
Development of Schiff base electrochemical sensors for the evaluation of polycyclic aromatic hydrocarbons in aqueous medium



BY
MERYCK WARD

A thesis submitted in partial fulfilment of the requirements for the degree
of Doctor Philosophiae in the Department of Chemistry,
University of the Western Cape.

Supervisors
Professor Priscilla G.L. Baker
Professor Pierre-Henri Aubert

Abstract

A novel monomer (N,N'-Bis-(1H-pyrrol-2-ylmethylene)-benzene-1,2-diamine-BPPD) was derived from the condensation reaction between o-phenylenediamine and a pyrrole derivative. The monomer was polymerized electrochemically to produce the new polymer material – polymerized(N,N'-Bis-(1H-pyrrol-2-ylmethylene)-benzene-1,2-diamine) PBPPD. This novel polymer material was deposited at the surface of a screen-printed carbon electrode, as a thin film, in the development of chemical sensors for the detection of polycyclic aromatic hydrocarbons (PAHs). The monomer material was characterized in terms of its optical (spectroscopy) and thermal properties. The polymer material was characterized in terms of its surface morphology and its redox electrochemistry. Fourier transform infrared spectroscopy (FTIR) was used to confirm the azomethine bond formation during the condensation reaction of an aldehyde and primary amine derivative. Thermal stability of the Schiff base material was determined by thermogravimetric analysis. Surface morphology of the polymer material prepared by cyclic voltammetry was studied to determine if the polymer material was prepared at the surface of the electrode. Redox behaviour was investigated by square wave voltammetry to determine electrochemical parameters such as diffusion coefficient, peak separation and formal potential. 12 PAHs were selected from the United States environmental protection agency (U.S EPA) priority listing of PAHs and these were evaluated at an unmodified and polymer modified screen printed carbon electrodes. 1-hydroxypyrene (1-OHP) and pyrene (PYR) displayed well defined peaks at +0.2 V and -0.54 V vs Ag/AgCl respectively when evaluated at the unmodified transducer. These 2 PAHs were quantitatively evaluated in two different electrolyte solutions (both pH < 7) in order to enhance electrochemical signal reporting. The limit of detection (LOD) for 1-OHP and PYR was found to be 6.00×10^{-4} ppb ($R^2 = 0.9924$) and 1.77×10^{-3} ppb ($R^2 = 0.9989$) respectively. Sensitivity of the transducer towards the detection of the analyte was determined from the slope of the linear portion of the calibration curve. The sensitivity for 1-OHP and PYR was found to be 585.81 $\mu\text{A/ppb}$ and 338.61 $\mu\text{A/ppb}$. Oxidative redox peaks were observed for anthracene (-0.93 V), benzo(a)pyrene (-0.73 V), chrysene (-0.58 V), naphthalene (+0.21 V) and phenanthrene (-0.55 V) vs Ag/AgCl. These PAHs redox peaks were observed at higher concentrations than 1-OHP and PYR. No redox response was observed for 7,12-dimethylbenz(a)anthracene, acenaphthylene,

benzo(b)fluoranthene and fluoranthene at the unmodified transducer. Benzo(a)pyrene (BaP) and fluoranthene (FLA) displayed well defined peaks at -0.68 V vs Ag/AgCl and -0.54 V vs Ag/AgCl respectively when evaluated at the polymer modified transducer, as single analytes as well as when combined as a mixed sample. Redox responses for BaP and FLA were determined in 0.1 M LiClO₄. The LOD for BaP and FLA was found to be 9.46×10^{-7} ppb ($R^2 = 0.9975$) and 1.07×10^{-7} ppb ($R^2 = 0.9941$) respectively. The sensitivity for BaP and FLA was found to be 712.04 μ A/ppb and 627.21 μ A/ppb. Oxidative redox peaks were observed for 1-OHP (-0.16 V), 7,12-dimethylbenz(a)anthracene (-0.46 V), acenaphthylene (-0.50 V), chrysene (-0.56 V), naphthalene (-0.62 V), pyrene (-0.43 V) and triphenylene (-0.58 V) vs Ag/AgCl. These PAHs species were not selected for quantitative analysis as their analytical signals became lost in a mixed sample. No redox peaks were observed for anthracene and phenanthrene. High performance liquid chromatography (HPLC) using an ultraviolet (UV) detector is one of the most common methods used for the determination of PAHs in mixed samples. PAHs species seldom occur as individual PAHs species and the standard analytical method for the priority PAHs is the HPLC-UV/fluorescence method. HPLC-UV was used to validate PAHs sample integrity and to compare with PAHs detection methods in literature. A multichannel multi array electrochemical analysis approach was tested, drawing on the data from individual PAH evaluation. The multichannel approach proposed incorporated the use of an 8 electrode array wall jet cell that can be individually optimized for up to 8 PAHs in one mixed sample. This was made possible by using a different electrode assembly that favours one individual PAH at each electrode, based on its specific requirements for electrochemical detection. The proposed multichannel approach proposed in this research is being developed in ongoing research development.

Keywords

N,N'-Bis-(1H-pyrrol-2-ylmethylene)-benzene-1,2-diamine

Schiff base

Zig-zag polymer

Conducting polymer

Actuator

Deformation

Expansion

Screen-printed carbon electrode

Polycyclic aromatic hydrocarbons

Multichannel

Multi array

High Performance Liquid Chromatography



Abbreviations

PAHs	:	Polycyclic aromatic hydrocarbons
WHO	:	World Health Organization
E.U.	:	European Union
U.S. EPA	:	United States Environmental Protection Agency
OSHA	:	Occupational Safety and Health Administration
NOISH	:	National Institute for Occupational Safety and Health
LMW	:	Low molecular weight
HMW	:	High molecular weight
1-OHP	:	1-hydroxypyrene
ANT	:	Anthracene
ANY	:	Acenaphthylene
BaP	:	Benzo(a)pyrene
BbF	:	Benzo(b)fluoranthene
CHR	:	Chrysene
DMBA	:	7,12-dimethylbenz(a)anthracene
FLA	:	Fluoranthene
NAPH	:	Naphthalene
PHEN	:	Phenanthrene
PYR	:	Pyrene
TRIP	:	Triphenylene
HPLC	:	High Performance Liquid Chromatography



GC	:	Gas Chromatography
AFM	:	Atomic Force Microscopy
CV	:	Cyclic Voltammetry
FTIR	:	Fourier Transform Infrared Spectroscopy
NMR	:	Nuclear Magnetic Resonance
SWV	:	Square Wave Voltammetry
SEM	:	Scanning Electron Microscopy
TGA	:	Thermogravimetric Analysis
LOD	:	Limit of Detection
LOQ	:	Limit of Quantification
SPCE	:	Screen printed carbon electrode
BPPD	:	N,N'-Bis-(1H-pyrrol-2-ylmethylene)-benzene-1,2-diamine
PBPPD	:	poly(N,N'-Bis-(1H-pyrrol-2-ylmethylene)-benzene-1,2-diamine)
oPD	:	o-phenylenediamine
P2C	:	Pyrrole-2-carboxaldehyde
USB	:	Universal serial bus
CDC	:	Carbide-derived-carbon
CP	:	Conducting Polymer
CPE	:	Constant Phase Element
EAP	:	Electroactive Polymer
ESI-MS	:	Electrospray Ionisation Mass Spectrometry
NQSA	:	1,4-Naphthaquinone Sulphonic Acid
PEDOT	:	Poly(3,4-ethylenedioxythiophene)

PPDP	:	Poly(phenazine- 2,3-diimino(pyrrole-2-yl))
PPy	:	Polypyrrole
PVDF	:	Polyvinylidene Fluoride
SCE	:	Saturated Calomel Electrode
TTFV	:	Tetrathiafulvalene



Declaration

I hereby declare that the work of '**Development of Schiff base electrochemical sensors for the evaluation of polycyclic aromatic hydrocarbons in aqueous medium**' which I now submit for the assessment on the programme of study leading towards the award of a doctoral degree, is entirely my own work; quotes and phrases obtained from the work of others have been fully acknowledged and referenced.



Signed:

.....

MERYCK WARD

Date: August 2017

Acknowledgements

I would like to express my gratitude to the people who showed continuous support and encouragement, without these significant people this thesis would not be possible. Constant guidance has allowed me to achieve this goal.

A day will come in every life, when appreciation is rendered. And this should be taken seriously, and given with love and tender. Anyone who deserves appreciation, must have done something great. So share with them the way you feel, and always treat them right. But keep in mind that appreciation, should be given again and again. If you truly appreciate, you'll remind them how great they've been. Do something special to thank the ones, who've made a difference to you.

But don't forget to thank them again, for everything they do.

Julie Hebert

My supervisor Prof. Priscilla Baker, thank you for the unwavering supervision, guidance and constant encouragement, which has allowed me to progress year by year towards this great achievement.

To my sensorlab colleagues, who have all become friend's thank you for all your help and support. The road to completion is a telling task without the help and support of friends to surround you.

To my parents Helen and Leslie Ward, thank you for the belief, guidance, support and so much more that words cannot describe. Every moment leading up to this would not have been achieved without your steadfast trust in my capabilities.

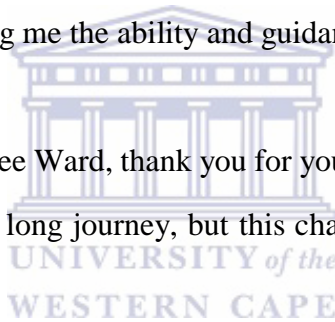
To my grandmother, Elizabeth O'Shea, for all her prayers, asking the Lord to guide me in the right direction and to allow me the opportunity to succeed in my career, thank you very much.

A family is like a circle, the connection never ends and even if at times it breaks, in time it always mends. A family is like the stars somehow they're always there. Families are those who help, who support and always care. A family is like a book, the endings never clear but through the pages of the book their love is always near. A family is many things with endless words that show who they are, what they do, how they teach you so you know, but don't be weary if it's broken or if through time its been so worn families are like that. They're split up and always torn but even if this happens your family will always be, they help define just who you are and will be a part of you eternally.

Nicole M. O'Neil

Thank you Lord for giving me the ability and guidance to complete this work.

To my rock, my amazing wife Aimee Ward, thank you for your support, encouragement and most of all your patience. It has been a long journey, but this chapter has finally been achieved with you by my side.

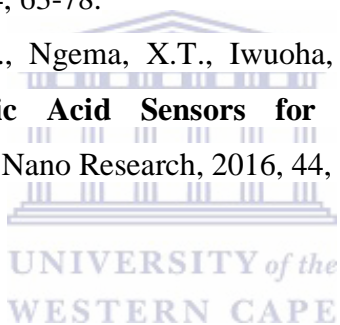


“We rejoice in our sufferings, knowing that suffering produces endurance, and endurance produces character, and character produces hope.”

Romans 5:3-4

Publications

1. **Ward, M.**, Baker, P., Iwuoha, E., Aubert, PH. and Plesse, C., **Polypyrrole Derivatives in the Design of Electrochemically Driven Actuators.** Mini-Reviews in Organic Chemistry, 2015, 12, 414-423.
2. **Ward, M.**, Botha, S., Iwuoha, E., Baker, P., **Actuation Behaviour of a Derivatized Pyrrole Accordion Type Polymer.** International Journal of Electrochemical Science, 2014, 9, 4776-4792.
3. Ngema, X. T., **Ward, M.**, Hamnca, S., Baker, P., Iwuoha, E., **Spectro-Electrochemical of Detection Anthracene at Electrodeposited Polyamic Acid Thin Films.** Journal of Nano Research, 2016, 44, 63-78.
4. Hamnca, S., **Ward, M.**, Ngema, X.T., Iwuoha, E.I., Baker, P., **Development of Graphenated Polyamic Acid Sensors for Electroanalytical Detection of Anthracene.** Journal of Nano Research, 2016, 44, 11-22.



Contents

Abstract	
Keywords	
Abbreviations	
Declaration	
Acknowledgements	
Publications	
Contents	
1. Polycyclic Aromatic Hydrocarbons.....	1
1.1 Polycyclic aromatic hydrocarbons.....	2
1.2 Sources of polycyclic aromatic hydrocarbons.....	2
1.3 Properties of polycyclic aromatic hydrocarbons	5
1.4 Formation of polycyclic aromatic hydrocarbons.....	10
1.5 Polycyclic aromatic hydrocarbons in the environment	11
1.6 Carcinogenicity of polycyclic aromatic hydrocarbons.....	11
1.7 Mutagenicity of polycyclic aromatic hydrocarbons	12
1.8 Human exposure to polycyclic aromatic hydrocarbons	14
1.9 Polycyclic aromatic hydrocarbons biomarkers.....	16
2. Multi-array Sensors Systems.....	22
2.1 Chemical sensors	22
2.2 Chemical sensors for polycyclic aromatic hydrocarbons	23
2.3 Array sensing	25
2.4 Multi-array sensor systems.....	25
2.5 Multichannel devices.....	29

2.6	Multichannel analysis case studies	31
2.6.1	Cantilever array sensing.....	31
2.6.2	High density temperature array sensing.....	32
2.6.3	Tactile array sensing	32
2.7	Proposed multichannel analytical protocol for polycyclic aromatic hydrocarbons ...	33
3.	Materials design and Methodology	36
3.1	Microscopy	38
3.2	Spectroscopy.....	39
3.3	Electrochemistry	39
3.4	Thermogravimetric analysis	40
4.	Electrochemical evaluation of Polycyclic Aromatic Hydrocarbons at a Bare Screen Printed Carbon Electrode	41
4.1	Bare screen-printed carbon electrode platform	43
4.2	Electrochemical screening of polycyclic aromatic hydrocarbons	44
4.3	Quantitative analysis of pyrene	52
4.4	Quantitative analysis of 1-hydroxypyrene.....	58
5.	Characterization of Schiff base materials (N,N'-Bis-(1H-pyrrol-2-ylmethylene)-benzene-1,2-diamine) and poly(N,N'-Bis-(1H-pyrrol-2-ylmethylene)-benzene-1,2-diamine) modified screen printed carbon electrode.....	65
5.1	Introduction	66
5.2	Introduction into Schiff base materials.....	66
5.3	Schiff base sensors	67
5.4	Monomer synthesis.....	68
5.5	Fourier transform infrared spectroscopy (FTIR)	69
5.6	Nuclear magnetic resonance (NMR)	72
5.7	UV-Vis analysis.....	76

5.8	Thermal analysis.....	78
5.9	Electrochemical preparation of poly(N,N'-Bis-(1H-pyrrol-2-ylmethylene)-benzene-1,2-diamine).....	80
5.10	Electrochemical characterization of poly(N,N'-Bis-(1H-pyrrol-2-ylmethylene)-benzene-1,2-diamine) prepared at the screen printed carbon electrode	83
5.10.1	Atomic force microscopy.....	83
5.10.2	Scanning electron microscopy	84
5.10.3	Electrochemical characterization	85
6.	Electrochemical evaluation of selected polycyclic aromatic hydrocarbons at poly(N,N'-Bis-(1H-pyrrol-2-ylmethylene)-benzene-1,2-diamine) modified screen printed carbon electrode.....	92
6.1	Electrochemical screening of polycyclic aromatic hydrocarbons	94
6.2	Quantitative Analysis of benzo(a)pyrene and fluoranthene	98
6.3	Quantitative analysis of a complex mixture containing benzo(a)pyrene and fluoranthene	104
7.	High Performance Liquid Chromatography Identification, Separation and Detection of Polycyclic Aromatic Hydrocarbons in the presence of Interfering Species	110
7.1	Introduction	110
7.2	Experimental.....	112
7.3	Standard solutions.....	112
7.4	Instrument and instrument conditions	112
7.5	Interference species and sample preparation	113
7.6	Results and Discussion	113
7.6.1	Chromatographic results of standard profiles	113
7.6.2	Chromatographic results for the complex mixture	122
8.	Conclusion and Future Work.....	127
8.1	Conclusion	127

References	135
9. Publication 1	158
Polypyrrole Derivatives in the Design of electrochemically Driven Actuators	158
9.1 Introduction	159
9.2 Bilayer actuators	161
9.3 Trilayer actuators	165
9.4 Polymer conformations influencing actuation	170
9.5 Conclusion	175



Table of Figures:

Figure 1. Contributing sources of PAHs emissions into the environment.....	3
Figure 2. Global PAHs emissions.....	4
Figure 3. Low Molecular Weight Polycyclic Aromatic Hydrocarbons.....	6
Figure 4. High Molecular Weight Polycyclic Aromatic Hydrocarbons.....	7
Figure 5. PAHs formation by pyrosynthesis process.[155].....	10
Figure 6. Identification of the bay-region in (a), (b), (c).	14
Figure 7. Percentage representation of the daily PAHs intake limits.....	16
Figure 8. A chemical sensor transforms chemical information into an analytical signal.....	23
Figure 9. Array sensors designed by MicruX technologies, A – dual sensor, B - tri sensor, C – 8x single-electrode chip, D – 16x single-electrode chip, E – multi-individual microelectrode array.....	26
Figure 10. Sensors designed by Dropsens, A – 4X screen printed carbon electrode, B – 8X screen printed carbon electrode, C – 96X screen printed carbon electrode.....	27
Figure 11. An array sensor designed by BVT technologies incorporating 8 working electrodes.....	27
Figure 12. Gwent technologies array sensor design incorporated 16 working electrodes in its geometrical design.....	28
Figure 13. Multichannel potentiostat produced by Dropsens, A - Bipotentiostat, B - multipotentiostat with 4 channels, C - multipotentiostat with 8 channels.....	30
Figure 14. VSP300 multipotentiostat developed by Bio-logic	30
Figure 15. Operating principle of the liquid-based sensing array.....	33
Figure 16. Principle operation of the wall-jet flow cell with 8 reservoirs being controlled by 2 pumps.....	35
Figure 17. Anchor molecules, (a) o-phenylenediamine and (b) 2,3-diaminophenazine.....	38
Figure 18. Structural images of the selected polycyclic aromatic hydrocarbons for this work... ..	42
Figure 19. Screen-printed carbon electrodes used for all electrochemical measurements.....	43
Figure 20. Evaluation of selected PAHs using CV at a bare SPCE in 0.1 M LiClO ₄ at 50mV/s.....	44
Figure 21. CV of naphthalene at a bare SPCE in 0.1 M LiClO ₄ at 50 mV/s displaying a reversible redox couple (A-A').	46

Figure 22. Electrochemical signature of (a) 1-OHP, (b) ANT, (c) ANY, (d) BaP, (e) BbF, (f) CHR, (g) DMBA, (h) FLA, (i) NAPH, (j) PHEN, (k) PYR and (l) TRIP at the bare SPCE.	50
Figure 23. SWV analysis of pyrene at a bare SPCE in 0.1 M LiClO ₄ in the concentration range 753 to 3420 ppb, at 50mV/s.	53
Figure 24. Calibration curve for the screening of pyrene.	55
Figure 25. SWV analysis of 1-hydroxypyrene at a bare SPCE in 0.1 M HCl in the concentration range 543 to 3435 ppb, at 50mV/s.....	58
Figure 26. Calibration curve of the detection of 1-hydroxypyrene.	60
Figure 27. Conclusions based on the information obtained during the evaluation of PAHs at the unmodified screen printed carbon electrode surface.	64
Figure 28. A Schiff base ligand 2-((2-sulfanylphenyl)ethanimidoyl)phenol.	67
Figure 29. FTIR spectra of o-phenylenediamine, pyrrole-2-carboxaldehyde and N,N'-Bis-(1H-pyrrol-2-ylmethylene)-benzene-1,2-diamine, between 400 and 4000 cm ⁻¹	69
Figure 30. FTIR spectra of o-phenylenediamine, pyrrole-2-carboxaldehyde and N,N'-Bis-(1H-pyrrol-2-ylmethylene)-benzene-1,2-diamine, between 2600 and 3600 cm ⁻¹	70
Figure 31. FTIR spectra of o-phenylenediamine, pyrrole-2-carboxaldehyde and N,N'-Bis-(1H-pyrrol-2-ylmethylene)-benzene-1,2-diamine, between 1500 and 1800 cm ⁻¹	71
Figure 32. NMR spectra of o-phenylenediamine in Acetone-d ₆	72
Figure 33. NMR spectra of pyrrole-2-carboxaldehyde in Acetone-d ₆	73
Figure 34. NMR spectra of BDDP in DMSO-d ₆	74
Figure 35. UV-Vis spectra of pyrrole-2-carboxaldehyde in Ethanol.	76
Figure 36. UV-Vis spectra of o-phenylenediamine in Ethanol.	77
Figure 37. UV-Vis of BPPD, O-phenylenediamine and Pyrrole-2-carboxaldehyde in Ethanol.	77
Figure 38. TGA decomposition analysis of BPPD.	78
Figure 39. Fragmentational loss during thermogravimetric analysis of BPPD.	79
Figure 40. Electrochemical polymerization of 20 mM BPPD at SPCE in DMF/0.1 M HCl at 50 mV/s for 15 cycles.	80
Figure 41. Electrochemical polymerization of oPD, P2C and PBPPD in an equivolume ratio of DMF:0.1M HCl.	81
Figure 42. AFM image of an unmodified screen printed carbon electrode.	83
Figure 43. AFM image of a screen printed carbon electrode modified with PBPPD.	83

Figure 44. SEM image of BPPD novel monomer.....	84
Figure 45. SEM image of the polymer material PBPPD.	85
Figure 46. Electrochemical signature of PBPPD in 0.1 M LiClO ₄ characterized by cyclic voltammetry.....	86
Figure 47. Electrochemical signature of PBPPD redox process by SWV, oxidation (above) and reduction (below) behaviours.	87
Figure 48. Plot of PBPPD based on the Cottrell equation.	89
Figure 49. Structural images of the selected polycyclic aromatic hydrocarbons evaluated at this novel platform.	93
Figure 50. Electrochemical signatures of (a) 1-OHP, (b) ANT, (c) ANY, (d) BaP, (e) BbF, (f) CHR, (g) DMBA, (h) FLA, (i) NAPH, (j) PHEN, (k) PYR and (l) TRIP at the modified polymer platform.....	96
Figure 51. SWV analysis of benzo(a)pyrene (B) at the modified polymer SPCE (A) in 0.1 M LiClO ₄ in the concentration range 939 to 4852 ppb, at 50mV/s.....	98
Figure 52. Calibration curve of the screening of BaP.....	100
Figure 53. SWV analysis of fluoranthene (B) at the modified polymer SPCE (A) in 0.1 M LiClO ₄ in the concentration range 252 to 4816 ppb, at 10mV/s.....	101
Figure 54. Calibration curve of the screening of FLA.....	102
Figure 55. Electrochemical screening of the complex matrix at the polymer platform.	104
Figure 56. Calibration curves for the complex matrix containing BaP (above) and FLA (below).	105
Figure 57. Conclusions based on the information obtained during the evaluation of PAHs at the polymer modified screen printed carbon electrode surface.....	109
Figure 58. Chemical structures of the polycyclic aromatic hydrocarbons is within this work..	112
Figure 59. Concentration profile of benzo(a)pyrene standard.	114
Figure 60. Calibration curve for benzo(a)pyrene standard solution.	115
Figure 61. Concentration profile of 1-hydroxypyrene standard.	116
Figure 62. Calibration curve for 1-hydroxypyrene standard solution.....	117
Figure 63. Concentration profile of fluoranthene standard.....	118
Figure 64. Calibration curve for fluoranthene standard solution.	119
Figure 65. Concentration profile of pyrene standard.	120

Figure 66. Combined cocktail standard containing: 1. 1-OHP, 2. FLA, 3. PYR, 4. BaP.....	122
Figure 67. Consecutive concentration additions of pyrene into the complex mixture.	123
Figure 68. Calibration curve of PYR in the complex PAHs matrix.	124
Figure 69. Proposed multi array setup for the simultaneous detection of polycyclic aromatic hydrocarbons.	132
Figure 70. Multichannel design for the evaluation of 1-hydroxypyrene, benzo(a)pyrene, fluoranthene and pyrene.	134
Figure 71. Possible deformation mechanism of an EAP.	160
Figure 72. (a) Bilayer actuator design, (b) Operating mechanism.....	162
Figure 73. (a) The bilayer actuator at rest covering a reservoir, (b) Electrical stimulus applied to the bilayer actuator causing displacement and revealing the opening to the reservoir.	163
Figure 74. Illustration of the behaviour of the trilayer actuator under electrical stimulus.	165
Figure 75. Trilayer experiences delamination due to excess number of actuation cycles.	168
Figure 76. (a) PPy is oxidized at the positive electrode causing anion movement from the PVDF layer into the PPY layer which causes volume expansion. Reduction occurs at the negative electrode resulting in volume reduction. (b) The trilayer actuator at rest with no electrical stimulus being applied. (c) Step A is repeated with the electrodes being switched around, allowing deformation to occur in the opposite direction.....	169
Figure 77. Zig-zag molecule containing calix(4)arene and quarterthiophene.	171
Figure 78. Helical Structure with Zn centre $\{Zn(SPh)_2(BPyVB)\}_n$	172
Figure 79. Organometallic framework.....	172
Figure 80. Molecular tweezers.....	173
Figure 81. Zig zag structural conformation of a phenazine hinged molecule interconnected by pyrrole chains.	174

List of Tables:

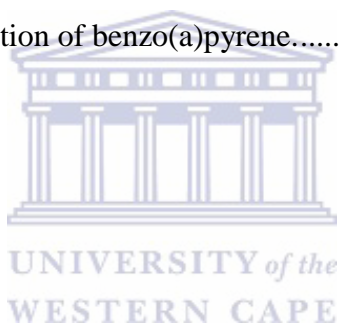
Table 1. The main sources responsible for PAHs emissions.	3
Table 2. Contribution towards total atmospheric PAHs emissions.	4
Table 3. Priority PAHs listed by the U.S. EPA.[29, 34, 101, 200]	8
Table 4. Priority PAHs listed by the E.U.[210]	9
Table 5. Levels of contamination in respective food groups.	15
Table 6. Environmental protection agency daily PAHs limits.	15
Table 7. PAHs biomarkers.....	20
Table 8. Array sensor systems developed by various companies.	29
Table 9. Commercially available multichannel potentiostats.	31
Table 10. Electrochemical evaluation of polycyclic aromatic hydrocarbons at bare screen printed carbon electrode.....	51
Table 11. Analytical and statistical data for pyrene detection at bare SPCE.....	57
Table 12. Analytical and statistical data for 1-hydroxypyrene detection at bare SPCE.....	61
Table 13. FTIR stretching frequency assignments	71
Table 14. ¹ H NMR data of starting materials and the new Schiff base material.	75
Table 15. AFM analysis obtained from the SPCE platform.	84
Table 16. Electrochemical parameters obtained from the characterization of PBPPPD.	90
Table 17. Diffusion coefficient values for PBPPD.	90
Table 18. Electrochemical screening of polycyclic aromatic hydrocarbons at the polymer modified bare screen printed carbon electrode.	97
Table 19. Electrochemical parameters and calibration data for BaP and FLA.	103
Table 20. Electrochemical parameters and calibration data for the species in the PAHs mixture.	106
Table 21. HPLC conditions used for the identification of PAHs.	113
Table 22. Chromatographic data for the BaP standard profile.	115
Table 23. Chromatographic data for the 1-hydroxypyrene standard profile.	117
Table 24. Chromatographic data for the fluoranthene standard profile.....	119
Table 25. Chromatographic data for the pyrene standard profile.	121
Table 26. Calibration standard profile data for PAHs determined from electrochemistry.	121

Table 27. PAHs complex matrix data.....	122
Table 28. Shift in retention times for PAHs.	124
Table 29. Modified polypyrrole bilayers.	162
Table 30. Modified polypyrrole trilayers.	166
Table 31. Interfacial capacitance of PPDP-PVSA.....	175



Table of Schemes:

Scheme 1. Metabolic pathway of carcinogenic PAHs.....	13
Scheme 2. Metabolism of Pyrene to 1-Hydroxypyrene.....	17
Scheme 3. Metabolism of benzo(a)pyrene to form the diol-epoxides.....	18
Scheme 4. Proposed electrochemical oxidation scheme of pyrene to pyrene-1,6-dione.....	54
Scheme 5. Proposed electrochemical oxidation mechanism of 1-hydroxypyrene.....	59
Scheme 6. Formation of Schiff base compound.....	66
Scheme 7. N,N'-Bis-(1H-pyrrol-2-ylmethylene)-benzene-1,2-diamine preparation by Schiff base synthesis.....	69
Scheme 8. Proposed structural formation of the polymerization observed at SPCE.....	82
Scheme 9. Proposed structural formation of the cyclization observed at GCE.....	82
Scheme 10. Electrochemical oxidation of benzo(a)pyrene.....	99



1. Polycyclic Aromatic Hydrocarbons

Environmental pollutants have a long lasting effect on the earth, humans and animals alike and may have drastic outcomes on life as we know it. This chapter introduces polycyclic aromatic hydrocarbons in terms of physical and chemical properties, how they are formed and how the environment is affected by their production. The major concerns relate to the adverse health effects on humans. Various health organizations have established guidelines for the safety limits to when humans are exposed to polycyclic aromatic hydrocarbons. Polycyclic aromatic hydrocarbons that enter the body are metabolized into DNA-adducts which have harmful effects on the human body, as extreme as cancer. Many methods have been explored for efficient and cost effective monitoring of polycyclic aromatic hydrocarbons in water, soil, food and in vitro. However, many challenges still remain.

1.1 Polycyclic aromatic hydrocarbons

Polycyclic Aromatic Hydrocarbons (PAHs) are a ubiquitous class of organic pollutants that are persistent in the environment. They result from the incomplete combustion or pyrolysis of many organic matter. PAHs are also known as polynuclear hydrocarbons (PNHs), polycyclic organic matter (POM) and polynuclear aromatics (PNAs). There are thousands of PAHs in the environment but they are usually found in complex mixtures rather than individual compounds. PAHs produce toxic and irritating fumes on decomposition and may also react violently with oxidizing agents. When dissolved in water or absorbed onto particulate matter, PAHs can undergo photodecomposition when exposed to ultraviolet light from solar radiation. The best known model PAHs compound is benzo(a)pyrene (BaP) due to its highly carcinogenic nature, based on the information provided by the World Health Organization (WHO).[32, 106, 127, 142, 149, 156]

1.2 Sources of polycyclic aromatic hydrocarbons

PAHs are produced mainly through the pyrolysis process, usually through incomplete combustion of organic materials. Both natural and anthropogenic sources are the major contributors to the release of PAHs into the environment. Natural sources include forest fires and volcanic eruptions, the main anthropogenic sources include vehicular emissions, residential wood burning, petroleum catalytic cracking and industrial combustion of fossil fuels. PAHs are widely distributed into the environment and was one of the first atmospheric pollutants to be classified as a potential carcinogen. The release of PAHs into the atmosphere allows for the possibility of the PAHs to be transported over great distances before deposition through atmospheric precipitation into waters, soils and vegetation's. A wide range of sources are responsible for the contribution to the total global atmospheric PAHs emissions including, industrial, agricultural, air, water, soil, foodstuffs and other sources such as medicines, dyes, plastics, pesticides and wood preservatives. Industrial emissions are produced by the burning of fuels such as gas, oil and coal, other industrial sources include the production of primary aluminium, coke, petrochemicals, rubber tires, cement manufacturing, bitumen, asphalt, wood preservation, commercial heat, power generation and waste incineration. Burning of brushwood, straw, moorland heather, stubble

are the main contributors from agricultural sources.[67, 130, 145] The main sources of PAHs emissions in air are directly related to the combustion processes such as domestic solid fuel burning and motor vehicles (**Table 1**). Each source plays a major role in the contribution of PAHs emissions into the environment, biofuel and wildfire being the major contributors (**Figure 1**).[2, 155]

Table 1. The main sources responsible for PAHs emissions.

Environmental Sources of PAHs	% Contribution
Biofuel	58
Wildfire	17
Consumed product use	7
Traffic oil	5
Domestic Coal	4
Coke Production	2
Petrol Refineries	2
Waste Management	1
Others	4

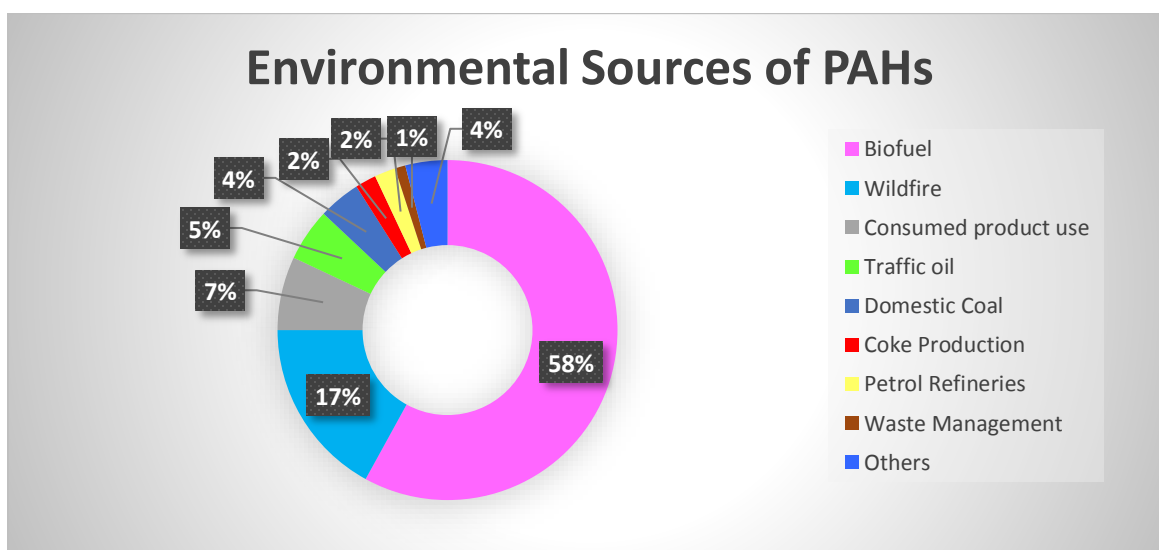


Figure 1. Contributing sources of PAHs emissions into the environment.

An estimation was made in 2004 that the total global atmospheric PAHs emission of the 16 priority PAHs was 520 giga grams per year ($Gg.y^{-1}$), with the major contributing continent being Asia (anthropogenic sources). The high percentage contribution from the African continent is due to the high amount of PAHs from natural sources such as savanna fires, similarly in the case of the South American continent where forest fires is the major source of PAHs emissions (**Figure 2**). PAHs emissions are spread globally with each continent contributing to the annual PAHs emissions (**Table 2**).[165, 214]

Table 2. Contribution towards total atmospheric PAHs emissions.

Country	Total Atmospheric PAHs Emissions ($Gg.y^{-1}$)	% Contribution
Asia	290	55
Africa	98	18.8
North America	42	8
Europe	49	9.5
South America	31	6
Oceania	8	11.5

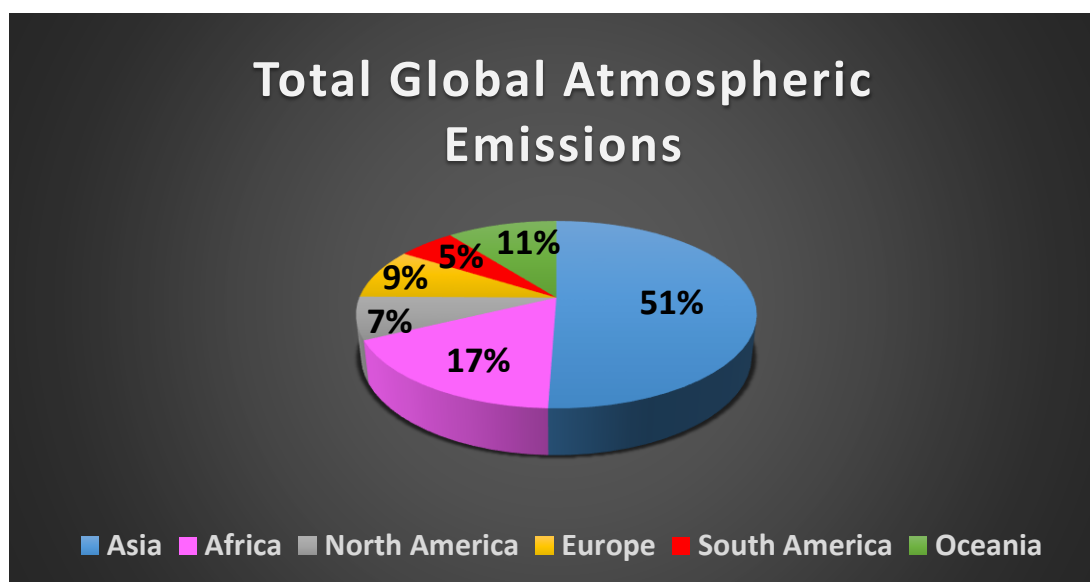


Figure 2. Global PAHs emissions.

1.3 Properties of polycyclic aromatic hydrocarbons

PAHs are colourless, white or pale yellow solids with relatively low solubilities in water, high boiling and melting points as well as low vapour pressures.[9, 93, 140] PAHs comprise of two or more fused benzene rings consisting mostly of carbon and hydrogen atoms, with a few exception which contain a nitrogen atom. PAHs are highly hydrophobic and easily adsorb onto the surface of organic matter of solid particles, resulting in the formation of persistent micropollutants in the environment.[26, 93, 95, 212] The physical properties of PAHs such as solubility vary with their structure and molecular weights, other properties include light sensitivity, heat resistance, conductivity, emittability, corrosion resistance and physiological action. PAHs are relatively insoluble in water with most of them being able to be photo-oxidized or degraded, but are however highly lipophilic. PAHs can be classed into two categories based on their relative insolubilities, (1) low molecular weight (LMW) PAHs and (2) high molecular weight (HMW) PAHs. Low molecular weight compounds which comprise of 2-3 rings (Naphthalenes, Flourenes, Phenanthrenes and Anthracenes) (**Figure 3**). With an increase in the molecular weight of the PAHs their respective solubility in water decreases, an increase in both the melting and boiling point and vapour pressure decreases.

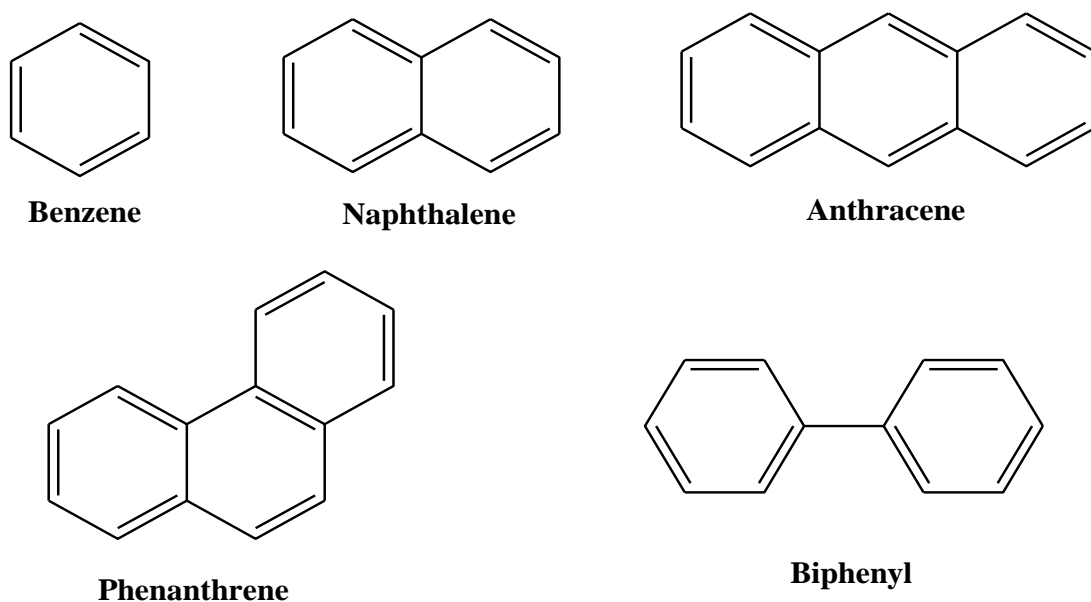


Figure 3. Low Molecular Weight Polycyclic Aromatic Hydrocarbons.

HMW PAHs compounds comprise of 4 or more rings (chrysenes and coronenes), with most of these HMW PAHs being carcinogenic (**Figure 4**).[170, 206] The list of priority PAHs vary with each country, but based on the carcinogenic nature of PAHs, the United States Environmental Protection Agency (U.S. EPA) and the European Union (E.U.) have listed 16 PAHs as priority. The U.S. EPA viewed these priority 16 organic compounds for their potential risk to human health via drinking water (**Table 3**).[10, 29, 121, 200] The E.U. studied the behaviour of the priority PAHs in food additives based on the recommendation from the European Commission (**Table 4**).[94, 148, 161]

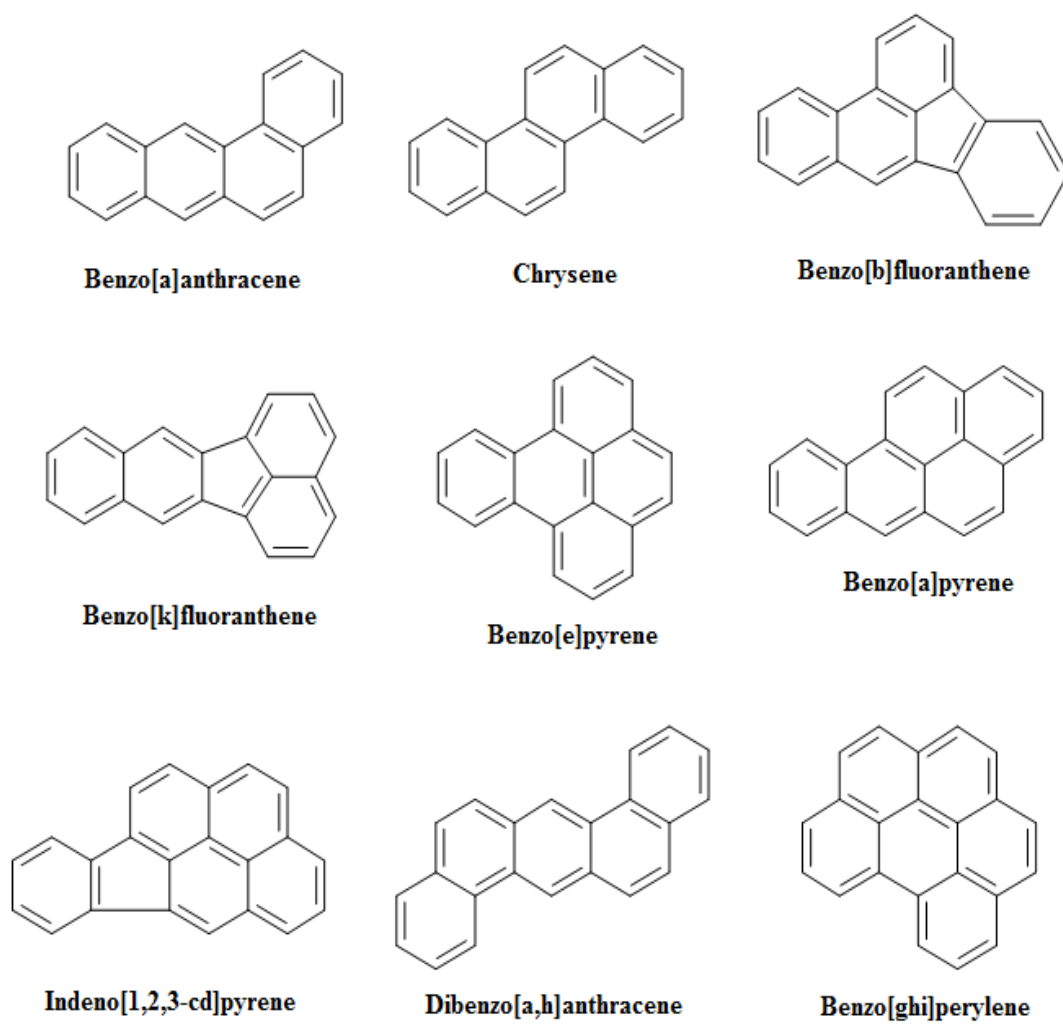


Figure 4. High Molecular Weight Polycyclic Aromatic Hydrocarbons.

Table 3. Priority PAHs listed by the U.S. EPA.[29, 34, 101, 200]

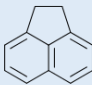
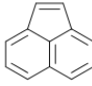
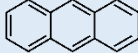
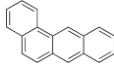
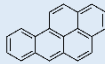
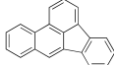
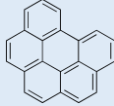
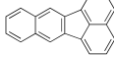
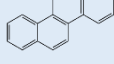
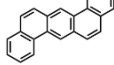
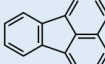
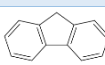
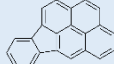
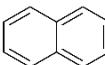
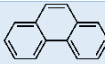
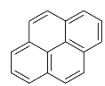
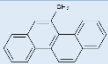
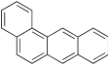
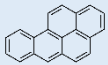
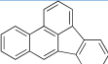
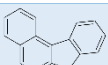
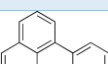
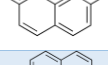
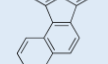
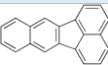
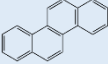
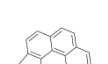
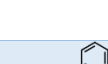
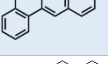
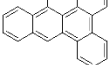
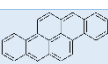
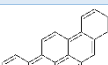
	PAHs Compound	Molecular Weight g.mol ⁻¹	Chemical Structure	Rings
1	Acenaphthene	154.21		3
2	Acenaphthylene	152.2		3
3	Anthracene	178.23		3
4	Benz(a)anthracene	228.29		4
5	Benzo(a)pyrene	252.32		5
6	Benzo(l)fluoranthene	252.31		5
7	Benzo(ghi)perylene	276.33		6
8	Benzo(k)fluoranthene	252.31		5
9	Chrysene	228.29		4
10	Dibenz(a,h)anthracene	278.35		5
11	Fluoranthene	202.25		4
12	Fluorene	166.22		3
13	Indeno(1,2,3-cd)pyrene	276.33		6
14	Naphthalene	128.17		2
15	Phenanthrene	178.23		3
16	Pyrene	202.25		4

Table 4. Priority PAHs listed by the E.U.[210]

	PAHs Compound	Molecular Weight g.mol ⁻¹	Chemical Structure	Rings
1	5-Methylchrysene	242.31		4
2	Benz(a)anthracene	228.29		4
3	Benzo(a)pyrene	252.31		5
4	Benzo(b)fluoranthene	252.31		5
5	Benzo(c)fluorene	216.28		4
6	Benzo(ghi)perylene	276.33		6
7	Benzo(j)fluoranthene	252.31		5
8	Benzo(k)fluoranthene	252.31		5
9	Chrysene	228.29		4
10	Cyclopenta(cd)pyrene	226.27		5
11	Dibenz(a,h)anthracene	278.35		5
12	Dibenzo(a,e)pyrene	302.37		6
13	Dibenzo(a,h)pyrene	302.37		6
14	Dibenzo(a,i)pyrene	302.1096		6
15	Dibenzo(a,l)pyrene	302.37		6
16	Indeno(1,2,3-cd)pyrene	276.33		6

1.4 Formation of polycyclic aromatic hydrocarbons

PAHs may be synthesized under oxygen deficient environments from saturated hydrocarbons. The two main mechanisms that are used in the explanation for the formation of PAHs include pyrosynthesis and pyrolysis. Pyrosynthesis occurs when low hydrocarbons are used in the formation of PAHs. At high temperatures ($> 500\text{ }^{\circ}\text{C}$) free radicals are formed when the bonds between the C-H and C-C are broken. These free radicals then combine to acetylene which further condense with aromatic ring structures, which are thermally resistant. (**Figure 5**). The formation of PAHs by pyrosynthesis from hydrocarbons varies in order of aromatics $>$ cycloolefins $>$ olefins $>$ parafins.[128]

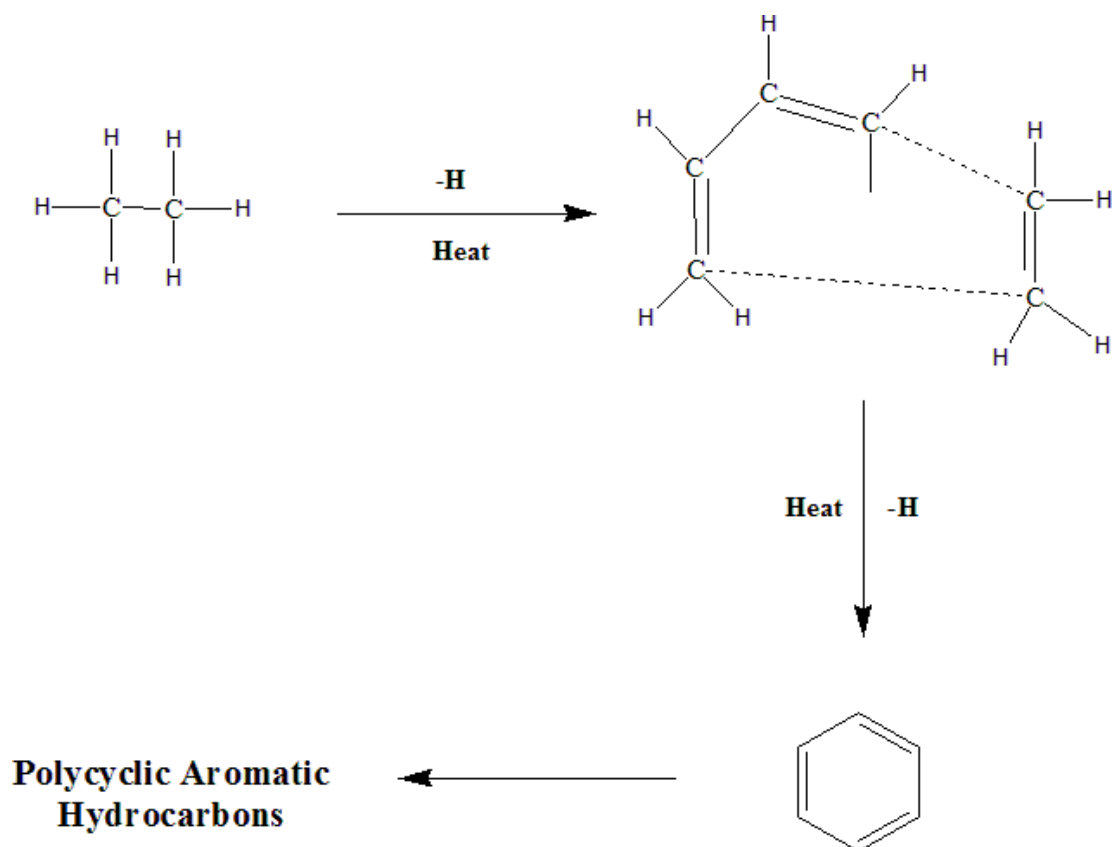


Figure 5. PAHs formation by pyrosynthesis process.[155]

Various mechanistic pathways were suggested by Haynes et., al 1991 for the PAHs formation during combustion.[23] These mechanistic pathways include slow Diels-Alder condensations, ionic, reaction mechanism and rapid radical reactions. Radicals from gaseous

hydrocarbons tend to quickly rearrange in order to provide the mechanism of PAHs formation and growth. The addition of these free radical hydrocarbons to lower molecular weight PAHs then lead, by alkyl PAHs to the formation of HMW PAHs.

1.5 Polycyclic aromatic hydrocarbons in the environment

Atmospheric PAHs are an important by-product of incomplete combustion or pyrolysis of organic material which include wood and biomass materials. Atmospheric PAHs are usually found in the form of both particulate and the gaseous phase matter which are dependent upon the vapor pressure. PAHs enter the environment due to evaporation from the earth's surface or human activity. Generally PAHs present in the gas phase dissolve within the clouds and into raindrops. However the majority of PAHs (70-90%) are adsorbed onto small inhalable particles with high concentrations, they tend to be removed via atmospheric precipitation. Once water clouds become saturated with PAHs, precipitations usually occur long distances from their origin resulting in the contamination of surface waters and land. HMW PAHs (> 5 benzene rings) can be classified as low mobility and are often deposited rapidly close to the source. LMW PAHs (2-3 benzene rings) are abundant in the gas phase and worldwide dispersion occurs preferentially in the Polar Regions. Transportation, deposition and chemical transformation of PAHs are dependent on their respective gas phase partitioning. Gas phase partitioning occurs when gas molecules move from a phase of high partial pressure to an adjacent phase of lower partial pressure. Gas phase partitioning is affected by molecular weight, temperature, humidity, precipitation, vapor pressure, concentration and amount of PAHs and the type of fine particles present.[42, 155, 168]

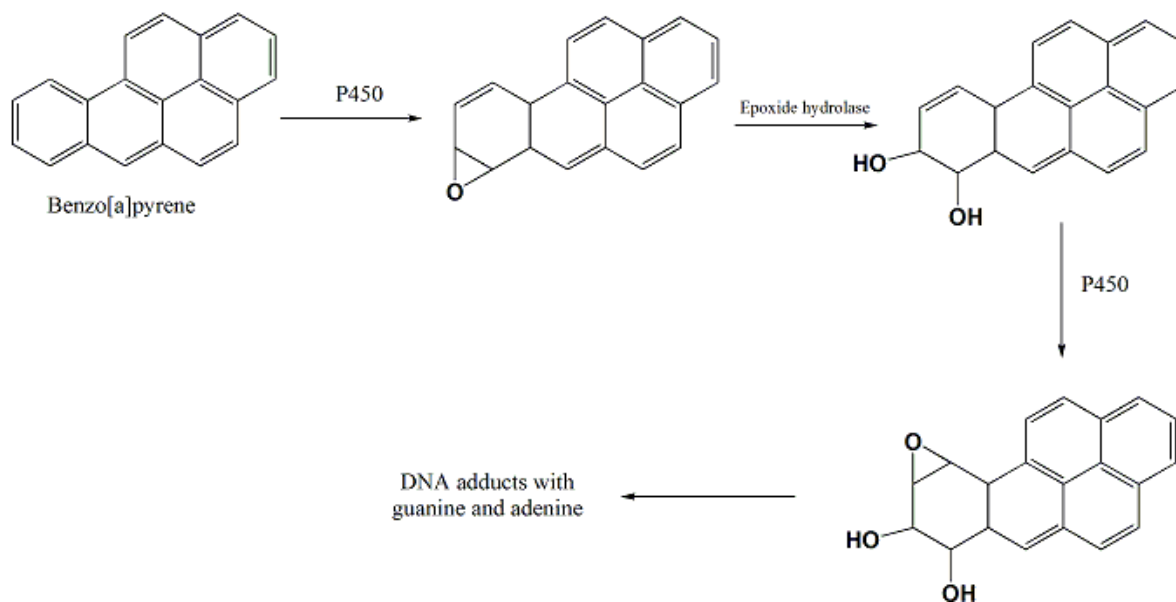
1.6 Carcinogenicity of polycyclic aromatic hydrocarbons

Consumer products such as toys, shoes and sporting goods, bicycle grips and tool handles still contain carcinogenic PAHs despite the known health hazards of these compounds. According to the European Chemical Agency (Anex XVII of Regulation (EC) 1907/2006 Reach Regulation) products containing these PAHs above the concentration limits have to be classified as carcinogenic and may not be sold publically.[5] The new E.U. Toy Directive (Directive 2009/48/EC) stipulates that the same concentration limits (dependent

upon which PAHs is responsible for the exposure) for known carcinogenic PAHs apply to toys.[157] The U.S. EPA has classified several PAHs as probable carcinogens, benzo(a)pyrene (BaP), benzo(a)anthracene (BaA), benzo(b)fluoranthene (BbF), benzo(k)fluoranthene (BkF), chrysene (CHR), dibenz(a,h)anthracene (DB(a,h)A) and Indeno(1,2,3-cd)pyrene (I(1,2,3-cd)P). These carcinogenic PAHs have been found in cigarette smoke, broiled foods and various polluted environments.[80] Synergistic and antagonistic effects by other compounds that are simultaneously emitted during incomplete combustion can have. Routes of exposure can determine the respective carcinogenic potency of these PAHs. BaP is highly carcinogenic and is often used as a marker for the presence of PAHs in environmental samples.[143]

1.7 Mutagenicity of polycyclic aromatic hydrocarbons

The ability of some PAHs to bind to cellular proteins and DNA with toxic effects poses a potential health risk.[15, 17] PAHs are able to attack DNA and form PAHs-DNA adducts through covalent bonding. The PAHs-DNA adducts have been identified as biomarkers for cancer.[91, 188, 199] Metabolic activation of PAHs occurs as a result of the interaction with microsomal enzymes (cytochrome P450, other proteins and UDP-glucuronyltransferase) present in many body cells with PAHs species. The interaction with the microsomal enzymes produce reactive epoxides which react with DNA and cause mutations of DNA. PAHs are initially metabolized to epoxides, the epoxides then couple to nucleic acids and introduce malignant transformations.[145] The oxidation of PAHs by the P450 enzyme is the initial step in the activation process, which then produces of a polar biochemically reactive electrophilic species. The electrophilic species is capable of interacting with cellular macromolecules (nucleic acid and proteins). A three enzyme-mediated reaction process is involved in the metabolic pathway of carcinogenic PAHs such as BaP (**Scheme 1**);



Scheme 1. Metabolic pathway of carcinogenic PAHs.

- The oxidation of a double bond which is catalyzed by the P450 enzyme to form the unstable arene oxides
- The hydrolysis process of the arene oxides by microsomal epoxide hydrolase to trans dihydrodiols
- A second enzyme (P450) catalyzed oxidation step at the double bond adjacent to the diol function which generates a vicinal diol epoxide.

This pathway may result in sterically hindered bay- or fjord-region diol epoxides, which are electrophiles that are capable of binding to DNA (**Figure 6**). Some other diol-epoxide stereoisomers of PAHs are found to be the ultimate carcinogens. PAHs classified in this category include benzo(a)pyrene, chrysene, 5-methylchrysene (5-MCR), phenanthrene (PHEN), benzo(c)phenanthrene (BcP), benz(a)anthracene, 7,12-dimethyl-benz(a)anthracene (DMBA) and Dibenzo(a,l)pyrene (DB(a,l)P), which are all metabolized through this pathway.[199]

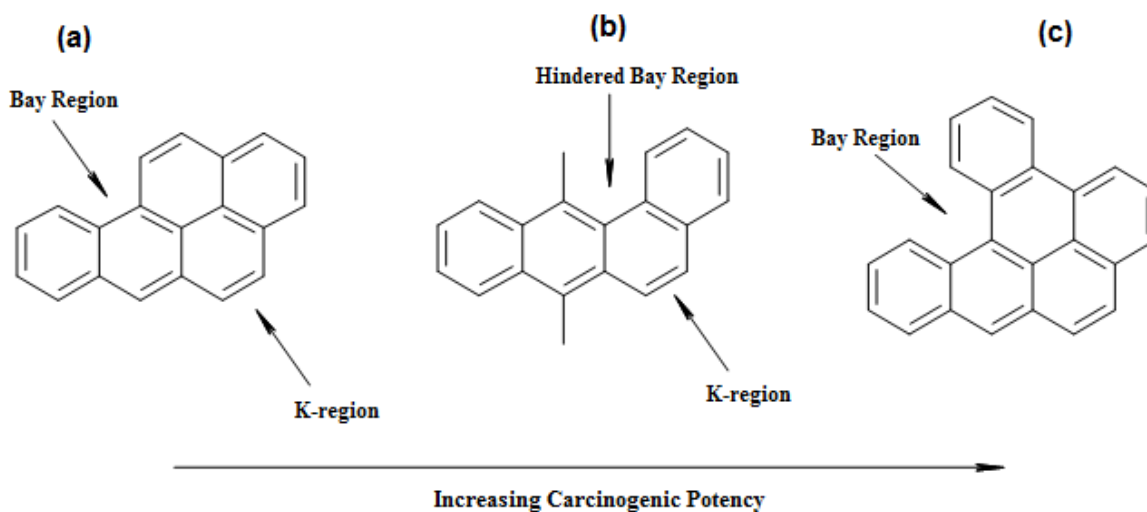


Figure 6. Identification of the bay-region in (a), (b), (c).

The structural features of PAHs contribute to the carcinogenicity with BaP being a known carcinogen which contains a bay-region. Methyl groups in DMBA and the extra benzene ring in DB(a,l)P hinder the structural feature further.[18] The bay-region is the space between the aromatic rings of the PAHs molecule. The change in potency of the diol epoxide can be attributed to the availability of the bay-region which predicts the reactivity and the mutagenicity of the PAHs. The bay-region is directly linked to the formation of diol epoxides in PAHs-DNA adducts.[75, 114, 158, 185]

1.8 Human exposure to polycyclic aromatic hydrocarbons

The main routes of PAHs intake in humans occur through diet and inhalation, with dietary intake being the main source of human exposure. Oil well fires, automotive exhaust fumes and tobacco smoking, represent alternative sources of human exposure. The population density increases the level of exposure, as well as exposure to mixed sources of PAHs. Human exposure to PAHs in bitumen fumes occur via several routes, e.g. inhalation, skin contamination or orally.[31, 97, 156] Plants have a relatively large surface area covered with waxes that facilitate the accumulation of PAHs. Atmospheric PAHs are generally transferred to plants by particle-phase deposition on the wax leaf cuticles or by uptake in the gas phase (stomata). Leaf features such as surface, cuticular waxes, hairs and number of stomata play an important role in the accumulation of PAHs. Foods can become

contaminated from particulate deposition on vegetables and fruit from air pollution and appears to be the main source of PAHs exposure to human. Consumers may be exposed to PAHs by consuming grilled or charred meats, contaminated cereals, flour and bread. BaP has been identified as the most carcinogenic PAHs, the levels of PAHs within the respective food groups reported as the levels of BaP. PAHs can accumulate in fish and shellfish, particularly bivalve molluscs, that are exposed to PAHs after an oil spill at sea (Table 5).[57, 172, 207]

Table 5. Levels of contamination in respective food groups.

<i>Food Groups</i>	<i>BaP Levels ($\mu\text{g}/\text{kg}$)</i>
<i>Grilled/Charred meats</i>	5.0
<i>Cereals</i>	1.0
<i>Flour</i>	0.1
<i>Bread</i>	0.1
<i>Bivalve Mollusks</i>	10.0
<i>Fish</i>	5.0
<i>Shellfish</i>	5.0

WESTERN CAPE

The environmental protection agency has suggested that the following amounts of daily PAHs intake is not likely to have harmful health effects to humans (Table 6). Each PAHs represents a specific percentage of the daily intake limit humans can be exposed to (Figure 7).

Table 6. Environmental protection agency daily PAHs limits.

<i>PAHs compound</i>	<i>Levels in Body (mg/kg)</i>
<i>Anthracene</i>	0.3
<i>Acenaphthene</i>	0.06
<i>Fluoranthene</i>	0.04
<i>Fluorene</i>	0.04
<i>Pyrene</i>	0.03

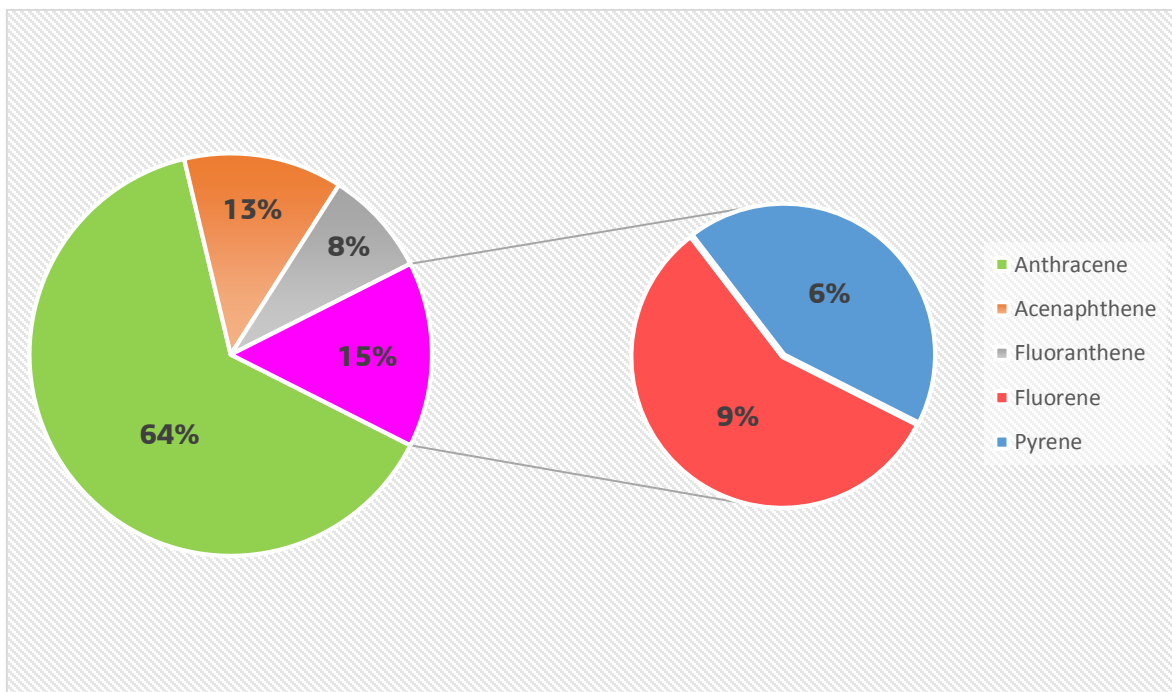


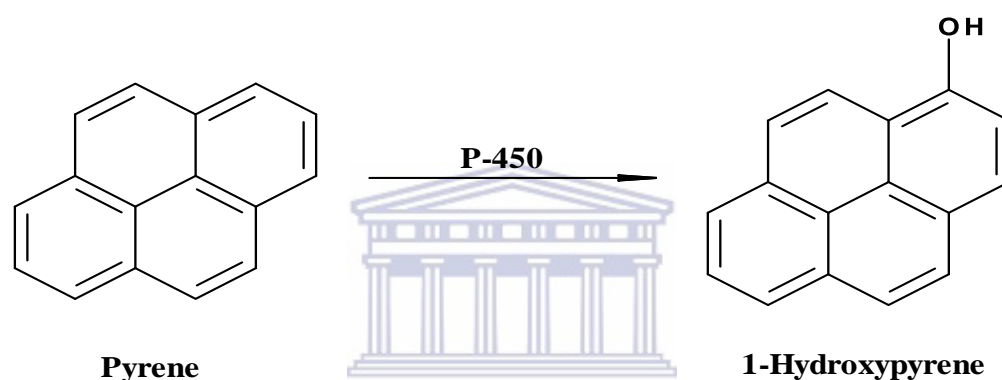
Figure 7. Percentage representation of the daily PAHs intake limits.

Toxicity of PAHs is dependent on exposure, the amount of PAHs exposed to, the various types of PAHs exposed to and the means of exposure (inhalation, skin contact or ingestion). [2, 156] Both short and long term exposure affects human health with longer term effects being more life threatening. Short term symptoms include; eye irritation, nausea, vomiting, diarrhea, skin irritation and inflammation. Long term exposure to pyrene (PYR) and BaP being identified as the two major PAHs responsible for causing cancer in lab animals. Long term effects include; skin, lung, bladder and gastrointestinal cancers. Cataracts, kidney damage, liver and jaundice, gene mutation and cardiopulmonary mortality. Redness and inflammation of the skin results from repeated contact with naphthalene (NAPH). Inhalation or swallowing large amounts of NAPH can cause a breakdown of red blood cells (hemolytic anemia).[1, 86] The harmful effects of PAHs depend on the mechanism of exposure; i.e. physical contact or chemical adduct formation.

1.9 Polycyclic aromatic hydrocarbons biomarkers

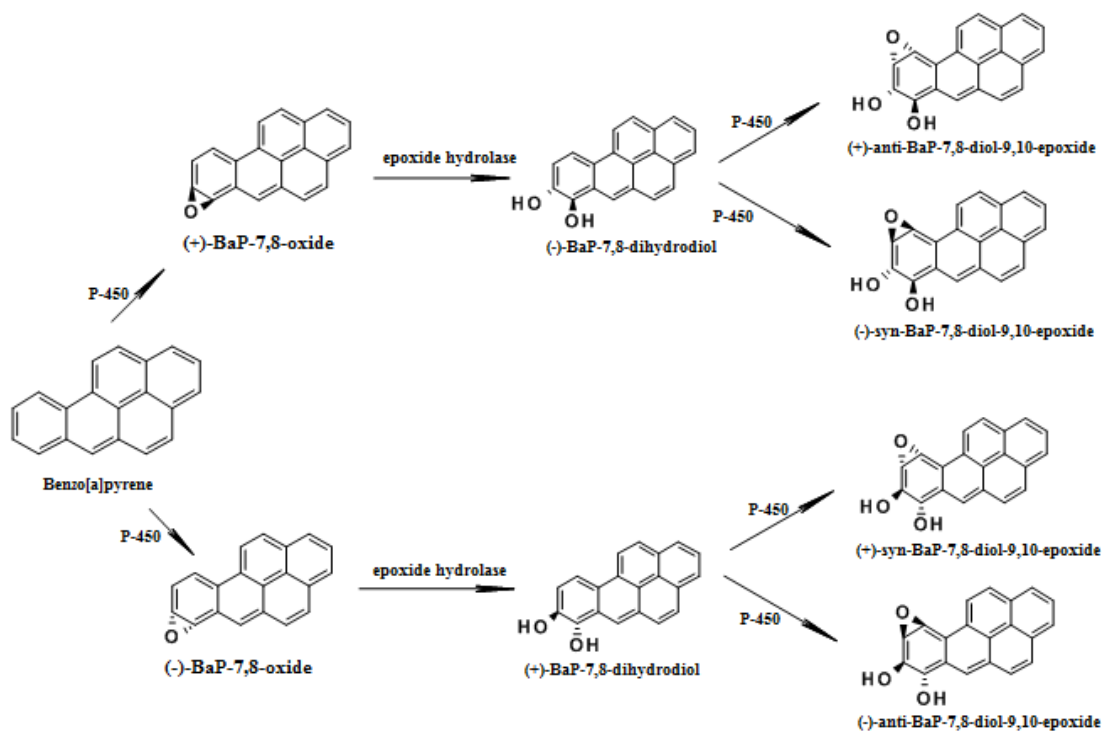
Biomarkers also known as biological markers are used in the assessment of health or disease state of an individual. Every biological system cardiovascular, metabolic

system and immune system has its own specific biomarker. An increase in the incidence of disease and pathological conditions in aquatic organisms has been identified as a relevant indicator of ecosystem health and potential human health risks. PYR is the one PAHs that is present in relatively high concentrations (between 2 - 10 %) of total PAHs. The relationship between PYR and BaP may vary considerably between different routes of exposure. Coal tar contains between 2 - 10 % PYR and between 0.4 – 0.6 % BaP. PYR is predominantly metabolized into 1-Hydroxypyrene (1-OHP) which is a urinary biomarker with a half-life between 18 - 20 hours (**Scheme 2**).



Scheme 2. Metabolism of Pyrene to 1-Hydroxypyrene.

The mutagenic and carcinogenic properties are acquired when BaP is bioactivated by enzymes such as cytochrome P450 (metabolic pathway in the human body usually the lungs). The metabolic activation of BaP to BaP-7,8-epoxide is the first step in the diol-epoxide formation (**Scheme 3**). This step is followed by hydrolysis by microsomal epoxide hydrolase to form the BaP-dihydrodiol metabolite. The metabolite is then further metabolized by P450 to form the mutagenic BaP species also known as the diol-epoxide. The BaP-diol-epoxide is extremely reactive and can bind to macromolecules such as DNA, RNA and proteins.[47, 81, 105, 133, 206]



Scheme 3. Metabolism of benzo(a)pyrene to form the diol-epoxides.

PAHs that bind to DNA-adducts within the body have half-lives which determines the time the adduct remains in the body before being reduced by half.

- DNA Adducts – order of months
- Protein Adducts – largely dependent on the type of protein where the bond is formed
- Albumin Adducts – 20 days
- Haemoglobin Adducts – 120 days

Various methods have been employed in the detection of these DNA-adducts, some of which include;

- enzyme-linked immunosorbent assay (ELISA) – measures DNA-adducts
- ^{32}P -postlabelling – determination of bulky DNA-adducts
- Gas chromatography-mass spectrometry/high performance liquid chromatography/enzyme-linked immunosorbent assay (GC-MS/HPLC/ELISA) – measurement of protein adducts mostly in blood proteins

The detection of BaP in drinking water can be directly attributed to the deterioration of coal tar. Many years ago coal tar was used to line water pipes, currently BaP is seldomly detected due to extensive water treatment and renewals, in line with drinking water standards – Water Supply Regulations 2000. Water contamination can occur as a result of leaching from soils into water, industrial effluents and accidental oil spills. BaP is often used as an environmental indicator for the pollution of water. Exposure to NAPH for individuals occur primarily indoors with residential sources such as pest control products, cigarette smoke, cooking and emissions from gasoline sources. Biomarkers may originate from specific sources some of which include biochemical, morphological and physiological changes occurring in organisms due to their exposure to foreign substances (**Table 7**). Biomarkers of NAPH, 1-naphthol and 2-naphthol exposure were explored by monitoring their behaviour in pregnant women (Canada), based on the analysis of urine and breast milk. Samples of naphthalene in breast milk was associated with 1-naphthol in urine where a 10% increase in 1-naphthol was associated with a 1.6% increase naphthalene present in breast milk.[192] Currently the urinary tetrahydroxylated BaP biomarker has been used for the monitoring of exposure to PAHs, however there is insufficient data for the monitoring of the concentration of this biomarker in hair. Initial studies for monitoring this biomarker was performed using hairs obtained from rats, exposure occurred under controlled conditions with exposure to individual BaP or to mixtures of PAHs. The suitability for the analysis of tetrahydroxylated BaP in hair as a biomarker for BaP exposure, the concentrations of this target analyte was compared to that of monohydroxylated and dihydroxylated BaP found in hair samples. This gas chromatography-tandem mass spectrometry (GC-MS/MS) method for monitoring of tetrahydroxylated BaP was tested on hair samples collected from human volunteers.[71] PYR a parent PAHs undergoes simple metabolism by P450 enzyme to produce 1-OHP, which is excreted in urine. The major routes of PYR exposure occur through inhalation or by skin contact, from sources including cigarette smoke, coal tar and petroleum distillates. PYR which is ever present within PAHs mixtures has become an indirect indicator for all PAHs as well as an indicator for PAHs exposure. The composition of the PAHs mixture vary in different environments especially in the case when individual PAHs are monitored or used as a marker.[92]

Table 7. PAHs biomarkers

Biomarkers	Source	Means of Infection	Body Parts Affected	Type of Biomarker	Method of Detection
1- and 2-naphthol Naphthalene	Coal tar Pesticides Mothballs	Inhalation Skin Contact	Skin Kidney Liver	Urine Breast milk	GC-MS/MS
Tetrahydroxylated -BaP (BaP)-associated DNA adducts Protein adducts Lipids	Coal tar Food	Inhalation Ingestion	Lung Liver Kidney	Urine Hair Blood	GC-MS/MS
1-Hydroxypyrene	Coal tar Cigarette Smoke Asphalt	Inhalation Skin Contact	Eyes Skin	Urinary	HPLC-UV HPLC-FLD

The most common methods for the monitoring and detection of 1-OHP is high performance liquid chromatography (HPLC) and fluorescence detection (FLD). Dietary intake is the major contributor of 1-OHP in urine for non-smokers without regular exposure to PAHs. However a shortfall of this biomarker is that it has is a short term measure of PAH exposure as it has a half-life between 6 to 35 hours, 1-OHP in urine has a representation of the last 24 hours.[37, 83]

Little or no information is available for studies performed on humans exposed to PAHs. Most information provided about the carcinogenic behaviour of PAHs have been performed on mice, under controlled exposure conditions (inhalation, contaminated food and skin contact). The damage (tumors, birth defects) due to exposure in mice, have led to the classification of PAH toxicity by federal agencies and health administrations. The Occupational Safety and Health Administration (OSHA), the National Institute for Occupational Safety and Health (NIOSH), the Environmental Protection Agency (EPA), World Health Organization (WHO), European Commission and Egyptian Environmental Affairs (EEA) agencies, and health administrations have provided occupational PAH exposure limits and guidelines. The Occupational Safety and Health Administration has set

a 0.2 mg/m³ limit of PAHs exposure of air during an 8 hour working day. The maximum contamination level from the U.S. EPA for PAHs in water (mainly due to BaP) is 0.2 ppb which can be attributed to leachin from water storage tanks and transportation pipes. The maximum levels of PAHs contamination (in µg/kg) various dependedent on the food group. Biomarkers play an important role in analytical methods as they allow for the identification PAHs present. There are different types of biomarkers (hair, blood, bile, urinary) but the major biomarker is the urinary biomarker. BaP the the most carcinogenic PAHs is often used as the indicator for the presence of PAHs in many analytical techniques. Many ananalytical methods (HPLC, GC, fluorescence, ultraviolet visible spectroscopy (UV-Vis)) have been used to monitor and detect these DNA-adducts within these various bodies (food, water and air). These methods tend to be relatively expensive and the sample preparation for these methods tend to be time consuming. Cheaper cost effective electrochemical methods have been explored where biosensors/immunosensors and polymer sensors have been employed as a electrochemical transducers for the detection of the PAHs. However only a hand full of PAHs have been detected using this technique and only by detecting them individually. Most simultaneous methods explored for PAHs detection has been performed by HPLC and GC. The need for a cheaper cost effective methods for simultaneous detection of PAHs, will be addressed in this work.

2. Multi-array Sensors Systems

This chapters explores the designs of chemical sensors, multi array sensor systems and the ability of multi-array sensors which employ various chemical sensors in an array setup. Multi array sensor systems allow for the simultaneous detection of multiple analytical species.

2.1 Chemical sensors

Chemical sensors are different from physical sensors in that an operable analytical signals are produced by various chemical components (concentration, chemical composition and partial pressure). Ideal chemical sensors would be inexpensive, portable and should be able to perform static and continuous measurements in any environment. Chemical sensors can be classed based on the phase of the chemical compound, gas, liquid and solid being the main categories. Electron transfer and charge polarization between chemical compounds and the electrode which produces an electrical signal is the principle mode of operation for electrochemical devices. Electrochemical sensors include metal oxide semiconductors, organic semiconductors, electrolytic conductivity sensors and electric permittivity sensors. Many existing chemical sensors have limiting features such as selectivity, sensitivity, limit of detection, response time and packaging size.

Chemical sensors function by detecting and immediately responding to the presence of analyte at an interface between the sensor and the sample matrix. The ideal sensor and the most important parameter associated with this sensor is selectivity, the sensor should be selective towards the specific analyte and not selective to the rest of the sample matrix.[61, 82, 162, 163] The composition of a chemical sensor employs two basic components which are connected in series; the chemical recognition system (molecular receptor) and the physicochemical transducer (**Figure 8**).

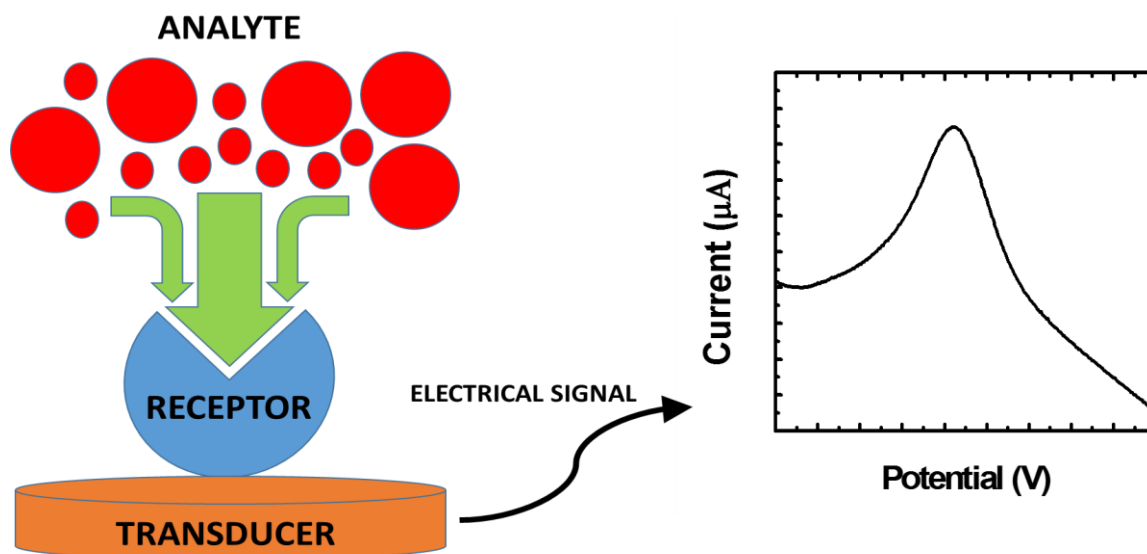


Figure 8. A chemical sensor transforms chemical information into an analytical signal.

The receptor is usually a thin film (layer) which is able to interact with analyte molecules, selectively catalyze a reaction or participate in a chemical equilibrium with the analyte. The receptor element is sensitive to stimuli produced by various chemical compounds. The transducer element generates a signal whose magnitude is related to the concentration of the analyte. The part of the chemical sensor is responsible for transforming the transported chemical information about the sample into a useful analytical signal.

2.2 Chemical sensors for polycyclic aromatic hydrocarbons

Recent developments of polymer sensors for PAHs detection have employed Overoxidized-polypyrrole(PPy)/Silver-Gold(Ag-Au) Alloy nanoparticles composite, dendrimers, polyaniline-graphene composite and polyaniline (PANI) as the materials for these sensors. Overoxidized PPy was electrochemically prepared on a glassy carbon electrode as a thin film. A nanoalloy (Ag-Au) was drop coated onto the surface of the thin film to create the composite material which was used as an electrochemical transducer. This new transducer was applied to the detection of anthracene (ANT) (prepared in acetonitrile), with the limit of detection of 1.69×10^{-7} M. The dendrimer was prepared at a gold electrode surface and was used in the detection of phenanthrene in a mixture of acetonitrile (MeCN) and water. The one major concern with electrochemical sensors for

PAHs detection is the possibility of fouling, which was not observed in composite material.[125] Various electrochemical techniques such as cyclic voltammetry (CV), square wave voltammetry (SWV) and alternating current voltammetry (ACV) was used in the detection of PHEN in water samples. Each of the electrochemical techniques CV, ACV and SWV provided different LOD, calculated LOD was found to be 4.74, 1.42, 3.24 nmol/L respectively. Interference studies were also performed during detection using metal (Na^+ , Cu^{2+} , Fe^{2+} , Cl^- , SO_4^{2-} and NO_3^-) and organic species (phenols and petroleum ether).[126, 154] A novel graphene-polyaniline composite was constructed by in-situ polymerization of aniline in a suspension of graphene oxide. This novel electroactive platform was used as an electrochemical sensor for that detection of ANT by using amperometric and voltammetric signal transductions. ANT was successfully detected using this electroactive platform, with a LOD found to be 4.4 nmol/L. The unique catalytic properties of graphene are responsible for the extensive dynamic linear range and the high sensitivity of the sensor.[179]

To a limited extent a few electrochemical (immunosensors, polymer sensors and DNA biosensors) sensors have been used. A PPy and benz(a)anthracene-7-12-dione (BaD) was electrochemically polymerized onto a graphite electrode. Due to specific interactions between BaD and benzo(k)fluoranthene (BkF), this sensor was used to quantitatively determine BkF in water samples obtained from coking plants. A wide linear range of BkF between 1.0×10^{-12} to 1.0×10^{-9} M with good linearity ($R^2 = 0.9962$) with a low LOD of 1.0×10^{-13} M ($S/N=3$). This sensor was found to have favourable properties such as good sensitivity, selectivity and reversibility. The developed method was rapid, relatively inexpensive and environmentally friendly.[215]

A sol-gel-derived array DNA biosensors coupled with a fluorescence detection system and a robotic pin-printing platform was fabricated and used in the detection of PAHs. This DNA biosensors have the ability to simultaneously detect at least 50 samples. The DNA biosensor was effectively used to detect NAPH and PHEN in water and serum samples in a concentration range between 0-10 mg/L. In aqueous solutions the DNA biosensor was sensitive to NAPH and PHEN, however it was not sensitive towards fluoranthene (FLA) and BaP. This unresponsive behaviour of the biosensor towards these PAHs can be attributed to

the solubility of these PAHs which have HMW. In the serum samples however the solubility of these PAHs were greatly enhanced. The high toxic effect of BaP at low concentrations in serum indicated that sol-gel-derived DNA biosensor exhibited effective ability to detect PAHs in both water and serum samples.[52]

An immunosensor coated with phenanthrene-9-carboxaldehyde coupled to bovine serum albumin (BSA) was developed at screen printed carbon electrodes. Cross-reactivities tests confirmed strongest interaction whilst benzo(g,h,i)perylene (B(g,h,i)P) and dibenzo(a,h)anthracene (DB(a,h)A) displayed no cross-reactivity. The immunosensor was not specific for PHEN detection but exhibited cross-reactivity of varying degrees towards other PAHs. The cross-reactivity of ANT and CHR was found to be 89.9 % and 64.5 % respectively in tap and river water samples.[56]

2.3 Array sensing

Array sensors employing conducting polymers, conductive polymer/carbon black composites, fluorescent dye/polymer systems, tin oxide sensors and polymer-coated surface acoustic wave devices have all been based on a variety of chemical interaction strategies. These systems were successful in the detection and differentiation of chemical vapours. However, the main challenge was in the detection of non-coordinating organic vapours. Many of the most toxic compounds which are metal binding species (amines, phosphines and thiols are excellent ligands for metal ions) have not been extensively studied. Sensor arrays exposed to the same sample can produce individual response as well as a pattern of responses.[115, 152, 153]

2.4 Multi-array sensor systems

Multi array sensor systems are made up of a group of sensors usually aligned in a certain geometrical design. Multi array sensor systems allow for the simultaneous detection of multiple analytes. These sensor types require multichannel potentiostat to control the multiple detections. Many commercial array sensors have been produced over the years some of which incorporate gold (Au), platinum (Pt), carbon (C) and silver (Ag)

platforms while others incorporate modified platforms (nanoalloys). Array sensor designs use various amounts of working electrodes (2 to 96 working electrodes) with different working electrode diameters (company specific) in its sensor design to simultaneously determine target analytes under investigation. Sensors are prepared on different substrates (ceramic, alumina ceramic and glass) which house these working electrodes in a specific geometrical design (**Table 8**). Technological companies such as MicruX, Dropsens, BVT and Gwent Sensors Ltd have produced array sensors employing different geometrical designs (varying amounts of working electrode) (**Figures 9-12**).

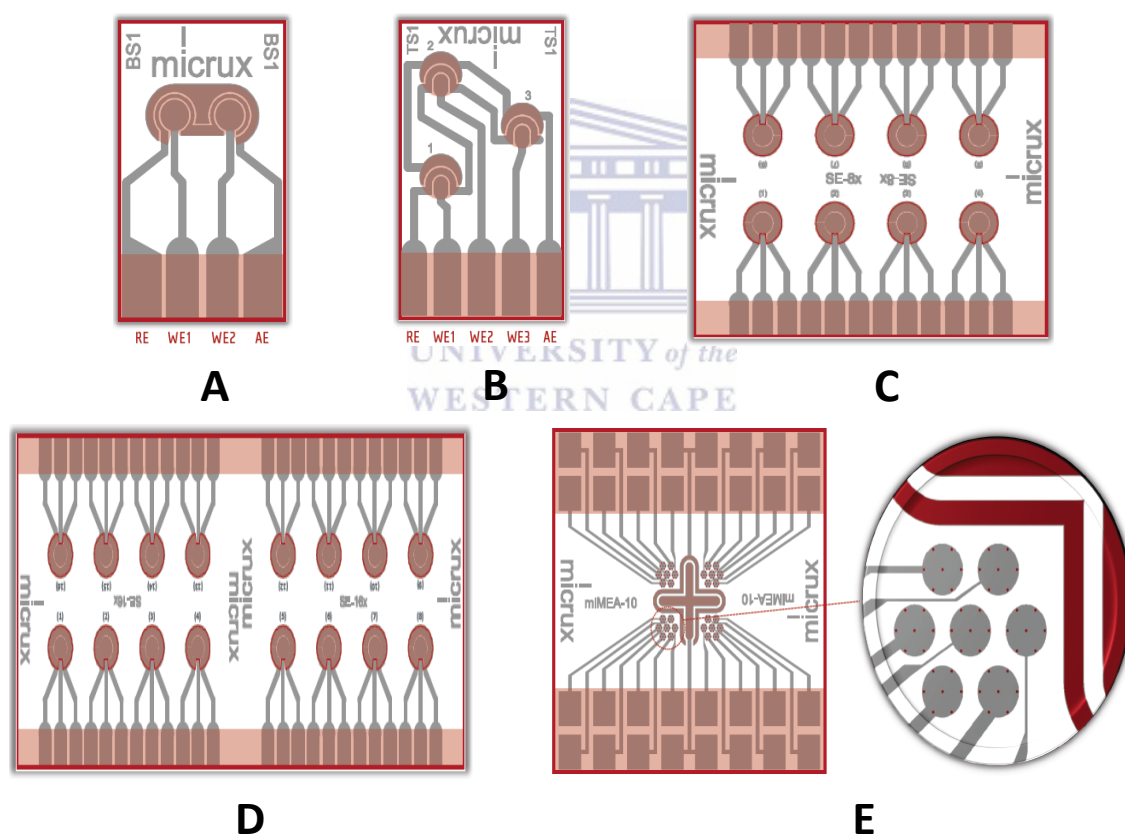


Figure 9. Array sensors designed by MicruX technologies, A – dual sensor, B - tri sensor, C – 8x single-electrode chip, D – 16x single-electrode chip, E – multi-individual microelectrode array.

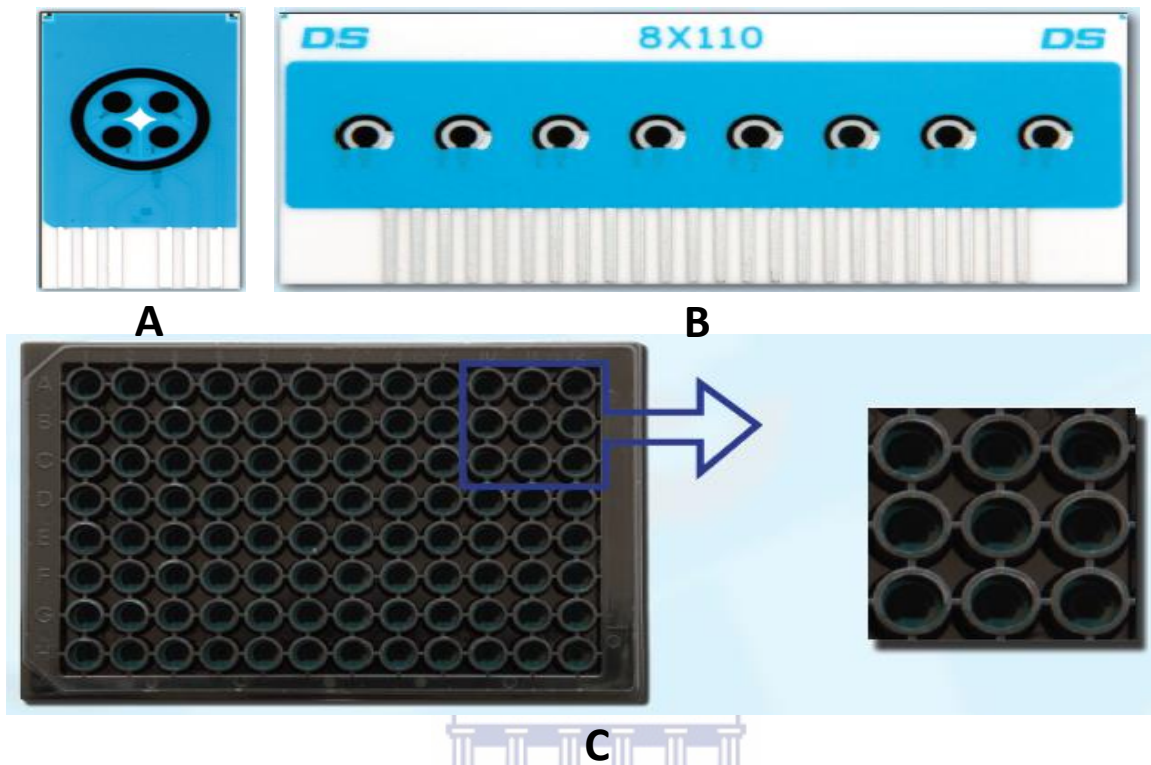


Figure 10. Sensors designed by Dropsens, A – 4X screen printed carbon electrode, B – 8X screen printed carbon electrode, C – 96X screen printed carbon electrode.

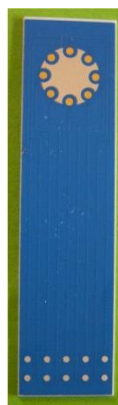


Figure 11. An array sensor designed by BVT technologies incorporating 8 working electrodes.

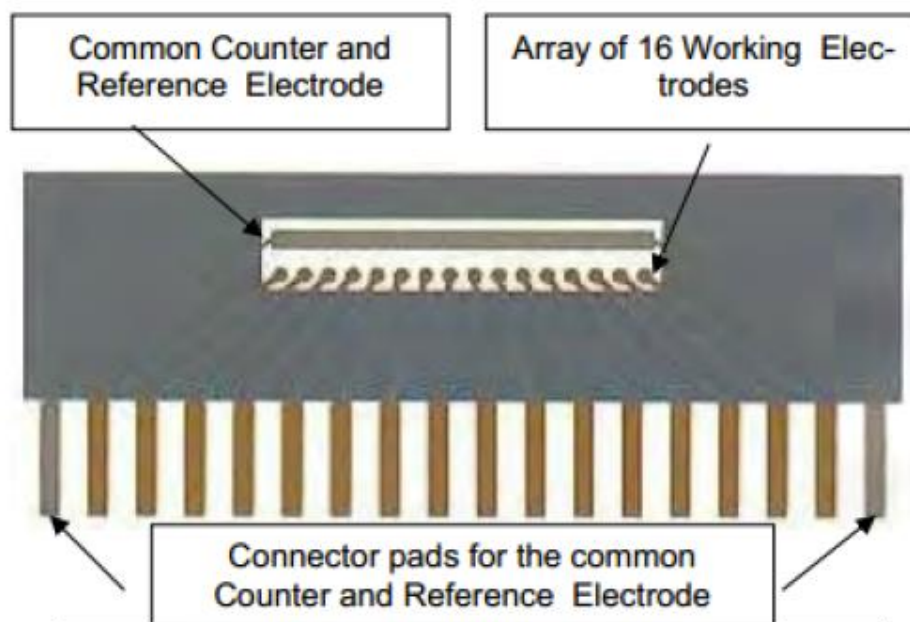
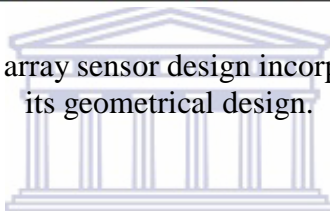


Figure 12. Gwent technologies array sensor design incorporated 16 working electrodes in its geometrical design.



The design of these sensors have favour microlitre volumes, in analyzing decentralized assays or to develop sensors for simultaneous analysis. A high number of working electrode on a substrate is usually indicative of applications for biological processes. These sensor array designs have been applied to analysis based on electrolysis, biomolecule modification, self assembled monolayers and redox active species. The array sensor developed by Dropsens has been designed in a way which allows for electrochemical detection to be easily coupled to ELISA assay using simple electrochemical instrumentation.

Table 8. Array sensor systems developed by various companies.

Company	No. of working electrodes	Electrode Materials	Substrate	Working Electrode Diameter (mm)
Dropsens	4	C (4W110) Au, Ag, Pt and C modified with nanoparticles	Ceramic	2.95
	8	Au (8X220) C (8X110) Pt (8X550)	Ceramic	2.56
	96	C (96X110) Au, Ag, Pt and C modified with nanoparticles	Ceramic	3.00
BVT Technologies	8	Au, Pt, Ag, Au-Py Alloy	Alumina Ceramic	1.00
Gwent Sensors Ltd	16	Au, C, Pt	Alumina Ceramic	0.84
MicruX Technologies	2	Pt, Au	Glass	1.01
	3	Pt, Au	Glass	0.62
	8	Pt, Au	Glass	1.01
	16	Pt, Au	Glass	1.01
	28	Pt, Au	Glass	0.01

2.5 Multichannel devices

Multichannel devices are potentiostats which provide electrochemical techniques such as amperometry and voltammetry that can be individually or simultaneously controlled (analysis dependent) at each working electrode. Many companies have developed multichannel potentiostats with a wide range of potential applications (**Table 9**). In this work we have used the Dropsens multi potentiostat with 8 channels. These potentiostats are light weight (easily portable) and are equipped with lithium ion batteries (**Figure 13**). These potentiostats can easily be connected to the computer via a USB cable or via bluetooth.

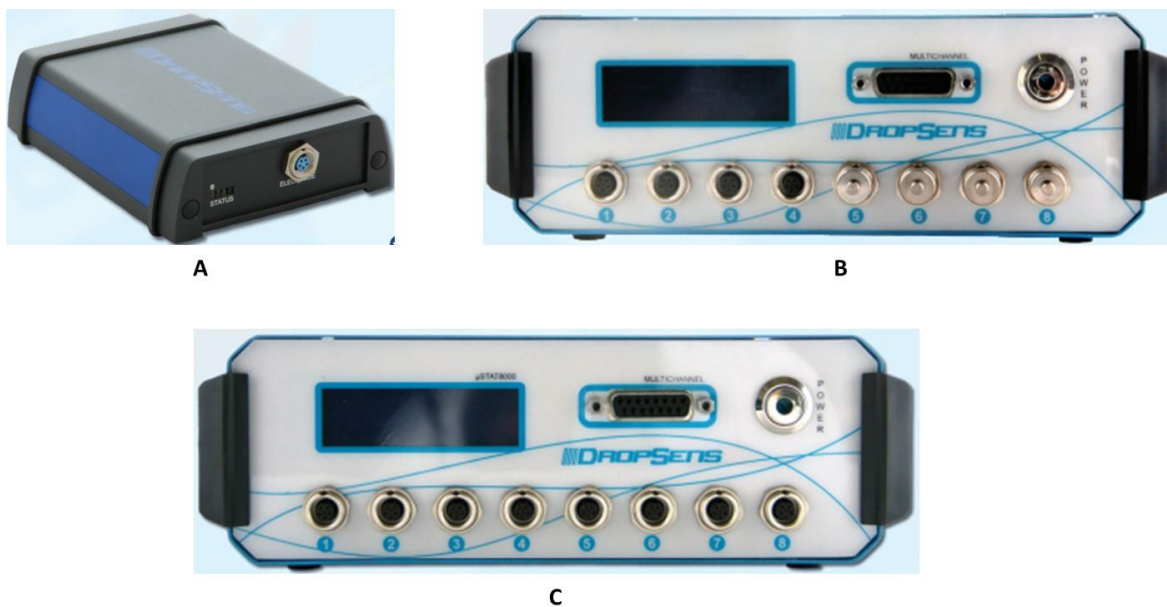


Figure 13. Multichannel potentiostat produced by Dropsens, A - Bipotentiostat, B - multipotentiostat with 4 channels, C - multipotentiostat with 8 channels.

The VSP300 multipotentiostat can be used for fundamental electrochemistry, corrosion experiments, fuel cells/batteries, photovoltaic/solar cells, coating/plating experiments (Figure 14). This versatile potentiostat with 6 channels incorporates the latest technology to ensure excellent performance, the instrument can also be independently controlled by several users via a LAN cable. Similar models are available for BioLogic, Uniscan and Autolab.

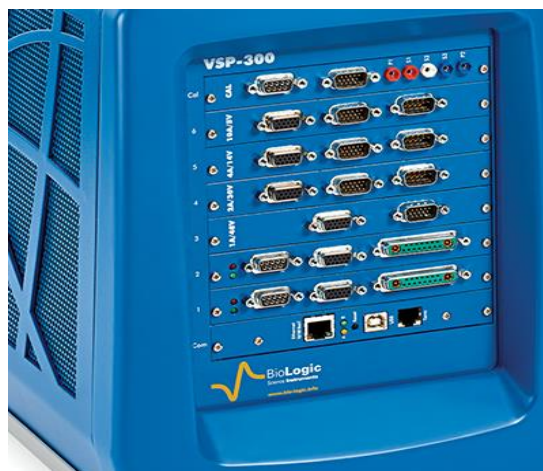


Figure 14. VSP300 multipotentiostat developed by Bio-logic

Table 9. Commercially available multichannel potentiostats.

Company	No. of Channels	Potential Range (V)	Current Ranges	Weight (kg)	Connection	Software
Dropsens	2 (μ Stat 300)	± 2	1 nA to 1 mA	0.48	USB Bluetooth	Dropview
	4 (μ Stat 4000P)	± 4	1 nA to 100 mA	1.6		
	8 (μ Stat 8000P)	± 4	1 nA to 100 mA	1.6		
Bio-Logic	6 (vsp300)	± 10	10 nA to 1 A	20	USB Ethernet	EC-Lab
Autolab	12 (M101)	± 10	10 nA to 10 mA	13	USB	Nova
Uniscan	2-14 (PG580RM)	± 8	1 nA to 10 mA	14	USB	UniEchem/UniEcorr
Ivium	64 (Ivium-n-stat)	± 10	10 nA to 10 A	11.8	USB	IviumSoft
CH Instruments	8 (1000C)	± 10	± 10 mA	5.4	USB Serial Port (RS-232)	CH electrochemical analyzer
PARASTAT	32 (PMC 1000A)	± 12	4 nA to 2 A		USB	VersaStudio
	32 (PMC 2000A)	± 30	4 nA to 1 A			

2.6 Multichannel analysis case studies

2.6.1 Cantilever array sensing

A carbohydrate-based cantilever microarray biosensor was applied to a variety of problems in order to detect molecular interactions. This array biosensor is robust and highly reliable in the detection of intermolecular binding events in both air and solutions. The array is extremely sensitive and have the ability to detect picomolar amounts of mRNA even in complex background. The array design was employed in a series of individual cantilevers which were modified with either immobilized trimannose, nonamannose or galactose. The principle operation behind the sensing mechanism is the transduction of the biomolecular interactions into a nanomechanical force. The receptor molecules bound to the surface of the cantilever tend to bind with the analyte, which causes a change in the surface stress as a result of steric and/or electrostatic repulsion or attraction. The generated nanomechanical force cause the cantilever to bend, analyte binding is measured as an optical

laser is deflected off the cantilever. The major advantages the cantilever array displays over other array sensors is its ability to measure binding interactions in real time, the capacity for multiple binding events which are simultaneously examined in up to 8 parallel channels.[72, 171]

2.6.2 High density temperature array sensing

This high-density array temperature sensor consists of up to 40 discrete optical sensors in a single optical fiber which can be spread for customized spatial resolution. This allows for fast thermal measurements with the ability to respond quickly to catastrophic steam breakthrough events in the longer horizontal well sections. These array sensors have unique advantages such as long term reliability, quick response times, fixed absolute data versus statistically averaged data and accurate, stable, high resolution, ultrahigh-temperature applications (up to 280°C). The unique ability of these sensors allows for it to be used in a wide range of applications including, thermal temperature, high rate, intelligent or multizone wells, thermal recovery monitoring, in-well flow temperature measurements, subcool monitoring and geothermal wells.[85] A robust sensor was developed using a quasi-distributing multi fiber sensors in a gas turbine environment, this sensors was used to accurately determine the temperature. The sensor displayed a unique advantage of determining the high-density as well as the multipoint and multifunctional capability by measuring both dynamic and static responses within the gas turbine.[195]

2.6.3 Tactile array sensing

The sensing array is made up of a deformable polydimethylsiloxane (PDMS) space layer, two aluminium (Al) glass substrates and two dielectric liquids. Sensing ranges can be alternated in the ranges of 0.05-0.29 N and 0.42-1.12 N, this is due to the principle operation of controlling the shape of the droplet. The adjustment of the electric flux passing through the electrodes for the contact angle of the droplet to be controlled. This sensor array can be used in the application for humanoid robots or artificial skin as tough interfaces to satisfy different required or dynamic sensing ranges.

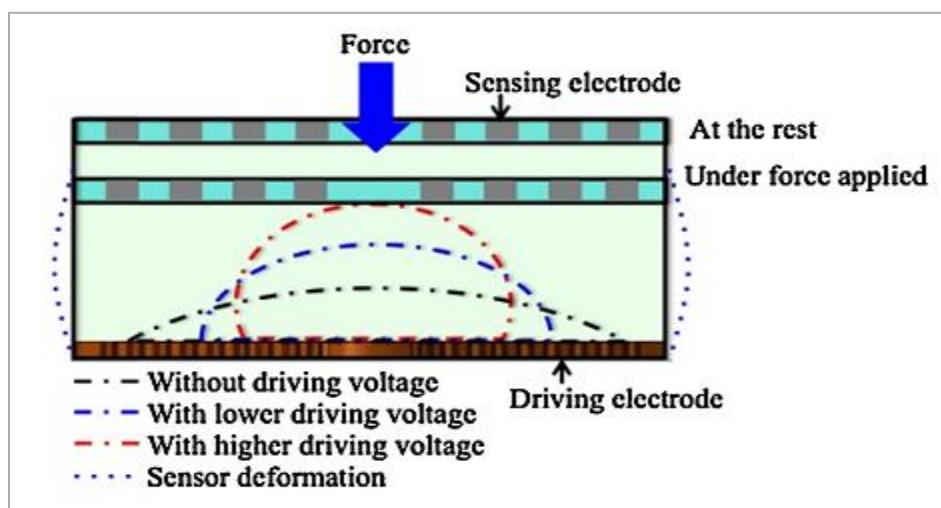


Figure 15. Operating principle of the liquid-based sensing array.

The sensing mechanism shows the electrode which is covered with the higher-dielectric liquid at the beginning. Due to the PDMS structure being deformed under an external applied force, the sensing electrode approaches closer and then attaching to the droplet (**Figure 15**).

Flexible tactile sensor arrays which employ patterned buckypaper as the sensing element, display advantages such as anisotropic sensing capability, flexibility, simple fabrication process and low costs. This array sensors has the ability to sense normal and shear forces, sensitivity can be enhanced by centralizing the applied force (achieved as the PDMS pumps are bonded to the top of each shear-force sensing cell).[117, 123]

2.7 Proposed multichannel analytical protocol for polycyclic aromatic hydrocarbons

In this thesis we have adopted the multichannel approach for analysis of selected PAHs at polymer modified screen printed carbon electrodes. After individual PAHs analysis was performed using a single potentiostat, the optimized analytical conditions were used to propose a multichannel approach. The proposed way forward in this work is to demonstrate the principle of detecting PAHs using the multi array setup. The dropsens working electrode multi array sensor was employed as the electrochemical transducer. A multichannel potentiostat was used for all measurements. A 2 pump peristaltic system with a flow rate in ml/min was used to drive the solution from the reservoirs to the working electrodes. The

multi array sensors was constructed inside a wall-jet flow cell. This cell allows for 8 different working solutions to pass simultaneously through the flow cell without any cross reactivity between cells. The software provided control over individual cells to be inactive (channels not in use) or active during measurements (**Figure 16**).



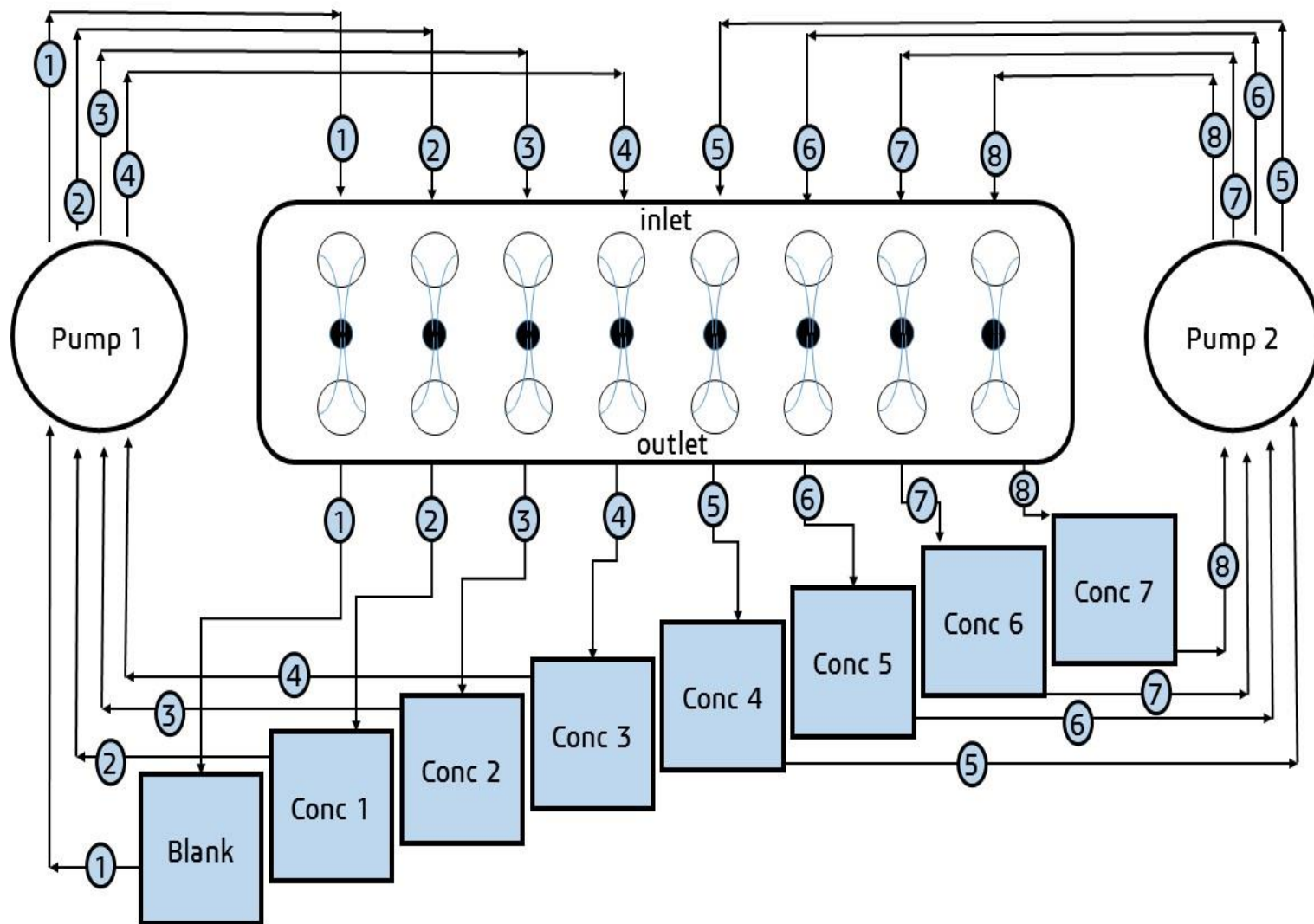


Figure 16. Principle operation of the wall-jet flow cell with 8 reservoirs being controlled by 2 pumps.

3. Materials design and Methodology

Recent developments in the field of biomimetic systems demand mechanical systems that are capable of delivering high power output per volume or mass. Volume changes within the conducting polymer layers are caused by the oxidation or reduction of the polymer. This volume change is the main source for actuators bending or deforming. Different actuator designs have been explored over the years to maximize bending, displacement or deformation. The bilayer design (two layers) incorporates a highly conductive metal layer along with the conducting polymer layer in its design. Trilayer designs (three layers) utilize an electrolyte storage layer to avoid delamination within the design. The storage layer allows for the trilayer design to operate freely in both liquid and air environments. To a limited extent zig zag conformations of polymers linked by small organic molecules or metal coordinating ligands have also been explored in the search for actuator materials with significant deformation and high current density. This review evaluates the contribution of polypyrrole and its derivatives in these actuator designs that impact on maximum displacement capability, current density and the lifetime of these actuator systems. Exploring actuators leads back to 1992 when the first design of an actuator (bilayer) was explored by T.F. Otero. This design employed two layers, one conductive polymer layer and the other a metal layer. Deformation (actuation) of the bilayer actuators occurred through the redox reactions of polymer layer which would then contract and expand upon applied potentials. The metal layer provided mechanical strength which supported the stimuli responsive polymer layer. The conducting polymer layer included conjugated polymers such as Polypyrrole (PPy), Polythiophene (PTH) and Polyaniline (PANI). Bilayer actuator displacement ranged from 60° - 120° between potential ranges -2 to +2 V. Applications for

the bilayer devices included release valves in drug delivery systems, mechanical microactuators, mechanical micromixing and microtweezers. Reduction in conductivity of the conducting polymer layers reduces the ability of the actuator to achieve high actuation speeds. This phenomena is the main reason for poor actuation performance. The introduction of trilayer actuators has been found to address the problems associated with the bilayer actuators. These trilayer actuator devices incorporate 2 conducting polymer layers and one electrolyte storage layer usually Polyvinylidene fluoride (PVDF). The PVDF storage layer allows for the actuator to be operated in both air and liquid environments. The trilayer actuator has the ability to bend in both directions when a potential is applied across the trilayer actuator. The redox processes involved during the applied potential caused the ions to move in and out of the polymer layer which caused expansion of the layers leading to deformation of the actuator. Trilayer actuators have favourable properties such as displacement ranges (18 to 60 mm), potential values (-1 to +3 V) and frequency ranges (0.05 to 4 Hz). The wide range of possible potential application which include microactuators, high speed response, improved performance and lifetime have made trilayer actuators well studied materials. Volume changes within the actuator layers have been linked to conformational changes generated by redox processes. The electrochemical simulation and generation of free volume is transformed into a stress gradient across the polymer-polymer interface which allowed the actuator to bend. The zig zag polymer conformation plays an important role in the actuation mechanism, which is not limited to only ion intercalation in the bulk polymer chain during electrochemical activation. Various zig zag conformation materials have been explored in this review some of which include helical structures (Zinc metal centre), organometallic frameworks (diplatinum(IV) complexes), molecular tweezers (Tetrathiafulvalene hinge) and Schiff base materials (Phenazine hinge with conducting polymer linker molecule). The desirable features of PPy such as large mechanical stress generation, large maximum strain values, high reversibility and safety at low voltage make them prime candidates for conducting polymer actuators. However poor actuation performance results due to the reduction in conductivity during the reduction process. Bilayer actuators the original actuator design was primarily used for actuation in liquid environments, delamination of the actuator layers being another disadvantage. The

introduction of the trilayer actuators devices have been found to overcome the shortcomings of the bilayer actuators by operating in both air and liquid environments.

The Schiff base polymers developed in our work was employed as direct chemical transducers for the electro analysis of selected PAHs. In related research the energy efficiency, capacitive behaviour and bilayer actuation properties have been explored. In collaboration with the physical chemical laboratory of polymers and interfaces (LPPI) at the University of Cergy-Pontoise the Schiff polymer material was further optimized and extensively characterized. The zig-zag polymer conformation was explored using different anchor molecules, o-phenylenediamine and 2,3-diaminophenazine coupled to pyrrole-2-carboxaldehyde (**Figure 17**).

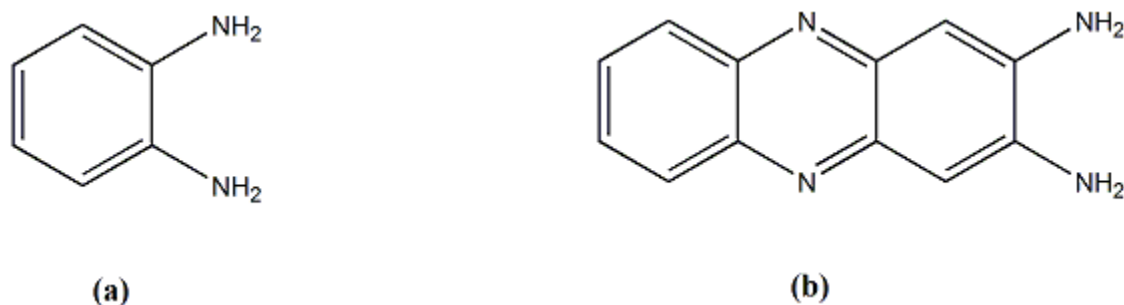


Figure 17. Anchor molecules, (a) o-phenylenediamine and (b) 2,3-diaminophenazine.

The 2,3-diaminophenazine anchor was used in the development of a bilayer actuator based on its excellent mechanical processibility. O-phenylenediamine was employed in the development of thin film chemical sensors for electro-analytical application, based on its feasibility for electropolymerization and controlled thin film formation. Here we report on the electro-analysis of 8 selected PAHs at the electropolymerized polymer N,N'-Bis-(1H-pyrrol-2-ylmethylene)-benzene-1,2-diamine (PBPPD). Various analytical techniques have been used to extensively characterize the spectroscopic properties, morphology and electrochemical characteristics of PBPPD.

3.1 Microscopy

Atomic force microscopy (AFM) and scanning electron microscopy (SEM) were used to study the morphological and surface features of samples for AFM and SEM analysis. Surface features were evaluated as topography profiles, surface roughness and

morphology imaging. The roughness of the Schiff base material which was prepared at the screen printed carbon electrode surface was compared to a bare screen printed carbon electrode, the information was captured on the Nanosurf Easyscan 2 instrument. The AFM instrument used in the Chemistry department at UWC.

SEM images (3D) are produced when a focused beam of electrons interacts with the atoms within the sample. The electrons interact with the samples causing scattering of secondary electrons which provide information about the surface composition and topography of the material. All SEM imaging was done using the Auriga high-resolution (HR) SEM which is located at the department of Physics at UWC.

3.2 Spectroscopy

Fourier transform infrared spectroscopy (FTIR) is a technique used in the determination of the infrared absorption or emission spectra of solids, liquids and gases. FTIR provided useful quantitative and qualitative information about various organic and inorganic materials. FTIR was used to determine the bond vibration of the fundamental groups in the novel Schiff base material and provided a means to differentiate between the starting materials and the monomer material. The FTIR instrument used at UCP-LPPI was the Bruker Tensor 27 with OPUS software.

Nuclear magnetic resonance (NMR) spectroscopy is a technique that explores the magnetic properties of atomic nuclei. Proton (^1H) NMR was used to study the magnetic resonance of the hydrogen nuclei within the molecules. The NMR instrument used at UCP-LPPI was a Bruker Avance DPX 250 MHz spectrometer. At UWC a Bruker Avance IIIHD Nanobay 400 MHz spectrometer equipped with a 5 mm broadband observe (BBO) probe at room temperature (298K) was used. ^1H NMR was revealed that the structure of the materials differed from each other, the monomer material displayed properties similar to that of a Schiff base.

3.3 Electrochemistry

Square wave voltammetry, cyclic voltammetry and electrochemical impedance spectroscopy was used as the electrochemical characterization of materials as well

as the evaluation of analytical performance. Biologic VSP300 potentiostat (UCP-LPPI) and the PalmSens 3 electrochemical interface potentiostat (UWC) was used respectively. Cyclic voltammetry (CV) can be used to provide quantitative information about the electrochemical processes under controlled conditions, i.e. the reversibility of the reaction as well as the intermediates in the redox reactions. CV was used to determine the electron stoichiometry, diffusion coefficient of analytes and formal reduction potentials of the materials under investigation. CV was also used to electrochemically polymerize and dimerize novel polymer and dimer platforms.

Square Wave Voltammetry (SWV) a linear potential sweep technique which was used for the quantitative measurements of electroactive species within the electrolyte solution. Various electrochemical parameters such as formal potential, potential peak separation, diffusion coefficient (Cottrell plot) were obtained using this technique. The sensitivity of the SWV technique was an added advantage in the detection of the PAHs.

3.4 Thermogravimetric analysis

This technique studied the change in weight as a function of increasing temperature or a function of time, in the presence of an inert gas. The effect of mass change causes changes in the physical (gas adsorption, gas desorption, phase transition) and chemical properties (decomposition, break down reactions, gas reactions, chemisorption) of the material. The thermal stability of the monomer material over a wide range of temperature was evaluated by TGA.

4. Electrochemical evaluation of Polycyclic Aromatic Hydrocarbons at a Bare Screen Printed Carbon Electrode

In this chapter redox behaviours of selected polycyclic aromatic hydrocarbons will be explored at the surface of an unmodified screen printed carbon surface, using cyclic voltammetry and square wave voltammetry.

Cyclic voltammetry is a potential sweep technique that allows us to detect oxidative and reductive processes in a single sweep. Cyclic voltammetry was performed by cycling the potential range from -1.0 to +1.5 V at a scan rate of 50mV/s for 1 cycle. The working electrode in the 3 electrode electrochemical cell was a SPCE and the electrolyte solution was 0.1 M LiClO₄.

Square wave voltammetry is a technique which allows us to evaluate Faradaic processes in the absence of dominant capacitive currents. The electrochemical windows selected for the oxidative SWV of the selected PAHs was set at -1.0 to +1.0 V. A scan rate of 50 mV/s was achieved by setting the frequency at 10 Hz and the step potential at 5 mV. The working electrode in the 3 electrode electrochemical cell was a SPCE and the electrolyte solutions were 0.1 M HCl and 0.1 M LiClO₄.

PAHs were selected based on their solubility in aqueous medium, which was related to their molecular weights. Lower molecular weight PAHs tend to have better solubility in aqueous. We purposefully avoided the use of acetonitrile, an organic solvent into which most PAHs will dissolve, with the aim of keeping the method as environmentally friendly as possible. The species selected for the inclusion in this study were ANT, acenaphthylene (ANY), BaP, BbF, CHR, FLA, NAPH, PHEN, PYR, 1-OHP, triphenylene (TRIP) and 7,12-dimethylbenz(a)anthracene (DMBA) (**Figure 18**). BaP in particular, was identified from

literature, as a reference for the carcinogenicity of PAHs. Very little is reported on the redox behaviour of PAHs species, and the study of redox behaviours at the unmodified screen printed carbon electrode was necessary and was reported here for the first time in a comprehensive manner.

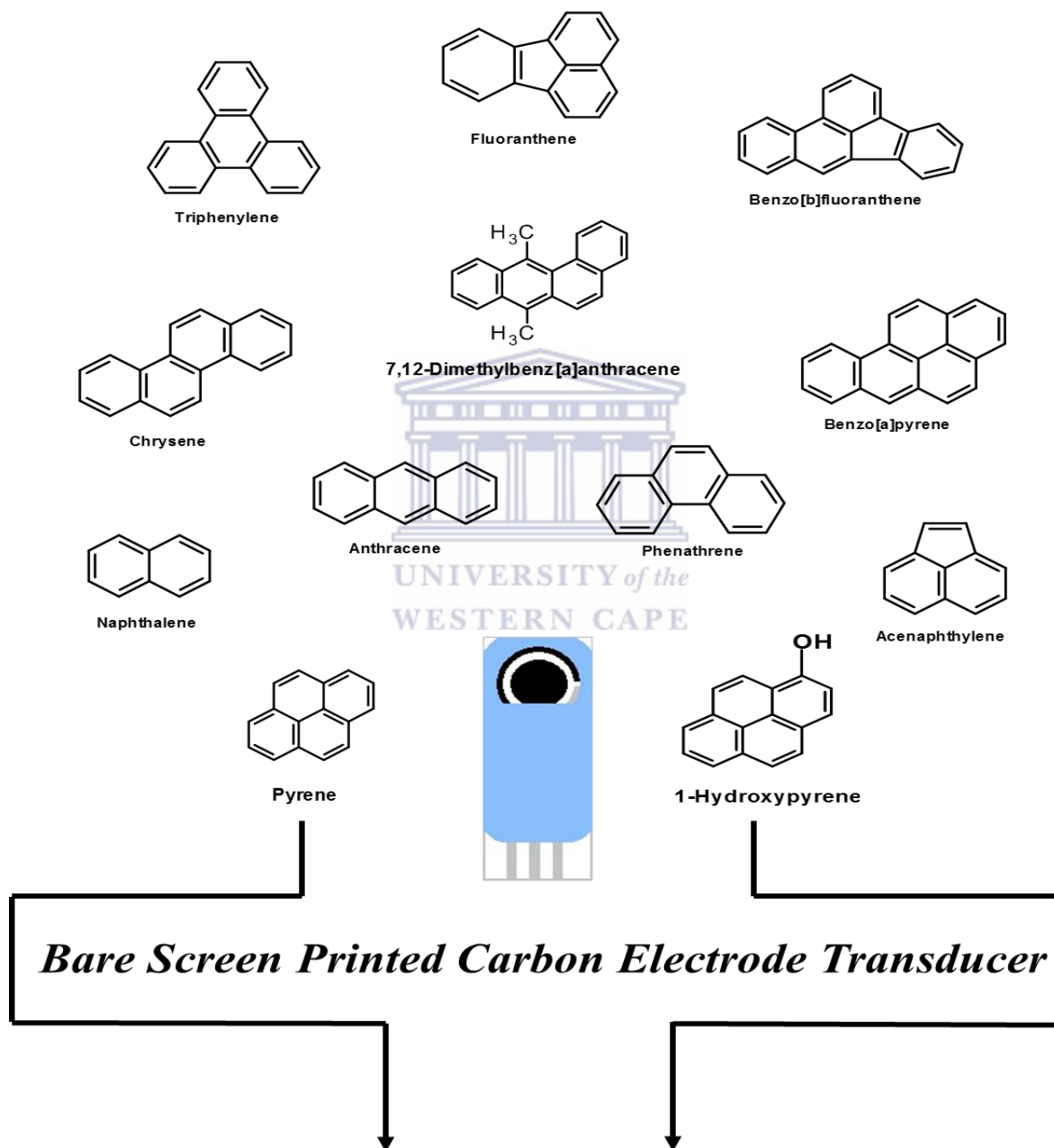


Figure 18. Structural images of the selected polycyclic aromatic hydrocarbons for this work.

4.1 Bare screen-printed carbon electrode platform

Screen-printed electrodes (SPE) were used as the electrochemical transducers for the screening of PAHs. The fabrication of these printed devices on pliable substrates have allowed for the development of a wider range of new electrode systems. This pliable substrate allows for the complete electrode system to be placed on the same surface (**Figure 19**). The global biosensor which is used for diabetes is the most commercialized screen-printed electrode, with a billion dollar yearly global market.[79, 184] These electrodes are low cost, disposable devices which were designed to work with microlitre volumes of a sample. SPE are based on carbon, gold, silver, platinum and carbon nanotubes ink, for all electrochemical measurements in this work the screen-printed carbon electrodes (SPCE) were used (ref. 110). The adaptability of these electrodes is of vital importance as the ability to modify these electrodes with ease through many techniques allows for specific target analytes to be determined.

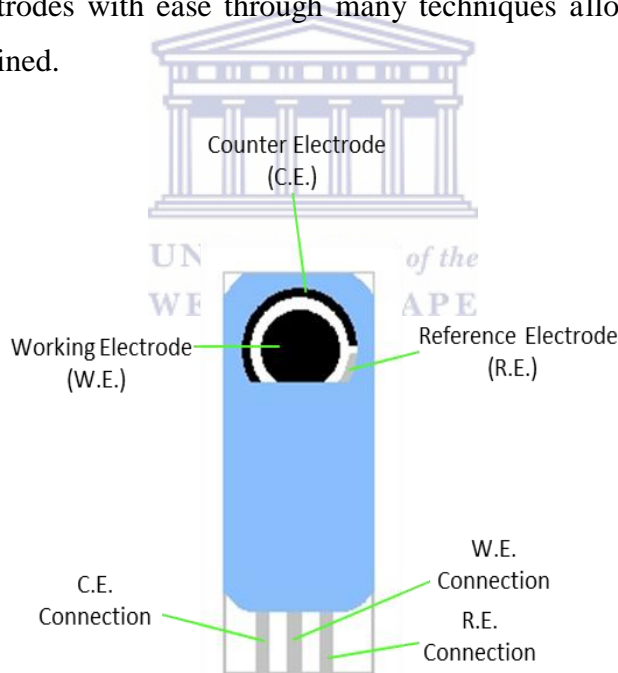


Figure 19. Screen-printed carbon electrodes used for all electrochemical measurements.

The electrode consists of a 3 electrodes on one chemically inert substrate, the counter, the reference and the working electrode. The chemical reaction or biological event occurring at the working electrode is converted to an electrochemical signal.[54, 79, 174]

This chapter explores the electrochemical behaviour of various PAHs studied at the surface of a bare SPCE in aqueous media. PAHs selected for the electrochemical screening process was based on their respective solubilities, lower molecular weight PAHs (priority 16 PAHs) were targetted for this investigation. Evaluated PAHs included. BaP was selected due to the fact that it has been well studied as a reference for the carcinogenicity of PAHs. The electrochemical technique used in the screening process was square wave voltammetry.

4.2 Electrochemical screening of polycyclic aromatic hydrocarbons

Cyclic voltammetry was performed by cycling the potential range from -1.0 to +1.5 V at a scan rate of 50mV/s for 1 cycle (Figure 20). The working electrode in the 3 electrode electrochemical cell was a SPCE and the electrolyte solution was 0.1 M LiClO₄. A bare SPCE was used as the electrochemical transducer in the of selected PAHs in 4 mL 0.1 M LiClO₄ (electrolyte solution). The selection of the wide potential window resulted in a cathodic peak being observed at +0.6 V vs Ag/AgCl which was attributed to the behaviour of the SPCE electrode itself.

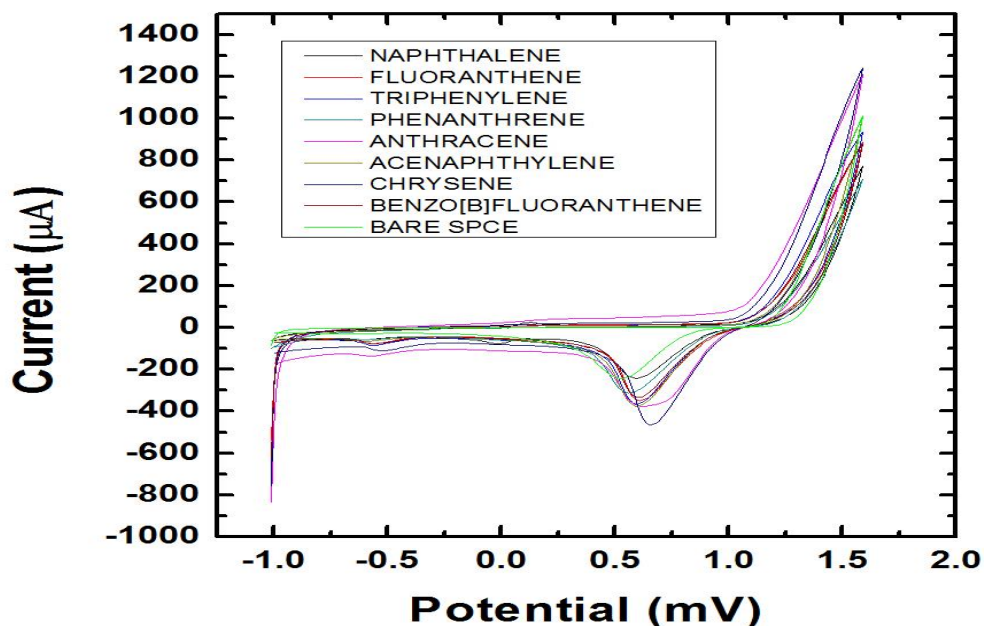


Figure 20. Evaluation of selected PAHs using CV at a bare SPCE in 0.1 M LiClO₄ at 50mV/s.

Based on literature reports for PAHs there is a lack of information regarding the reporting of the redox ability of CHR, ANY and BbF in terms of cyclic voltammetry. Anthracene one of the more commonly explored PAHs is usually evaluated predominantly in organic medium such as acetonitrile and dimethylformamide at a glassy carbon or gold disk electrode. Anthracene evaluated in acetonitrile at a GCE gave rise to a sharp, irreversible peak at +1.5 V vs Ag/AgCl at scan rate of 0.1 V/s. The irreversible nature of ANT results from the follow-up chemistry which causes the ANT radical to undergo another reactivity such as dimerization before reduction occurs at the electrode.[98] The cyclic voltammograms of all PAH experiments showed no distinct redox peaks with the exception of naphthalene which showed a reversible couple at +0.16 V vs Ag/AgCl. PHEN evaluated in 1 M HCl at a GCE, GCE/polyaniline (PANI) and GCE/PANI-Nickel Oxide (NiO) using cyclic voltammetry displayed anodic peaks at +1.54 V vs Ag/AgCl, +1.55 vs Ag/AgCl and +1.65 V vs Ag/AgCl, respectively. The effect of scan rate on PHEN was explored which resulted in the increase in anodic peak current as the scan rate increased. It was also determined that the oxidation peak potential shifted to more positive potentials which is a confirmation of a diffusion controlled process.[60] FLA evaluated in dichloromethane at a platinum disk electrode displayed 2 anodic peak at +1.6 V vs Ag/AgCl and +1.9 V vs Ag/AgCl, with one reduction peak at +1.4 V vs Ag/AgCl.[22] Triphenylene evaluated at a GCE in acetonitrile and dichloromethane displayed reversible couples at approximately -2.0 V and +1.2 V respectively.[6]

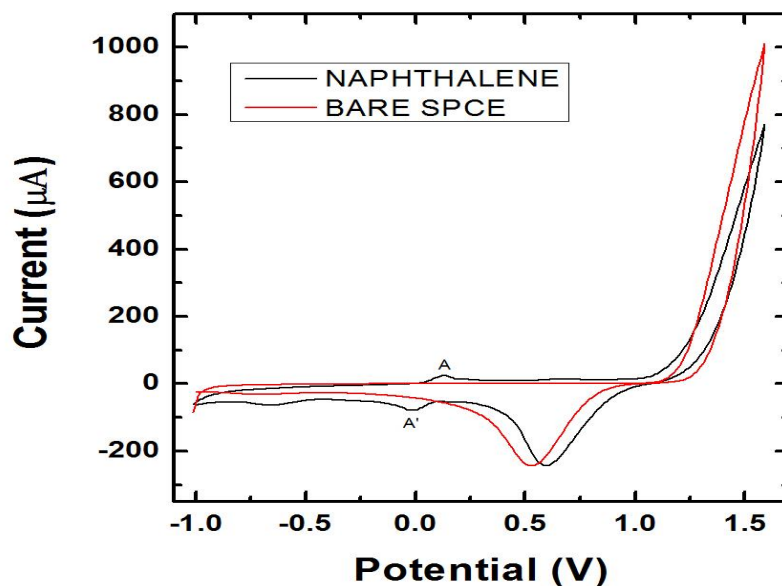


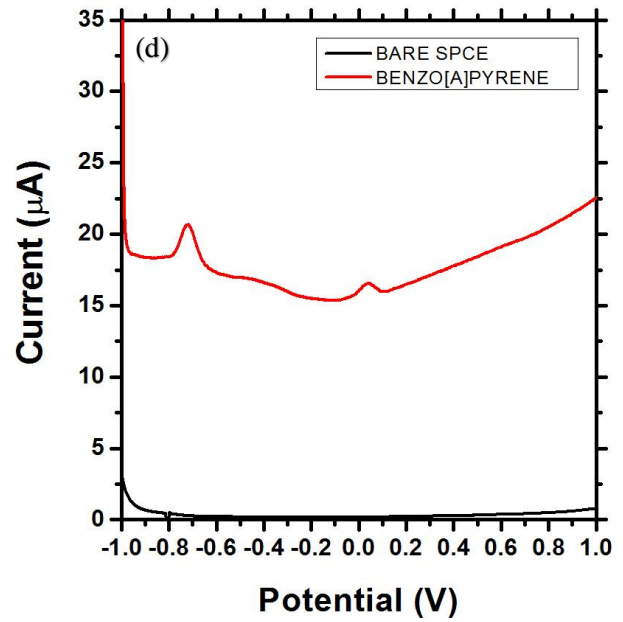
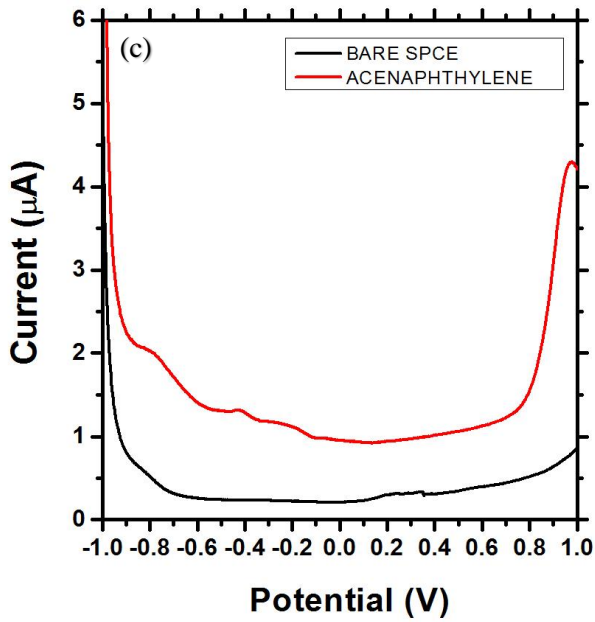
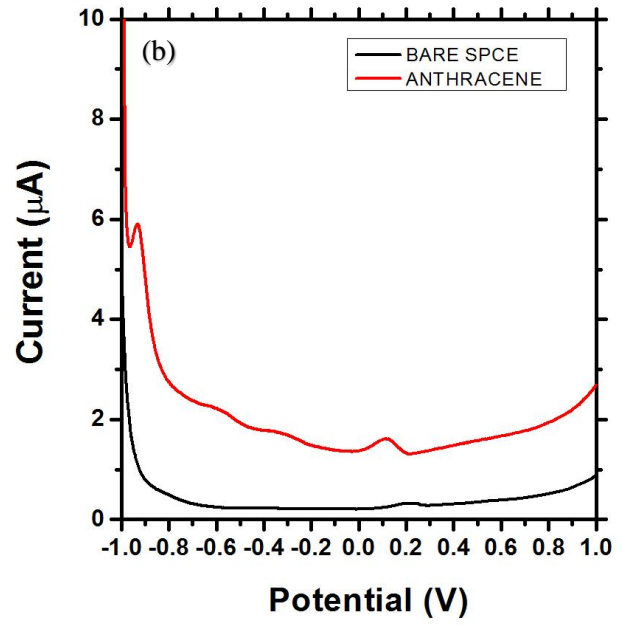
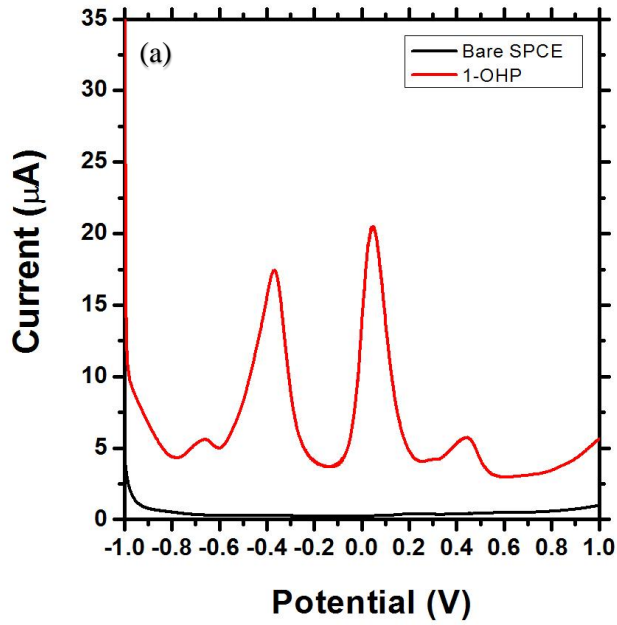
Figure 21. CV of naphthalene at a bare SPCE in 0.1 M LiClO₄ at 50 mV/s displaying a reversible redox couple (A-A').

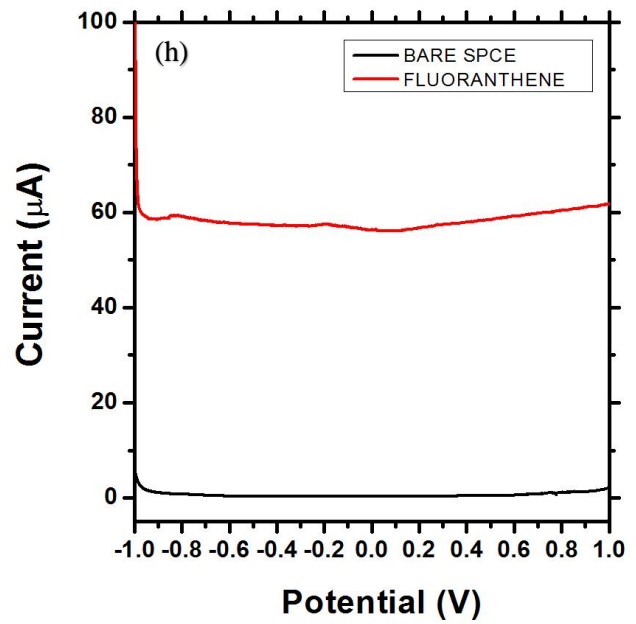
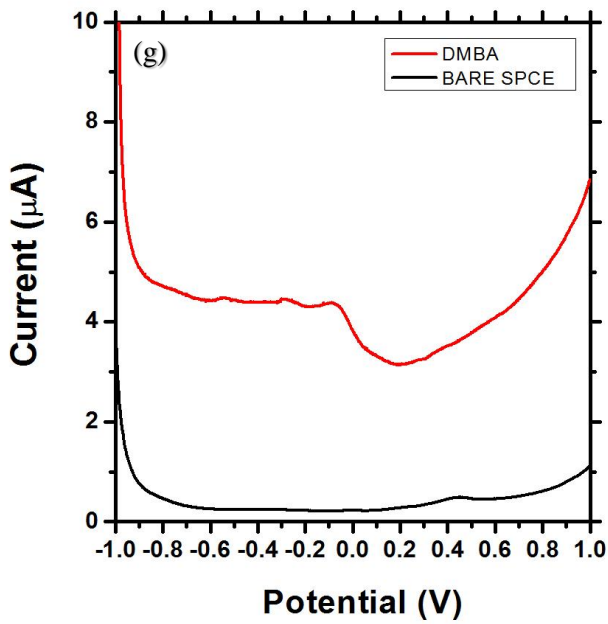
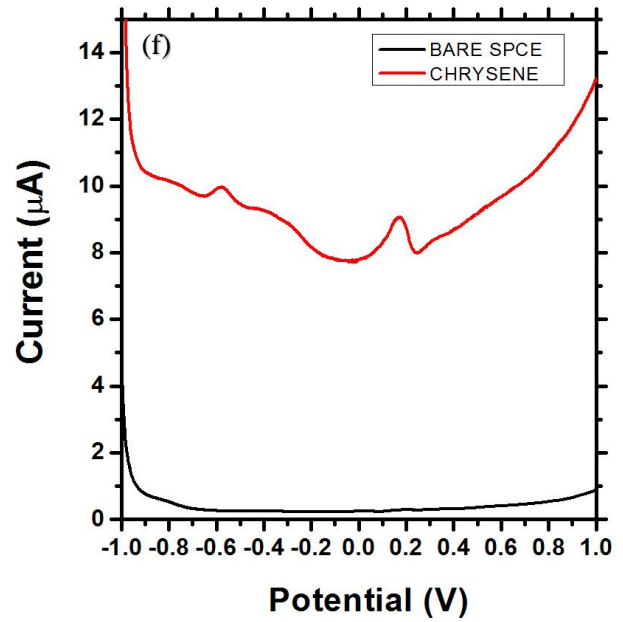
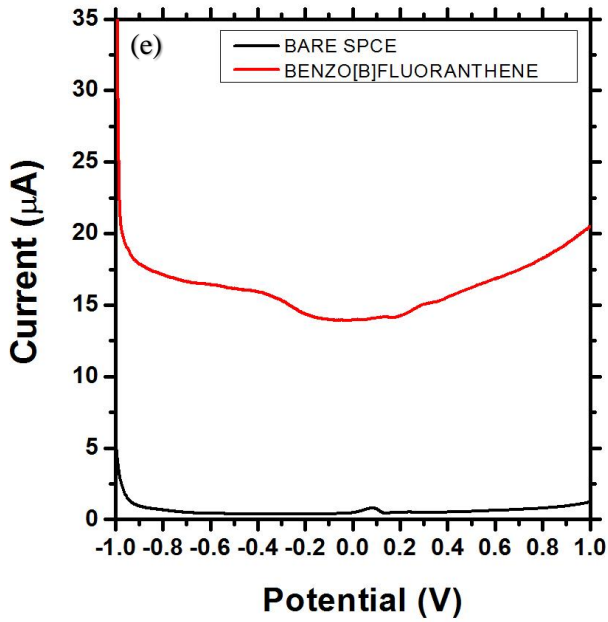
During the evaluation of naphthalene however a reversible couple is evident in the CV scan, the size of the peak attributed the bare SPCE dominated the naphthalene couple (**Figure 21**). Reproducibility of CV analysis for NAPH detection proved unsuccessful at the bare SPCE, this can be attributed to the unpredictable behaviour of the SPCE. NAPH evaluated at the surface of platinum electrodes in acetonitrile and a Brij 35 solution (nonionic detergent used for various protein methods) displayed irreversible redox couples. Oxidative sweep peaks can be observed at +1.40 V and +1.62 V in Brij 35 solution and acetonitrile respectively. The absence of the reversible couple in the voltammetry of the NAPH is indicative of a very short lifetime of the NAPH radicals or a fast follow-up reaction which is couple to the charge transfer.[46] Information obtained from cyclic voltammetry experiments and literature, it was determined that the preferred electrochemical technique for the evaluation of PAHs was square wave voltammetry. Literature reported that reversible redox couples were observed at higher scan rates while others reported that due to the short lifetime of PAHs, peaks were only observed in the oxidative scan in cyclic voltammetry. The lack of reversible couples

for PAHs also resulted due to the follow-up chemistry. Based on these problems cyclic voltammetry was omitted as the principle technique for PAHs evaluation in this work.

The redox behaviour of the 12 selected PAHs was performed by SWV in 0.1 M LiClO₄. The electrochemical window used for the oxidative SWV was set at -1.0 to +1.0 V. A scan rate of 50 mV/s was achieved by setting the frequency at 10 Hz and the step potential to 5 mV vs Ag/AgCl. An oxidative scan as opposed to reductive scan was selected from the initial CV screening, using the same parameters as SWV (**Figure 22**).







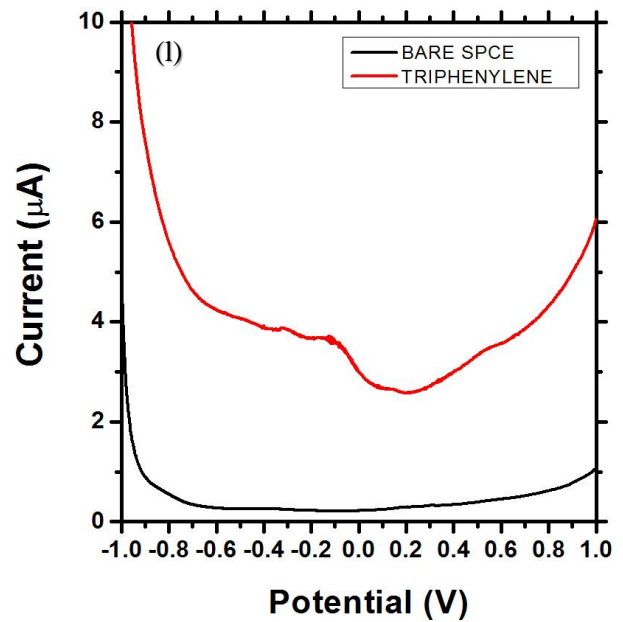
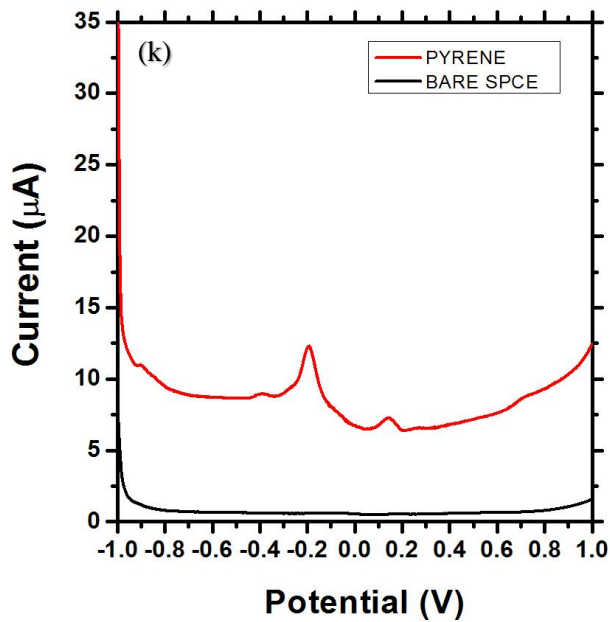
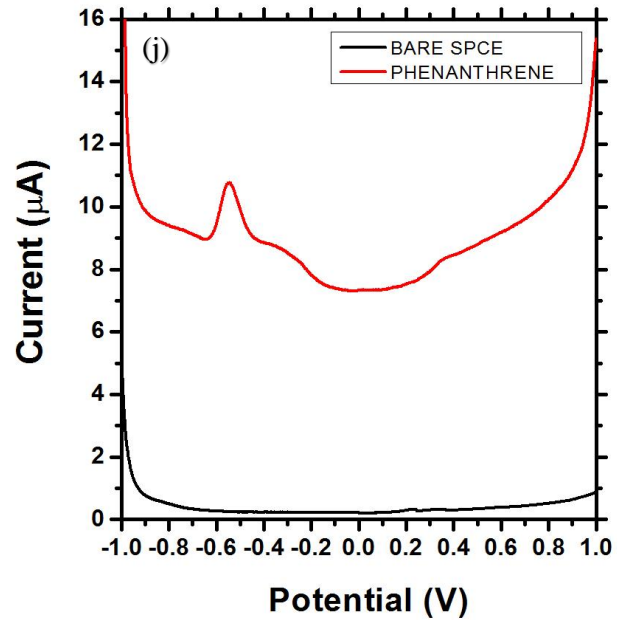
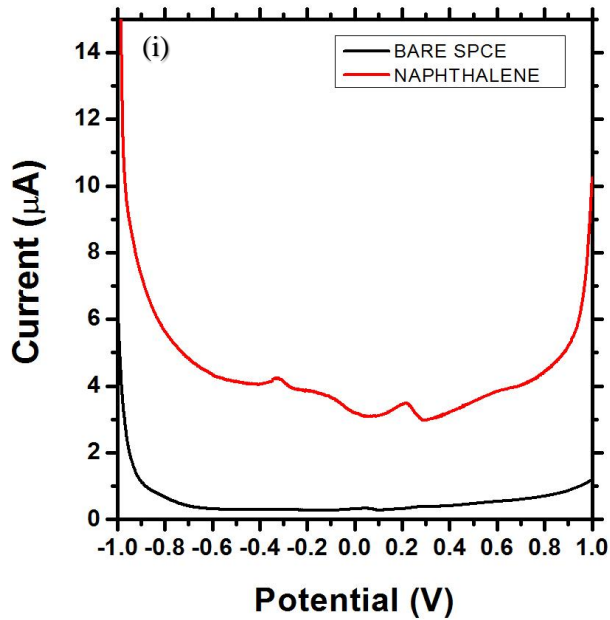


Figure 22. Electrochemical signature of (a) 1-OHP, (b) ANT, (c) ANY, (d) BaP, (e) BbF, (f) CHR, (g) DMBA, (h) FLA, (i) NAPH, (j) PHEN, (k) PYR and (l) TRIP at the bare SPCE.

The strongest anodic peak currents were observed for 1-OHP and PYR, for which quantitative analysis was performed. For all other PAH species, inconsistent peak responses were recorded as a function of increasing concentration (**Table 10**).

Table 10. Electrochemical evaluation of polycyclic aromatic hydrocarbons at bare screen printed carbon electrode.

PAHs	Concentration (ppb)	Peak Potential (V)	Concentration (ppb)	Peak Potential (V)
	SWV		CV	
1-hydroxypyrene	2720	-0.37 +0.05	--	--
7,12-dimethylbenz(a)anthracene	3200	No peak	--	--
Acenaphthylene	2850	No peak	1217	No peak
Anthracene	5550	-0.93 +0.11	3013	No peak
Benzo(a)pyrene	12530	-0.73 +0.05	--	--
Benzo(b)fluoranthene	9450	No peak	3376	No peak
Chrysene	8550	-0.58 +0.16	10377	No peak
Fluoranthene	10080	No peak	4355	No peak
Naphthalene	3200	-0.32 +0.21	1102	+0.13 -0.18
Phenanthrene	660	-0.55	663	No peak
Pyrene	1890	-0.20 +0.14	2784	No peak

The more commonly explored methods for PAH detection is differential pulse voltammetry (DPV) and square wave anodic stripping voltammetry. Based on the information from literature and the use of these techniques there is a lack of information about ANY, BbF, CHR, FLA and NAPH, in terms of SWV. ANT and PHEN in acetonitrile were evaluated at a GCE in 0.1 M LiClO₄ (electrolyte solution) with peak potentials found at +1.18 V vs Ag/AgCl and +1.60 V vs Ag/AgCl respectively. The detection limits determined for these 2 PAHs compounds were found to be 30 and 285 ppb respectively.[124] BaP evaluated at a pencil graphite electrode in acetate buffer (pH 4.8) gave rise to a peak at a potential of +1.15

V vs Ag/AgCl using a scan rate of 200 mV/s. The frequency was set at 25 Hz and the potential step being set at 8 mV vs Ag/AgCl. The detection limit for BaP was found to be 6.82 ppb.[103] DMBA evaluated in acetate buffer (pH 4.8) at a GCE provided a detection limit of 0.05 ppb at +1.15 V vs Ag/AgCl, using a scan rate of 200 mV/s.

PAHs generally exhibit a decrease in solubility while the hydrophobicity increases with an increase in the number of fused benzene rings. Dissolving PAHs in an appropriate organic solvent is required to overcome this poor solubility. Solvent effects are influenced by factors such as conductance, solubility of the electrolyte and the reactivity with electrolytic products. Organic solvents such as acetonitrile, ethanol, methanol and methylene chloride explored by Fry and Britton, 1984, was suggested as appropriate solvents for oxidative electrochemistry. Dimethylsulfoxide and Dimethylformamide however was suggested as good solvents for reductive electrochemistry.[107] Most literature reports for PAHs analysis involves the use of acetonitrile as the solvent of interest. However, the non-aqueous nature of acetonitrile still requires some supporting electrolyte to improve conductivity and to reduce double-layer and migration currents.

4.3 Quantitative analysis of pyrene

A 101125 ppb stock concentration of PYR was prepared in methanol (MeOH). The electrochemical window used for the oxidative SWV of PYR was set at -1.0 to +1.0 V. A scan rate of 50 mV/s was achieved by setting the frequency at 10 Hz and the step potential at 5 mV. A bare SPCE was used as the electrochemical transducer in the quantitative determination of PYR in 4 mL 0.1 M LiClO₄ (electrolyte solution). Consecutive concentration additions of PYR within a concentration range of 753 to 3420 ppb was then added to the electrolyte solution.

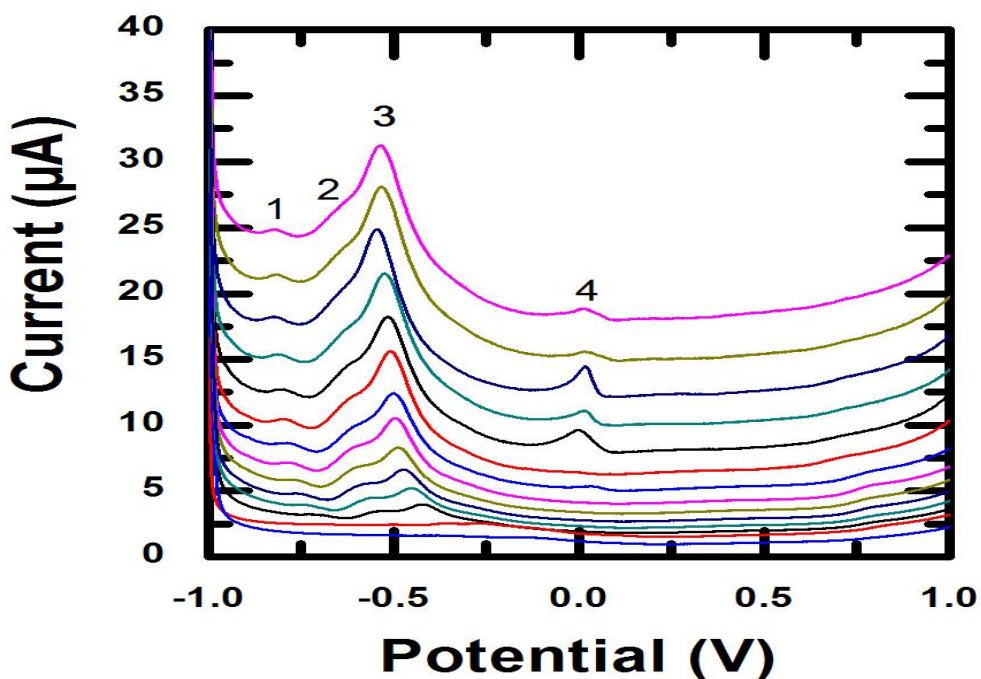
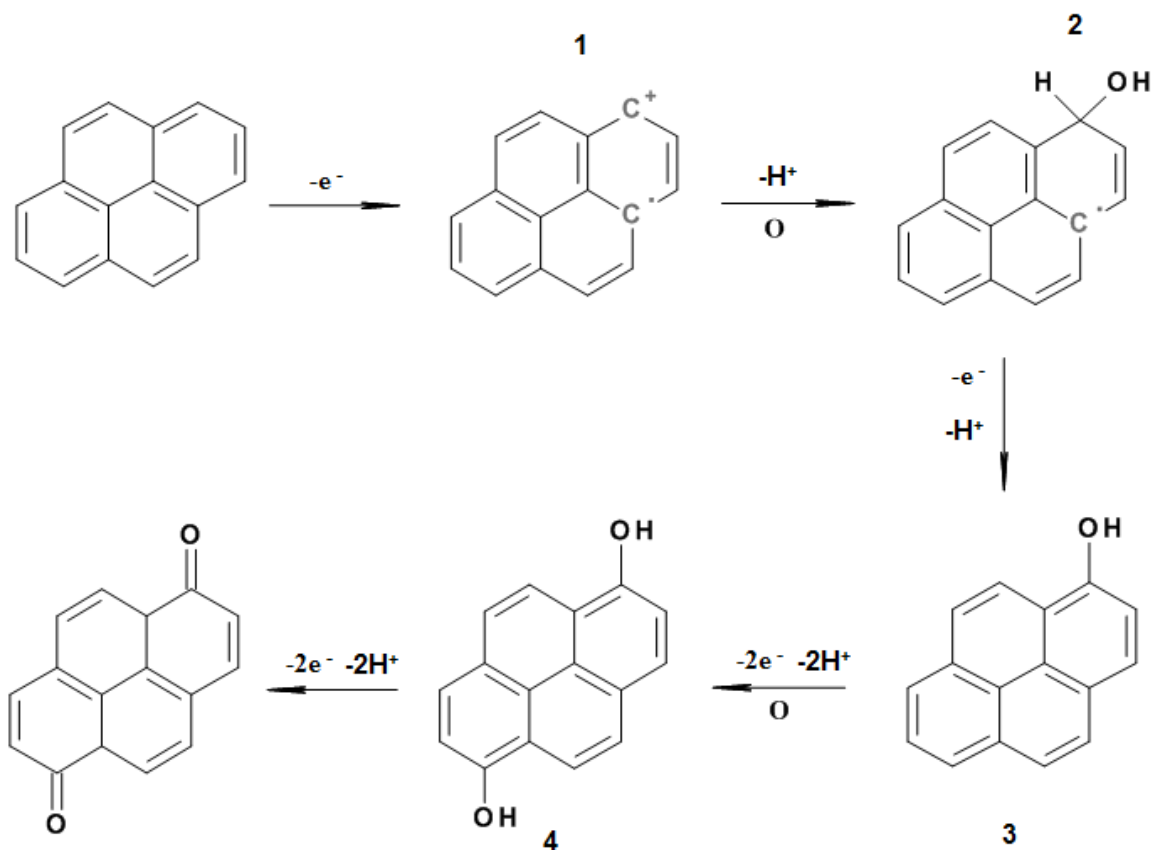


Figure 23. SWV analysis of pyrene at a bare SPCE in 0.1 M LiClO₄ in the concentration range 753 to 3420 ppb, at 50mV/s.

4 peaks of PYR were identified at potentials of 1. -0.82 V vs Ag/AgCl, 2. -0.66 V vs Ag/AgCl, 3. -0.54 V vs Ag/AgCl and 4. +0.02 V vs Ag/AgCl (**Figure 23**). The peaks represented by the voltammogram of PYR was attributed to the respective steps in the oxidation mechanism of PYR. It was suggested from the formation of the hydroquinone structure in the mechanism that the process in the voltammogram was irreversible. A clear increase in peak current in the oxidation scan with each concentration addition was observed. The electrochemical degradation of PAHs may occur via multiple steps, the degradation occurred via a direct one electron transfer from the adsorbed PAHs to the electrode surface forming radical cations. This step was then followed by nucleophilic attack by water at the carbon atoms with the highest positive charge density resulting in the formation of hydroxyquinones, dihydroxyquinones and ultimately diones. The formation and the possible reaction mechanism was used in the explanation of the screening of PYR (**Scheme 4**). [116, 169]



Scheme 4. Proposed electrochemical oxidation scheme of pyrene to pyrene-1,6-dione.

The change in peak current at -0.54 V vs Ag/AgCl occurred as a result of consecutive concentration additions which was then used to plot a calibration curve of current versus concentration. The calibration curve for PYR provided useful quantitative analysis in the determination of the LOD. The LOD was related to the minimum concentration that was detected by the system.

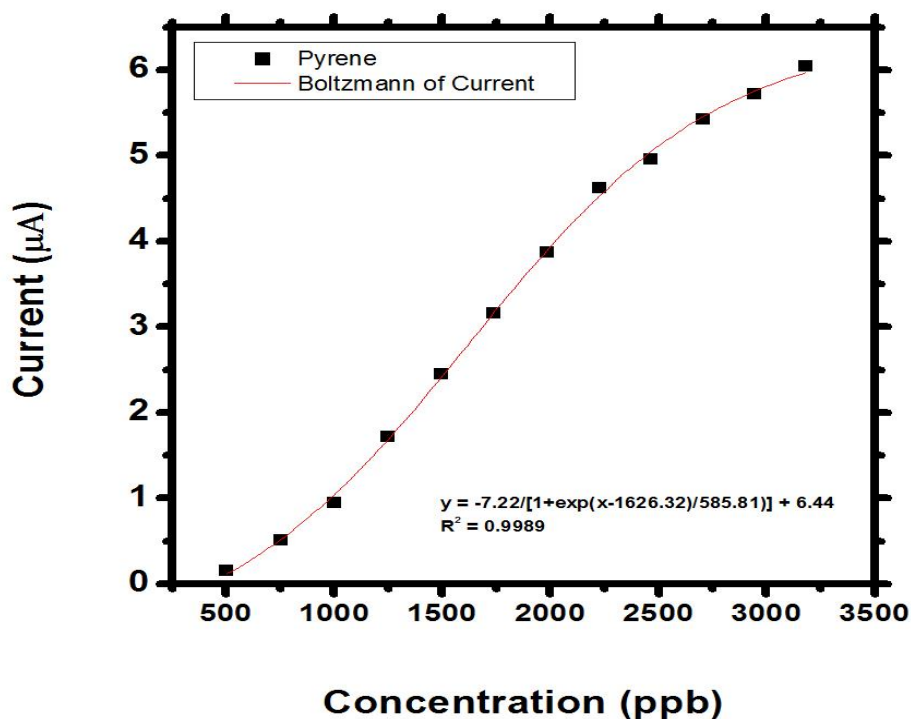


Figure 24. Calibration curve for the screening of pyrene.

An electrochemical reaction occurred via contact between the analyte molecule and the reactive surface. Based on the above calibration curve it was evident that the data followed an S-shaped calibration curve, indicative of competition for attachment to the available binding sites at low concentrations (**Figure 24**). This may be due to the size of the analyte molecules and possible flow parameters which affect the binding. Hydrophobicity was another factor influencing the competition at the binding sites as the binding affinity of PAHs (cross-reactivity) predominantly contributed to the analytical signal. These influences at the binding sites give rise to an S-shaped calibration, indicating initial adsorption followed by the linear response to concentration and eventually saturation.[49] The initial adsorption process indicated the amount of molecules the surface of the electrode can take up is dependent upon temperature, surface area and porosity of the electrode surface. The calibration data was modelled as a Boltzmann fit which is based on the non-linear least squares method.[102] The sensitivity of the transducer to the analyte species was evaluated from the linear region in the

Sigmoidal curve (S). The Boltzmann equation used to fit the s-shaped calibration curve was indicated using **(Equation 1)**. [33]

$$y = \frac{A1-A2}{1+e^{(x-x_0)/dx}} + A2 \dots \dots \dots \text{Equation 1}$$

Where;

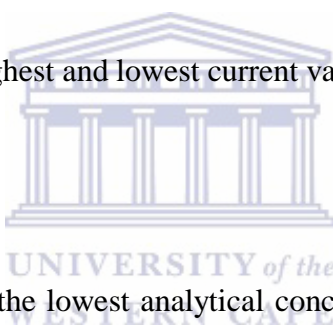
A1: lowest current values

A2: highest current values

x₀: midpoint between the highest and lowest current values

x: observed current value

dx: slope of the linear region



The LOD is the point at which the lowest analytical concentration can be determined, not always quantitatively. LOQ is the lowest analytical concentration that can be precisely and accurately determined **(Equation 2)**. [167]

$$LOD \text{ or } LOQ = \frac{F X SD}{b} \dots \dots \dots \text{Equation 2}$$

Where;

LOD: Limit of detection

LOQ: Limit of quantification

F: Factor of 3.3 (LOD) and 10 (LOQ) respectively

SD: Standard deviation of blank

b: Slope of the regression line

When the calibration curve is a straight line the slope of the curve determines the sensitivity of the system, based on the mathematical equation $y = mx + c$ where m is the slope. When the curve is not a straight line then the sensitivity is determined as a function of the analyte concentration.[77] The slope of the Sigmoidal curve is determined using the **Equation 1**, where the dx is the slope of the linear region. The slope indicated the steepness or sensitivity of the curve.[33] The electrochemical parameters selected for the detection of PAHs as well as the results determined from the calibration plot have been tabulated below (**Table 11**). The RSD value is an indication of the dispersion or spread of the data results, for $n=3$.

Table 11. Analytical and statistical data for pyrene detection at bare SPCE.

Pyrene	
Electrolyte Solution	0.1 M LiClO ₄
Potential Window (V)	-1.00 to +1.00
Scan Rate (mV/s)	50
Peak Potential (V)	-0.54
LOD (ppb)	1.77×10^{-3}
LOQ (ppb)	5.85×10^{-3}
R²	0.9989
Slope (μA/ppb)	585.81
% RSD	12.62 (n=3)

The LOD for PYR was found to be 1.77×10^{-3} ppb with a correlation coefficient of 0.9989. The sensitivity of the system determined from the slope of the calibration was found to be 585.81 μA/ppb based on the non-linear least squares method. Literature reports where pyrene was detected at a overoxidized polypyrrole metal nanoparticle modified glassy carbon electrode, a limit of detection of 546 ppb was achieved. The sensitivity and linear regression obtained using SWV for the detection of pyrene was found to be 1.07×10^{-6} μA/ppb and 0.9970 respectively.[124] A graphenated polyaniline doped tungsten trioxide material at a glassy carbon electrode surface was used to detect pyrene by cyclic voltammetry. This composite material was able to detect pyrene at a limit of 0.3 ppb with a linear regression of 0.9959. The sensitivity of the system towards pyrene was found to be 6.07×10^{-4} μA/ppb.[180] A modified GCE with multi walled carbon nanotubes and cobalt oxide was

used to determine pyrene at a limit of detection of 0.3 ppb. The sensitivity and linear regression based on the detection of pyrene was found to be $0.9 \mu\text{A/ppb}$ and 0.9997, respectively.[28] Comparing the detection limit and the sensitivity of the system towards pyrene in this work to literature, it was found that both parameters exceeded the reports from literature.

4.4 Quantitative analysis of 1-hydroxypyrene

The behaviour of 1-OHP was explored by initially preparing a stock solution of 109125 ppb in MeOH. The electrochemical window used for the oxidative SWV of 1-OHP was set at -1.0 to +1.0 V. A scan rate of 50 mV/s was achieved by setting the frequency at 10 Hz and the step potential at 5 mV. A bare SPCE was used as the electrochemical transducer in the quantitative determination of PYR in 4 mL 0.1 M HCl (electrolyte solution). Consecutive concentration additions of 1-OHP within a concentration range of 753 to 3420 ppb was then added to the electrolyte solution.

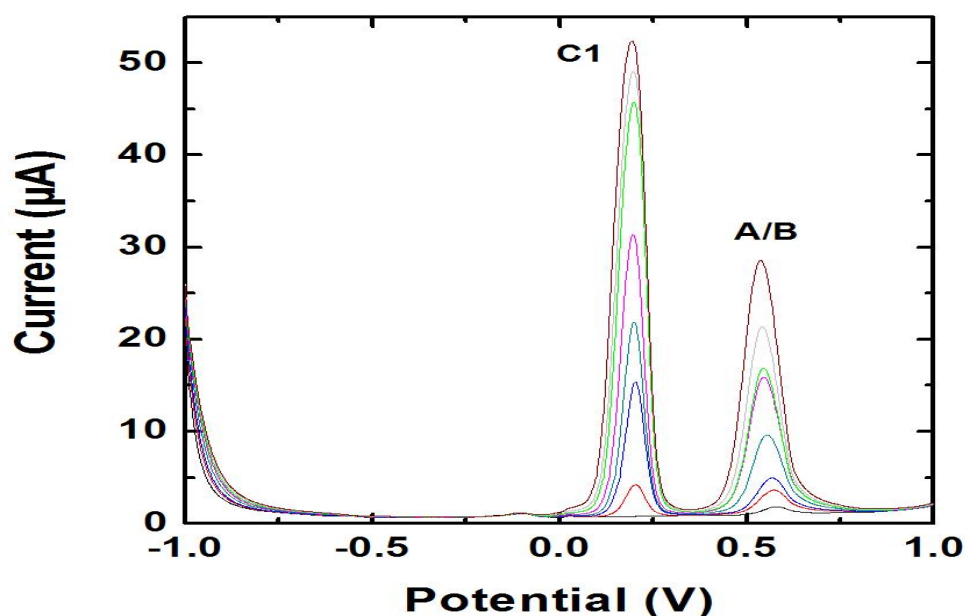
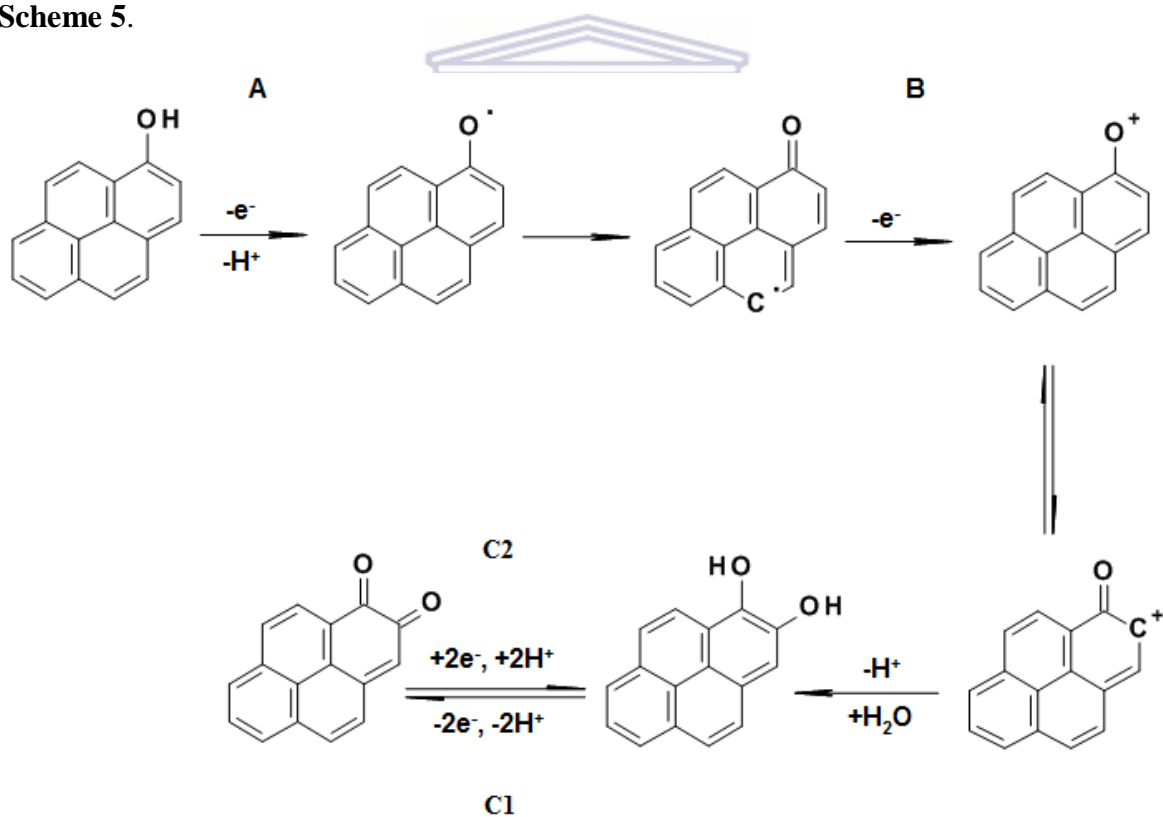


Figure 25. SWV analysis of 1-hydroxypyrene at a bare SPCE in 0.1 M HCl in the concentration range 543 to 3435 ppb, at 50mV/s.

2 electrochemical oxidation peaks (**Figure 25**) at +0.20 V and +0.54 V vs Ag/AgCl were observed during the oxidative SWV analysis which was attributed to the cation (B) and quinoid (C1) species. At lower pH < 7 the oxidation peak (B) is an amalgamation of 2 electron processes (A and B), the peak relating to process B was found to be independent of pH. The combination of peak A/B can be considered as a result of an initial one-electron one proton oxidation (1-OHP) step to give rise to radical species, peak A (step 2). Peak B (step 4) results due to further one-electron oxidation process of step 2 which gives rise to the cation species. The quinoid species observed in step 7 (peak C1) results from the oxidation process where $2e^-$ and $2H^+$ species were consumed during this step. The quinoid structure is also known as pyrene-1,2-dione. The oxidation of 1-OHP proceeded via an electron transfer-chemical reaction-electron transfer (ECE) mechanism which resulted in the proposed **Scheme 5**.



Scheme 5. Proposed electrochemical oxidation mechanism of 1-hydroxypyrene.

The change in peak current at -0.20 V vs Ag/AgCl as a result of consecutive concentration addition was used to plot a calibration curve of current versus concentration.

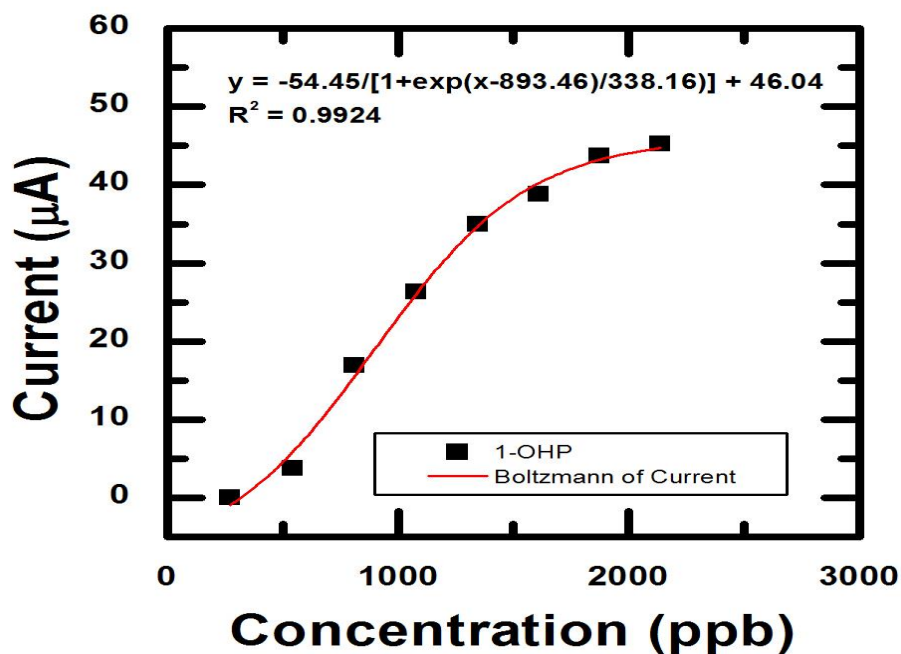


Figure 26. Calibration curve of the detection of 1-hydroxypyrene.

An electrochemical reaction occurred via contact between the analyte molecule and the reactive surface. Based on the above calibration curve it was evident that the data followed a sigmoidal calibration curve, indicative of competition for attachment to the available binding sites at low concentrations (**Figure 26**). The calibration data was modelled as a Boltzmann fit which is based on the non-linear least squares method. The Boltzmann equation used to fit the s-shaped calibration curve was indicated using (**Equation 1**). The electrochemical parameters selected for the detection of PAHs as well as the results determined from the calibration plot have been tabulated below. The RSD value is an indication of the dispersion or spread of the data results, for n=3 (**Table 12**).

Table 12. Analytical and statistical data for 1-hydroxypyrene detection at bare SPCE.

1-Hydroxypyrene	
Electrolyte Solution	0.1 M HCl
Potential Window (V)	-1.00 to +1.00
Scan Rate (mV/s)	50
Peak Potential (V)	+0.20
LOD (ppb)	6.00×10^{-4}
LOQ (ppb)	1.80×10^{-3}
R²	0.9924
Slope (μA/ppb)	338.61
% RSD	14.78 (n=3)

The LOD (n=3) for 1-OHP was found to be 6.00×10^{-4} ppb with a correlation coefficient of 0.9924. The sensitivity of the system determined from the slope of the calibration was found to be 338.61 μA/ppb based on the non-linear least squares method. A thin film mercury electrode was used in the investigation of the urinary biomarker 1-OHP using SWV adsorptive stripping voltammetry. The limit detected for 1-OHP was determined to be 0.2 ppb with a sensitivity of 2.40×10^{-1} μA/ppb. A linear regression of the system towards 1-OHP was found to be 0.9960.[39] A graphene oxide polymer composite modified GCE used in the detection of 1-OHP by DPV in phosphate buffer solution (PBS – pH 2.0) buffer containing sodium chloride (NaCl – 0.2 M). The limit of detection and linear regression of the system towards 1-OHP was found to be 8 ppb and 0.9950, respectively.[166] 1-OHP was detected at a molecular imprinted titanium dioxide (TiO₂) gel film using cyclic voltammetry in a 2 mM potassium ferrocyanide (K₃[Fe(CN)₆]) solution with 1 M potassium chloride (KCl). The sensitivity of the system was found to 6.60×10^{-2} μA/ppb, with a limit of detection and linear range of 0.07 ppb and 0.9700.[201] The limit of 6.00×10^{-4} ppb indicated that the unmodified SPCE sensor system was more sensitive towards 1-OHP compared to some other electrochemical techniques, reported in literature.

Aromatic compounds tend to interact with graphite walls and resulted in the stacking onto carbon materials via non-covalent bonding. After the PAHs concentrated onto the surface of the electrode an electrochemical operation was applied which resulted in the detection of the

PAHs. The exploration of these PAHs at a bare SPCE using 0.1 M LiClO₄ and 0.1 M HCl allowed for the detection of both PYR and 1-OHP. Redox behaviours and the plot of peak current versus concentration gave rise to the LOD of PYR and 1-OHP which were found to be 1.77x10⁻³ ppb and 6.00x10⁻⁴ ppb respectively. The detection of both PAHs in a complex mixture was also explored, however the sensitive electrochemical response of the 1-OHP completely dominated the electrochemistry of PYR at a SPCE. A second electrolyte solution 0.1 M HCl was employed to find an alternative background for the recording of PYR and 1-OHP electrochemistry. However the sensitivity of the SPCE towards 1-OHP was better in 0.1 M HCl. As a result PYR analysis was recommended in 0.1 M LiClO₄ and 1-OHP in 0.1 M HCl in the multichannel protocol proposed for mixed samples. Currently, according to the U.S. EPA there is insufficient information about PYR to classify it a potential cancer causing substance. Further investigation into PYR could lead to proper classification as either a probable or not probable carcinogen towards humans. High performance liquid chromatography the most common method in the study of PAHs was used to determine limits for PYR, limits determined for UV and FLD were 0.01 ppb and 0.01 ppb respectively. Methods developed by the U.S. EPA (610 and 550.1) for the determination of PAHs found limits for PYR to be 0.27 ppb and 0.13 ppb respectively. Based on the determined limits from the electrochemical detection, the limits for PYR are within the range of HPLC detection and the limits detected using the U.S. EPA methods. The limits determined from the electrochemical methods are more sensitive and provides a cheaper alternative to the more expensive HPLC methods. HPLC-(UV/FLD/DAD) however has the ability to simultaneously determine a large number of PAHs in one analytical run. The problem with HPLC is the sample preparation, if the sample is incorrectly prepared problems could arise during the integration of the data. The mobility of the HPLC instrument is also limited to the laboratory desktop compared to the lightweight potentiostat used for electrochemical measurements. The potentiostat which is very portable uses a lithium ion battery and can be connected to a smart device via bluetooth or USB cable, can be used for on-site analysis. Electrochemical methods provided a good basis for cheaper, on-site measurements with the ability to measure at low detection limits. Various occupational limits for 1-OHP have been determined by various health agencies in America, Canada and Australia. These

occupational limits for 1-OHP ranged between 1.00 to 10.00 ppb. The electrochemical work performed in this chapter determined limits that fell below these occupational limits. The selective determination of these PAHs as individuals in alternative electrolyte medium provided a means in principle to employ them in a multichannel design (**Figure 27**). The electrode employed in the multichannel design consisted of 8 working electrodes.



BARE SCREEN PRINTED CARBON ELECTRODE

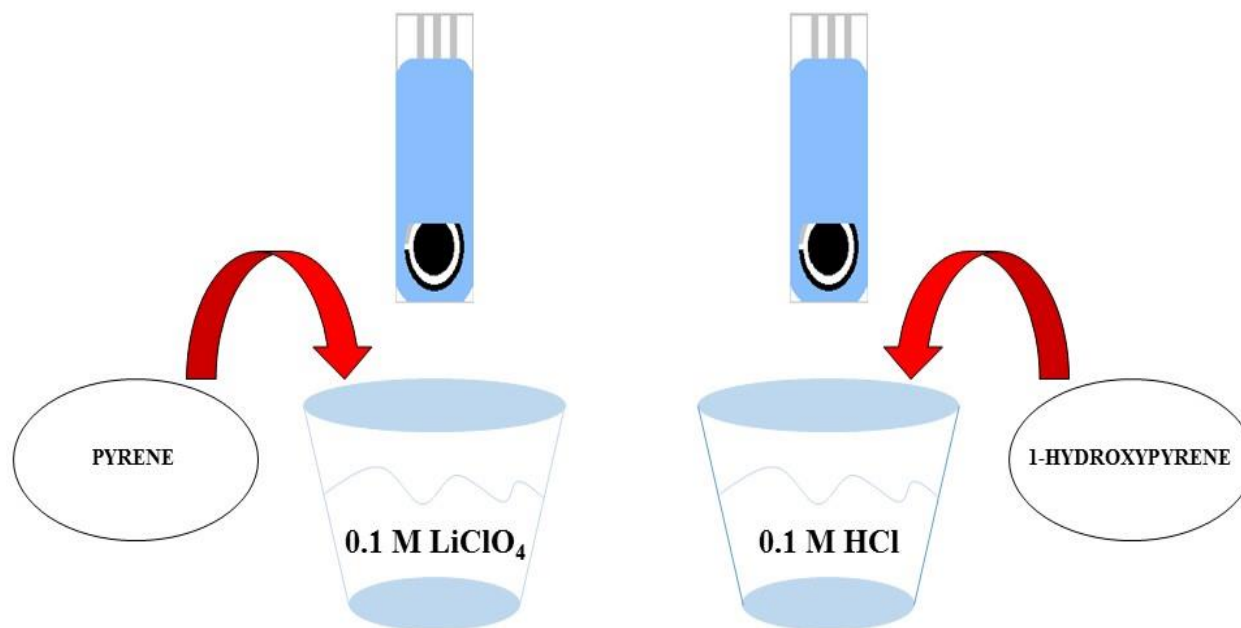


Figure 27. Conclusions based on the information obtained during the evaluation of PAHs at the unmodified screen printed carbon electrode surface.

5. Characterization of Schiff base materials (N,N'-Bis-(1H-pyrrol-2-ylmethylene)-benzene-1,2-diamine) and poly(N,N'-Bis-(1H-pyrrol-2-ylmethylene)-benzene-1,2-diamine) modified screen printed carbon electrode



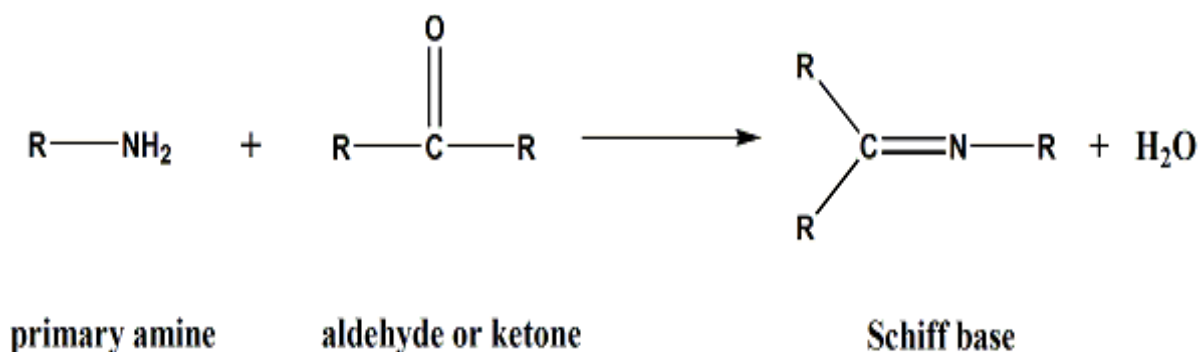
The novel Schiff base monomer was electropolymerized at a SPCE to produce the polymer modified electrode. Spectroscopy techniques was used to confirm the Schiff base formation through the azomethine bond. The electrochemically produced polymer material will be characterized by atomic force microscopy, scanning electron microscopy, cyclic voltammetry and square wave voltammetry.

5.1 Introduction

A Novel Schiff base material was prepared under a reflux condensation reaction and was sufficiently dried before characterization and analysis. This novel material was extensively characterized in terms of spectroscopy, microscopy and electrochemical techniques to confirm the successful linking of starting materials and to study the morphology and topography of the material at a microscopic level. Thin films of the Schiff base polymer was deposited at the surface of screen printed carbon electrodes by electrochemical polymerization. The freshly prepared thin film sensor was used as the transducer for the evaluation of polycyclic aromatic hydrocarbons.

5.2 Introduction into Schiff base materials

A natural products chemist named Hugo Schiff discovered a class of compounds which were formed when primary amines reacted with an aldehyde or a ketone under specific reaction conditions. This new class of compounds known as Schiff bases are also known as imines or azomethine is a nitrogen analogue in which a carbonyl attached to an aldehyde or ketone is replaced by an azomethine group (**Scheme 6**). The formation of these compounds tend to be a reversible process therefore usually occurs under acidic or basic conditions during heating. [68, 159, 211]



Scheme 6. Formation of Schiff base compound.

Schiff base compounds are widely used organic compounds that have been used as pigments, dyes, catalysts, intermediates in organic synthesis and as polymer stabilisers. Schiff bases of aliphatic aldehydes are very unstable and are readily polymerizable with aromatic aldehydes, having an effect on the conjugation system resulting in more stable complexes. These Schiff

bases are usually tri and bi dentate ligands which are capable of forming very stable complexes with transition metals of various oxidation states. Some Schiff bases and their respective metal complexes have antibacterial and antitumor activity which make them an interesting topic for discussion.[48, 108]

5.3 Schiff base sensors

Schiff base materials have been used for a wide range of potential sensors including fluorescence, membrane, colorimetric, metal ions and chemical sensors. Fluorescence Schiff base sensors have been found to display remarkable fluorescent behaviour towards metals ions including Al^{3+} , Mg^{2+} , Hg^{2+} and Zn^{2+} . [76, 96, 150, 198] Schiff base materials have also been reported to be used in metal ion sensors, especially for $\text{Hg}(\text{II})$ detection. [129, 151, 187] A new cellulose –lysine-Schiff-base-based sensor-absorbent was developed for the selective detection of mercury as well as its removal from water. Results revealed that this sensor displayed rapid and high removal capacity and easily visible detection within a defined limit of 10 ppm and higher. This range was explored to cover both high and low concentrations of $\text{Hg}(\text{II})$. The material displayed a high maximum removal capacity and good reusability up to 8 cycles. [110] Schiff base ligands (**Figure 28**) have been used in the construction of membrane sensors due to its ability to form stable complexes with metal ions. Good selectivity, sensitivity and stability is produced for specific ions. A schiff base ligand was covalently immobilized on an agrose membrane which was used as an effective ionophore in the construction of a selective optical sensor. This sensor was used for the spectrophotometric determination of $\text{Hg}(\text{II})$ in aqueous solutions.

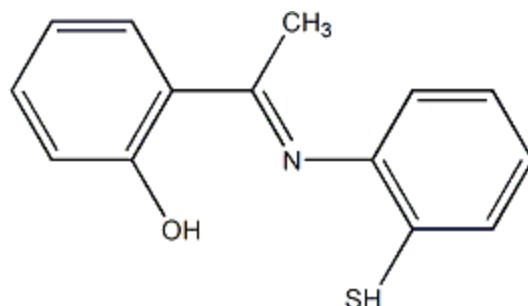


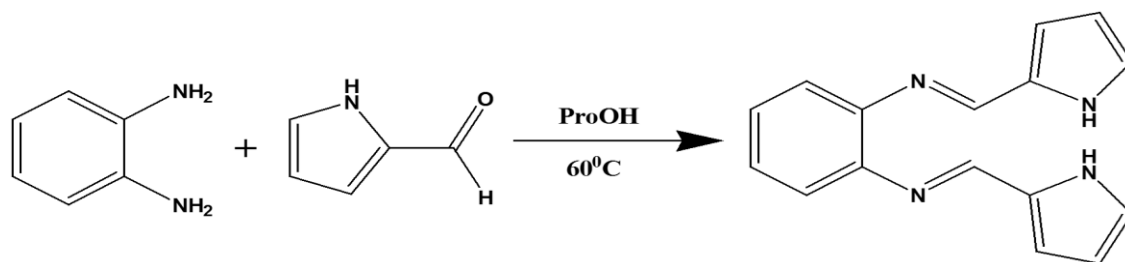
Figure 28. A Schiff base ligand 2-((2-sulfanyphenyl)ethanimidoyl)phenol.

The optical sensor displayed favourable properties such as, high selectivity, good lifetime, fast and reproducible regeneration, low cost, simple fabrication and easy handling. In addition the sensor showed quick response time, good linear calibration curve and low detection limits. The optical was used for quantitative and qualitative analysis for the determination of Hg(II) ions even in the presence of other metal ion species.[8]

Most work performed using Schiff bases as sensor have been done on detecting or monitoring metal ions. Little to no work has been done using Schiff base sensors for PAHs detection. A few reports have revealed that PAHs have been linked to Schiff bases to produce sensors for the detection and monitoring metal ions. A novel Schiff based linked PAHs (NAPH, ANT and PYR) sensor which was utilized as selective fluorescent and colorimetric sensors for the detection of Cu(II) and Hg(II) in aqueous medium.[183] A chemosensor based on a NAPH Schiff base was used for the fluorometric and colorimetric sensing of Hg(II) ions via twisted intramolecular charge transfer mechanism.[204]

5.4 Monomer synthesis

A novel Schiff base material was synthesized by a reflux condensation reaction, which produced the novel azomethine material, N,N'-Bis-(1H-pyrrol-2-ylmethylene)-benzene-1,2-diamine (BPPD). The condensation reaction mixture consisted of 0.5 mmol o-phenylenediamine (oPD) which was reacted with 1 mmol pyrrole-2-carboxaldehyde (P2C) in the presence of propanol (**Scheme 7**). The reaction mixtures was kept under argon gas to avoid overoxidation of pyrrole. The reaction proceeded overnight, the initial colour (light brown) disappeared and a new bright orange colour was observed. The reaction was then stopped and the solvent was duely evaporated by rotary evaporation leaving a red oily like substance. This oily substance was then precipitated by using cold chloroform, once the oily substance precipitated further evaporation was performed to remove any remaining organic solvents. A light orange precipitate was obtained with a percentage yield of 80%.



Scheme 7. N,N'-Bis-(1H-pyrrol-2-ylmethylene)-benzene-1,2-diamine preparation by Schiff base synthesis.

5.5 Fourier transform infrared spectroscopy (FTIR)

FTIR spectra represent starting materials o-phenylenediamine (oPD), pyrrole-2-carboxaldehyde (P2C) and the monomer material N,N'-Bis-(1H-pyrrol-2-ylmethylene)-benzene-1,2-diamine (BPPD) (**Figure 29**). These are important regions as they indicated the presence of primary amines, carbonyl bonds and azomethine bonds. All FTIR spectra were recorded using the Bruker Tensor 27 with OPUS software, all materials used were a solid material. The important stretching frequency in Schiff base materials is the formation of the azomethine bond.

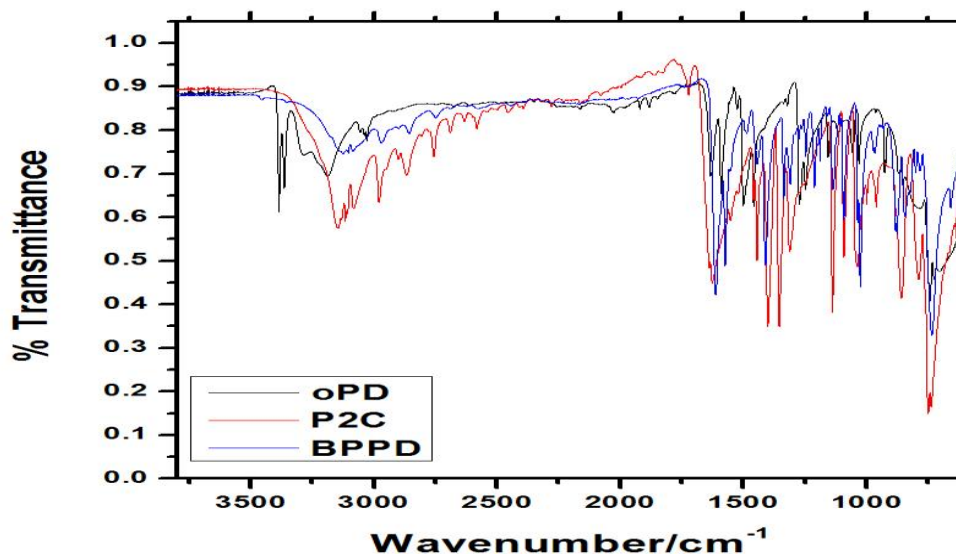


Figure 29. FTIR spectra of o-phenylenediamine, pyrrole-2-carboxaldehyde and N,N'-Bis-(1H-pyrrol-2-ylmethylene)-benzene-1,2-diamine, between 400 and 4000 cm^{-1} .

The stretching region where (1°, 2°, 3°) amines stretching bands were observed at 3100 to 3400 cm⁻¹ (**Figure 30**). The sharp intense stretching bands at 3384 cm⁻¹ and 3364 cm⁻¹ are attributed to the primary (1°) amine associated with the structure of oPD. The stretching band of the secondary (2°) amine present in the P2C can be seen at 3147 cm⁻¹. The stretching band present at 3126 cm⁻¹ is associated with the secondary (2°) amine of the BPPD.

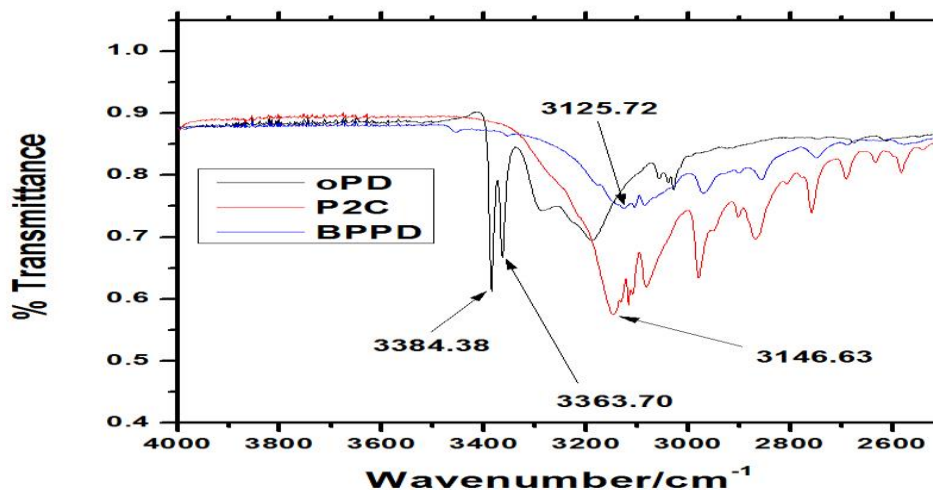


Figure 30. FTIR spectra of o-phenylenediamine, pyrrole-2-carboxaldehyde and N,N'-Bis-(1H-pyrrol-2-ylmethylene)-benzene-1,2-diamine, between 2600 and 3600 cm⁻¹.

The other important region for the determination of the azomethine bond is the stretching region where the aldehyde bond (H-C=O) and azomethine bond (C=N-H) is observed. The stretching range for the aldehyde bond is between 1740 to 1660 cm⁻¹ with the exact stretching band being dependent on the conjugation of the carbonyl bond (functional groups). The increase in the conjugation of the carbonyl bond decreases the stretching frequency.[73, 135] The range in which the azomethine bond was expected theoretically was between 1690 to 1520 cm⁻¹, again conjugation and side groups play an important role in the expected stretching frequency observed.[147]

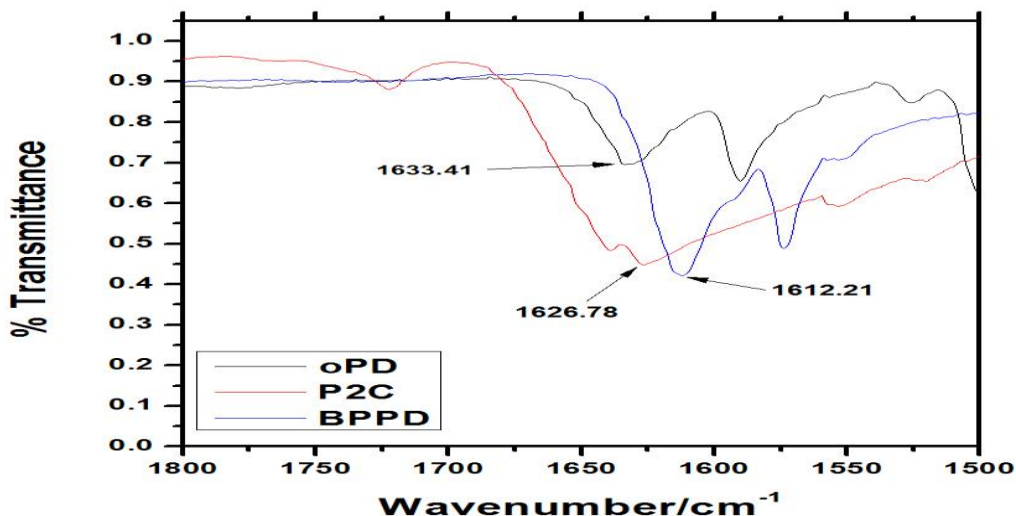


Figure 31. FTIR spectra of *o*-phenylenediamine, pyrrole-2-carboxaldehyde and *N,N'*-Bis-(1*H*-pyrrol-2-ylmethylene)-benzene-1,2-diamine, between 1500 and 1800 cm^{-1} .

In the region where the carbonyl stretching band was observed, P2C showed an intense stretching at 1627 cm^{-1} , associated with that of the carbonyl bond (C=O). The intense band associated with BPPD was attributed to the C=N bond at 1612 cm^{-1} . The broad band at 1633 cm^{-1} was associated with the *o*PD can be attributed to the C-N-bond (**Figure 31**).

Table 13. FTIR stretching frequency assignments

Material	Assignment	Frequency (cm^{-1})
<i>o</i> -phenylenediamine (<i>o</i> PD)	-NH ₂ C-N	3384 and 3364 1633
Pyrrole-2-carboxaldehyde (P2C)	-NH C=O	3147 1627
<i>N,N'</i> -Bis-(1 <i>H</i> -pyrrol-2-ylmethylene)-benzene-1,2-diamine (BPPD)	-NH C=N	3126 1612

The data obtained from the FTIR spectra indicating the important bands within each material have been tabulated (**Table 13**). The spectra and tabulated data of BPPD both indicated that there was an absence of both a primary (1°) amine and the intense carbonyl (C=O) band. The presence of the stretching frequency at 1612 cm^{-1} is indicative of the C=N bond, based on the above evidence the formation of the desired material in **Scheme 4** was achieved.

5.6 Nuclear magnetic resonance (NMR)

^1H -NMR spectra of oPD, P2C and BPPD were recorded in Acetone- d_6 and DMSO- d_6 respectively. Relevant spectra were recorded using a Bruker Avance DPX 250 MHz spectrometer. Subsequently the NMR data was confirmed using an alternative NMR namely the Bruker Avance IIIHD Nanobay 400 MHz spectrometer equipped with a 5 mm broadband observe (BBO) probe at room temperature (298K)

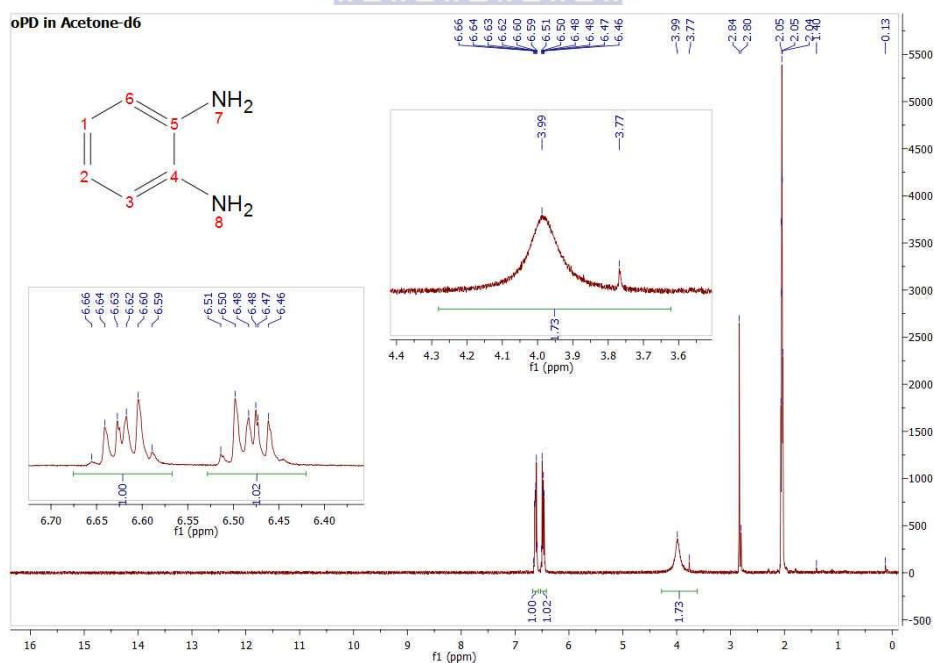


Figure 32. NMR spectra of o-phenylenediamine in Acetone- d_6 .

The NMR spectra of oPD revealed δ shifts at 3.99, 6.48 and 6.62 ppm, attributed to the $-\text{NH}_2$ (7/8 on the chemical structure), C-H (1 on the chemical structure) and C-H (6 on the chemical structure) bonds respectively. The NMR solvent acetone- d_6 and the water attributed

to the acetone-d₆ can be seen at 2.05 and 2.84 ppm respectively (**Figure 32**). The spectra of P2C displayed a range of δ shifts in the NMR spectrum using acetone-d₆.

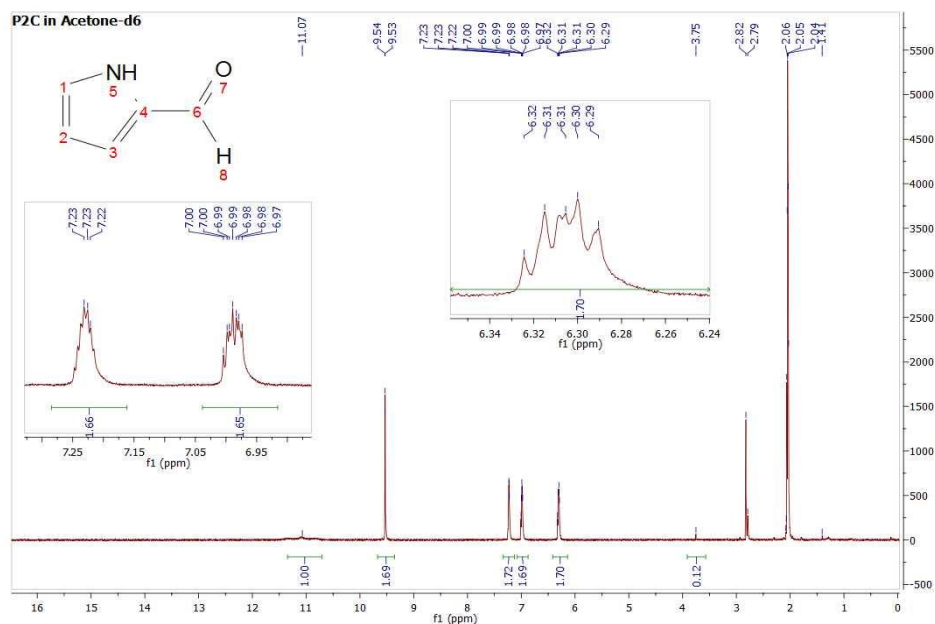


Figure 33. NMR spectra of pyrrole-2-carboxaldehyde in Acetone-d₆.

UNIVERSITY of the
WESTERN CAPE

The δ shift responsible for the C-H bonds can be seen at 6.30 (2), 6.99 (3) and 7.22 ppm (1) respectively. The proton attached to the carbonyl group is observed at a δ shift of 9.5 ppm (8). The proton attached to the nitrogen compound on the pyrrole ring can be seen at a δ shift at 11.07 ppm (5). The NMR solvent acetone-d₆ and water can be observed at δ shift of 2.05 and 2.84 ppm respectively (**Figure 33**). The spectra of BPPD dissolved in DMSO-d₆ was determined in order to confirm the presence of the azomethine bond. The chemical structure of BPPD was used to determine the respective δ shift in the NMR spectra.

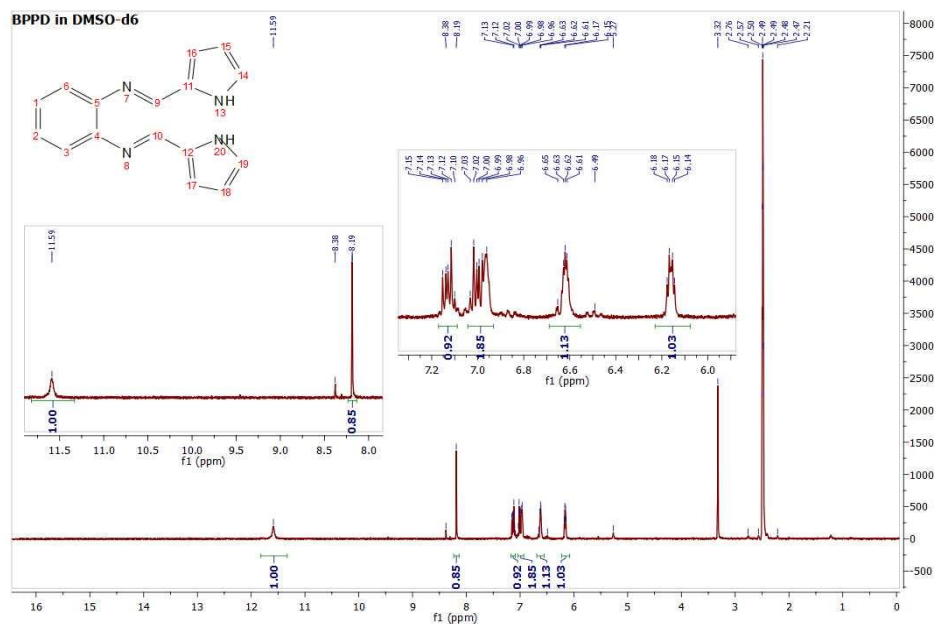


Figure 34. NMR spectra of BDDP in DMSO-d₆.

The main δ shift of interest in the BPPD spectrum revealed the azomethine bond (HC=N) at a δ shift of 8.19 ppm (9). The retention of protons from the two combining starting materials are evident within the BPPD spectra. The protons attributed to the pyrrole ring (C-H and –NH protons) could be seen at a δ shift of 6.15 (15), 6.62 (16), 6.98 (14) and 11.59 ppm (13) respectively. The δ shifts attributed to the oPD ring (C-H proton) could be seen at δ shifts of 6.96 (1) and 7.12 ppm (6) respectively (**Figure 34**).

Table 14. ¹H NMR data of starting materials and the new Schiff base material.

Material	δ shift (ppm)	Assignment
o-phenylenediamine (oPD)	3.99	(s, 1H)
	6.48	(m, 1H)
	6.62	(m, 1H)
Pyrrole-2-carboxaldehyde (P2C)	6.30	(m, 1H)
	6.99	(ddd, 1H)
	7.23	(m, 1H)
	9.53	(d, 1H)
N,N'-Bis-(1H-pyrrol-2-ylmethylene)-benzene-1,2-diamine (BPPD)	11.07	(s, 1H)
	6.15	(dd, 1H)
	6.62	(dd, 1H)
	6.98	(s, 1H)
	6.99	(m, 1H)
	7.12	(dd, 1H)
	8.19	(s, 1H)
11.59	(s, 1H)	

Data relating to the NMR spectra was tabulated (**Table 14**) for P2C, oPD and BPPD, displaying their relative NMR shifts. The δ shift of importance associated with o-phenylenediamine was found a 3.99 ppm (1° -NH₂) as a singlet in the high field region. The important δ shifts in the NMR spectra of P2C was observed in the low field region at δ 9.53 ppm (-CHO) as a singlet and δ 11.07 ppm (-NH₂) as a doublet. The formation of BPPD was indicated by the disappearance of the aldehydic proton (P2C) and the primary (1° -NH₂) amine

(oPD). Acetone was used as the NMR solvent for both starting materials, however due to the low solubility of BPPD in most solvents DMSO-d₆ was used.

5.7 UV-Vis analysis

The absorption spectra of BPPD, oPD and P2C were recorded over a wavelength range of 200 to 500 nm using a Nicolet Evolution 100 spectrophotometer at room temperature. Both starting materials and BPPD was dissolved in ethanol to prepare 20 mM solutions.

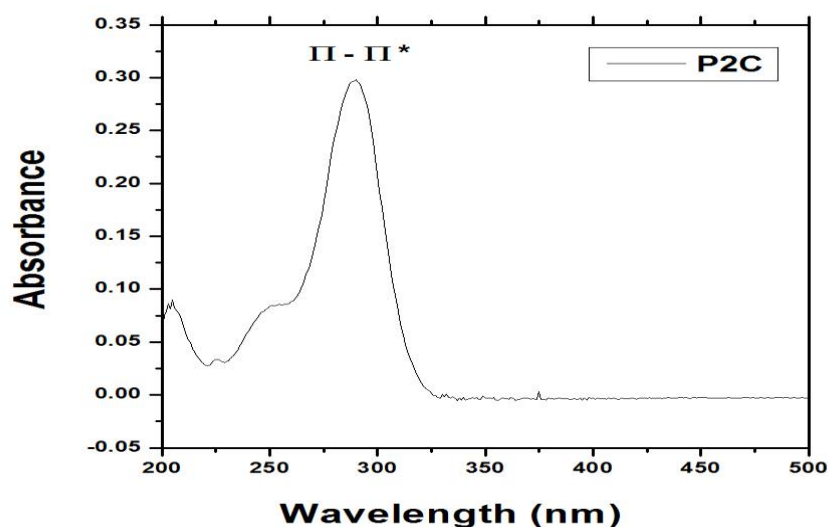


Figure 35. UV-Vis spectra of pyrrole-2-carboxaldehyde in Ethanol.

The spectra of P2C displayed a high energy π - π^* band (**Figure 35**) at 289 nm was attributed to the pyrrole ring.[203] The peaks (**Figure 36**) at 237 and 446 nm in the spectra of oPD was attributed to the benzene π - π^* electronic transition and the broad absorption to the n - π^* electronic transition.[217]

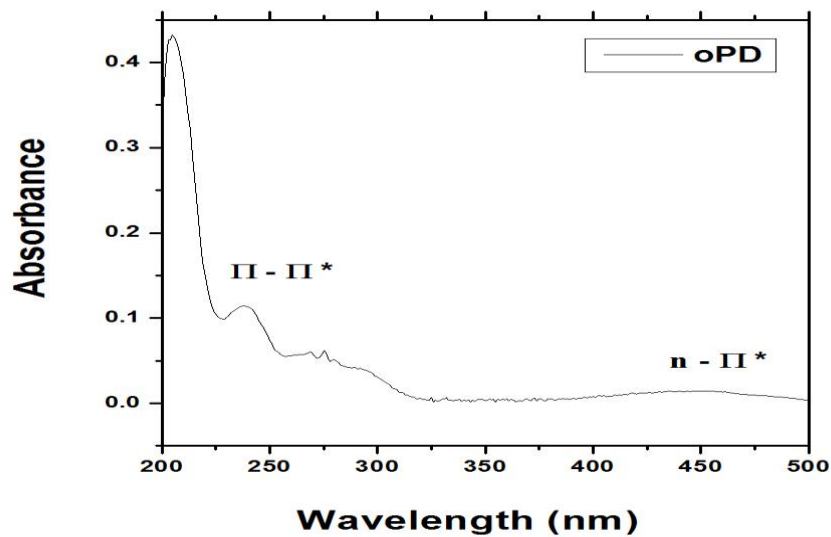


Figure 36. UV-Vis spectra of o-phenylenediamine in Ethanol.

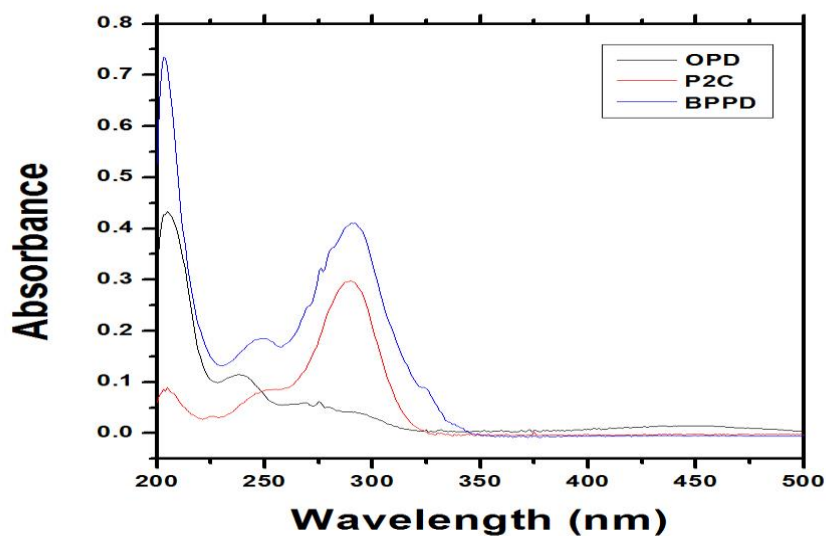


Figure 37. UV-Vis of BPPD, O-phenylenediamine and Pyrrole-2-carboxaldehyde in Ethanol.

The absorption band present at 291 nm was related to the pyrrole ring and the imine function (Figure 37).[203] The similarity of the UV-Vis spectra of the newly synthesized monomer and the starting materials was attributed to pyrrole ring (P2C), imine function (new bond

formation) and the benzene ring (oPD). This can also be observed in the reaction mechanism of the monomer formation (**Scheme 4**).

5.8 Thermal analysis

Thermogravimetric analysis (TGA) of the BPPD was used to determine the thermal stability of the material. In this TGA investigation the heating rates was controlled at 20.00 °C/min under an Argon atmosphere, with the weight loss being measured from room temperature up to 700 °C (**Figure 38**).

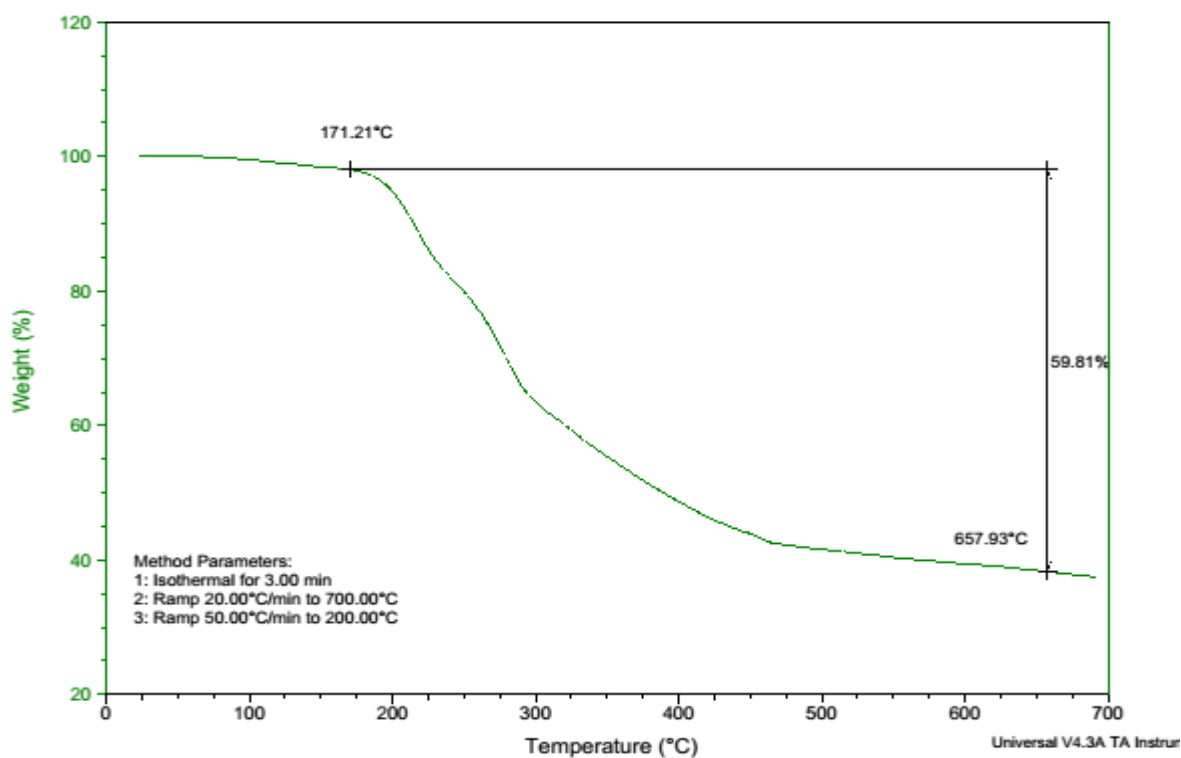


Figure 38. TGA decomposition analysis of BPPD.

The TGA revealed that BPPD is thermally stable up to 171.12 °C, before thermal decomposition begins. BPPD decomposes up to 60 % (4.0459 mg loss) before decomposition process is complete, a mass of 6.0211 mg remains after the decomposition process.

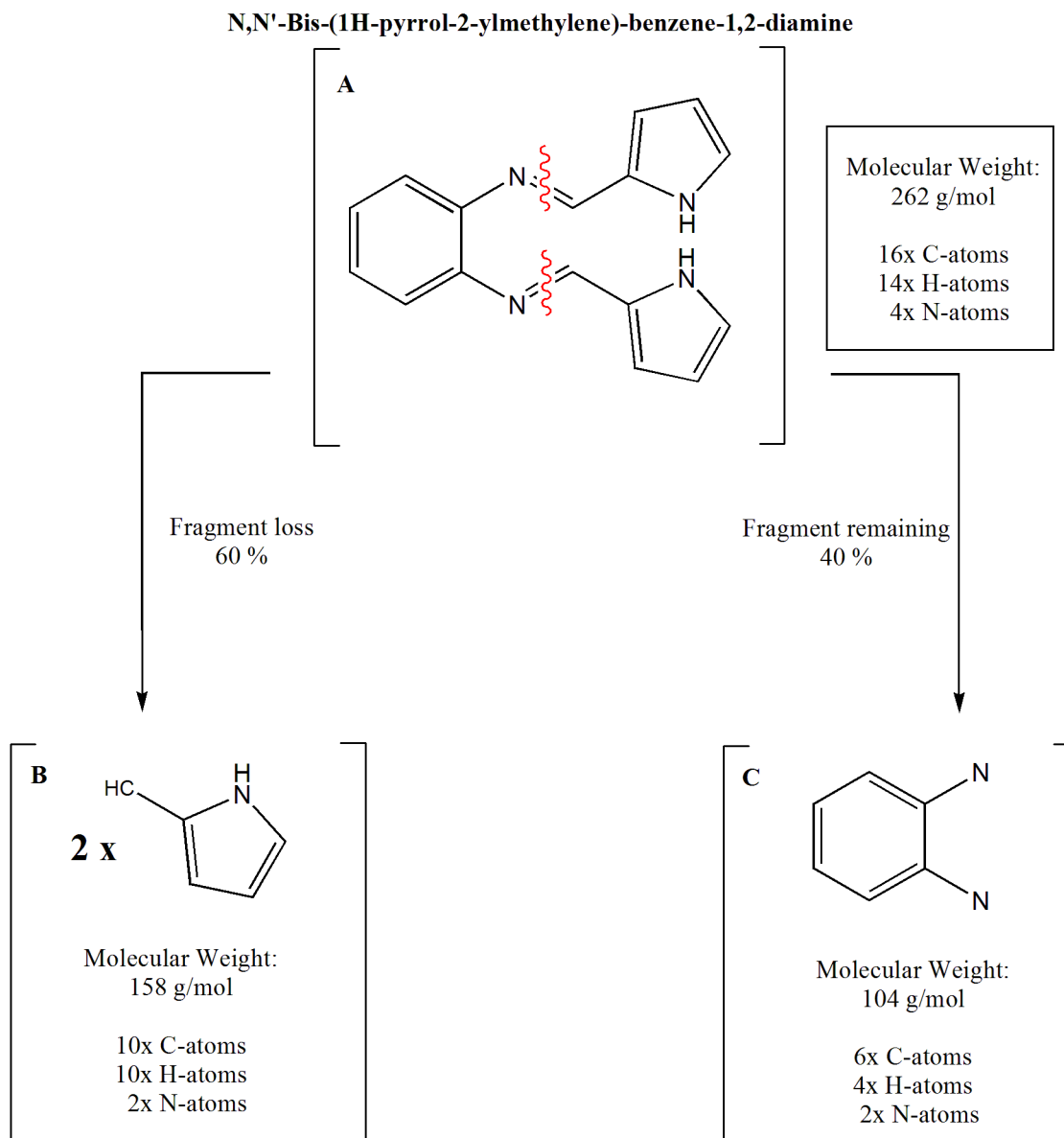


Figure 39. Fragmentational loss during thermogravimetric analysis of BPPD.

The molecular mass of BPPD (A) is 262 g/mol which comprises of carbon, nitrogen and hydrogen. The overall fragment lost (B) during the thermal analysis can be attributed to a molecular weight of 158 g/mol (60 % loss). The remaining fragment (C) has a molecular weight of 104 g/mol which accounts for the remaining 40 % (**Figure 39**).

5.9 Electrochemical preparation of poly(N,N'-Bis-(1H-pyrrol-2-ylmethylene)-benzene-1,2-diamine)

The polymer material was deposited as a thin film at the surface of a screen printed carbon electrode. This thin film was electropolymerized by cycling between a potential window of -0.7 to +0.7 V at a scan rate of 50 mV/s for 15 cycles. The electrochemical technique employed for the polymerization of BPPD was cyclic voltammetry. A 20 mM solution of oPD, P2C and PBPPD were prepared by dissolving in an equivolume ratio of DMF:0.1 M HCl (1:1).

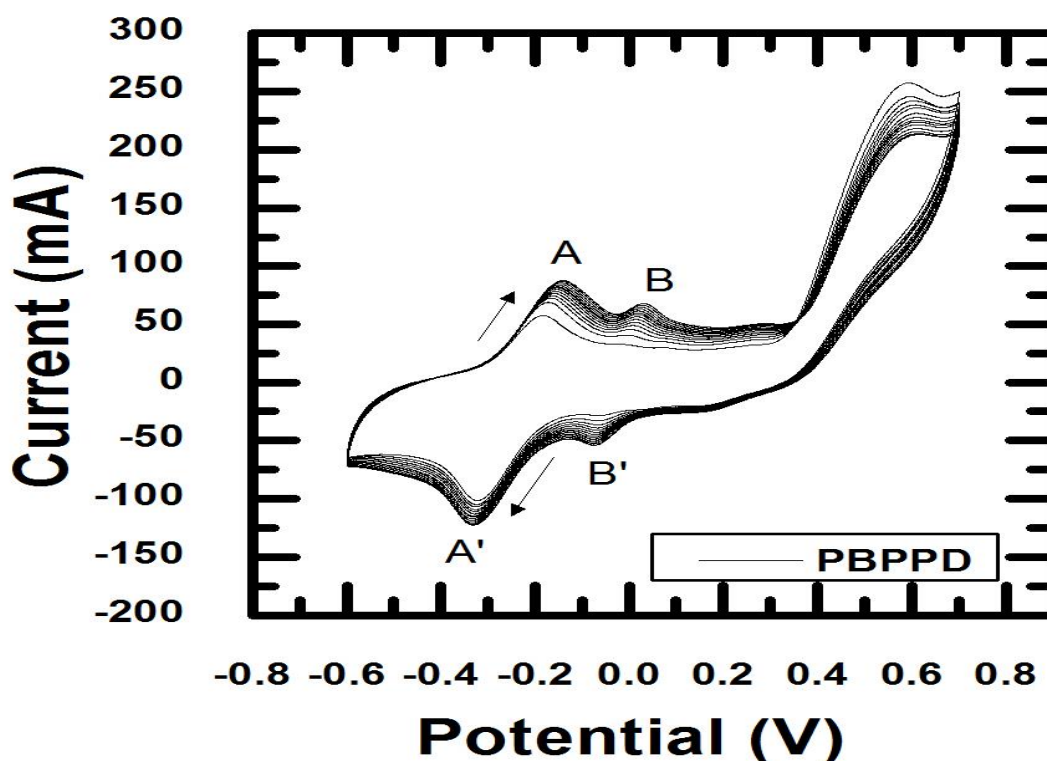


Figure 40. Electrochemical polymerization of 20 mM BPPD at SPCE in DMF/0.1 M HCl at 50 mV/s for 15 cycles.

The growth of the polymer material at the surface of a SPCE was monitored by cyclic voltammetry where an increase in peak current is observed in the oxidation sweep (peak A). The reductive sweep indicated an effective immobilization of the adsorption of the polymer material (peak A'). The same process can be observed for the B-B' peak couple (**Figure 40**).

As the polymer material grows the chain length of the conducting polymer increases. Starting materials were polymerized in order to observe their electropolymerization behaviour.

Similarly to the electrochemical method and parameters selected for the polymerization of BPPD, oPD and P2C were also polymerized at the surface of a SPCE.

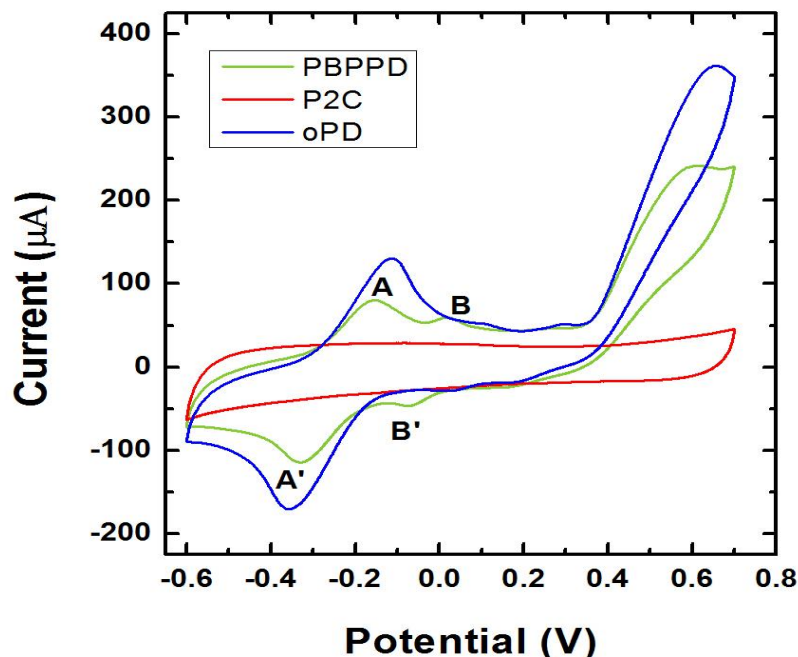
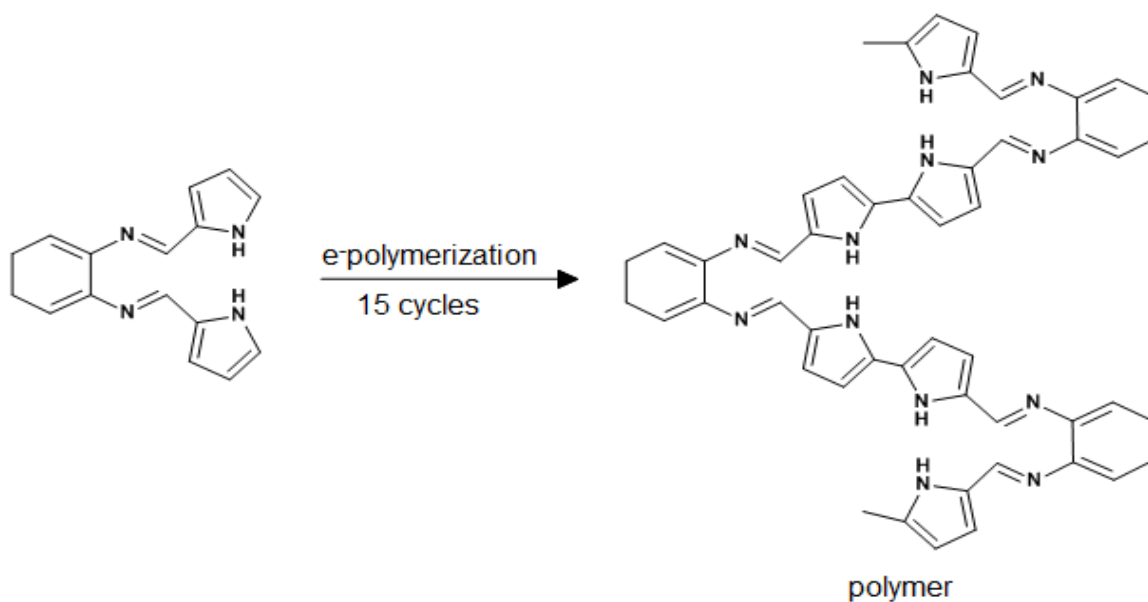


Figure 41. Electrochemical polymerization of oPD, P2C and PBPPD in an equivolume ratio of DMF:0.1M HCl.

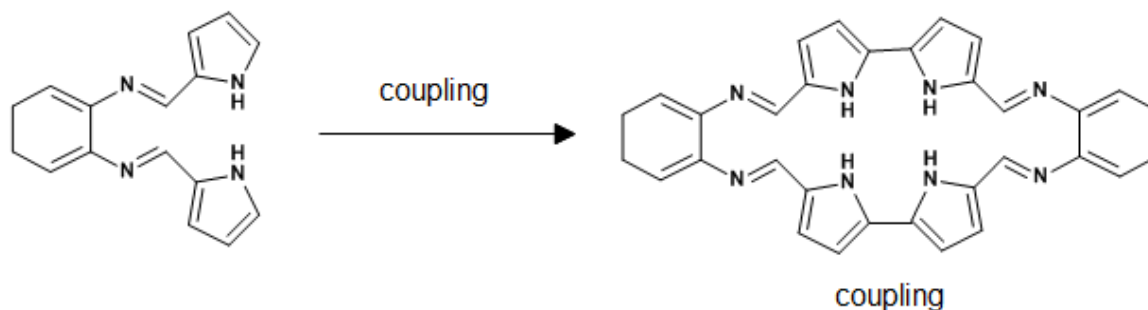
The voltammograms of the polymerization of both starting materials and the polymerized monomer were overlaid and used to determine the characteristics of the polymer material (**Figure 41**). The polymer material displayed a reversible couple (A-A') attributed to oPD, however a new reversible couple (B-B') is displayed. This couple was attributed to the newly formed azomethine bond, as P2C does not display any redox peaks. The thin film at the surface of the screen printed carbon electrode was called poly(N,N'-Bis-(1H-pyrrol-2-ylmethylene)-benzene-1,2-diamine) – PBPPD. The two structural formations below are proposed methods of the electrochemical preparation of the polymer material, the pyrrole linkage to produce the zig-zag polymer (**Scheme 8**) or the coupling material (**Scheme 9**).

Scheme 8 can be attributed to polymerization of the monomer where the peak current grows with each cycle. Scheme 9 is based on the preparation at a glassy carbon electrode surface, where the same electrochemical parameters are applied. However during the polymerization cycles the materials peak current only grows for 2 polymerization cycles and thereafter the peak current decreases. The two possibilities include polymerization or cyclization



WESTERN CAPE

Scheme 8. Proposed structural formation of the polymerization observed at SPCE.



Scheme 9. Proposed structural formation of the cyclization observed at GCE.

5.10 Electrochemical characterization of poly(N,N'-Bis-(1H-pyrrol-2-ylmethylene)-benzene-1,2-diamine) prepared at the screen printed carbon electrode

This novel polymerized material was characterized microscopically (atomic force microscopy and scanning electron microscopy) and electrochemically in 0.1 M LiClO₄ in terms of CV and SWV to evaluate the electrochemical signature within this aqueous media. This novel thin film was characterized by differentiating between a bare screen printed electrode and the modified screen printed carbon electrode.

5.10.1 Atomic force microscopy

The images below were obtained using the atomic force microscopy technique, the images display the differences between an unmodified (**Figure 42**) and polymer modified (**Figure 43**) SPCE.

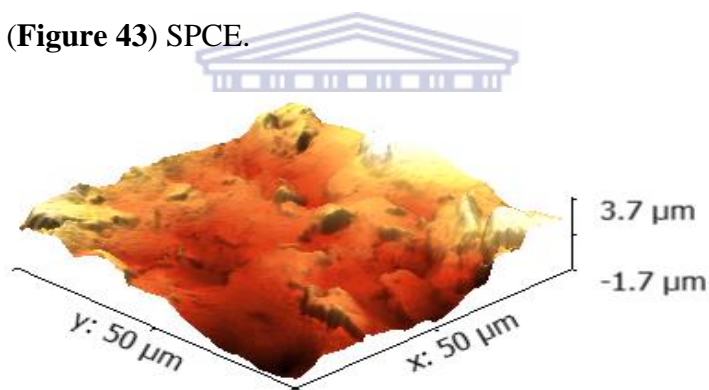


Figure 42. AFM image of an unmodified screen printed carbon electrode.

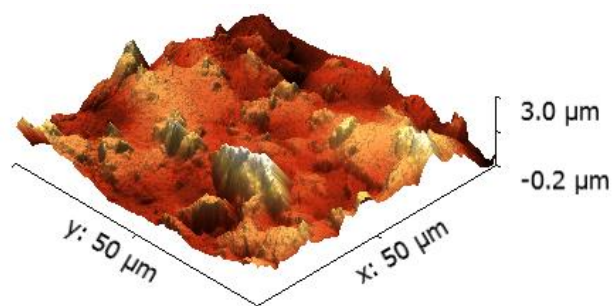


Figure 43. AFM image of a screen printed carbon electrode modified with PBPPD.

Table 15. AFM analysis obtained from the SPCE platform.

Material	Image Size (μm)	Line Roughness (mV)	Area Roughness (mV)
Bare SPCE	50	45.96	49.25
PBPPD	50	52.34	44.60

The polymer material at the surface of the SPCE has a maximum height of $3.0 \mu\text{m}$, $0.7 \mu\text{m}$ less than that of the bare SPCE. This is also observed from the line and area roughness obtained for the electrodes (bare vs modified SPCE) (**Table 15**).

5.10.2 Scanning electron microscopy

The 3-dimensional images of the monomer (solid chemical) and the polymer material prepared at the screen printed carbon electrode surface. The difference between the two materials is that the monomer (BPPD) displayed a significantly different image compared to the of the polymer (PBPPD) material.

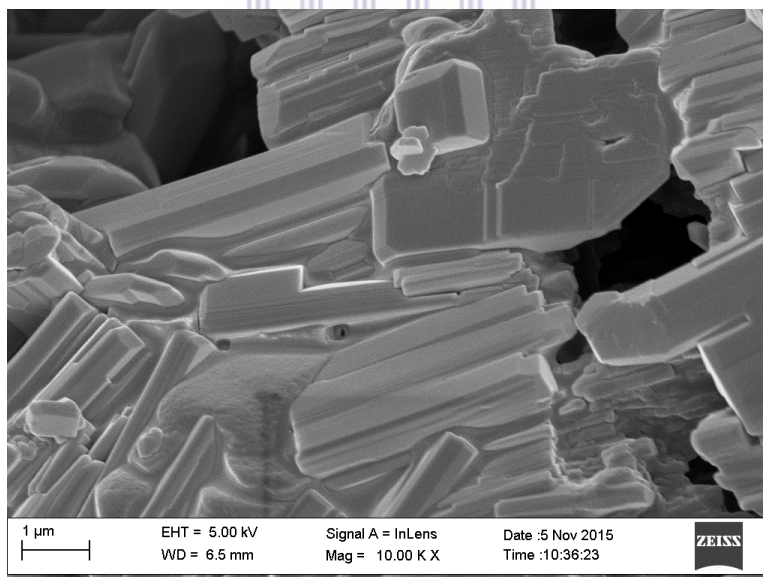


Figure 44. SEM image of BPPD novel monomer.

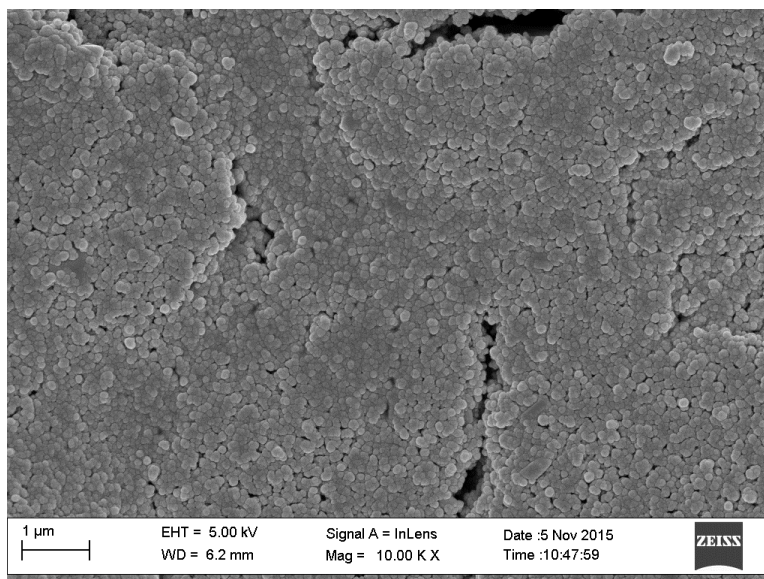


Figure 45. SEM image of the polymer material PBPPD.

The images revealed that the monomer material (BPPD) showed characteristics of a rod-like structure (**Figure 44**). The image of the polymer material displayed layers upon layers of a globular shaped structure (**Figure 45**). These globular shaped structure reminiscent of polymerized polypyrrole, using the oxidant iron (III) chloride.[43]

5.10.3 Electrochemical characterization

The electrochemical behaviour of the polymer material was explored using the CV technique in a 0.1 M LiClO₄ electrolyte solution. A CV technique was used to characterize the polymer, by sweep cycling the potential from -1.0 to +1.0 V and then back to -1.0 V. A scan dependent analysis was performed in order to determine the diffusion coefficient of the polymer material.

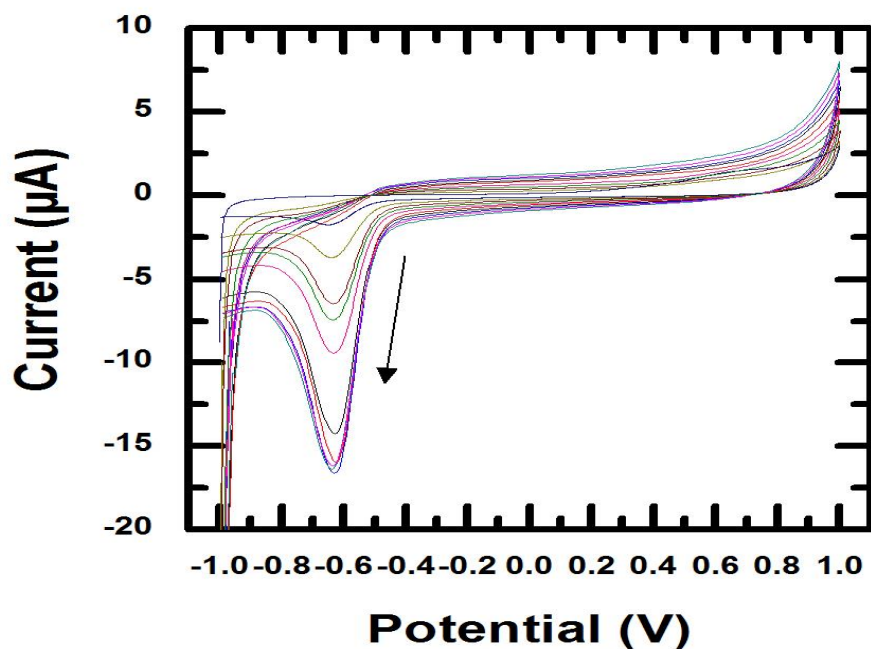


Figure 46. Electrochemical signature of PBPPD in 0.1 M LiClO₄ characterized by cyclic voltammetry.

The electrochemical signature obtained using this CV technique revealed one reduction peak with increasing peak current at lower scan rates (10 – 80 mV/s). At higher scan rates the peak current behaviour became erratic (90 - 100 mV/s) (**Figure 46**). SWV analysis revealed a different electrochemical signature compared to that of the CV technique. The more sensitive nature of the SWV technique allows for reversible couples to be explored as this technique focusses on individual sweeps rather than the complete cycling process. The same electrochemical potential window for CV was used in the SWV. The SWV of the polymer was also studied by a scan rate dependent analysis. The scan rate used in SWV is determined by the frequency (Hz) and potential step (V) parameters.

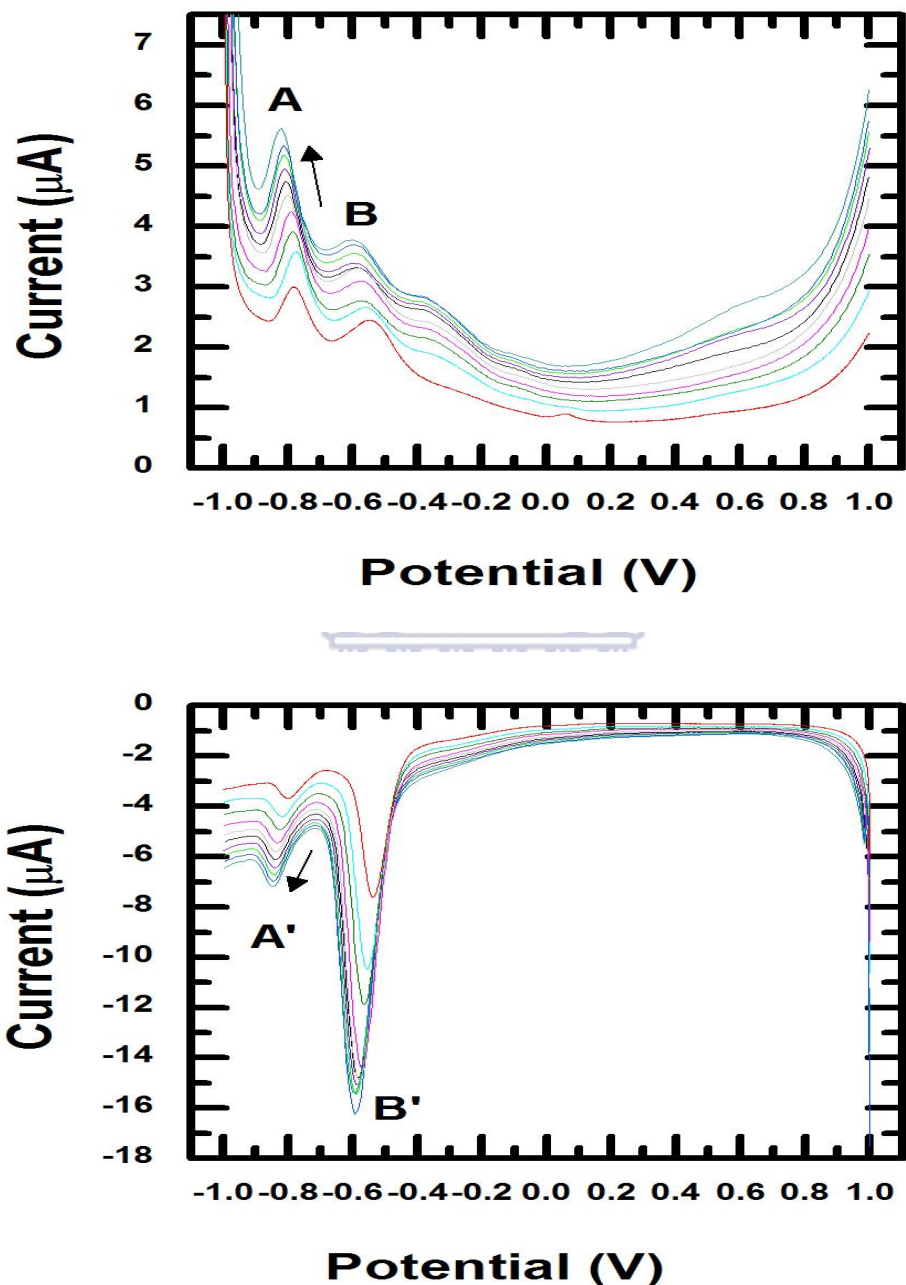
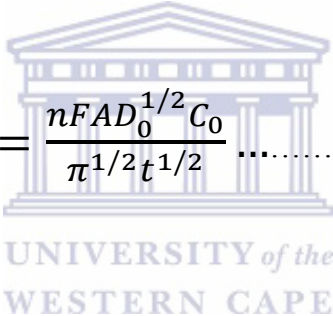


Figure 47. Electrochemical signature of PBPPD redox process by SWV, oxidation (above) and reduction (below) behaviours.

The SWV displayed 2 reversible peaks, however the A-A' couple was the more consistent of the redox couples and was used for quantitative analysis (Figure 47). The other redox couple displayed erratic electrochemical behaviour. Data provided in the SWV technique was scan

rate dependent ranging from low (10 mV/s) to high (100 mV/s) ranges. The SWV technique displayed an increase in peak current with each scan rate, high scan rates resulted in higher peak current values allowing for the determination of electrochemical properties (diffusion coefficient, number of moles, a change in potential, formal potential) at a frequency of 10 Hz. The diffusion coefficient for a square wave controlled experiment was determined using the more concise form of the Cottrell equation (**Equation 3**).[21] The measured current was dependent upon the rate at which the analyte diffused to the SPCE surface. Under semi-infinite conditions for linear diffusion, the current behaves as a function of time which can be denoted by the Cottrell equation. Based on Fick's second law of diffusion, Frederick Gardner Cottrell (1903) derived the relationship between an electrical current and time in an electrochemical experiment.



$$i_p = \frac{nFAD_0^{1/2}C_0}{\pi^{1/2}t^{1/2}} \dots \text{Equation 3}$$

Where;

- i_p : peak current (anodic or cathodic)
- n: number of electrons
- F: Faradaic constant (96485 C/mol)
- A: Area of the electrode (cm²)
- D₀: Diffusion coefficient (cm²/s)
- C₀: Concentration of electrolyte (mol/cm⁻³)
- t: Time (s), pulse width

Scan rate (v) for a square wave voltammetry experiment was determined by **Equation 4**;[87, 209]

$$\text{scan rate (mVs}^{-1}\text{)} = \frac{E_{step} \text{ (mV)}}{t \text{ (sec)}} \dots\dots\dots \text{Equation 4}$$

Based on the inversely proportional relationship between the scan rate and time ($v \propto 1/t$), the $1/t^{1/2}$ in equation 2 was replaced with $(v/E_{step})^{1/2}$.

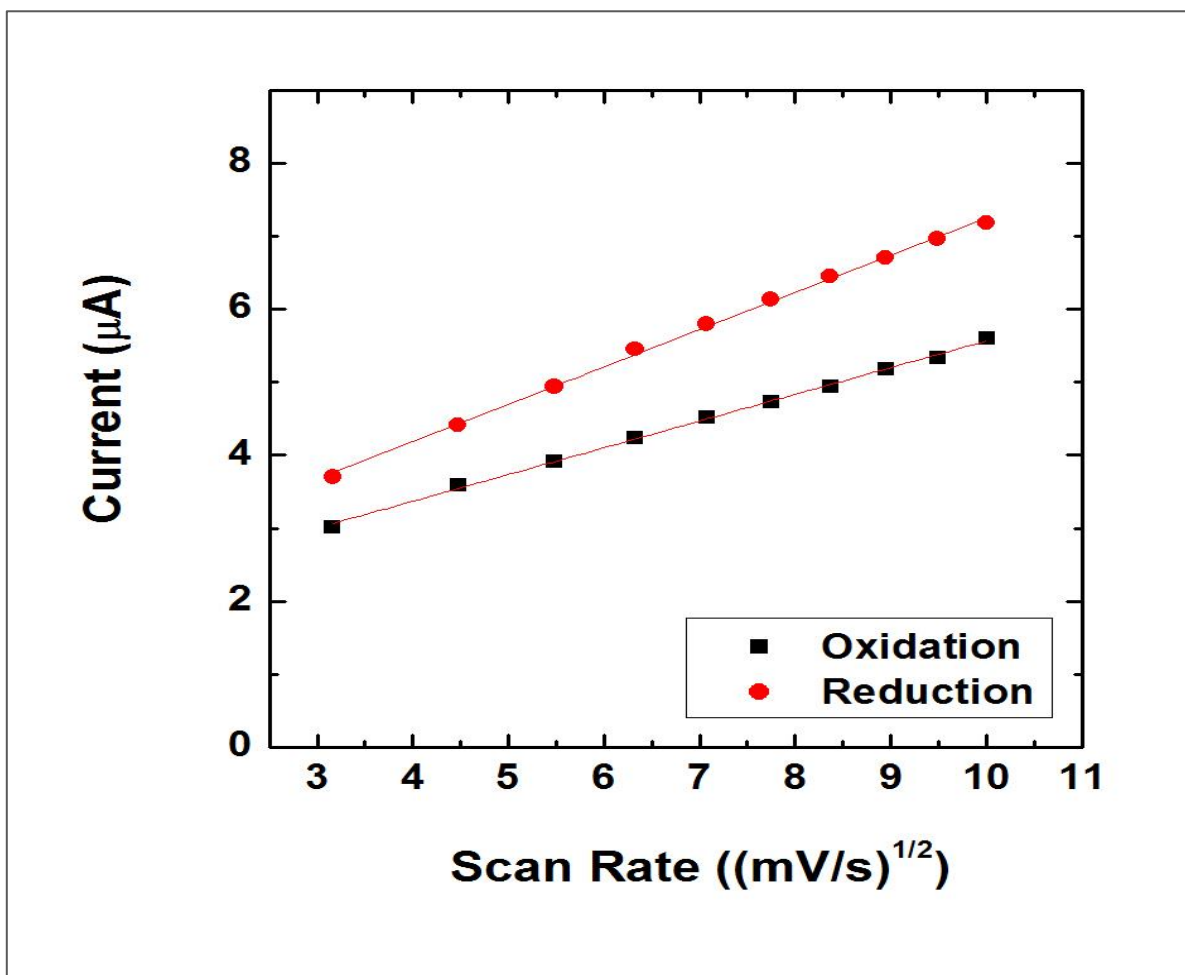


Figure 48. Plot of PBPPD based on the Cottrell equation.

The respective diffusion coefficient was determined by plotting the peak current versus the scan rate based on the Cottrell equation for SWV voltammetry (**Figure 48**). Since the diffusion coefficient was calculated from the slope of the plot of current versus $(\text{scan rate})^{1/2}$

from the linear curve, the approximation of E_{step} led to the approximation of the diffusion coefficient. The Cottrell equation was further summarized to determine the diffusion coefficient by using the slope of the peak current versus scan rate graph in **Equation 5**.

$$D_0 = \left(\frac{\text{slope} \cdot \pi^{1/2}}{nAF C_0} \right)^2 \dots\dots\dots \text{Equation 5}$$

Electrochemical information such as formal potential (E°), peak separation (ΔE_p) and the number of electrons (n) (**Table 16**) was obtained based on the respective SWV voltammograms. The diffusion coefficient (D_0) values were obtained using the Cottrell equation for SWV measurements (**Table 17**).

Table 16. Electrochemical parameters obtained from the characterization of PBPPD.

Scan rate (mV/s)	$E_{p,a}$ (mV)	$E_{p,c}$ (mV)	ΔE_p (mV)	E°	n
10	-781	-800	19.0	-790.5	3.16
20	-774	-820	46.0	-797	1.30
30	-784	-824	40.0	-804	1.50
40	-788	-834	46.0	-811	1.30
50	-800	-839	39.0	-819.5	1.54
60	-807	-839	32.0	-823	1.88
70	-809	-842	33.0	-825.5	1.82
80	-813	-846	33.0	-829.5	1.82
90	-813	-847	34.0	-830	1.76
100	-821	-847	26.0	-834	2.31

Table 17. Diffusion coefficient values for PBPPD.

Peak	Redox Potential	Slope ($\mu\text{A}/\text{V}\cdot\text{s}^{-1}$)	D_0 ($\text{cm}\cdot\text{s}^{-1}$)	R^2
A	Oxidation	3.66×10^{-01}	4.47×10^{-15}	0.9983
A'	Reduction	5.10×10^{-01}	8.70×10^{-15}	0.9983

Based on the information obtained from the electrochemical measurements from square wave voltammetry for the polymer material, the diffusion coefficient for the oxidation process is quicker than that of the reduction process. This indicated that the electrons in solution moved quicker to the surface of the electrode in the oxidation process (Table 17).

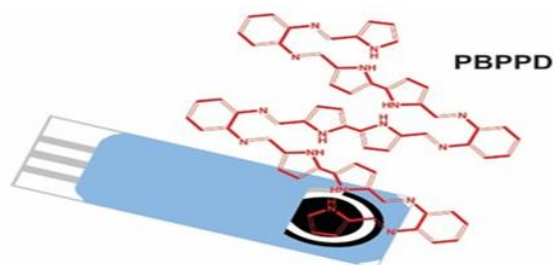
The spectroscopy characterization provided clear information about the structural behaviour of the resulting Schiff base material. The regions of interest in the FTIR spectrum were the regions where the presence of primary amines, carbonyl group and the azomethine bond were observed. The linkage between the aldehyde derivative and the primary amine was confirmed by the presence of the azomethine bond. Absorption bands in the Schiff base material displayed properties of both the primary amine and the aldehyde derivative. The Schiff base materials was exposed to high temperatures to determine the thermal stability of the material, the thermal stability of the material was up to 171.12 °C. Electrochemical preparation of the polymer material at the screen printed carbon electrode surface was performed using the cyclic voltammetry technique, 15 cycles. Two proposed structures are possible during the electrochemical polymerization, either the zig zag conformation or the coupling conformation. The electrochemical signature of the polymer material in 0.1 M LiClO₄ displayed a reversible couple present at negative potentials. Microscopy techniques provided a way to observe the materials at a microscopic level to determine the presence of a thin film at the screen printed carbon electrode.

6. Electrochemical evaluation of selected polycyclic aromatic hydrocarbons at poly(N,N'-Bis-(1H-pyrrol-2-ylmethylene)-benzene-1,2-diamine) modified screen printed carbon electrode

This chapter describes the application of the polymer platform to the electrochemical evaluation of the 12 selected PAHs. As before SWV was used to evaluate the 12 selected PAHs.

Square wave voltammetry is a technique which allowed us to evaluate Faradaic processes in the absence of dominant capacitive currents. The electrochemical windows selected for the oxidative SWV of the selected PAHs was set at -1.0 to +1.0 V. A scan rate of 50 mV/s was achieved by setting the frequency at 10 Hz and the step potential at 5 mV. The working electrode in the 3 electrode electrochemical cell was a SPCE and the electrolyte solutions were 0.1 M HCl and 0.1 M LiClO₄.

The species selected for the inclusion at this novel polymer platform were ANT, ANY, BaP, BbF, CHR, FLA, NAPH, PHEN, PYR, 1-OHP, TRIP and DMBA (**Figure 49**). The study of PAHs redox behaviours at this novel polymer platform was reported here for the first time in a comprehensive manner.



poly(N,N'-Bis-(1H-pyrrol-2-ylmethylene)-benzene-1,2-diamine)

Detection of PAHs at PBPPD Platform

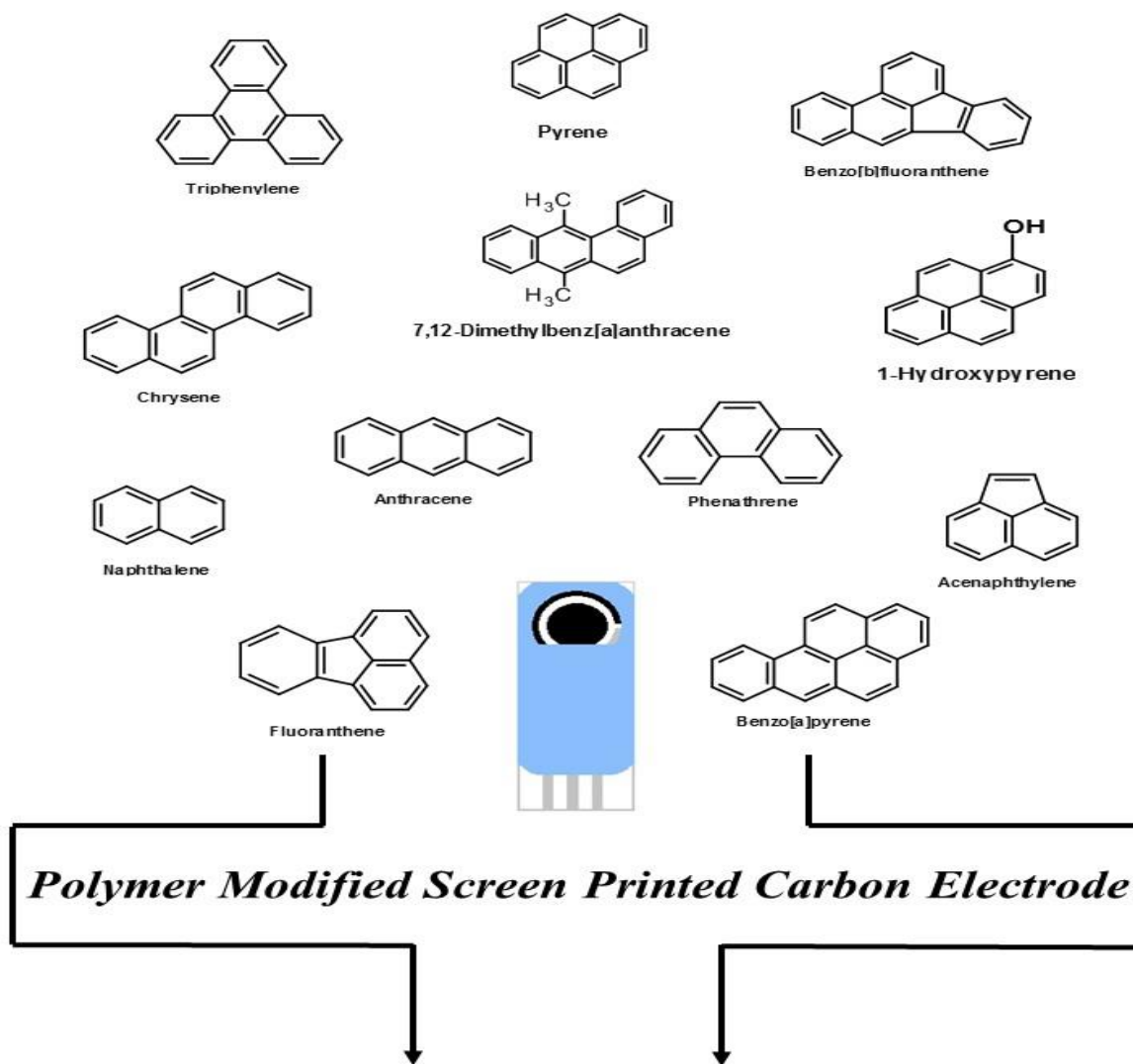
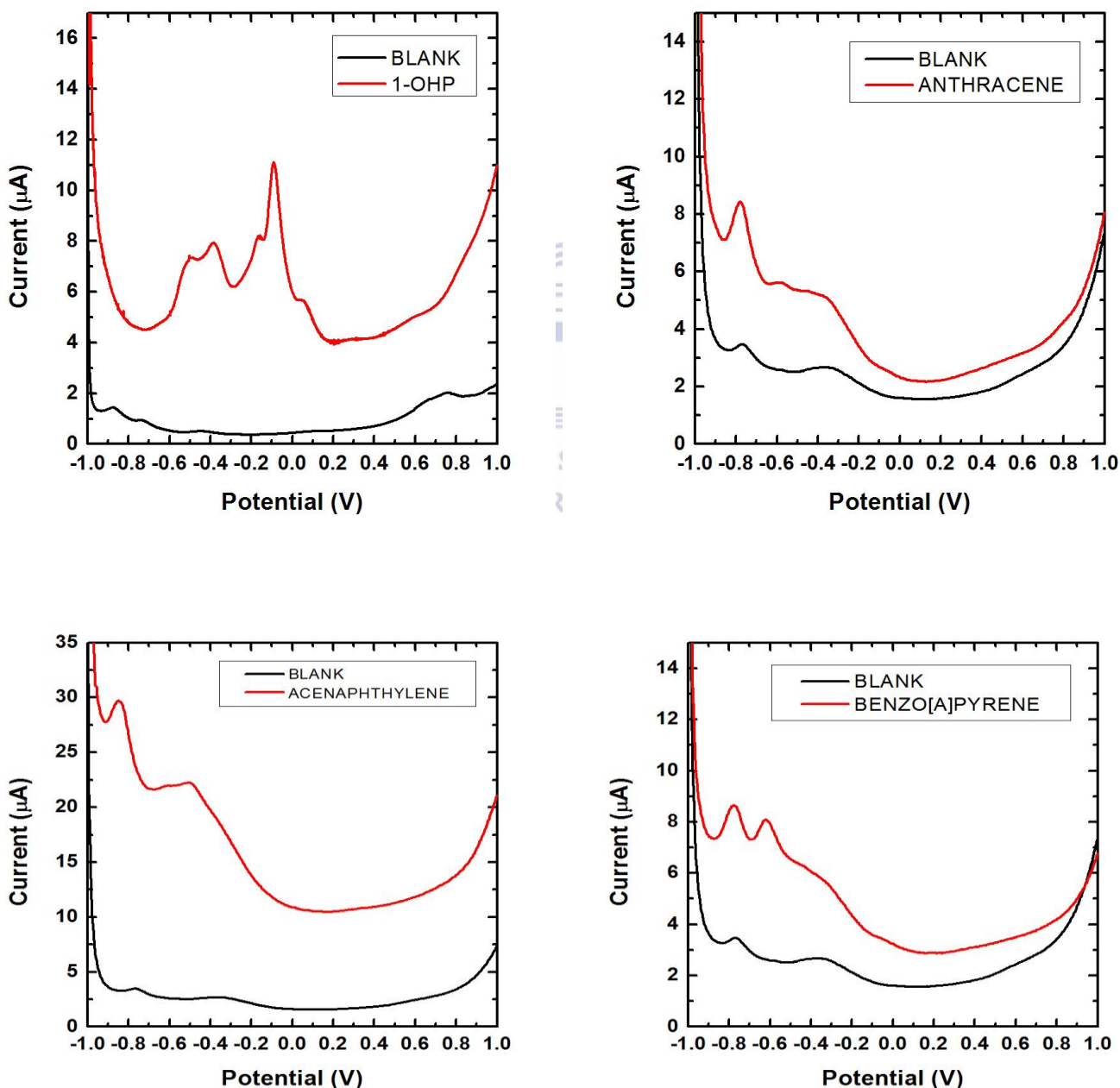
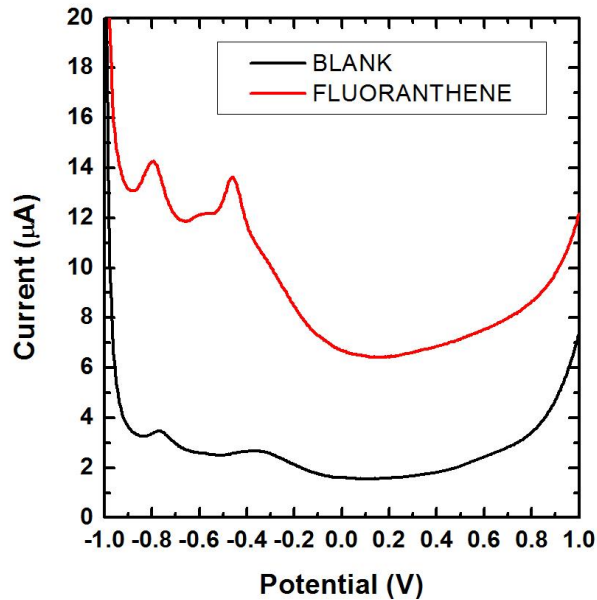
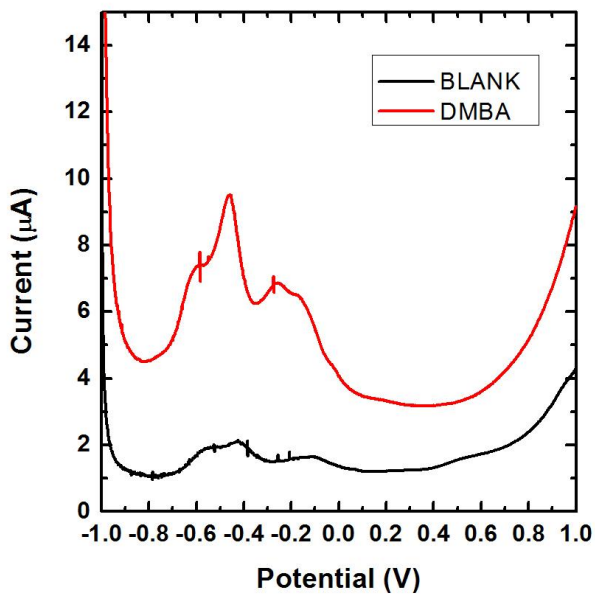
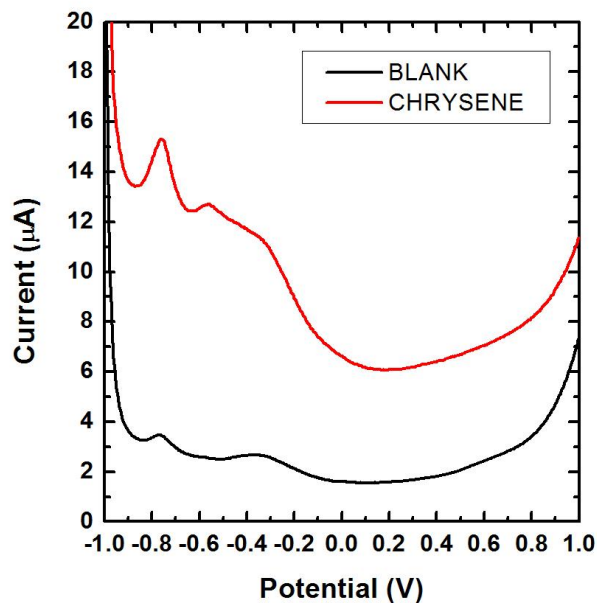
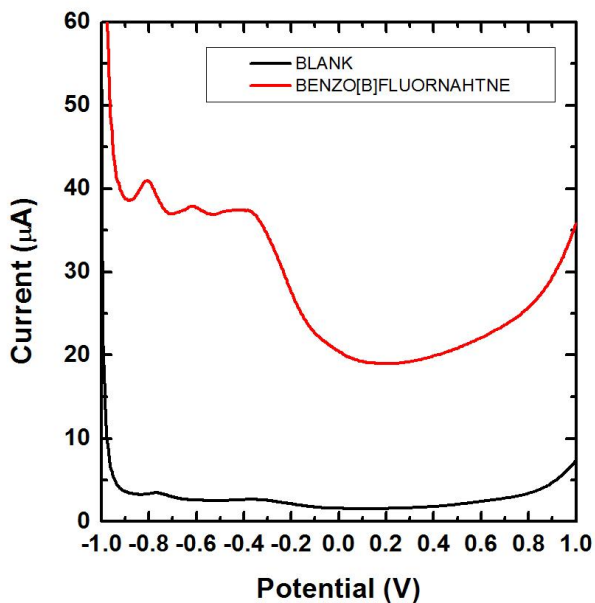


Figure 49. Structural images of the selected polycyclic aromatic hydrocarbons evaluated at this novel platform.

6.1 Electrochemical screening of polycyclic aromatic hydrocarbons

The redox behaviour of the 12 selected PAHs was performed by SWV in 0.1 M LiClO₄. The electrochemical window used for the oxidative SWV was set at -1.0 to +1.0 V. A scan rate of 50 mV/s was achieved by setting the frequency at 10 Hz and the step potential to 5 mV vs Ag/AgCl (Figure 50).





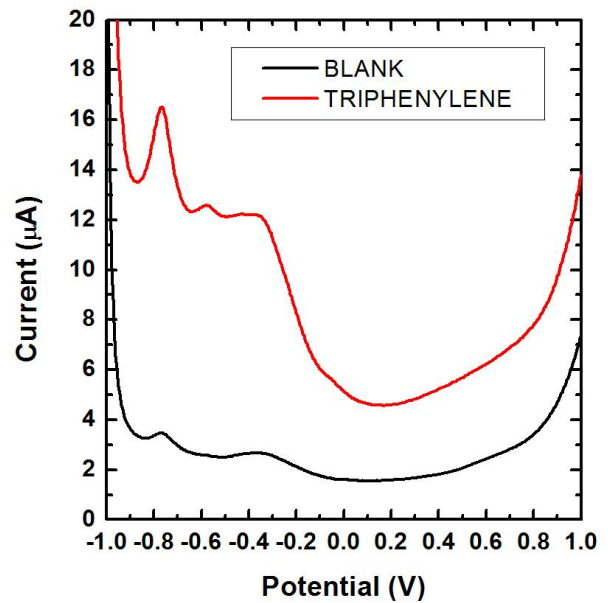
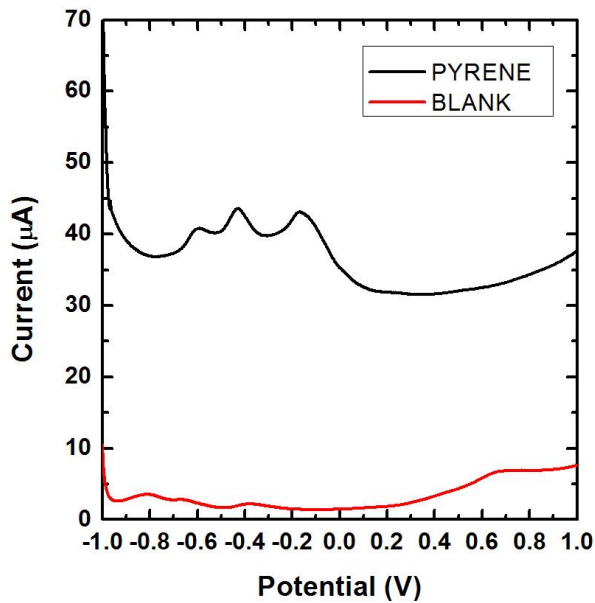
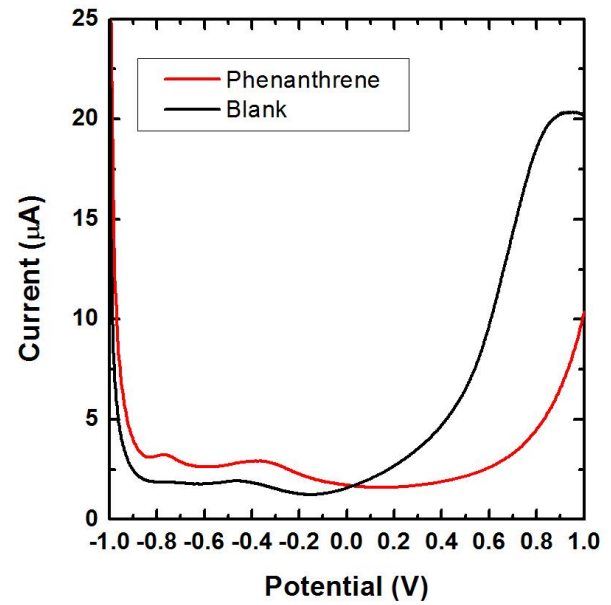
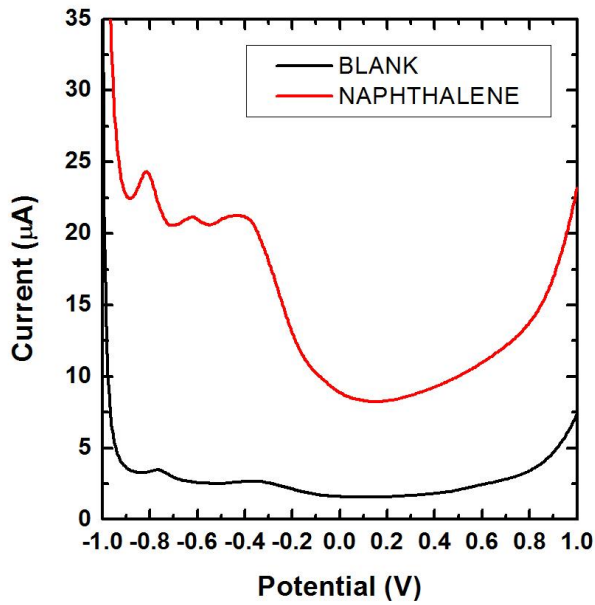


Figure 50. Electrochemical signatures of (a) 1-OHP, (b) ANT, (c) ANY, (d) BaP, (e) BbF, (f) CHR, (g) DMBA, (h) FLA, (i) NAPH, (j) PHEN, (k) PYR and (l) TRIP at the modified polymer platform.

The strongest anodic peak currents were observed for 1-OHP, BaP, DMBA, FLA and PYR. The selected PAHs for evaluation at the novel polymer platform was BaP and FLA, for which quantitative analysis was performed. For all other PAH species inconsistent peak response was recorded as a function of increasing concentration (**Table 18**).

Table 18. Electrochemical screening of polycyclic aromatic hydrocarbons at the polymer modified bare screen printed carbon electrode.

PAHs	Concentration (ppb)	Peak Potential (V)
	SWV	
1-hydroxypyrene	1088	-0.50 -0.38 -0.16 -0.09
7,12-dimethylbenz(a)anthracene	1269	-0.59 -0.46 -0.26 -0.17
Acenaphthylene	660	-0.50
Anthracene	663	No peak
Benzo(a)pyrene	2321	-0.62
Benzo(b)fluoranthene	1557	-0.62
Chrysene	709	-0.56
Fluoranthene	2772	-0.46
Naphthalene	791	-0.62
Pyrene	1512	-0.60 -0.43 -0.17
Phenanthrene	1640	No peak
Triphenylene	990	-0.58

Similarly to literature reports explored at the bare SPCE, there is a lack of information regarding the SWV behaviour of PAHs

Responses of the selected PAHs displayed well defined electrochemical signatures for both BaP and FLA (**Table 18**). The information obtained for these 2 PAHs indicated their sensitive nature towards the polymer platform at low concentrations. Further screening of

these 2 PAHs in aqueous media would better describe their respective behaviours at the polymer platform. Consecutive concentration analysis would determine their limit of detection within an aqueous media. Electrochemical oxidation mechanisms for the selected PAHs helped in the explanation of the observed electrochemical signatures.

6.2 Quantitative Analysis of benzo(a)pyrene and fluoranthene

Stock solutions of BaP (126155 ppb) and FLA (101130 ppb) were prepared in methanol. The electrochemical window used for the oxidative SWV of BaP and FLA was set at -1.0 to +1.0 V. A scan rate of 10 mV/s and 50 mV/s was achieved by setting the frequency at 10 Hz and the step potential at 1 mV vs Ag/AgCl and 5 mV vs Ag/AgCl, respectively. A modified polymer transducer was used in the quantitative determination of BaP and FLA in 4 mL 0.1 M LiClO₄ (electrolyte solution). Consecutive concentration additions of BaP within a concentration range of 939 to 4852 ppb was then added to the electrolyte solution respectively (Figure 51).

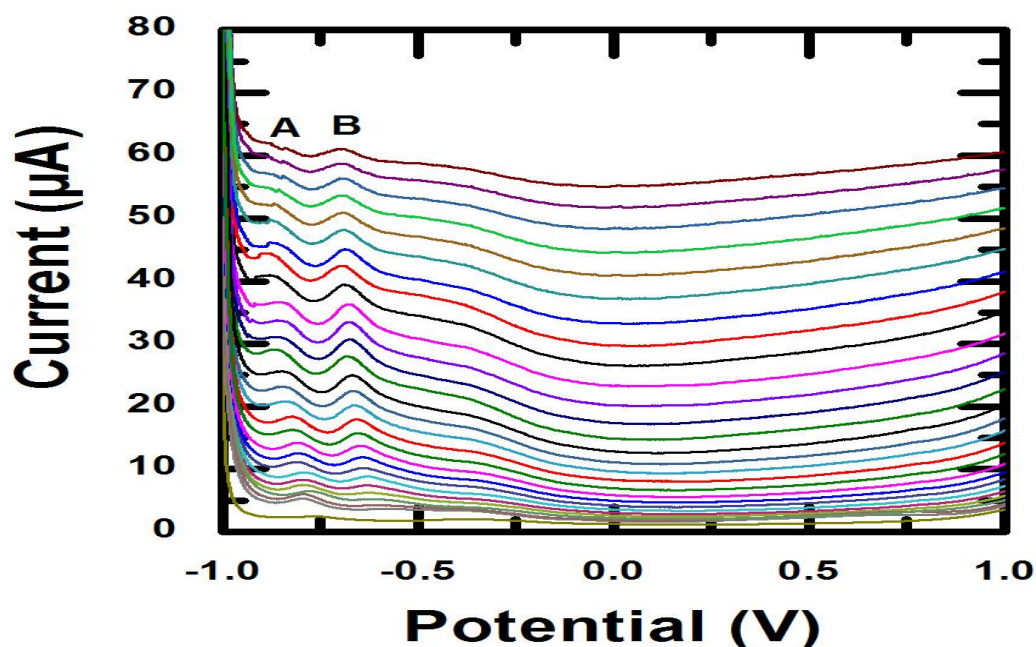
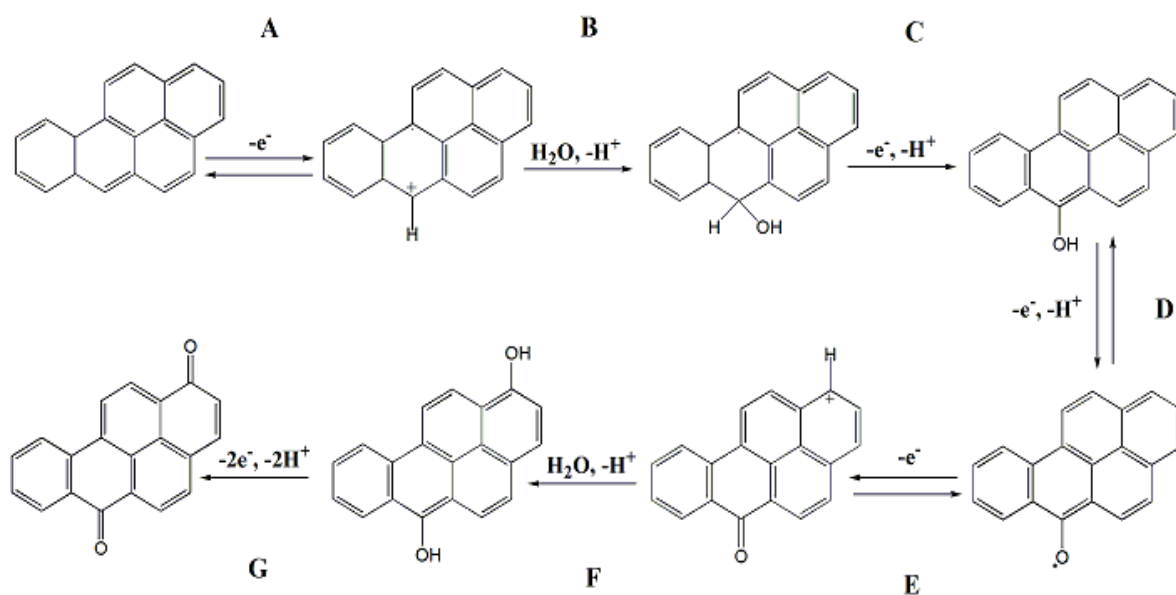


Figure 51. SWV analysis of benzo(a)pyrene (B) at the modified polymer SPCE (A) in 0.1 M LiClO₄ in the concentration range 939 to 4852 ppb, at 50mV/s.

2 peaks were identified during the evaluation of BaP at potentials of -0.85 V vs Ag/AgCl and -0.67 V vs Ag/AgCl attributed to the polymer peak and BaP peak (**Figure 51**). The peaks represent by the voltammogram of BaP can be attributed to the respective steps in the oxidation mechanism of BaP. The change in observed peak currents occur as a result of consecutive concentration addition which was used to plot a calibration curve of current versus concentration. The calibration curve for BaP provided useful quantitative analysis in the determination of the LOD. The LOD was related to the minimum concentration that can be detected by the system.



Scheme 10. Electrochemical oxidation of benzo(a)pyrene.

The initial step in the oxidation process of BaP is a one-electron transfer process which results in the formation of radical ion species. Nucleophilic attack by water occurred at the carbon atom with the highest positive charge density. This then led to the formation of the hydroquinone structure (**Scheme 10**).[90, 113]

The high capacitive background current was attributed to the charging and discharging of the electrochemical double layer at the surface of the electrode. The use of the SPCE and the modification of its surface with the polymer material both contributed to the high capacitive current. Similarly during the detection of the PAHs at the bare screen printed carbon platform

a sigmoidal curve was employed. The Boltzmann fit was used for fitting the data in the calibration curve (**Figure 52**).

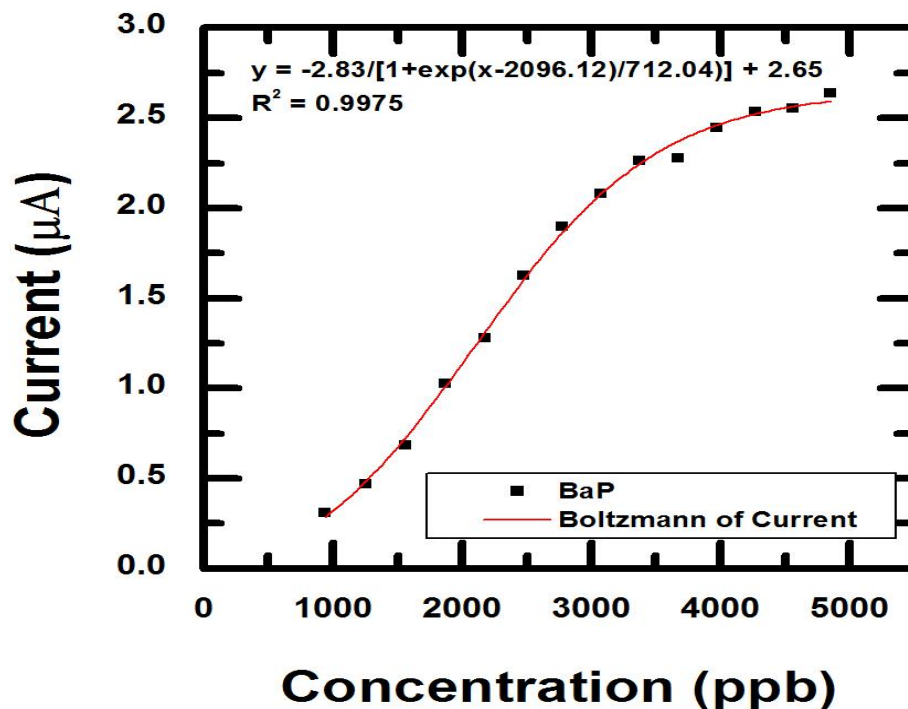


Figure 52. Calibration curve of the screening of BaP.

The background capacitive still remained high due to the polymer material at the surface of the screen printed carbon electrode. The peak current versus the concentration of the FLA gave rise to a sigmoidal calibration curve. Hydrophobicity is another factor influencing the competition at the binding sites as the binding affinity of PAHs (cross-reactivity) predominantly contributes to the analytical signal. The hydrophobicity of porous films can be attributed to the trapped air within the pores, this causes the prevention of water from entering the pores resulting in a higher contact angle. The hydrophobicity of the polymer material is greatly dependent on the type of dopant used.[197] Consecutive concentration additions of FLA within a concentration range of 252 to 4816 ppb was then added to the electrolyte solution respectively (**Figure 53**).

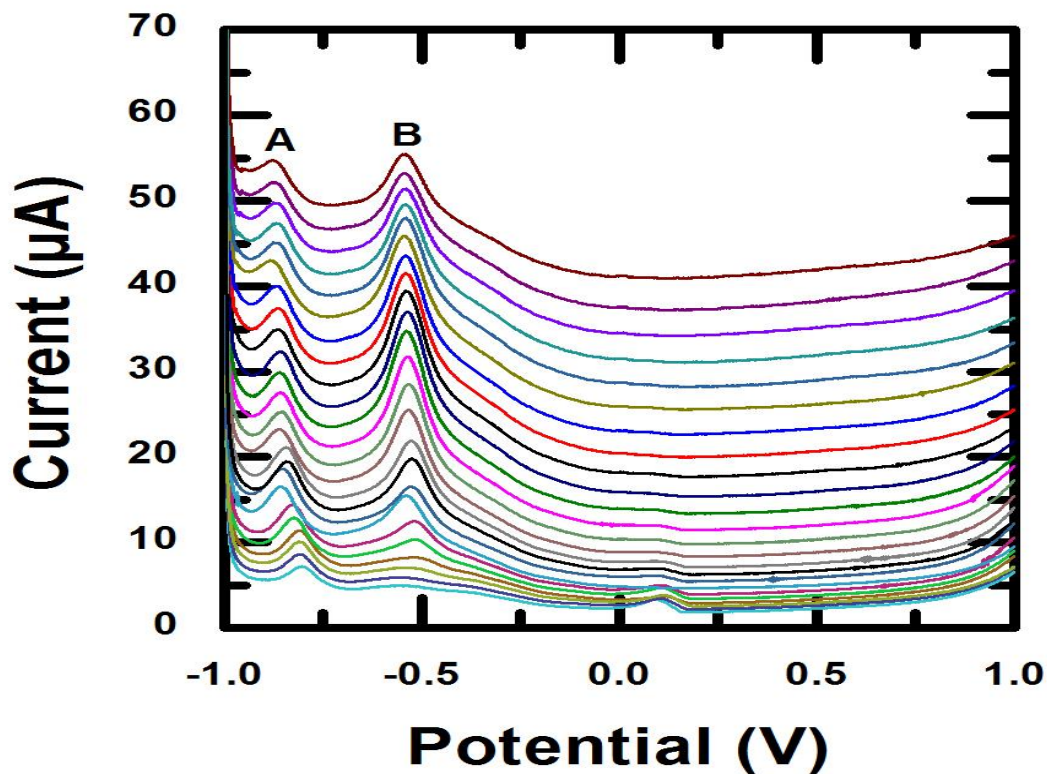


Figure 53. SWV analysis of fluoranthene (B) at the modified polymer SPCE (A) in 0.1 M LiClO₄ in the concentration range 252 to 4816 ppb, at 10mV/s.

2 peaks were identified during the evaluation of FLA at potentials of -0.85 V vs Ag/AgCl and -0.54 V vs Ag/AgCl attributed to the polymer peak and FLA peak. The peaks represent by the voltammogram of FLA can be attributed to the respective steps in the oxidation mechanism of FLA. The change in observed peak currents occur as a result of consecutive concentration addition which was used to plot a calibration curve of current versus concentration. The calibration curve for FLA provided useful quantitative analysis in the determination of the LOD. The LOD was related to the minimum concentration that can be detected by the system.

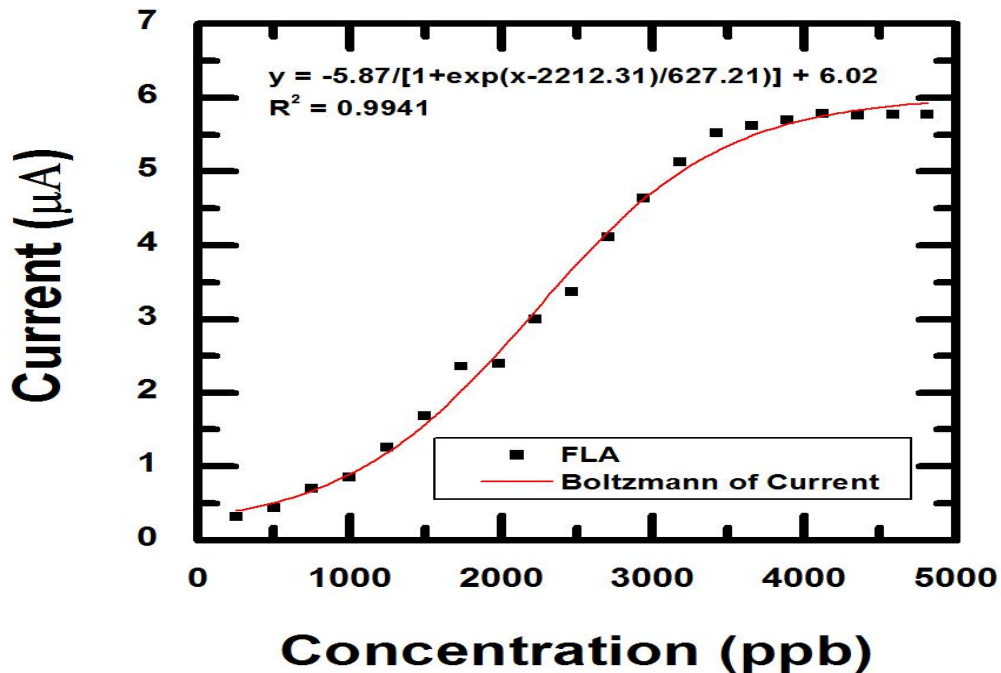


Figure 54. Calibration curve of the screening of FLA.

Based on the above calibration curve it is evident that the data follows a sigmoidal calibration curve, indicative of competition for attachment to the available binding sites at low concentrations (**Figure 54**). The calibration data was modelled as a Boltzmann fit which is based on the non-linear least squares method. The electrochemical parameters selected for the detection of PAHs as well as the results determined from the calibration plot have been tabulated below. The RSD value is an indication of the dispersion or spread of the data results, for n=3 (**Table 19**).

Table 19. Electrochemical parameters and calibration data for BaP and FLA.

Polycyclic Aromatic Hydrocarbons		
	BaP	FLA
Potential Window (V)	-1.0 to +1.0	
Scan Rate (mV/s)	50	10
Peak Potential (V)	-0.68	-0.54
LOD (ppb)	9.46×10^{-7}	1.07×10^{-9}
LOQ (ppb)	3.12×10^{-6}	3.54×10^{-9}
R²	0.9975	0.9941
Slope (μA/ppb)	712.04	627.21
% RSD	11.5	11.5

Calibration data for individual PAHs species using the Boltzmann plot gave rise to a LOD (n=3) for BaP and FLA, found to be 9.46×10^{-7} and 1.07×10^{-9} ppb respectively. The Boltzmann provided high sensitivity (slope of the linear region in the curve) of 712.04 μA/ppb and 627.21 μA/ppb respectively. Linearity coefficient (R²) was determined to be 0.9975 and 0.9941 for BaP and FLA. The voltammetry of urine sample containing BaP was explored at a pencil graphite electrode using adsorptive stripping SWV. This technique was used to determine BaP with a limit of detection of 33 ppb, with a sensitivity and linear regression of 161.54 μA/ppb and 0.9970 respectively.[103] An immunosensor prepared at a GCE was used to detect BaP in phosphate buffer (pH 7.4) using CV. The detection of BaP at immunosensor produced a sensitivity of 0.30 μA/ppb with a limit of detection of 8×10^{-5} ppb (R² = 0.9853).[213] DPV was used to detect BaP at a bare GCE in 0.2 M NaClO₄, a limit of detection of 0.17 ppb was obtained. The sensitivity of the system towards BaP was found to be 3×10^{-3} μA/ppb, with a linear regression of 0.9980.[53] The lack of literature for the detection of FLA results as it is no longer considered as a potential carcinogen to humans. However, the more common methods for the evaluation of FLA is fluorescence spectroscopy and high performance liquid chromatography.

6.3 Quantitative analysis of a complex mixture containing benzo(a)pyrene and fluoranthene

A complex sample matrix was prepared by combining stock volumes of BaP and FLA (1:1) into one solution. The electrochemical window used for the oxidative SWV of BaP and FLA was set at -1.0 to +1.0 V. A scan rate of 10 mV/s was achieved by setting the frequency at 10 Hz and the step potential at 1 mV vs Ag/AgCl. The modified polymer transducer was used in the quantitative determination of BaP and FLA in 4 mL 0.1 M LiClO₄ (electrolyte solution). Consecutive concentration additions of the complex mixture was then added to the electrolyte solution respectively (**Figure 55**).

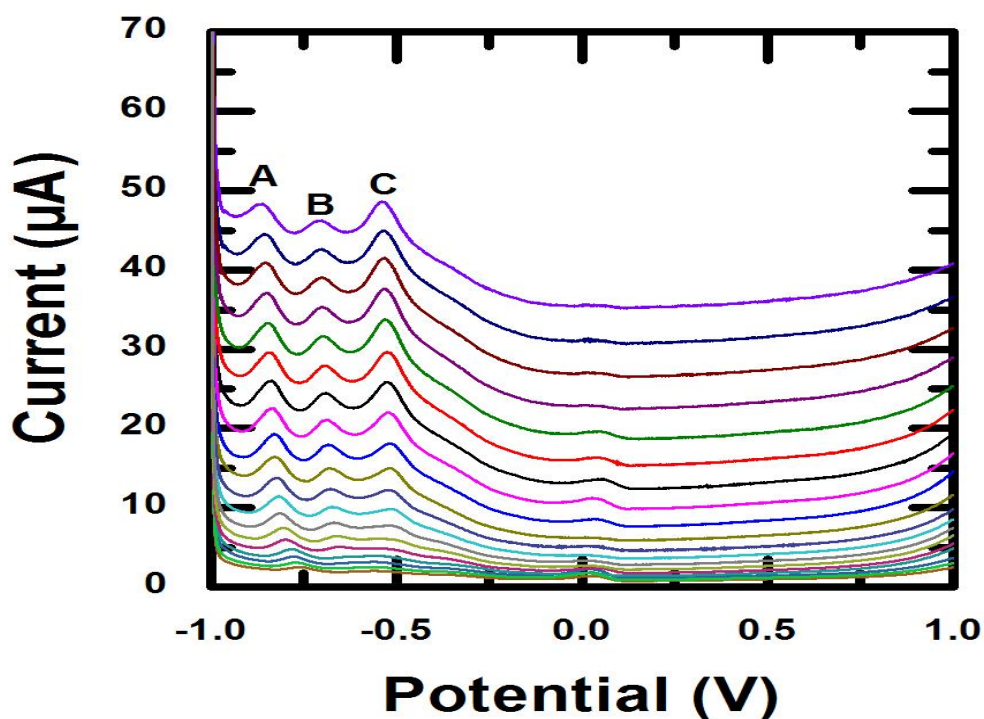


Figure 55. Electrochemical screening of the complex matrix at the polymer platform.

The SWV voltammogram revealed 3 well defined peak attributed to the polymer (A), BaP (B) and FLA (C). These peaks are observed at -0.86 V vs Ag/AgCl, -0.70 V vs Ag/AgCl and -0.54 V vs Ag/AgCl for the polymer, BaP and FLA respectively (**Figure 55**). Evidence from the voltammogram for the complex matrix can be used to clearly distinguish between the polymer and PAHs peaks. The PAHs are well defined and clearly be identified and

quantified within the complex matrix. Similarly during the detection of the BaP and FLA at the polymer platform a sigmoidal curve was employed. The Boltzmann fit was used for fitting the data in the calibration curve.

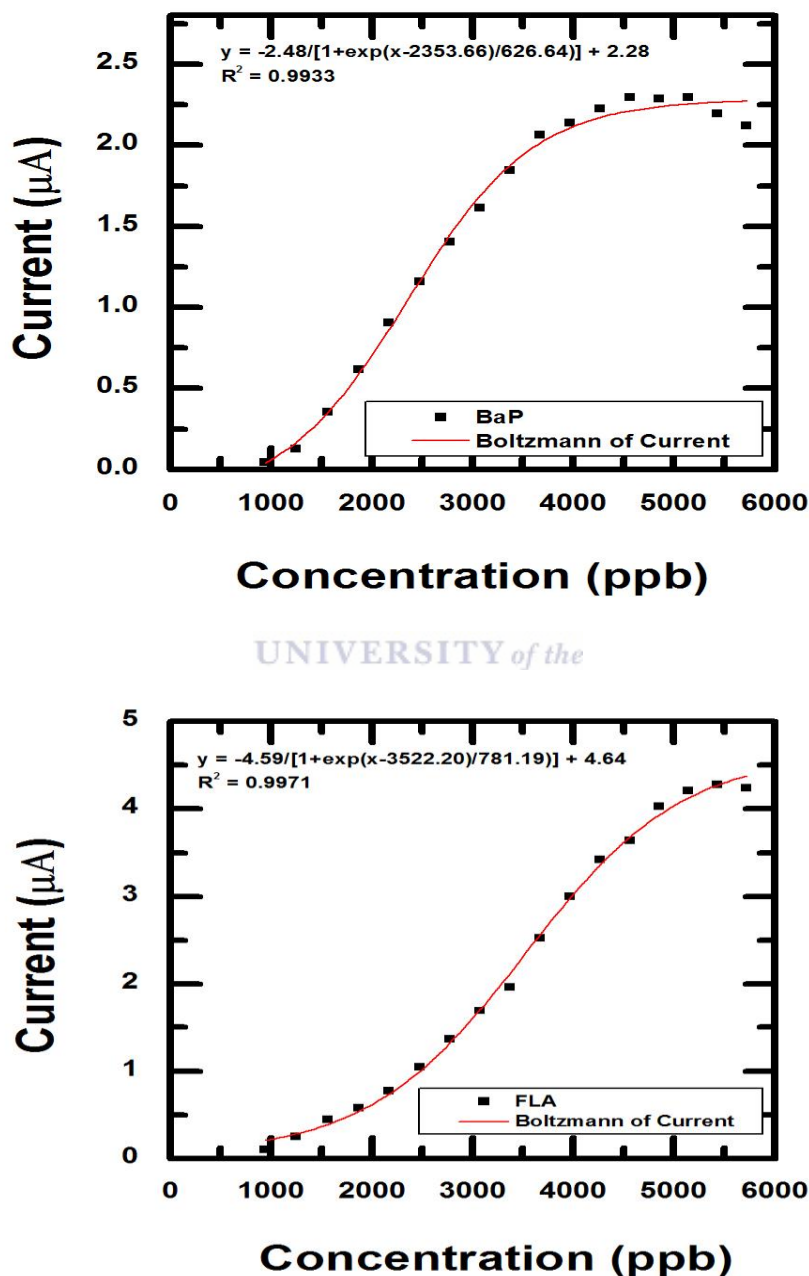


Figure 56. Calibration curves for the complex matrix containing BaP (above) and FLA (below).

The calibration curve provided data that followed a sigmoidal calibration curve, indicative of competition for attachment to the available binding sites at low concentrations (**Figure 56**). The calibration data was modelled as a Boltzmann fit which is based on the non-linear least squares method. The electrochemical parameters selected for the detection of PAHs as well as the results determined from the calibration plot have been tabulated below. The RSD value is an indication of the dispersion or spread of the data results, for n=3 (**Table 20**).

Table 20. Electrochemical parameters and calibration data for the species in the PAHs mixture.

Polycyclic Aromatic Hydrocarbons		
	BaP	FLA
Potential Window (V)	-1.0 to +1.0	
Scan Rate (mV.s⁻¹)	10	
Peak Potential (V)	-0.70	-0.54
LOD (ppb)	4.10x10 ⁻⁹	2.17x10 ⁻⁹
LOQ (ppb)	1.35x10 ⁻⁸	7.16x10 ⁻⁹
R²	0.9933	0.9971
Slope (µA/ppb)	626.64	781.19
% RSD	14.7 (n=3)	27.8(n=3)

Calibration data for individual PAHs species within the mixture using the Boltzmann plot gave rise to a LOD (n=3) for BaP and FLA, which was found to be 4.10x10⁻⁹ ppb and 2.17x10⁻⁹ ppb. The Boltzmann provided high sensitivity (slope of the linear region in the curve) of 626.64 µA/ppb (BaP) and 781.19 µA/ppb (FLA) respectively. Linearity coefficient (R²) was determined to be 0.9933 and 0.9971 for BaP and FLA. Many literature reports have evaluated these complex PAHs mixtures using HPLC and GC methods. No information is provided in literature about the detection of these 2 PAHs species in a complex mixture using voltammetric techniques. Studies have been performed to determine the possible toxic effects of these PAHs species on human breast cell line (MCF-7 cells).

Acute toxicity of these PAHs have been rarely reported in humans, fish or other wildlife species due to low limits of exposure to an individual PAHs species. PAHs are however

associated with chronic risks which have the potential to lead to cancer. Chronic risks result from the exposure to complex PAHs mixtures rather than individual PAHs species. Based on the initial evaluation of the selected PAHs at the polymer modified electrode, it was determined from the oxidation SWV that BaP and FLA provided the most well defined redox peaks. Further evaluation of the selected 2 PAHs was performed to better understand the redox behaviours in aqueous medium. Information obtained from the individual PAHs behaviour allowed for the BaP and FLA to be combined into a complex matrix. The evaluation of the complex matrix revealed 3 well defined electrochemical peaks attributed to the polymer material, BaP and FLA. BaP is the most commonly evaluated PAHs due to its carcinogenic ability, it has therefore been extensively explored by HPLC, GC and electrochemical methods. The maximum contamination level for BaP determined by the U.S. EPA (1974) was 0.2 ppb in drinking water with the WHO determining a limit of 0.7 ppb. FLA currently is not considered a significant health risk PAHs in drinking water.

HPLC using FLD, UV and DAD detectors have all been used in the determination of both BaP and FLA. Detection limits determined from HPLC for BaP range between 1.00×10^{-3} to 8.30×10^{-3} ppb, whereas FLA detection limits range from 9.00×10^{-3} to 2.00×10^{-2} ppb. Wide ranges of PAHs in a complex sample matrix was determined by HPLC. A wide range of electrochemical sensors were employed in the detection of BaP, with sensors including Immunosensors, DNA-biosensors, unmodified glassy carbon and boron doped diamond electrodes. Electrochemical techniques such as amperometry, differential pulse voltammetry and electrochemiluminescence were performed to find detection limits for BaP in the range of 6.00×10^{-3} to 146 ppb. Not much information is provided about the electrochemical detection of fluoranthene. However a Hg film sensor was developed for the detection of multiple PAHs such as phenanthrene, pyrene, anthracene and fluoranthene. The limit of detection for FLA was found to be 3.20×10^{-1} and 2.60×10^{-1} ppb for seawater and buffer solutions respectively. Very few information is provided on chemical sensors for the evaluation of multiple PAHs in a complex mixture.

The selective determination of these PAHs as individuals and in a complex mixture provided a principle basis for these PAHs to be determined in a multichannel design. The electrode

employed in the multichannel design consisted of 8 working electrodes. The screening of BaP and FLA allows for the possibility to employ the use of the 3rd and 4th working electrodes in the multichannel design. The complex mixture allows for these 2 PAHs to be screened at 1 working electrode rather than 2 working electrodes in the multichannel setup (**Figure 57**).



POLYMER MODIFIED SCREEN PRINTED CARBON ELECTRODE

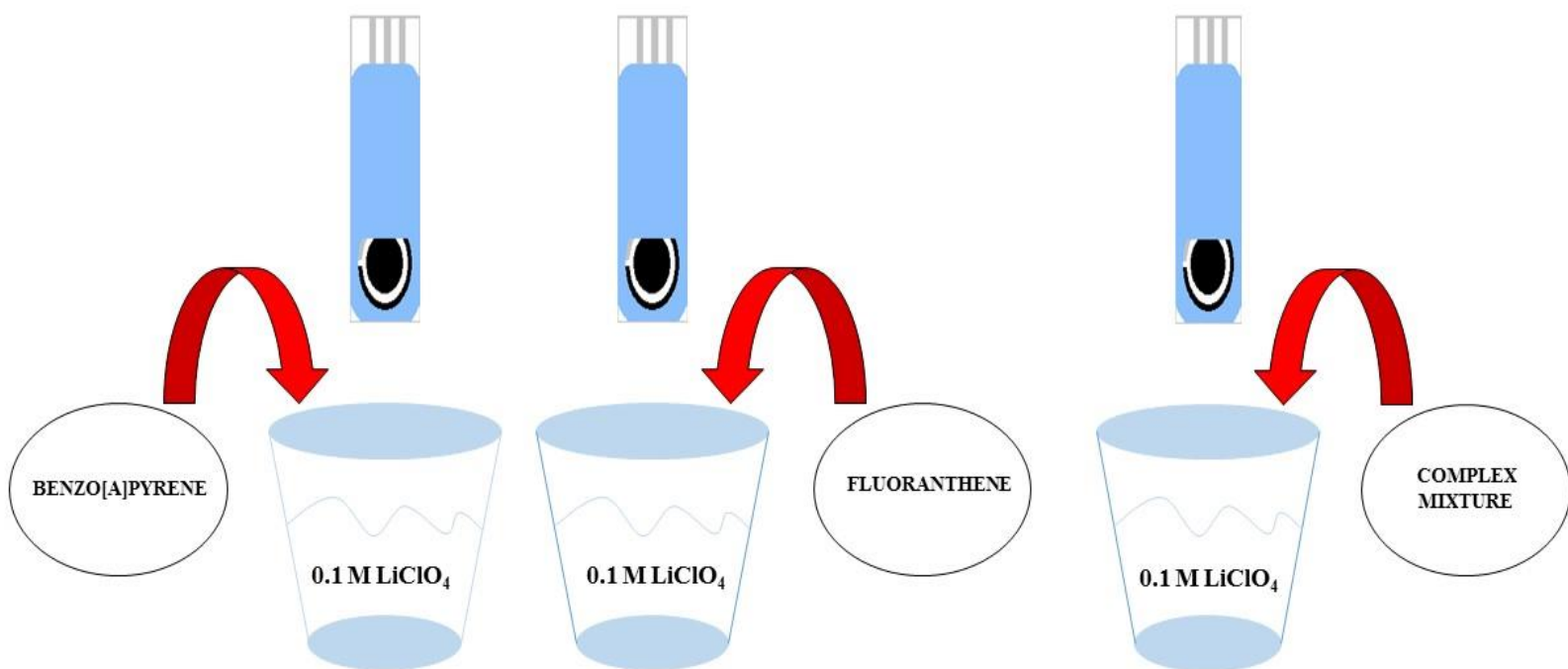


Figure 57. Conclusions based on the information obtained during the evaluation of PAHs at the polymer modified screen printed carbon electrode surface.

7. High Performance Liquid Chromatography Identification, Separation and Detection of Polycyclic Aromatic Hydrocarbons in the presence of Interfering Species

The separation of 8 PAHs using HPLC-UV method allows for retention times to be determined and used for quantitative and qualitative analysis. The quantification of an individual polycyclic aromatic hydrocarbon will be explored within a mixture.

7.1 Introduction

PAHs have traditionally been separated by GC and HPLC, with HPLC methods being useful for PAHs analysis as UV and fluorescence detection have been found to offer enhanced selectivity.[78, 122, 191] HPLC instruments can be equipped with three different detectors of which include UV, FLD and diode array detector (DAD). HPLC methods can perform suitable analysis of compounds with higher boiling points and molecular weights. HPLC methods were developed for simultaneous determination of PAHs, however there are alternative methods for PAHs detection such as FLD due to the fact that most PAHs compounds have high natural fluorescence.[36, 132] A newly developed method efficient and reliable analytical method was developed for sensitive and selective quantification of PAHs in soot samples. LOQ limits ranged between 0.64 (BaP) to 19.0 (indeno(1,2,3-cd)pyrene – I(1,2,3-cd)P) ng/kg in soot samples. Recoveries from spiked real soot samples were approximately 90 %.[11] Smoked fish products from a Turkish market were evaluated in order to determine the levels of potentially carcinogenic PAHs. This method

was used for the simultaneous detection of 16 PAHs salmon and trout samples, the concentration range of total PAHs varied between 23.83 to 79.74 ug/kg. Analysis revealed that LMW PAHs were in higher levels than HWM PAHs. Levels of the carcinogenic compounds which include BaA, benzo(b)fluoranthene (BbF), BkF and B(g,h,i)P was found to be between 0.44 to 9.55 ug/kg.[24] A validation method was developed for the extraction and determination of 16 PAHs from waste water and sediments. Calibration curves provided good linearity for all investigated PAHs compounds, R^2 between 0.991 to 0.996 in a concentration range between 2 to 300 ppb. Analysis obtained from spiked water and sediment samples gave rise to recoveries between 78 to 100 % and 82 to 106 % respectively. Determined LOD and LOQ from the samples were found to be between 0.01 to 0.51 ppb and 0.03 to 1.71 ppb respectively.[109] Sixteen PAHs in fish fillets were determined by HPLC-UV and FLD, with the method employing a multiresidue sample preparation method. Wavelengths used in the analysis of these PAHs compounds were 230 nm (UV) and varying wavelengths for FLD (dependent upon the fluorescent ability of the PAHs). Determined recovery values were found range between 83.4 to 101 % with relative standard deviation between 0.6 to 1.9 %. LOD and LOQ values were found to range between 0.04 to 0.84 ng/g and 0.1 to 2.80 ng/g respectively.[25]. Other methods used for PAHs detection include various electrochemical biosensors, adsorptive stripping voltammetric determination or electrochromatography with mass detection.[19, 50, 66, 202, 218] The major problems associated with using HPLC analysis is that PAHs give rise to structural similarities, which PAHs peaks tend to overlap resulting in problems during identification. These many interferences when performing HPLC analysis is of great concern. PAHs determined from oils and fats samples are time consuming and expensive due to the lipophilic matrices which are complex to isolate from one another.[141] BaP one of the most occurring and problematic (potent) PAHs and various other PAHs have been classified as probable human carcinogens.[70]

In this chapter selected PAHs based on electrochemical measurements were evaluated using an HPLC-UV detection. Concentration profiles of the selected PAHs were studied, to determine their respective retention times. A complex matrix of 4 selected PAHs were

evaluated to determine the behaviour of the PAHs in the complex matrix. PYR was selected as the PAHs of interest due to its close relationship (retention time) with other PAHs. Consecutive concentration additions of PYR were determined within the complex matrix and its respective detection limit was determined.

7.2 Experimental

Reagents and Chemicals

All reagents were analytical or HPLC grade. Acetonitrile (CH_3CN) and all PAHs were purchased from Sigma-Aldrich. PAHs used in the study include BaP, FLA, PYR and 1-OHP, whose chemical structures can be seen below (**Figure 58**).

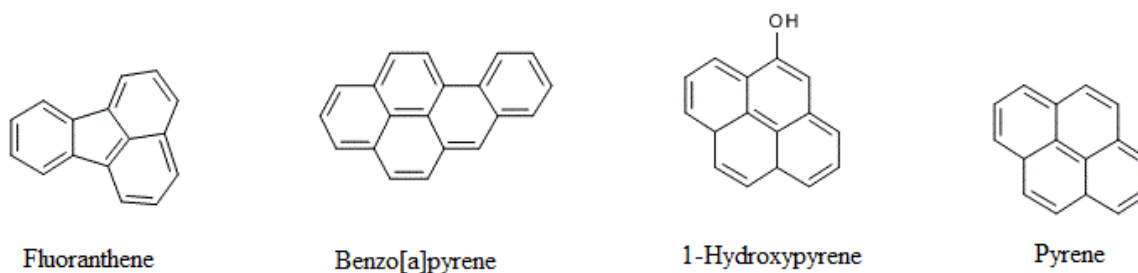


Figure 58. Chemical structures of the polycyclic aromatic hydrocarbons is within this work.

7.3 Standard solutions

Stock standard solutions were prepared by dissolving 10 mg of the desired PAHs in 20 mL CH_3CN . Sonication was used to assist the dissolving of the PAHs, when completely dissolved the PAHs stock standards were further diluted to 50 mL with CH_3CN . Appropriate dilutions were made of the respective PAHs standards in order to simulate the electrochemical screening of the PAHs. Initial work involved the profiling of the relative standards before a mixture of all individual standards was prepared. The mixture was prepared by pipetting 1 mL from from each individual stock standard.

7.4 Instrument and instrument conditions

All analysis was performed using an Agilent 1200 Series HPLC equipped with a UV detector set at a wavelength of 254 nm and a capillary pump.[3, 16, 136, 160] All

data obtained was processed using HPLC 3D ChemStation Software, with HPLC conditions being tabulated below (**Table 21**).

Table 21. HPLC conditions used for the identification of PAHs.

<i>Column</i>	Agilent Eclipse XDB C18 5µm 4.6 x 150mm
<i>Flow Rate</i>	1ml/min
<i>Column Temperature</i>	Room temperature
<i>Injection Volume</i>	20µl
<i>Run Time</i>	20min
<i>Mobile Phase (Isocratic)</i>	75% CH ₃ CN : 25% H ₂ O
<i>Detection</i>	UV at 254 nm

7.5 Interference species and sample preparation

All other PAHs used in the combined stock standard besides the target PAHs (PYR) was used as interfering species. The sample preparation involved adding excess volumes (varying concentrations) of BaP into the combined stock standard, this allowed for a concentration profile of BaP to be determined.

7.6 Results and Discussion

7.6.1 Chromatographic results of standard profiles

HPLC analysis was conducted by using 20 µL injections of the combined stock standards, detection occurred via UV at 254 nm. The mobile phase (75% CH₃CN : 25% H₂O) solvents required thorough degassing prior to use. Initial HPLC work was performed on individual PAHs stock standards, with each PAHs being clearly identified. Standard profiles of the PAHs compounds found to be sensitive during the electrochemical screening process were determined. BaP a marker for the indication for the presence of PAHs contamination was studied by consecutive concentration of BaP (2.04 to 204000 ppb) to determine its respective standard profile (**Figure 59**). Data from the BaP chromatogram was tabulated and used in the determination of the calibration curve(**Table 22**).

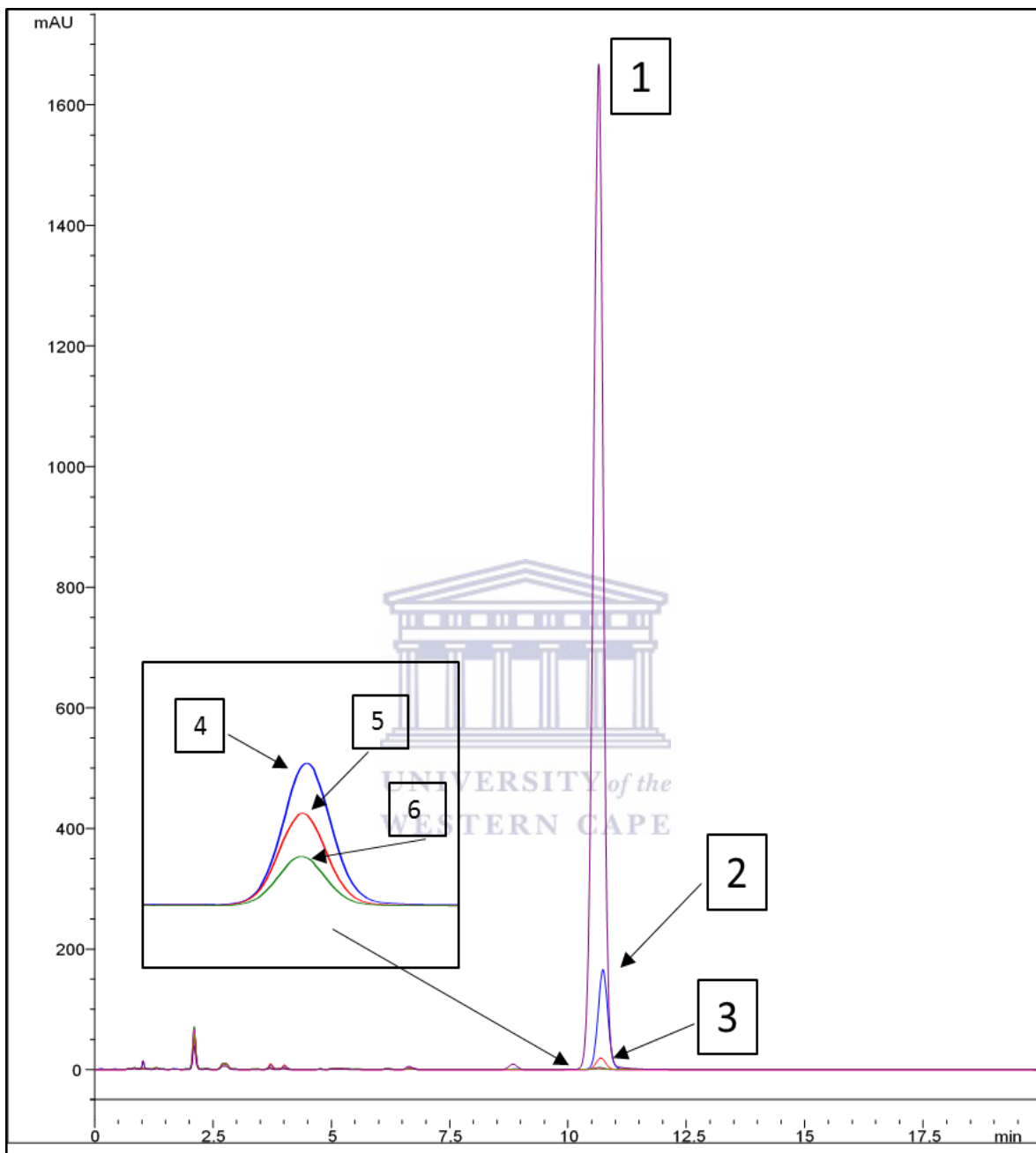


Figure 59. Concentration profile of benzo(a)pyrene standard.

Table 22. Chromatographic data for the BaP standard profile.

BaP STD SAMPLES	Concentration (ppb)	Peak Area (mAU)
1 (Stock)	204000	24793.50
2	20400	2438.47
3	2040	283.59
4	204	48.43
5	20.4	31.36
6	2.04	16.65

The calibration curve profile for the BaP standard was determined and a linear regression of 0.9999 was found (**Figure 60**). The sensitivity of BaP was determined to be 0.1214 mAU/ppb.

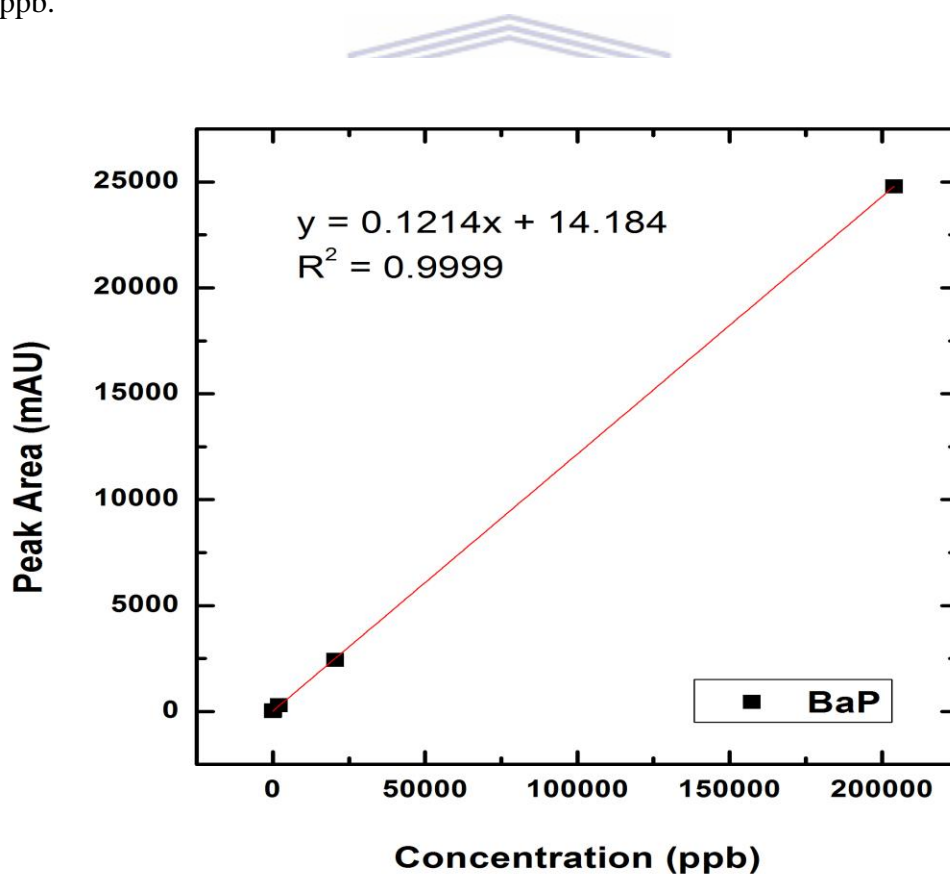


Figure 60. Calibration curve for benzo(a)pyrene standard solution.

1-hydroxypyrene a urinary biomarker was also studied as a standard profile by HPLC. Concentration values ranged between 2.06 to 206000 ppb which gave rise to the concentration profile in the chromatogram (**Figure 61**).

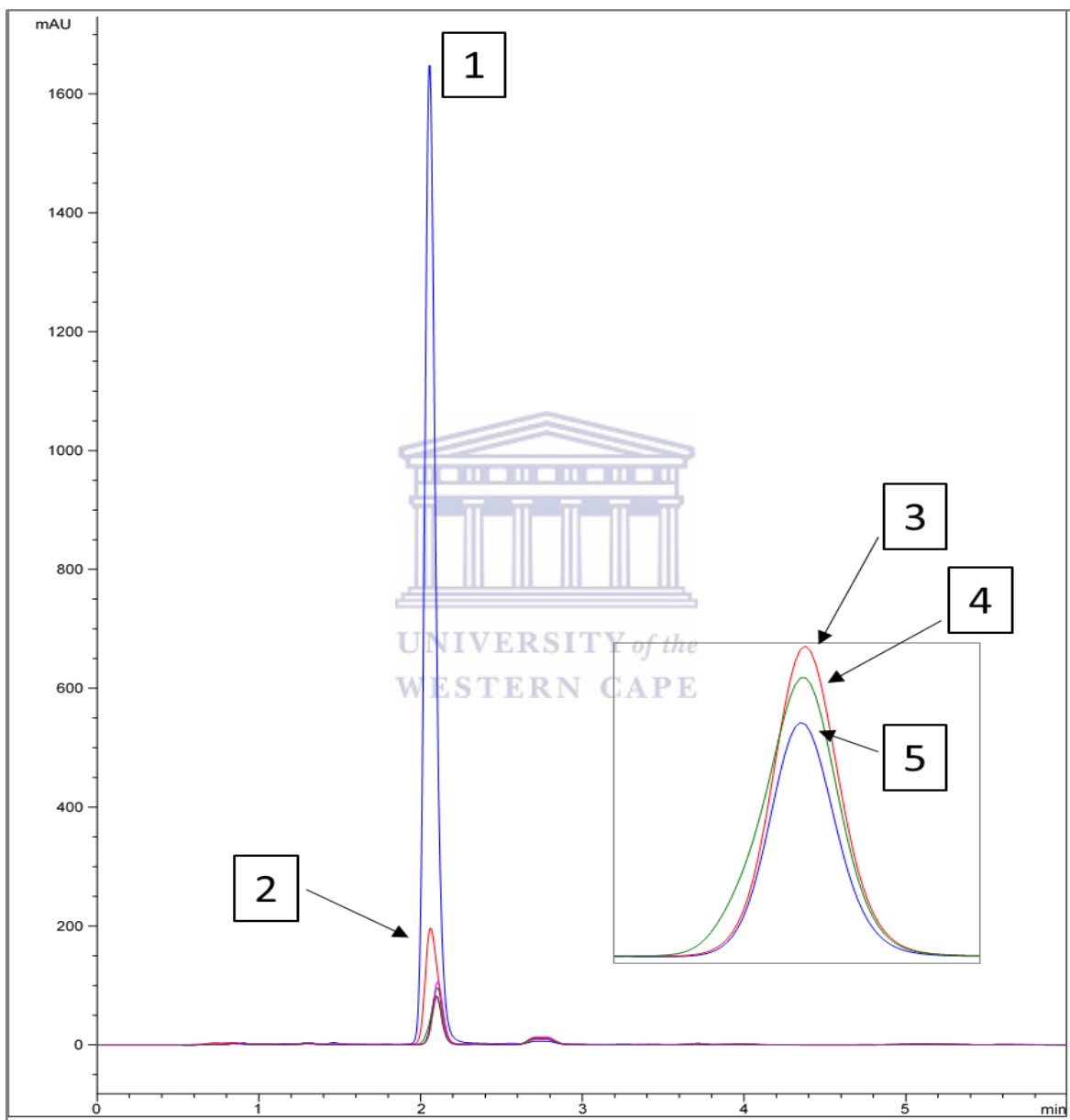


Figure 61. Concentration profile of 1-hydroxypyrene standard.

Peak areas were plotted against their respective concentration values to determine the calibration curve of 1-hydroxypyrene (**Table 23**). The calibration curve provided information such as slope (sensitivity) and linear regression.

Table 23. Chromatographic data for the 1-hydroxypyrene standard profile.

BaP STD SAMPLES	Concentration (ppb)	Peak Area (mAU)
1 (Stock)	206000	7863.48
2	20600	1130.63
3	2060	502.09
4	206	490.82
5	20.6	368.39
6	2.06	379.33

The linear regression and sensitivity of 1-OHP was found to be 0.9998 and 3.61×10^{-2} mAU/ppb respectively (**Figure 62**).

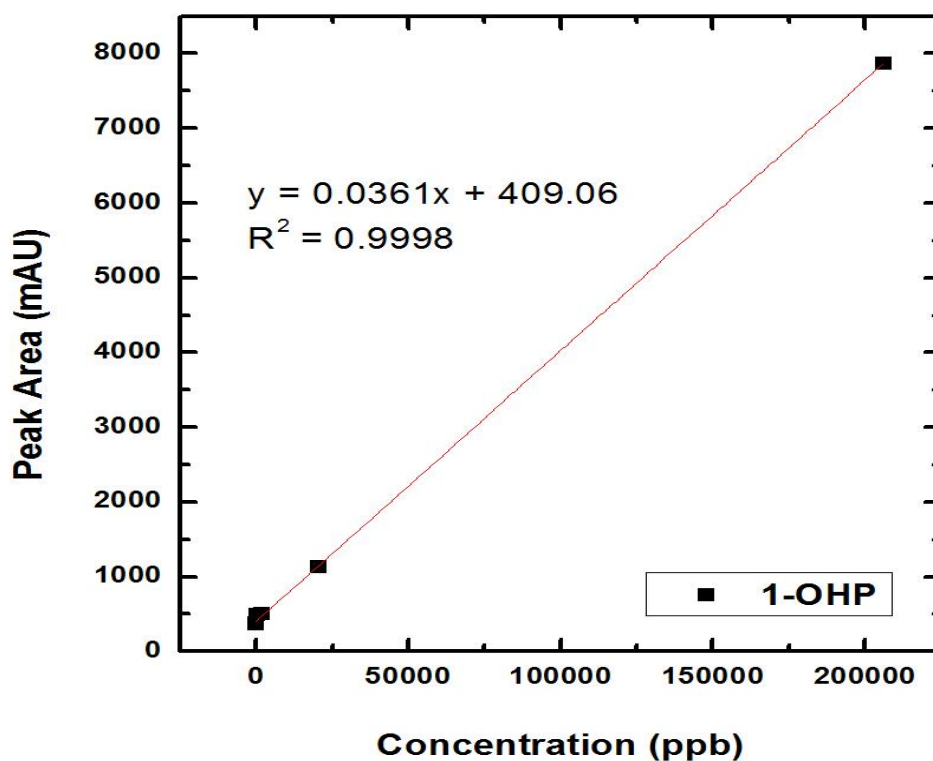


Figure 62. Calibration curve for 1-hydroxypyrene standard solution.

The standard profile of FLA was studied by consecutive concentration additions which ranged between 2.06 to 206000 ppb (**Figure 63**). Information based on the consecutive concentration additions was tabulated and used in the determination of the calibration curve (**Table 24**).

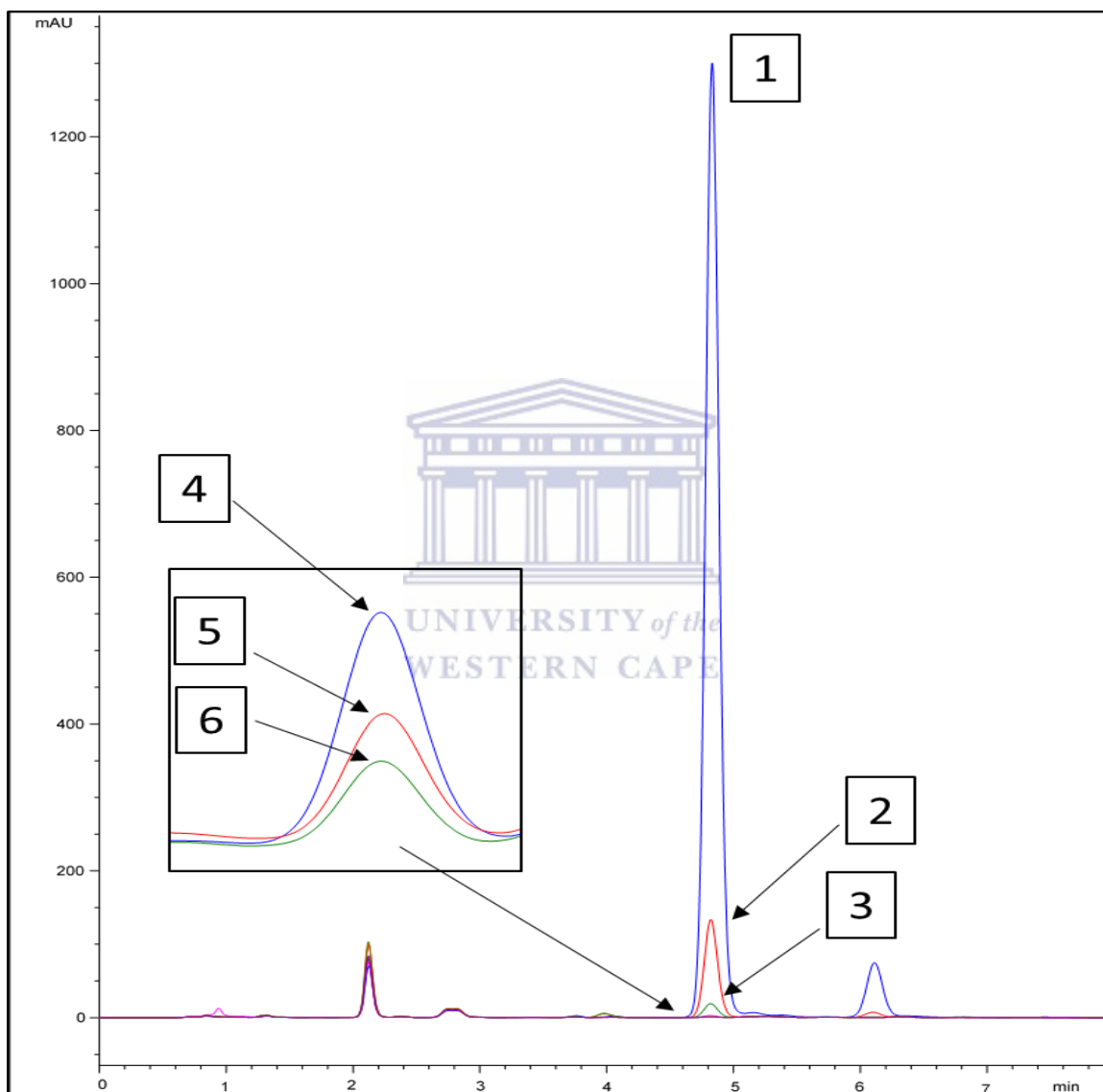


Figure 63. Concentration profile of fluoranthene standard.

Table 24. Chromatographic data for the fluoranthene standard profile.

BaP STD SAMPLES	Concentration (ppb)	Peak Area (mAU)
1 (Stock)	206000	7863.48
2	20600	1130.63
3	2060	502.09
4	206	490.82
5	20.6	368.39
6	2.06	379.33

A linear regression of 0.9999 and a sensitivity of 4.85×10^{-2} mAU/ppb was respectively determined from the calibration curve of FLA (**Figure 64**).

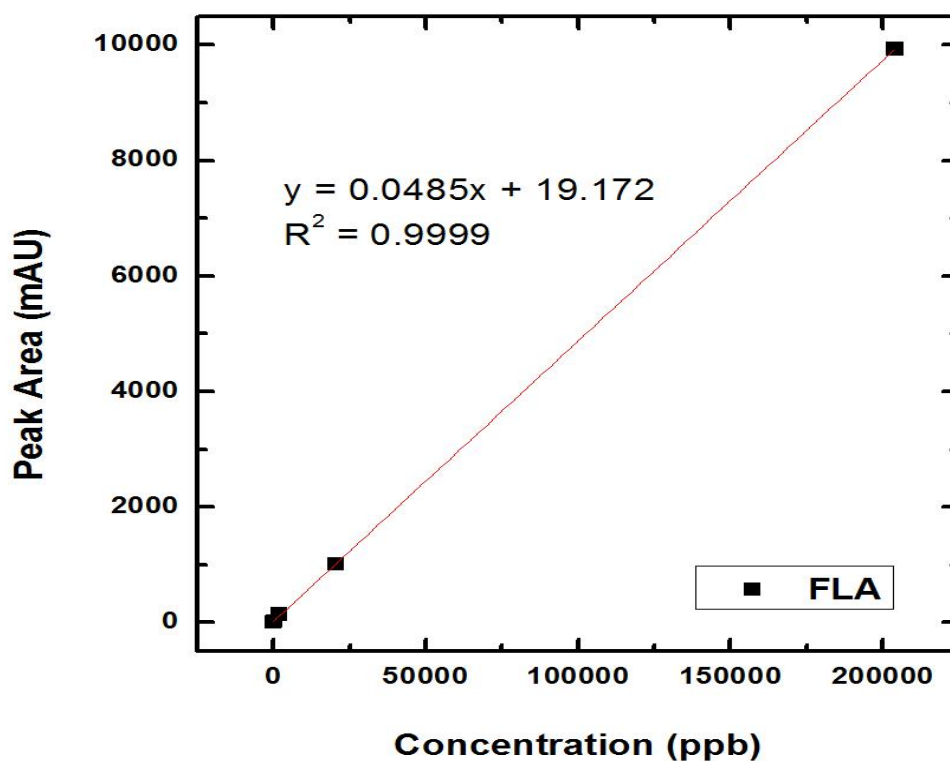


Figure 64. Calibration curve for fluoranthene standard solution.

The final PAHs selected for the HPLC evaluation was PYR represented in the chromatogram below (**Figure 65**). A consecutive concentration profile of PYR (2.12 to 212000 ppb) was determined using this HPLC method (**Table 25**).

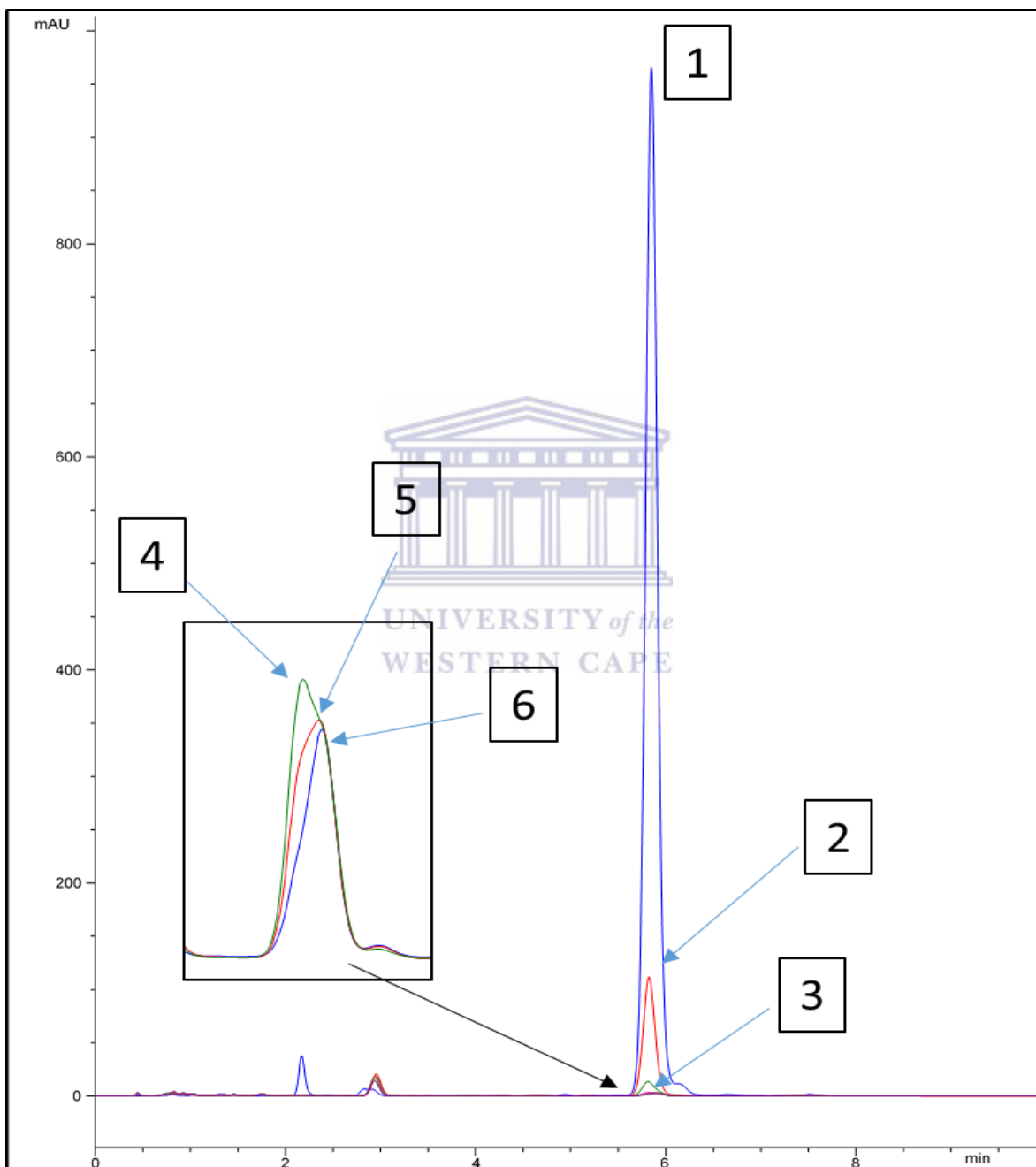


Figure 65. Concentration profile of pyrene standard.

Table 25. Chromatographic data for the pyrene standard profile.

BaP STD SAMPLES	Concentration (ppb)	Peak Area (mAU)
1 (Stock)	212000	8618.42
2	21200	1016.47
3	2120	143.60
4	212	48.34
5	21.2	41.96
6	2.12	33.96

Table 26. Calibration standard profile data for PAHs determined from electrochemistry.

PAHs standard	Slope (Sensitivity) (ppb/mAU)	Linear Regression (R^2)	Retention Time (min)
BaP	1.21×10^{-1}	0.9999	10.7
FLA	4.85×10^{-2}	0.9999	4.8
1-OHP	3.61×10^{-2}	0.9998	2.1
PYR	4.039×10^{-2}	0.9998	5.8

UNIVERSITY of the

Information obtained from the standard profile of the selected PAHs, included retention times, slope sensitivity and linear regression. Retention times of the selected PAHs allowed for each PAHs to be clearly identified and separated (**Table 26**).

7.6.2 Chromatographic results for the complex mixture

The chromatogram shows the behaviour of the complex mixture where the PAHs can be clearly separated and identified (**Figure 66**).

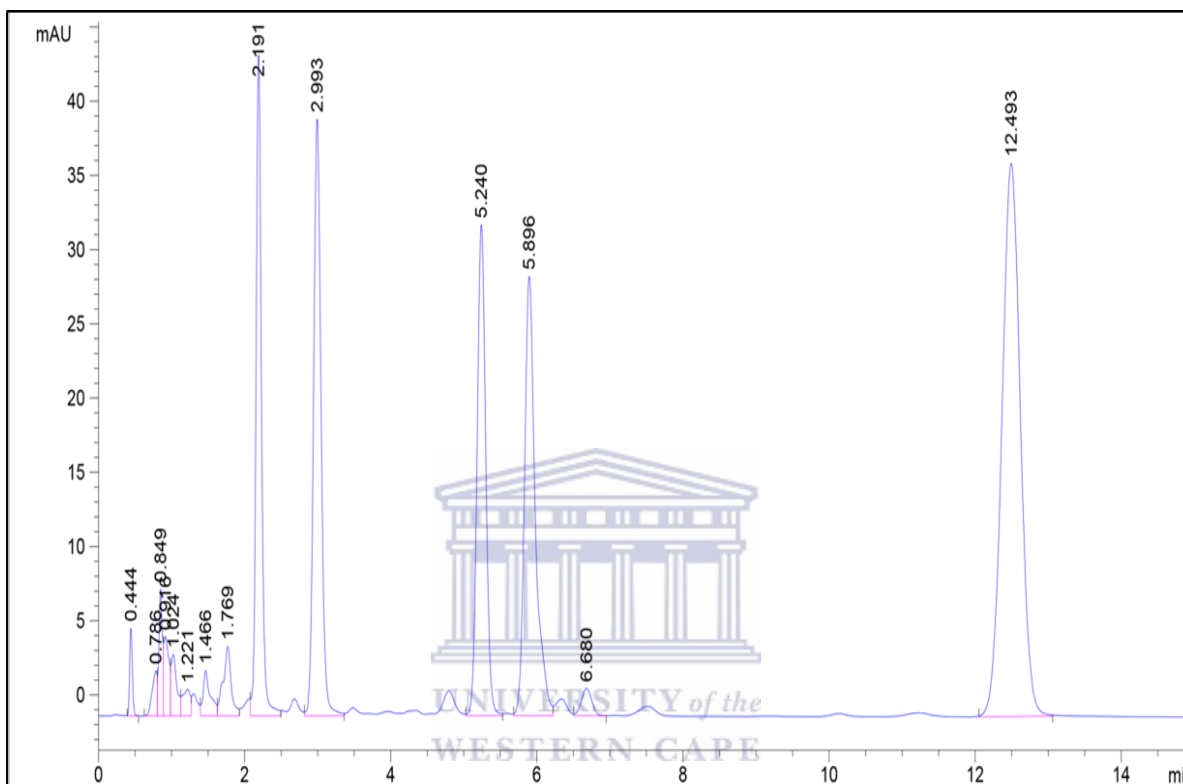


Figure 66. Combined cocktail standard containing: 1. 1-OHP, 2. FLA, 3. PYR, 4. BaP. The concentration levels within the complex matrix ranged between 5100 to 5300 ppb. Retention of the selected PAHs in the complex matrix were determined based on the chromatographic results (**Table 27**).

Table 27. PAHs complex matrix data.

PAHs standard	Concentration (ppb)	Retention Time (min)
BaP	5100	12.49
FLA	5100	5.24
1-OHP	5150	2.19
PYR	5300	5.89

An extra peak is observed in the PAHs complex matrix, however this is observed in the standard profiles of the individual PAHs (**Figure 67**). The reason the peak is observed is due to the low concentrations of the PAHs in the complex mixture. In the stock PAHs concentrations the peak area of the additional peak is relatively low, 177 mAU. PYR was selected for consecutive concentration additions due to its close relationship (retention times) with FLA.

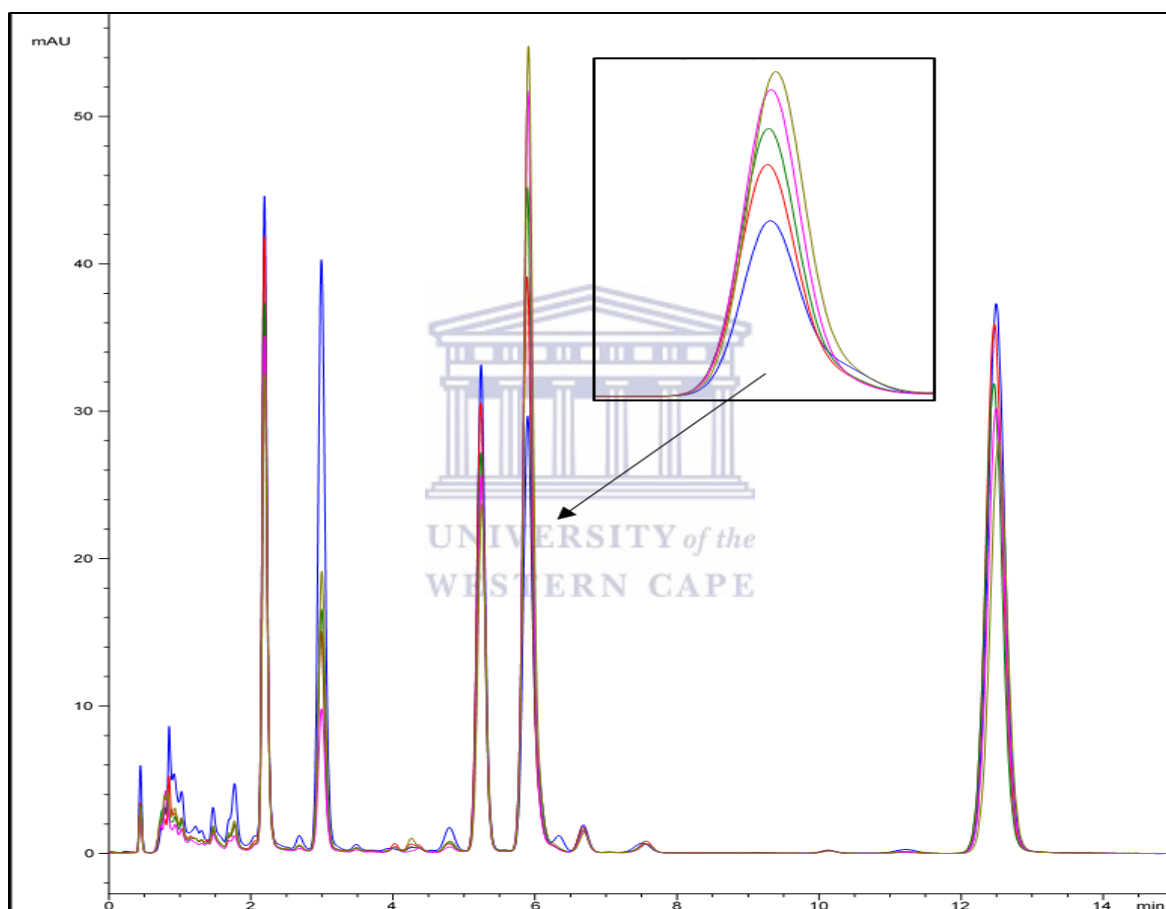


Figure 67. Consecutive concentration additions of pyrene into the complex mixture.

An increase in the PYR peak area is observed as the concentration is increased, however as the concentration of the PYR is increased the concentration of the other standards decrease. The peak area of the other PAHs decrease with an increase in the peak area of PYR. A slight shift in the retention times from the individual to the complex mixture can be observed (**Table 28**).

Table 28. Shift in retention times for PAHs.

PAHs standard	Individual Retention Time (min)	Complex Mixture Retention Times (min)
BaP	10.7	12.6
FLA	4.8	5.3
1-OHP	2.1	2.2
PYR	5.8	5.9

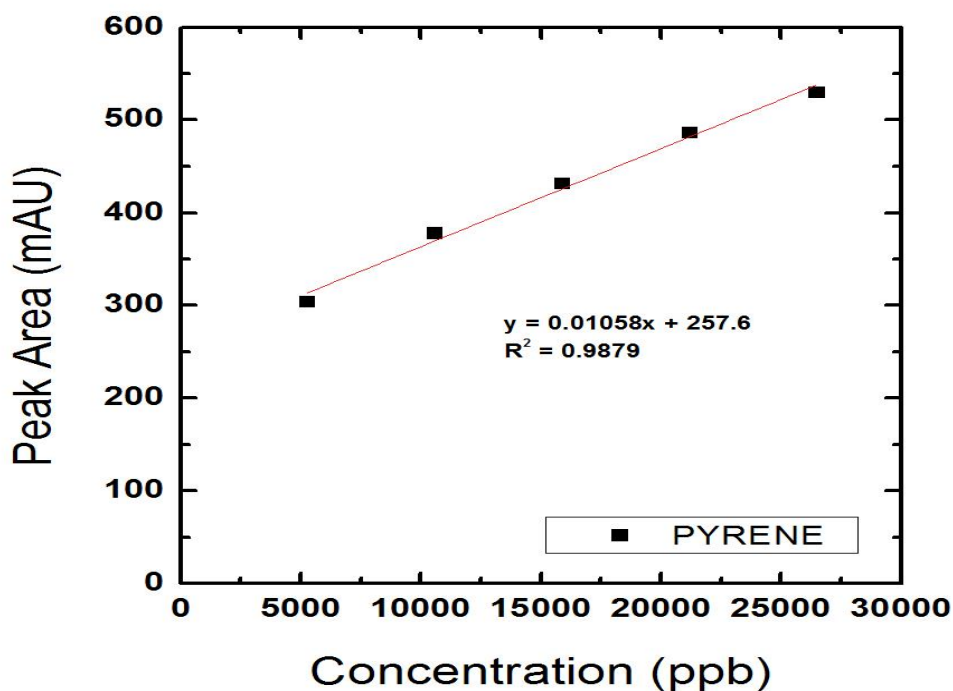


Figure 68. Calibration curve of PYR in the complex PAHs matrix.

The sensitivity of the PYR was found to be 0.01058 mAU/ppb, with a limit of detection of 136 ppb ($R^2 = 0.9879$) (Figure 68). The more commonly used method for PAHs detection has been explored and it has been determined that PAHs can be identified and separated using the method within this chapter. The mobile phase (75% CH_3CN : 25% H_2O) used, was degassed before use in order to avoid any other interfering factors during analysis. The other PAHs species within the complex matrix was used as interfering species and the evidence

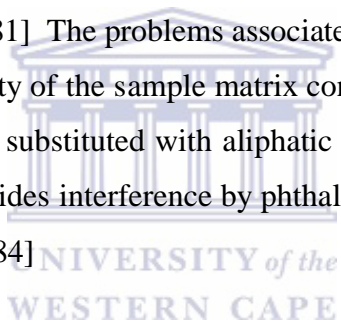
clearly indicated that there was no effect on the PYR peak. The developed method has proven that PYR was identified, separated and detected at consecutive concentrations. The CH₃CN has proven to be an excellent solvent in the identification and separation of PAHs, however CH₃CN is not environmentally friendly and is relatively expensive to purchase. Due to this fact it tends to make the method fairly expensive for identification and separation of PAHs. Further optimization to improve the limit of detection is possible, provided that the initial starting concentration is at a low enough concentration. The main aim of the HPLC experiment was to demonstrate the principle of identifying the selected PAHs from the electrochemical evaluation of PAHs.

Many HPLC methods have been used to evaluate a wide range of PAHs including the PAHs determined by the electrochemical methods in this work. An HPLC technique using an acetonitrile gradient mobile phase was used to evaluate a complex mixture of 18 PAHs. Of the 18 PAHs evaluated PYR, FLA and BaP were among them. A detection limit for these 3 PAHs were determined to be 0.02, 0.14 and 0.01 ppb. The detectors employed by the technique have an influence of the limits of detection, where FLD has better limits of detection compared to the photodiode array (PDA) detector.[175] An HPLC-FLD method was used in the determination of the priority pollutants using a gradient solvent program (acetonitrile). Respective retention times of FLA, PYR and BaP were determined by fluorescence and were found at 24.3, 25.4 and 33.9 min respectively. The column used for the evaluation of these PAHs species was Supelcosil C₁₈ column (4.6 x 250 mm, 5 µm particle size).[193] 1-OHP and PYR were determined by HPLC-FLD using an acetonitrile mobile phase, 60 % for 1-OHP and 85 % for PYR. A Kaseisorb column (250 x 4.6 mm) was used at a flow rate of 1.0 ml/min. The retention times determined for 1-OHP and PYR were 4.8 min and 11.8 min with a limit of detection of 0.05 ppb and 0.025 ppb, respectively.[111] The limit of detection of PYR determined from literature and the guidelines determined by the WHO are greater than the limit determined within this work. Retention times differ which can be attributed to the column used.

The stationary phase in the HPLC column is the most important factor when selecting columns for HPLC separation. Silica columns are the most often used as they are able to

work under pressure and has a neutral pH. The stationary phase has a major effect on the resolution, stability, retention time, reproducibility and peak shape. The standard column often employed for HPLC analysis is the column containing a stationary phase with particle sizes between 5 to 10 μm in a 250 x 4.6 mm length column. Smaller particle sizes (3.0 and 3.5 μm) in short columns can give rise to higher efficiency and high resolution within a short time.[40]

Interfering species can be classified into two categories, those that are already present in the matrix (endogenous suppressors) and those not originally in the matrix (exogenous suppressors). The endogenous suppressors include salts, highly polar compounds, surfactants and various other organic compounds (carbohydrates, amines, lipids, peptides). The exogenous suppressors include plastic, polymer residue, phthalates, ion pairing reagents, organic acids and buffers.[13, 181] The problems associated with low levels of detection of PAHs results from the complexity of the sample matrix containing PAHs by products. The petroleum matrix contain PAHs substituted with aliphatic or alicyclic groups.[69] For the determination of PAHs in pesticides interference by phthalate esters, a large eluting peak is observed in the chromatogram.[84]



8. Conclusion and Future Work

8.1 Conclusion

Electrochemical sensors are usually robust, relatively inexpensive and easy to prepare. Electrochemical sensors used in the detection of organic pollutants in a multi array design has not been greatly explored due to the lack of simultaneous detection ability. A new design incorporating electrochemically prepared materials into a multi array design for the simultaneous detection of PAHs is needed.

A novel Schiff base monomer material was prepared under controlled reflux condensation reaction. This novel material was then extensively characterized in terms of spectroscopy and microscopy in order to confirm the new azomethine bond in the aldol condensation product. This bond is evident in Schiff base materials, resulting from the reaction between an aldehyde derivative and a primary amine. The Schiff base monomer was then electrochemically polymerized onto the surface of a screen-printed carbon electrode as a thin film. This novel polymer material was then electrochemically evaluated to determine its redox properties. The electrochemically synthesized polymer material was used as the electrochemical transducer in the evaluation of selected PAHs. PAHs are a ubiquitous group of organic pollutants which result from incomplete combustion of fossil fuels. PAHs are released into the atmosphere as particulate matter, they can be transported over great distances depending on their half-life and molecular weight. The most widely reported PAH is benzo(a)pyrene and has been labelled along with other PAHs as potential carcinogens to humans by different environmental protection agencies. The carcinogenic PAHs metabolize within the human body to form DNA adducts which ultimately result in mutation in the body that predispose cancer. The environmental protection agencies (U.S EPA and E.U EPA) have declared a respective list of priority PAHs based on the threat to human health. Most detection, monitoring and screening work has been performed on these priority 16 PAHs. Literature reports typically focus on sensors for individual PAH species during analysis. The more

common methods for evaluating PAHs are differential pulse voltammetry, anodic stripping square wave voltammetry, amperometry and cyclic voltammetry. Cyclic and square wave voltammetry of the selected PAHs were explored and through the determination of their redox behaviour using these techniques, it was determined that square wave voltammetry would be the principle technique. In this work, square wave voltammetry was explored as the principle technique to evaluate the interaction between the selected PAHs species and the novel polymer electrochemical platform. Screening of a wide range of PAHs in aqueous media (deliberately avoiding acetonitrile in the development of this method) showed that 1-hydroxypyrene and pyrene produced the best defined peaks at +0.20 V and -0.54 V vs Ag/AgCl respectively. These 2 selected PAHs species were quantitatively assessed by standard addition method analysis using square wave voltammetry. The electrochemical window selected for the oxidative SWV was -1.0 to +1.0 V. A scan rate of 50 mV/s was achieved by setting the frequency at 10 Hz and the step potential at 5 mV. The working electrode in the 3 electrode electrochemical cell was a SPCE and the electrolyte solutions were 0.1 M HCl and 0.1 M LiClO₄, in separate experiments. The LOD for pyrene was found to be 1.77×10^{-3} ppb with a correlation coefficient of 0.9989. The sensitivity of the system determined from the slope of the calibration was found to be 585.81 μ A/ppb based on the non-linear least squares method of data fitting. The LOD (n=3) for pyrene was determined to be 6.00×10^{-4} ppb with a correlation coefficient of 0.9924. The sensitivity of the system determined from the slope of the calibration was found to be 338.61 μ A/ppb. These calibration curves obeyed a sigmoidal regression analysis fit, indicative of competition for attachment to the available binding sites at low concentrations due to the size of the molecule. The calibration data was modelled as a Boltzmann fit which was based on the non-linear least squares method, while the sensitivity of the system was determined from the linear region of the resulting plot. According to the U.S EPA there is insufficient information about pyrene to classify it as a potential cancer causing substance. Information obtained in this work was compared to literature reports and the limits of detection obtained are greater than those from literature. Literature reports by Mailu, S.N et. al; Tovide, O.O. et, al, and Boikanyo, D. et.al, cite detection limits for pyrene using polymer based chemical sensors of 546 ppb, 0.3 ppb and 0.3 ppb respectively. Health organizations and safety agencies have developed

occupational limits for 1-hydroxypyrene which ranged between 1.00 to 10.00 ppb. Literature reports by Castro, A.A. et al., 2004, Shen, C. et al., 2012, and Yang, D.-H. et al., 2017 on chemical sensors used for the detection of 1-hydroxypyrene, report detection limit of 0.2 ppb, 8 ppb and 0.07 ppb respectively. The limits obtained within this work are below those set by various health organization, safety agencies and literature reports for the detection of 1-hydroxypyrene. Other PAH species were more difficult to conclusively analyse, displaying variable redox behaviour under the predetermined electrochemical conditions i.e. anthracene (-0.93 V), benzo(a)pyrene (-0.73 V), chrysene (-0.58 V), naphthalene (+0.21 V) and phenanthrene (-0.55 V) vs Ag/AgCl, reported oxidation peaks that did not show consistent concentration dependence for effective analytical evaluation. The remaining evaluated PAHs showed no identifiable electrochemical signal under the experimental conditions i.e. 7,12-dimethylbenz(a)anthracene, acenaphthylene, benzo(b)fluoranthene and fluoranthene. It is well known that these fused ring systems require high oxidation potentials, further development of the analytical conditions and suitable platforms may be required for effective analysis of the whole range of PAHs under investigation. Literature reports that reversible PAHs redox couples are observed when using higher scan rates (< 1 V/s). The solubility of PAHs plays an important role in the detection as high molecular weight PAHs which tend to be problematic to dissolve. PAHs solutions for analysis were prepared in the mmol/L concentration range. Future work will focus on fast scan rate electrochemistry as another possible way to enhance detection of these PAHs at the novel polymer electrode developed in this work.

Conducting polymers are materials which have a wide range of favourable properties which can be manipulated to trap simple anions and to produce materials with different conductivities, capacitance or redox properties. PPy a material that has been extensively studied due its ability to operate in a wide range of potential applications and the mimicking of biological systems is an example of these CP materials. Actuators using these polymer materials can deform or bend into a different shape due to the response of being electrically stimulated. Polymer conformations in a zig zag design play an important role in the actuation mechanism. Volume changes within the polymer materials generated by the presence of

redox processes can be linked to conformation changes. The expansion and contraction of the polymer materials in the zig zag conformation have the potential to trap anions within the free volume space between the polymer backbones. These polymer materials in the zig zag conformation bodes well for the use in the detection of PAHs.

The novel Schiff base polymer platform that was used for the evaluation of the selected PAHs in 0.1 M LiClO₄. Benzo(a)pyrene and fluoranthene, displayed the best defined peaks in square wave voltammetry and as a result was quantitatively determined. Calibration data for individual PAHs species using the Boltzmann plot gave rise to a LOD (n=3) of 9.46x10⁻⁷ and 1.07x10⁻⁹ ppb for benzo(a)pyrene and fluoranthene respectively. The Boltzmann fit provided high sensitivities (slope of the linear region in the curve) of 712.04 μA/ppb and 627.21 μA/ppb respectively. Linearity coefficient (R²) was determined to be 0.9975 and 0.9941 for benzo(a)pyrene and fluoranthene. Literature reports for benzo(a)pyrene included Keskin, E. et al., 2010, Zhang, Y. et al., 2014 and Du, C. et al., 2015 all of which determined limits of detection for benzo(a)pyrene. Keskin, E. et al., 2010, and Du, C. et al., 2015 determined limits of detection of 33 ppb and 0.17 ppb using a chemical sensor. An immunosensor developed by Zhang, Y. et al., 2014 was used to determine a detection limit of 8x10⁻⁵ ppb. The presence of fluoranthene in drinking is very low which led to the world health organization not recognising fluoranthene as a potential hazard to human health. However, the more common methods for the evaluation of fluoranthene, is fluorescence spectroscopy and high performance liquid chromatography. The maximum contamination level for benzo(a)pyrene in drinking water according to the world health organization is 0.7 ppb. The novel polymer electrode reported strong analytical signals for 1-OHP (-0.16 V), 7,12-dimethylbenz(a)anthracene (-0.46 V), acenaphthylene (-0.50 V), chrysene (-0.56 V), naphthalene (-0.62 V), pyrene (-0.43 V) and triphenylene (-0.58 V) vs Ag/AgCl when evaluated as individual species. These PAHs species however were difficult to quantify in mixed samples, the analytical signals became suppressed or completely lost during voltammetric screening. No redox peaks were observed for anthracene and phenanthrene at the polymer electrode. The novel actuator type polymer facilitated the detection of PAHs at lower levels of detection compared to those stipulated by the world health organization. A

mixed sample of benzo(a)pyrene and fluoranthene in 0.1 M LiClO₄ was evaluated in the same manner as the individual PAHs species. The LOD (n=3) for benzo(a)pyrene and fluoranthene was found to be 4.10x10⁻⁹ ppb and 2.17x10⁻⁹ ppb, respectively. High sensitivities (slope of the linear region in the curve) of 626.64 μA/ppb (BaP) and 781.19 μA/ppb (FLA) were obtained with a linearity coefficient (R²) of 0.9933 and 0.9971 for BaP and FLA. To the best of our knowledge this work represents the first report for chemical sensors applied to a mixed sample of benzo(a)pyrene and fluoranthene. However, the polymer platform exhibits high background capacitive current, which can have a negative influence on detection in the lower concentration range. Slow scan rates used for the detection of PAHs at the polymer platform (similarly to the unmodified platform) may also affect the reversible nature of the PAH electrochemistry at these electrodes.

The most commonly used methods to detect multiple PAH species remain the chromatography techniques, notably HPLC (ultraviolet, fluorescence and diode array detectors) and GC. A wide range of PAHs have been detected using these methods, however, they also have their inherent disadvantages. In our work HPLC was used in the validation of standards to evaluate the calibration trends as a framework supported by literature. HPLC used for multi analysis, typically employed pyrene as the marker compound due to its ability to be clearly identified in close proximity to other PAH species.

As a first step towards multi element analysis by electrochemical methods, we explored the use of a multichannel potentiostat coupled to an 8 electrode array in a wall jet configuration. Electrochemical sensors that have been explored have only detected individual PAHs rather than PAHs in a mixed sample or the simultaneous detection of PAHs. The multi array analytical protocol has the potential to overcome the limitations of individual sensors. The sensors developed in this work (and others) may be incorporated onto a SPCE (DRP-8X110) array electrode with eight working electrode sites.

Combined with a multichannel potentiostat (μStat 8000P) individual samples or mixed samples, optimized for up to 8 individual analyte species, may be evaluated. A peristaltic pump dosing system may be employed to deliver the sample to the respective electrode,

where electrochemical parameters are selectively controlled. Such an experimental setup is proposed (**Figure 72**) for multi-element analysis of PAH species.

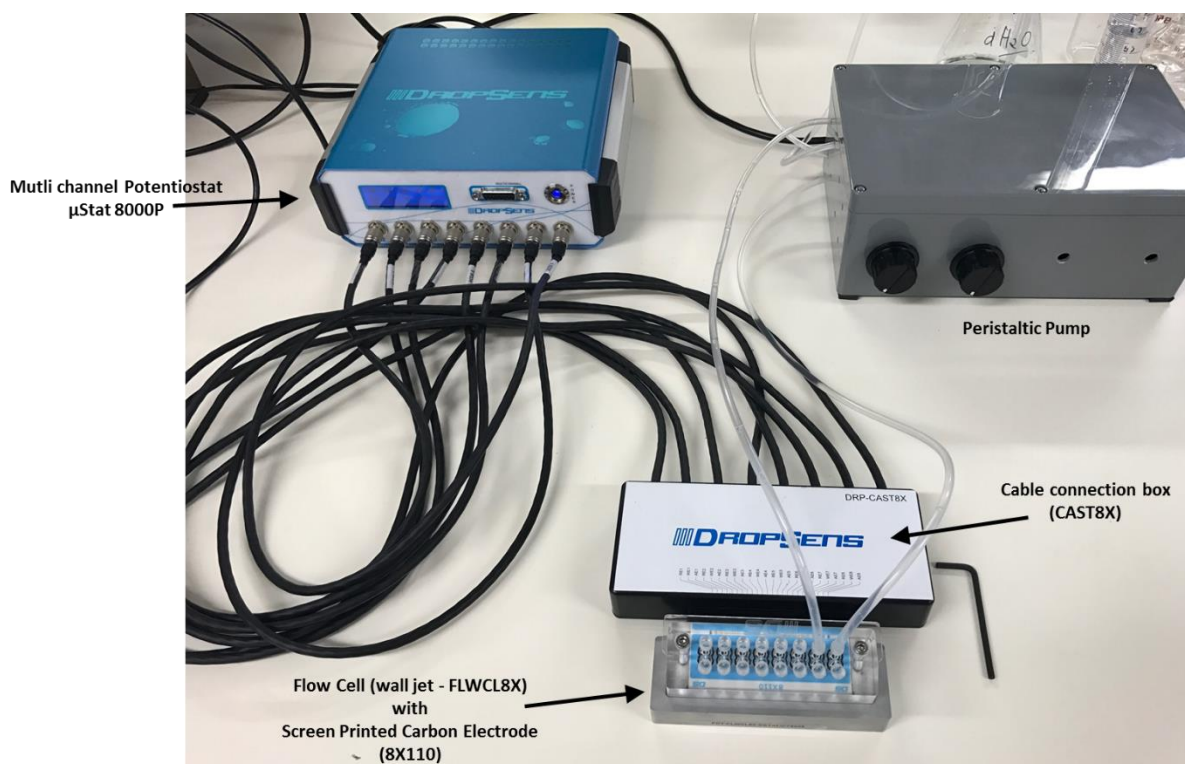


Figure 69. Proposed multi array setup for the simultaneous detection of polycyclic aromatic hydrocarbons.

Initial developmental work (subject to resources) has been attempted in our current project, but requires further major development and optimization to produce reliable and reproducible multi-element PAH analysis comparable to HPLC methods. Based on the preliminary work on the provisional multichannel setup constructed in our laboratory, which was tested for up to 4 PAHs, we confidently propose the hypothesis for the development of the multichannel approach for analysis of up to 8 PAH species in future research in this field (**Figure 73**).

The Schiff base polymer holds great promise for alternative applications such as organic solar cells, supercapacitor materials as well as sensors for metal ions and PAHs detection. The use of Schiff base metal complexes as photovoltaic materials have gained interest due to the ease

of synthesis and complexation with metal ions. The favourable properties of these Schiff base materials and their metal complexes include high thermal stability, wider range of absorption, lower band gap and good electrical conductivity properties. These favourable properties make these materials attractive for application in energy storage systems such as supercapacitors. Supercapacitors or double-layer supercapacitors are devices that have the ability to store energy due to the charging of the double electric layer at the electrode surface and electrolyte interface. Supercapacitors have the advantage of lower specific energy properties, compared to other batteries. Other attractive features include highly reversible charge-storage performance, longer cycle lives and rapid charge and discharge ability at high power densities (1 kW/kg). Overwhelming evidence in literature supports the use of Schiff base complexes in energy application such as photovoltaics and supercapacitors.



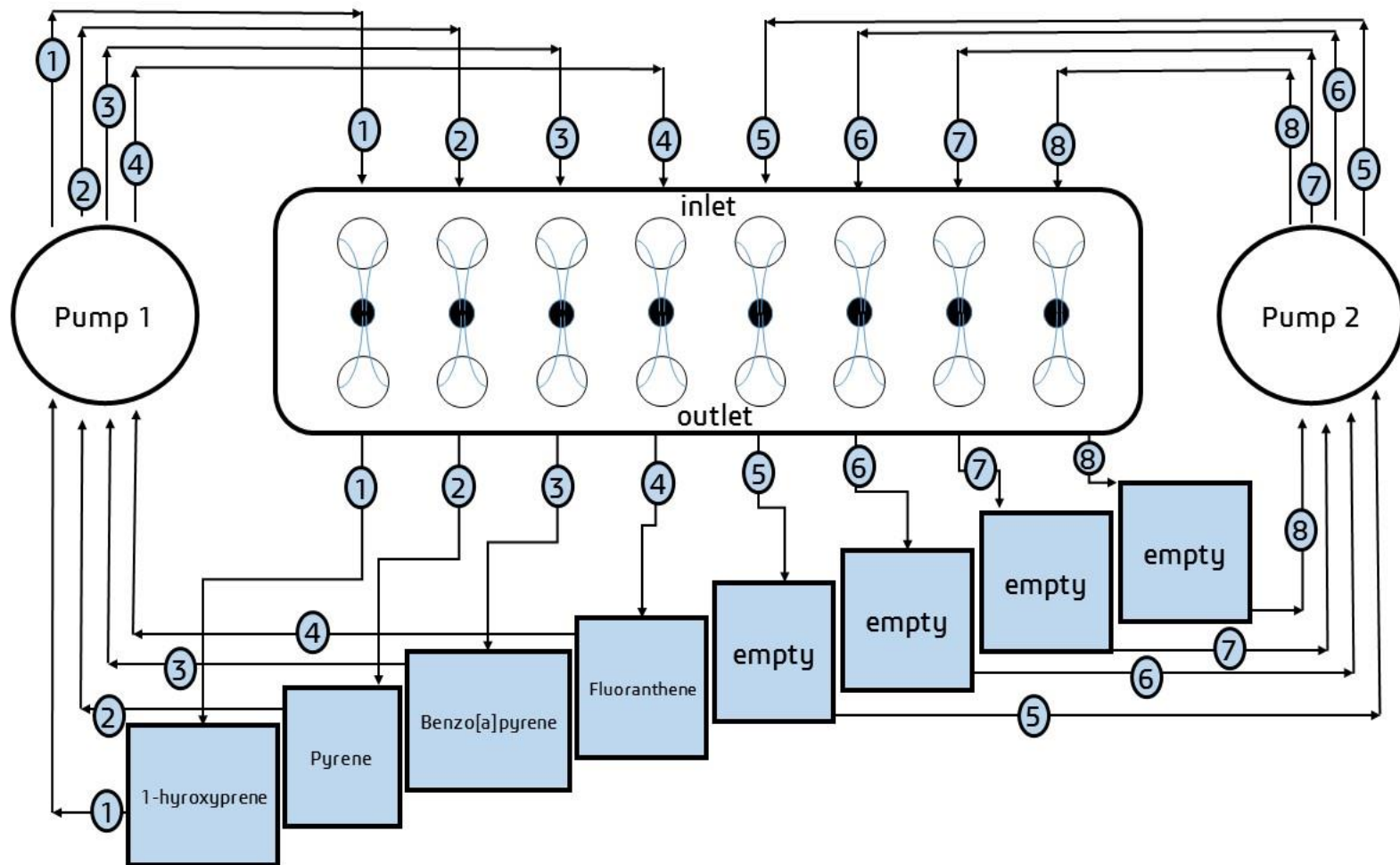


Figure 70. Multichannel design for the evaluation of 1-hydroxypyrene, benzo(a)pyrene, fluoranthene and pyrene.

References

- [1] (ATSDR), A.f.T.S.a.D.R., Toxicological profile for polycyclic aromatic hydrocarbons (PAHs), Atlanta, GA: U.S. Department of Health and Human Services, Public Health Service (1995).
- [2] Abdel-Shafy, H.I., Mansour, M.S.M., A review on polycyclic aromatic hydrocarbons: Source, environmental impact, effect on human health and remediation, Egyptian Journal of Petroleum 25 (2016) 107-123.
- [3] Abdul-Rasheed, O.F., Ali, N.M., Development of a new modified method for polyaromatic hydrocarbons (PAHS) measurement in sera samples of healthy individuals by high performance liquid chromatography technique, International Journal of Research in Pharmacy and Chemistry 3 (2013) 2231-2781.
- [4] Aczél, Á., Modelling of an Electroactive Polymer Actuator, Procedia Engineering 48 (2012) 1-9.
- [5] Agency, E.C., Registration, Evaluation, Authorisation and Restriction of Chemicals (REACH) Regulation (EC) No 1907/2006 (2006).
- [6] Ahmida, M.M., Eichhorn, S.H., Measurements and Prediction of Electronic Properties of Discotic Liquid Crystalline Triphenylenes and Phthalocyanines, ECS Transactions 25 (2010) 1-10.
- [7] Alici, G., Metz, P., Spinks, G.M., A mathematical model to describe bending mechanics of polypyrrole (PPy) actuators, Advanced Intelligent Mechatronics. Proceedings, 2005 IEEE/ASME International Conference on, 2005, pp. 1029-1034.
- [8] Alizadeh, K., Parooi, R., Hashemi, P., Rezaei, B., Ganjali, M.R., A new Schiff's base ligand immobilized agarose membrane optical sensor for selective monitoring of mercury ion, Journal of Hazardous Materials 186 (2011) 1794-1800.
- [9] Amos-Tautua, B.M.W., Inengite, A.K., Abasi, C.Y., Amirize, G.C., Evaluation of polycyclic aromatic hydrocarbons and some heavy metals in roasted food snacks in Amassoma, Niger Delta, Nigeria, African Journal of Environmental Science and Technology 7 (2013) 961-966.

- [10] Andersson, J.T., Achten, C., Time to Say Goodbye to the 16 EPA PAHs? Toward an Up-to-Date Use of PACs for Environmental Purposes, *Polycyclic Aromatic Compounds* 35 (2015) 330-354.
- [11] Andrade-Eiroa, A., Leroy, V., Dagaut, P., Bedjanian, Y., Determination of Polycyclic Aromatic Hydrocarbons in kerosene and bio-kerosene soot, *Chemosphere* 78 (2010) 1342-1349.
- [12] Anquetil, P.A., Yu, H.-h., Madden, J.D., Madden, P.G., Swager, T.M., Hunter, I.W., Thiophene-based conducting polymer molecular actuators, 2002, pp. 424-434.
- [13] Antignac, J.-P., de Wasch, K., Monteau, F., De Brabander, H., Andre, F., Le Bizec, B., The ion suppression phenomenon in liquid chromatography-mass spectrometry and its consequences in the field of residue analysis, *Analytica Chimica Acta* 529 (2005) 129-136.
- [14] Arias-Pardilla, J., Otero, T.F., Martínez, J.G., Ismail, Y.A., Biomimetic Sensing - Actuators Based on Conducting Polymers, in: Motheo, A.d.J., (Ed.), *Aspects on Fundamentals and Applications of Conducting Polymers*, InTech, Janeza Trdine 9, 51000 Rijeka, Croatia, 2012.
- [15] Armstrong, B., Hutchinson, E., Unwin, J., Fletcher, T., Lung Cancer Risk after Exposure to Polycyclic Aromatic Hydrocarbons: A Review and Meta-Analysis, *Environmental Health Perspectives* 112 (2004) 970-978.
- [16] Asadi, M., Shayegan, J., Alaie, E., Photocatalytic Degradation of PAHs Contaminated Soil in South Pars Economic and Energy Zone with TiO₂ Nanocatalyst *Iranian Journal of Chemical Engineering* 4 (2007) 14-20.
- [17] Bach, Q.D., Kim, S.J., Choi, S.C., Oh, Y.S., Enhancing the intrinsic bioremediation of PAH-contaminated anoxic estuarine sediments with biostimulating agents, *J Microbiol* 43 (2005) 319-324.
- [18] Baird, W.M., Hooven, L.A., Mahadevan, B., Carcinogenic polycyclic aromatic hydrocarbon-DNA adducts and mechanism of action, *Environmental and Molecular Mutagenesis* 45 (2005) 106-114.
- [19] Bandowe, B.A.M., Wilcke, W., Analysis of Polycyclic Aromatic Hydrocarbons and Their Oxygen-Containing Derivatives and Metabolites in Soils All rights reserved.

No part of this periodical may be reproduced or transmitted in any form or by any means, electronic or mechanical, including photocopying, recording, or any information storage and retrieval system, without permission in writing from the publisher, *Journal of Environmental Quality* 39 (2010) 1349-1358.

- [20] Bar-Cohen, Y., *Electroactive Polymer (EAP) Actuators as Artificial Muscles: Reality, Potential, and Challenges*, Society of Photo Optical, **2004**.
- [21] Bard, A., Faulkner, L., *Electrochemical Methods: Fundamentals and Applications*, John Wiley & Sons, Inc, **2001**.
- [22] Bard, A.J., *Electroanalytical Chemistry: A Series of Advances*, Taylor & Francis, **1988**.
- [23] Bartok, W., Sarofim, A.F., *Fossil Fuel Combustion: A Source Book*, Wiley, **1991**.
- [24] Basak, S., Şengör, G.F., Karakoç, F.T., *The Detection of Potential Carcinogenic PAH Using HPLC Procedure in Two Different Smoked Fish, Case Study: Istanbul/Turkey*, *Turkish Journal of Fisheries and Aquatic Sciences* 10 (2010) 351-355.
- [25] Bellah, P., Lesego, M., Nelson, T., *Analysis of Polycyclic Aromatic Hydrocarbons in Fish with Agilent Bond Elut QuEChERS AOAC Kit and HPLC-FLD*, *Agilent Technologies* (2012) 5990-5441.
- [26] Bezza, F.A., Nkhalambayausi-Chirwa, E.M., *Desorption kinetics of polycyclic aromatic hydrocarbons (PAHs) from contaminated soil and the effect of biosurfactant supplementation on the rapidly desorbing fractions*, *Biotechnology and Biotechnological Equipment* 29 (2015) 680-688.
- [27] Biddiss, E., Chau, T., *Electroactive polymeric sensors in hand prostheses: Bending response of an ionic polymer metal composite*, *Medical Engineering & Physics* 28 (2006) 568-578.
- [28] Boikanyo, D., *Electrochemical study of pyrene using glassy carbon electrode modified with metal-oxide nanoparticles and a graphene oxide/multi walled carbon nanotubes nanoplatfrom*, *Chemistry*, North-West University, Potchefstroom, **2015**, pp. 148.
- [29] Bojes, H.K., Pope, P.G., *Characterization of EPA's 16 priority pollutant polycyclic aromatic hydrocarbons (PAHs) in tank bottom solids and associated contaminated*

- soils at oil exploration and production sites in Texas, *Regulatory Toxicology and Pharmacology* 47 (2007) 288-295.
- [30] Braga, D., Grepioni, F., Biradha, K., Pedireddi, V.R., Desiraju, G.R., Hydrogen Bonding in Organometallic Crystals. 2. C-H...O Hydrogen Bonds in Bridged and Terminal First-Row Metal Carbonyls, *Journal of the American Chemical Society* 117 (1995) 3156-3166.
- [31] Brandt, H.C., Watson, W.P., Monitoring human occupational and environmental exposures to polycyclic aromatic compounds, *Ann Occup Hyg* 47 (2003) 349-378.
- [32] Bressan, L.P., do Nascimento, P.C., Schmidt, M.E.P., Faccin, H., de Machado, L.C., Bohrer, D., Salting-out assisted liquid-liquid extraction and partial least squares regression to assay low molecular weight polycyclic aromatic hydrocarbons leached from soils and sediments, *Spectrochimica Acta Part A: Molecular and Biomolecular Spectroscopy* 173 (2017) 749-756.
- [33] Brown, A.M., A step-by-step guide to non-linear regression analysis of experimental data using a Microsoft Excel spreadsheet, *Computer Methods and Programs in Biomedicine* 65 (2001) 191-200.
- [34] Bruzzoniti, M.C., Fungi, M., Sarzanini, C., Determination of EPA's priority pollutant polycyclic aromatic hydrocarbons in drinking waters by solid phase extraction-HPLC, *Analytical Methods* 2 (2010) 739-745.
- [35] Burchell, T.J., Eisler, D.J., Jennings, M.C., Puddephatt, R.J., Ring-opening polymerization of gold macrocycles and self-assembly of a coordination polymer through hydrogen-bonding., *The Royal Society of Chemistry, Chemical Communication*, 2003, pp. 2228-2229.
- [36] Camargo, M.C.R., Antonioli, P.R., Vicente, E., HPLC-FLD simultaneous determination of 13 polycyclic aromatic hydrocarbons: validation of an analytical procedure for soybean oils, *Journal of the Brazilian Chemical Society* 22 (2011) 1354-1361.
- [37] Carmella, S.G., Le, K.-A., Hecht, S.S., Improved Method for Determination of 1-Hydroxypyrene in Human Urine, *Cancer Epidemiology Biomarkers & Prevention* 13 (2004) 1261-1264.

- [38] Casadevall i Solvas, X., Lambert, R., Kulinsky, L., Rangel, R., Madou, M., Micromixing and flow manipulation with polymer microactuators, *Microfluidics and Nanofluidics* 11 (2011) 405-416.
- [39] Castro, A.A., Wagener, A.d.L.R., Farias, P.A.M., Bastos, M.B., Adsorptive stripping voltammetry of 1-hydroxypyrene at the thin-film mercury electrode—basis for quantitative determination of PAH metabolite in biological materials, *Analytica Chimica Acta* 521 (2004) 201-207.
- [40] Cazes, J., *Encyclopedia of Chromatography*, Taylor & Francis, 2005.
- [41] Chen, G., Bouzan, S., Zhao, Y., Synthesis and properties of TTFV-hinged molecular tweezers, *Tetrahedron Letters* 51 (2010) 6552-6556.
- [42] Chen, Y., Feng, Y., Xiong, S., Liu, D., Wang, G., Sheng, G., Fu, J., Polycyclic aromatic hydrocarbons in the atmosphere of Shanghai, China, *Environmental Monitoring and Assessment* 172 (2010) 235-247.
- [43] Chitte, H.K., Bhat, N.V., Walunj, V.E., Shinde, G.N., Synthesis of Polypyrrole Using Ferric Chloride (FeCl₃) as Oxidant Together with Some Dopants for Use in Gas Sensors *Journal of Sensor Technology* 1 (2011) 47-56.
- [44] Cohen, J., *Electroactive Polymers as Artificial Muscles—A Primer*, bearing dates of (2003) 1-14.
- [45] Cortes, M., Otero, T., Vazquez, A., Boyano, I., Electrochemomechanical Actuators Based on Polypyrrole: Influence of the Dimensions on the Movement, *Portugaliae Electrochimica Acta* 19 (2001).
- [46] Cortona, M.N., Vettorazzi, N.R., Silber, J.J., Sereno, L.E., Electrochemical nitration of naphthalene in micellar systems, *Journal of the Brazilian Chemical Society* 8 (1997) 377-382.
- [47] Crowell, S.R., Hanson-Drury, S., Williams, D.E., Corley, R.A., In vitro metabolism of benzo[a]pyrene and dibenzo[def,p]chrysene in rodent and human hepatic microsomes, *Toxicology Letters* 228 (2014) 48-55.
- [48] da Silva, C.M., da Silva, D.L., Modolo, L.V., Alves, R.B., de Resende, M.A., Martins, C.V.B., de Fátima, Â., Schiff bases: A short review of their antimicrobial activities, *Journal of Advanced Research* 2 (2011) 1-8.

- [49] Davenport, A.P., Receptor Binding Techniques, Humana Press, **2005**.
- [50] Del Carlo, M., Di Marcello, M., Perugini, M., Ponzielli, V., Sergi, M., Mascini, M., Compagnone, D., Electrochemical DNA biosensor for polycyclic aromatic hydrocarbon detection, *Microchimica Acta* 163 (**2008**) 163-169.
- [51] Deshpande, S.D., Kim, J., Yun, S.-R., New electro-active paper actuator using conducting polypyrrole: actuation behaviour in LiClO₄ acetonitrile solution, *Synthetic Metals* 149 (**2005**) 53-58.
- [52] Doong, R.-a., Shih, H.-m., Lee, S.-h., Sol-gel-derived array DNA biosensor for the detection of polycyclic aromatic hydrocarbons in water and biological samples, *Sensors and Actuators B: Chemical* 111-112 (**2005**) 323-330.
- [53] Du, C., Hu, Y., Li, Y., Fan, L., Li, X., Electrochemical detection of benzo(a)pyrene in acetonitrile-water binary medium, *Talanta* 138 (**2015**) 46-51.
- [54] Du, C.X., Han, L., Dong, S.L., Li, L.H., Wei, Y., A novel procedure for fabricating flexible screen-printed electrodes with improved electrochemical performance, *Materials Science and Engineering* 137 (**2016**) 1-7.
- [55] Elices, M., *Structural Biological Materials: Design and Structure-Property Relationships*, First ed., Elsevier Science, Kidlington, Oxford, **2000**.
- [56] Fähnrich, K.A., Pravda, M., Guilbault, G.G., Disposable amperometric immunosensor for the detection of polycyclic aromatic hydrocarbons (PAHs) using screen-printed electrodes, *Biosensors and Bioelectronics* 18 (**2003**) 73-82.
- [57] Falco, G., Domingo, J.L., Llobet, J.M., Teixido, A., Casas, C., Muller, L., Polycyclic aromatic hydrocarbons in foods: human exposure through the diet in Catalonia, Spain, *J Food Prot* 66 (**2003**) 2325-2331.
- [58] Fang, Y., Pence, T.J., Tan, X., Nonlinear elastic modeling of differential expansion in trilayer conjugated polymer actuators, *Smart Materials and Structures* 17 (**2008**) 065020.
- [59] Fang, Y., Tan, X., Shen, Y., Xi, N., Alici, G., A scalable model for trilayer conjugated polymer actuators and its experimental validation, *Materials Science and Engineering: C* 28 (**2008**) 421-428.

- [60] Fayemi, O.E., Adekunle, A.S., Ebenso, E.E., Electrochemical Detection of Phenanthrene Using Nickel Oxide Doped PANI Nanofiber Based Modified Electrodes, *Journal of Nanomaterials* 2016 (**2016**) 12.
- [61] Fraden, J., *Handbook of Modern Sensors*, 4th ed., Springer, United States of America, **2010**.
- [62] Fraser, C.S.A., Eisler, D.J., Puddephatt, R.J., Self-assembly of organometallic polymers through hydrogen bonding: A diplatinum(IV) complex with a single bridging halide ligand, *Polyhedron* 25 (**2006**) 266-270.
- [63] Gaihre, B., Alici, G., Spinks, G.M., Cairney, J.M., Effect of electrolyte storage layer on performance of PPy-PVDF-PPy microactuators, *Sensors and Actuators B: Chemical* 155 (**2011**) 810-816.
- [64] Gaihre, B., Alici, G., Spinks, G.M., Cairney, J.M., Synthesis and performance evaluation of thin film PPy-PVDF multilayer electroactive polymer actuators, *Sensors and Actuators A: Physical* 165 (**2011**) 321-328.
- [65] Gaihre, B., Ashraf, S., Spinks, G.M., Innis, P.C., Wallace, G.G., Comparative displacement study of bilayer actuators comprising of conducting polymers, fabricated from polypyrrole, poly(3,4-ethylenedioxythiophene) or poly(3,4-propylenedioxythiophene), *Sensors and Actuators A: Physical* 193 (**2013**) 48-53.
- [66] Gallotta, F.D.C., Lourenço, R.A., de Araújo, L.F.M., Evaluation of Holding Time for Polycyclic Aromatic Hydrocarbon (PAH) Analysis in Saline Water Samples, *Environmental Forensics* 11 (**2010**) 309-314.
- [67] Gan, S., Lau, E.V., Ng, H.K., Remediation of soils contaminated with polycyclic aromatic hydrocarbons (PAHs), *Journal of Hazardous Materials* 172 (**2009**) 532-549.
- [68] Gharamaleki, J.A., Akbari, F., Karbalaei, A., Ghiassi, K.B., Olmstead, M.M., Synthesis, Characterization and Crystal Structure of a New Schiff Base Ligand from a Bis(Thiazoline) Template and Hydrolytic Cleavage of the Imine Bond Induced by a Co(II) Cation, *Journal of Inorganic Chemistry* 6 (**2016**) 76-88.
- [69] Gilgenast, E., Boczkaj, G., Przyjazny, A., Kamiński, M., Sample preparation procedure for the determination of polycyclic aromatic hydrocarbons in petroleum

- vacuum residue and bitumen, *Analytical and Bioanalytical Chemistry* 401 (2011) 1059-1069.
- [70] Gratz, S., Mohrhaus, A., Gamble, B., Gracie, J., Jackson, D., Ciolino, L., Mccauley, H., Schneider, G., Crockett, D., Krol, W., Arsenault, T., White, J., Flottmeyer, M., Johnson, Y., Heitkemper, D., Fricke, F., Screen for the presence of polycyclic aromatic hydrocarbons in select seafood using LC-Fluorescence, Food and Drug Administration, Cincinnati, 2010.
- [71] Grova, N., Hardy, E.M., Meyer, P., Appenzeller, B.M.R., Analysis of tetrahydroxylated benzo[a]pyrene isomers in hair as biomarkers of exposure to benzo[a]pyrene, *Analytical and Bioanalytical Chemistry* 408 (2016) 1997-2008.
- [72] Gruber, K., Horlacher, T., Castelli, R., Mader, A., Seeberger, P.H., Hermann, B.A., Cantilever Array Sensors Detect Specific Carbohydrate-Protein Interactions with Picomolar Sensitivity, *ACS Nano* 5 (2011) 3670-3678.
- [73] Hall, H.K., Zbinden, R., *Infrared Spectra and Strain in Cyclic Carbonyl Compounds*, *Journal of the American Chemical Society* 80 (1958) 6428-6432.
- [74] Han, G., Shi, G., Conducting polymer electrochemical actuator made of high-strength three-layered composite films of polythiophene and polypyrrole, *Sensors and Actuators B: Chemical* 99 (2004) 525-531.
- [75] Hand, O.W., Winger, B.E., Cooks, R.G., Enhanced silver cationization of polycyclic aromatic hydrocarbons containing bay regions in molecular secondary ion mass spectrometry, *Biological Mass Spectrometry* 18 (1989) 83-85.
- [76] Hariharan, P.S., Anthony, S.P., Selective fluorescence sensing of Mg²⁺ ions by Schiff base chemosensor: effect of diamine structural rigidity and solvent, *RSC Advances* 4 (2014) 41565-41571.
- [77] Harvey, D., *Analytical Chemistry 2.0*, *Analytical Chemistry 2.0*, McGraw-Hill Companies, California, 2008, pp. 1134.
- [78] Hassan, J., Izadi, M., Homayonnejad, S., Application of low density homogeneous liquid-liquid extraction combined with GC for TPH and PAH determination in semi-micro solid samples, *Journal of the Brazilian Chemical Society* 24 (2013) 639-644.

- [79] Hayat, A., Marty, J.-L., Disposable Screen Printed Electrochemical Sensors: Tools for Environmental Monitoring, *Sensors* (2014) 10432-10453.
- [80] Hecht, S., Carcinogen derived biomarkers: applications in studies of human exposure to secondhand tobacco smoke, *Tobacco Control* 13 (2004) i48-i56.
- [81] Hongtao Yu, Qingsu Xia, Jian Yan, Diogenes Herreno-Saenz, Yuh-Shen Wu, I-Wah Tang, Fu, P.P., Photoirradiation of Polycyclic Aromatic Hydrocarbons with UVA Light - A Pathway Leading to the Generation of Reactive Oxygen Species, Lipid Peroxidation, and DNA Damage, *International Journal of Environmental Research and Public Health* 3 (2006) 348-354.
- [82] Hulanicki, A., Geab, S., Ingman, F., Chemical Sensors Definitions and Classification, *Pure and Applied Chemistry* 63 (1991) 1247-1250.
- [83] Ifegwu, C., Osunjaye, K., Fashogbon, F., Oke, K., Adeniyi, A., Anyakora, C., Urinary 1-Hydroxypyrene as a Biomarker to Carcinogenic Polycyclic Aromatic Hydrocarbon Exposure, *Biomarkers in Cancer* 4 (2012) 7-17.
- [84] Incorporated, C.P.E.T., The Determination of Polycyclic Aromatic Hydrocarbons (PAH), Polychlorobiphenyls (PCB) and Organochlorine compounds (OC) in ambient arctic air, Atmospheric Environment Service, Toronto, Ontario, 1999.
- [85] International, W., High-Density-Array Temperature Sensor, in: *Monitoring, O.P.a.R.*, (Ed.), 2014.
- [86] J.C, I., O, U.P., Environmental Effects of Polycyclic Aromatic Hydrocarbons, *Journal of Natural Sciences Research* 5 (2015) 117-131.
- [87] Jadreško, D., Zelić, M., Lovrić, M., A formal scan rate in staircase and square-wave voltammetry, *Journal of Electroanalytical Chemistry* 645 (2010) 103-108.
- [88] Jager, E.W.H., Inganäs, O., Lundström, I., Microrobots for Micrometer-Size Objects in Aqueous Media: Potential Tools for Single-Cell Manipulation, *Science* 288 (2000) 2335-2338.
- [89] Jager, E.W.H., Masurkar, N., Nworah, N.F., Gaihre, B., Alici, G., Spinks, G.M., Individually controlled conducting polymer tri-layer microactuators, *Solid-State Sensors, Actuators and Microsystems (TRANSDUCERS & EUROSENSORS*

- XXVII), 2013 Transducers & Eurosensors XXVII: The 17th International Conference on, **2013**, pp. 542-545.
- [90] Jeftic, L., Adams, R.N., Electrochemical oxidation pathways of benzo[a]pyrene, *Journal of the American Chemical Society* 92 (**1970**) 1332-1337.
- [91] Ji, G., Gu, A., Zhou, Y., Shi, X., Xia, Y., Long, Y., Song, L., Wang, S., Wang, X., Interactions between Exposure to Environmental Polycyclic Aromatic Hydrocarbons and DNA Repair Gene Polymorphisms on Bulky DNA Adducts in Human Sperm, *PLoS ONE* 5 (**2010**) e13145.
- [92] Jongeneelen, F.J., Benchmark guideline for urinary 1-hydroxypyrene as biomarker of occupational exposure to polycyclic aromatic hydrocarbons, *Ann Occup Hyg* 45 (**2001**) 3-13.
- [93] Juhasz, A.L., Britz, M.L., Stanley, G.A., Degradation of fluoranthene, pyrene, benz[a]anthracene and dibenz[a,h]anthracene by *Burkholderia cepacia*, *Journal of Applied Microbiology* 83 (**1997**) 189-198.
- [94] Jung, S.-Y., Park, J.-S., Chang, M.-S., Kim, M.-S., Lee, S.-M., Kim, J.-H., Chae, Y.-Z., A simple method for the determination of polycyclic aromatic hydrocarbons (pah) in edible oil employing solid phase extraction (SPE) cartridge purification, *Food Science and Biotechnology* 22 (**2013**) 241-248.
- [95] Kalmykova, Y., Moona, N., Strömvall, A.-M., Björklund, K., Sorption and degradation of petroleum hydrocarbons, polycyclic aromatic hydrocarbons, alkylphenols, bisphenol A and phthalates in landfill leachate using sand, activated carbon and peat filters, *Water Research* 56 (**2014**) 246-257.
- [96] Kao, M.-H., Chen, T.-Y., Cai, Y.-R., Hu, C.-H., Liu, Y.-W., Jhong, Y., Wu, A.-T., A turn-on Schiff-base fluorescence sensor for Mg²⁺ ion and its practical application, *Journal of Luminescence* 169, Part A (**2016**) 156-160.
- [97] Karaman, A., Pirim, I., Exposure to bitumen fumes and genotoxic effects on Turkish asphalt workers, *Clin Toxicol (Phila)* 47 (**2009**) 321-326.
- [98] Katz, E., *Molecular and Supramolecular Information Processing: From Molecular Switches to Logic Systems*, Wiley, **2013**.

- [99] Kaynak, A., Beltran, R., Effect of synthesis parameters on the electrical conductivity of polypyrrole-coated poly(ethylene terephthalate) fabrics, *Polymer International* 52 (2003) 1021-1026.
- [100] Kaynak, A., Yang, C., Lim, Y.C., Kouzani, A., Electrochemical fabrication and modelling of mechanical behavior of a tri-layer polymer actuator, *Materials Chemistry and Physics* 125 (2011) 113-117.
- [101] Keith, L.H., The Source of U.S. EPA's Sixteen PAH Priority Pollutants, *Polycyclic Aromatic Compounds* 35 (2015) 147-160.
- [102] Kelley, C.T., *Iterative Methods for Optimization*, Society for Industrial and Applied Mathematics, 1999.
- [103] Keskin, E., Yardım, Y., Şentürk, Z., Voltammetry of Benzo[a]pyrene in Aqueous and Nonaqueous Media: Adsorptive Stripping Voltammetric Determination at Pencil Graphite Electrode, *Electroanalysis* 22 (2010) 1191-1199.
- [104] Kiefer, R., Weis, D.G., Aabloo, A., Urban, G., Heinze, J., Dependence of polypyrrole bilayer deflection upon polymerization potential, *Synthetic Metals* 172 (2013) 37-43.
- [105] Kim, J.H., Stansbury, K.H., Walker, N.J., Trush, M.A., Strickland, P.T., Sutter, T.R., Metabolism of benzo[a]pyrene and benzo[a]pyrene-7,8-diol by human cytochrome P450 1B1, *Carcinogenesis* 19 (1998) 1847-1853.
- [106] Kim, K.-H., Jahan, S.A., Kabir, E., Brown, R.J.C., A review of airborne polycyclic aromatic hydrocarbons (PAHs) and their human health effects, *Environment International* 60 (2013) 71-80.
- [107] Kissinger, P.T., Heineman, W.R., *Laboratory techniques in electroanalytical chemistry*, Dekker, New York, 1984.
- [108] Kumar, A., *Synthesis and biological evaluation of novel heterocyclic analogues*, Department of Pharmacy, Punjab Technical University, India, 2011, pp. 100.
- [109] Kumar, B., Verma, V.K., Gaur, R., Kumar, S., Sharma, C.S., Akolkar, A.B., Validation of HPLC method for determination of priority polycyclic aromatic hydrocarbons (PAHS) in waste water and sediments, *Advances in Applied Science Research* 5 (2014) 201-209.

- [110] Kumari, S., Chauhan, G.S., New Cellulose-Lysine Schiff-Base-Based Sensor-Adsorbent for Mercury Ions, *ACS Applied Materials & Interfaces* 6 (2014) 5908-5917.
- [111] Kuo, C.-T., Chen, H.-W., Chen, J.-L., Determination of 1-hydroxypyrene in children urine using column-switching liquid chromatography and fluorescence detection, *Journal of Chromatography B* 805 (2004) 187-193.
- [112] Kwon, K.-S., Ng, T.N., Improving electroactive polymer actuator by tuning ionic liquid concentration, *Organic Electronics* 15 (2014) 294-298.
- [113] Lee-Ruff, E., Kazarians-Moghaddam, H., Katz, M., Controlled oxidations of benzo[a]pyrene, *Canadian Journal of Chemistry* 64 (1986) 1247-1253.
- [114] Lehr, R.E., Kumar, S., Levin, W., Wood, A.W., Chang, R.L., Conney, A.H., Yagi, H., Sayer, J.M., Jerina, D.M., The Bay Region Theory of Polycyclic Aromatic Hydrocarbon Carcinogenesis, *Polycyclic Hydrocarbons and Carcinogenesis*, American Chemical Society, 1985, pp. 63-84.
- [115] Li, C., Yang, Y., Wei, L., Wang, X., Wang, Z., Yin, Y., Li, G., An Array-Based Approach to Determine Different Subtype and Differentiation of Non-Small Cell Lung Cancer, *Theranostics* 5 (2015) 62-70.
- [116] Liang, Y., Gardner, D.R., Miller, C.D., Chen, D., Anderson, A.J., Weimer, B.C., Sims, R.C., Study of Biochemical Pathways and Enzymes Involved in Pyrene Degradation by Mycobacterium sp. Strain KMS, *American Society for Microbiology* 72 (2006) 7821-7828.
- [117] Liao, K.-W., Hou, M.T., Fujita, H., Andrew Yeh, J., Liquid-based tactile sensing array with adjustable sensing range and sensitivity by using dielectric liquid, *Sensors and Actuators A: Physical* 231 (2015) 15-20.
- [118] Liu, A., Yuan, W., Shi, G., Electrochemical actuator based on polypyrrole/sulfonated graphene/graphene tri-layer film, *Thin Solid Films* 520 (2012) 6307-6312.
- [119] Liu, J., Wang, Z., Xie, X., Cheng, H., Zhao, Y., Qu, L., A rationally-designed synergetic polypyrrole/graphene bilayer actuator, *Journal of Materials Chemistry* 22 (2012) 4015-4020.

- [120] Liu, Y., Yu, L.-M., Loo, S.C.J., Blair, R.G., Zhang, Q., Co-assembly of Zn(SPh)₂ and organic linkers into helical and zig-zag polymer chains, *Journal of Solid State Chemistry* 191 (2012) 283-286.
- [121] Loibner, A.P., Szolar, O.H.J., Braun, R., Hirmann, D., Toxicity Testing of 16 Priority Polycyclic Aromatic Hydrocarbons Using Lumistox, *Environmental Toxicology and Chemistry* 23 (2004) 557-564.
- [122] Lung, S.-C.C., Liu, C.-H., Fast analysis of 29 polycyclic aromatic hydrocarbons (PAHs) and nitro-PAHs with ultra-high performance liquid chromatography-atmospheric pressure photoionization-tandem mass spectrometry, *Scientific Reports* 5 (2015) 12992.
- [123] Ma, C.-W., Hsu, L.-S., Kuo, J.-C., Yang, Y.-J., A flexible tactile and shear sensing array fabricated using a novel buckypaper patterning technique, *Sensors and Actuators A: Physical* 231 (2015) 21-27.
- [124] Mailu, S.N., Development of electrochemical sensors containing bimetallic silver and gold nanoparticles, *Chemistry*, University of the Western Cape, Cape Town, 2010, pp. 183.
- [125] Mailu, S.N., Waryo, T.T., Ndangili, P.M., Ngece, F.R., Baleg, A.A., Baker, P.G., Iwuoha, E.I., Determination of Anthracene on Ag-Au Alloy Nanoparticles/Overoxidized-Polypyrrole Composite Modified Glassy Carbon Electrodes, *Sensors* 10 (2010) 9449-9465.
- [126] Makelane, H.R., Tovide, O., Sunday, C.E., Waryo, T., Iwuoha, E.I., Electrochemical Interrogation of G3-Poly(propylene thiophenimine) Dendritic Star Polymer in Phenanthrene Sensing, *Sensors* 15 (2015) 22343-22363.
- [127] Maliszewska-Kordybach, B., Sources, Concentrations, Fate and Effects of Polycyclic Aromatic Hydrocarbons (PAHs) in the Environment. Part A: PAHs in Air, *Polish Journal of Environmental Studies* 8 (1999) 131-136.
- [128] Manahan, S.E., *Environmental Chemistry*, 6th Edition ed., Lewis Publisher, New York, 1994.

- [129] Mashhadizadeh, M.H., Sheikhshoae, I., Mercury(II) ion-selective polymeric membrane sensor based on a recently synthesized Schiff base, *Talanta* 60 (2003) 73-80.
- [130] Mastral, A.M., Callén, M.S., A Review on Polycyclic Aromatic Hydrocarbon (PAH) Emissions from Energy Generation, *Environmental Science & Technology* 34 (2000) 3051-3057.
- [131] Melvin, G.J.H., Ni, Q.-Q., Natsuki, T., Bending actuation and charge distribution behavior of polyurethane/carbon nanotube electroactive nanocomposites, *Polymer Composites* (2014) n/a-n/a.
- [132] Meyer, S., Cartellieri, S., Steinhart, H., Simultaneous Determination of PAHs, Hetero-PAHs (N, S, O), and Their Degradation Products in Creosote-Contaminated Soils. Method Development, Validation, and Application to Hazardous Waste Sites, *Analytical Chemistry* 71 (1999) 4023-4029.
- [133] Miller, K.P., Ramos, K.S., Impact of Cellular Metabolism on the Biological Effects of Benzo[A]pyrene and related hydrocarbons, *Drug Metabolism Reviews* 33 (2001) 1-35.
- [134] Mirfakhrai, T., Madden, J.D.W., Baughman, R.H., Polymer artificial muscles, *Materials Today* 10 (2007) 30-38.
- [135] Mobaraki, N., Hemmateenejad, B., Structural characterization of carbonyl compounds by IR spectroscopy and chemometrics data analysis, *Chemometrics and Intelligent Laboratory Systems* 109 (2011) 171-177.
- [136] Mottier, P., Parisod, V., Turesky, R.J., Quantitative Determination of Polycyclic Aromatic Hydrocarbons in Barbecued Meat Sausages by Gas Chromatography Coupled to Mass Spectrometry, *Journal of Agricultural and Food Chemistry* 48 (2000) 1160-1166.
- [137] Mukai, K., Yamato, K., Asaka, K., Hata, K., Oike, H., Actuator of double layer film composed of carbon nanotubes and polypyrroles, *Sensors and Actuators B: Chemical* 161 (2012) 1010-1017.

- [138] Mulla, K., Zhao, Y., TTFV molecular tweezers with phenylboronic acid and phenylboronate endgroups: modular synthesis and electrochemical responses to saccharides and fluoride ion, *Tetrahedron Letters* 55 (2014) 382-386.
- [139] Mutlu, R., Alici, G., Weihua, L., Kinematic analysis of electroactive polymer actuators as soft and smart structures with more DoF than inputs, *Advanced Intelligent Mechatronics (AIM)*, 2012 IEEE/ASME International Conference on, 2012, pp. 484-489.
- [140] Nassef, E.M.R., Removal of polyaromatic hydrocarbons from waste water by electrocoagulation, *Journal of Petroleum and Gas Engineering* 5 (2014) 32-42.
- [141] Nederal, S., Pukec, D., Škevin, D., Kraljić, K., Obranović, M., Zrinjan, P., On-line DACC-HPLC analysis of polycyclic aromatic hydrocarbons in edible oils, *Croatian Journal of Food Technology, Biotechnology and Nutrition* 8 (2013) 74-81.
- [142] Oliveira, M., Slezakova, K., Alves, M.J., Fernandes, A., Teixeira, J.P., Delerue-Matos, C., Pereira, M.d.C., Morais, S., Polycyclic aromatic hydrocarbons at fire stations: firefighters' exposure monitoring and biomonitoring, and assessment of the contribution to total internal dose, *Journal of Hazardous Materials* 323, Part A (2017) 184-194.
- [143] Organization, W.H., *Air Quality Guidelines for Europe*, 2nd ed., World Health Organization Regional Office for Europe, Copenhagen, 2000.
- [144] Otero, T.F., Angulo, E., Rodríguez, J., Santamaría, C., Electrochemomechanical properties from a bilayer: polypyrrole / non-conducting and flexible material – artificial muscle, *Journal of Electroanalytical Chemistry* 341 (1992) 369-375.
- [145] Pashin, Y.V., Bakhitova, L.M., Mutagenic and carcinogenic properties of polycyclic aromatic hydrocarbons, *Environmental Health Perspectives* 30 (1979) 185-189.
- [146] Phuengphai, P., Youngme, S., Chaichit, N., Reedijk, J., New 3D supramolecular networks built from 1D and 2D frameworks via $\pi - \pi$ and H-bonding interactions: Topology and catalytic properties, *Inorganica Chimica Acta* 403 (2013) 35-42.
- [147] Pretsch, E.,ühlmann, P.B., Badertscher, M., *Structure Determination of Organic Compounds*, Springer, Germany, 2009

- [148] Purcaro, G., Moret, S., Conte, L.S., Rapid SPE-HPLC determination of the 16 European priority polycyclic aromatic hydrocarbons in olive oils, *Journal of Separation Science* 31 (2008) 3936-3944.
- [149] Pushparajah, D., Lewis, D.F.V., Ioannides, C., Up-regulation of CYP1A1 and phase II enzymes by 5-ring isomeric polycyclic aromatic hydrocarbons in precision-cut rat hepatic slices: Importance of molecular shape, *Toxicology in Vitro* 40 (2017) 203-213.
- [150] Qin, J.-C., Cheng, X.-y., Fang, R., Wang, M.-f., Yang, Z.-y., Li, T.-r., Li, Y., Two Schiff-base fluorescent sensors for selective sensing of aluminum (III): Experimental and computational studies, *Spectrochimica Acta Part A: Molecular and Biomolecular Spectroscopy* 152 (2016) 352-357.
- [151] Quang, D.T., Wu, J.-S., Luyen, N.D., Duong, T., Dan, N.D., Bao, N.C., Quy, P.T., Rhodamine-derived Schiff base for the selective determination of mercuric ions in water media, *Spectrochimica Acta Part A: Molecular and Biomolecular Spectroscopy* 78 (2011) 753-756.
- [152] Rakow, N.A., Suslick, K.S., A colorimetric sensor array for odour visualization, *Nature* 406 (2000) 710-713.
- [153] Rana, S., Singla, A.K., Bajaj, A., Elci, S.G., Miranda, O.R., Mout, R., Yan, B., Jirik, F.R., Rotello, V.M., Array-Based Sensing of Metastatic Cells and Tissues Using Nanoparticle-Fluorescent Protein Conjugates, *ACS Nano* 6 (2012) 8233-8240.
- [154] Rassie, C., Olowu, R.A., Waryo, T.T., Wilson, L., Williams, A., Baker, P.G., Iwuoha, E.I., Dendritic 7T-Polythiophene Electro-Catalytic Sensor System for the Determination of Polycyclic Aromatic Hydrocarbons, *International Journal of Electrochemical Science* 6 (2011) 1949-1967.
- [155] Ravindra, K., Sokhi, R., Van Grieken, R., Atmospheric polycyclic aromatic hydrocarbons: Source attribution, emission factors and regulation, *Atmospheric Environment* 42 (2008) 2895-2921.

- [156] Rengarajan, T., Rajendran, P., Nandakumar, N., Lokeshkumar, B., Rajendran, P., Nishigaki, I., Exposure to polycyclic aromatic hydrocarbons with special focus on cancer, *Asian Pacific Journal of Tropical Biomedicine* 5 (2015) 182-189.
- [157] Riskiobewertung), B.B.f., Carcinogenic polycyclic aromatic hydrocarbons (PAHs) in consumer products to be regulated by the EU - risk assessment by BfR in the context of a restriction proposal under REACH, BfR Opinion Nr. 032/2010 (2010) 20.
- [158] Rummel, A.M., Trosko, J.E., Wilson, M.R., Upham, B.L., Polycyclic aromatic hydrocarbons with bay-like regions inhibited gap junctional intercellular communication and stimulated MAPK activity, *Toxicological Sciences* 49 (1999) 232-240.
- [159] S.Arulmurugan, Kavitha, H.P., Venkatraman, B.R., Biological Activities of Schiff Base and its Complexes: A Review, *Rasayan Journal of Chemistry* 3 (2010) 385-410.
- [160] Sahu, S.K., Pandit, G.G., Puranik, V.D., Dry Deposition of Polycyclic Aromatic Hydrocarbons Associated with Atmospheric Particulate Matters in an Urban Site, Mumbai, India *Aerosol and Air Quality Research* 8 (2008) 437-446.
- [161] Schulz, C.M., Fritz, H., Ruthenschror, A., Occurrence of 15 + 1 EU priority polycyclic aromatic hydrocarbons (PAH) in various types of tea (*Camellia sinensis*) and herbal infusions, *Food Addit Contam Part A Chem Anal Control Expo Risk Assess* 31 (2014) 1723-1735.
- [162] Sciences, N.A.o., *Expanding the Vision of Sensor Materials*, National Academy Press, United States of America, 1995.
- [163] Sekhar, P.K., Brosha, E.L., Mukundan, R., Garzon, F.H., *Chemical Sensors for Environmental Monitoring and Homeland Security*, The Electrochemical Society Inter face (2010) 35-40.
- [164] Shankar, R., Ghosh, T.K., Spontak, R.J., Mechanical and actuation behavior of electroactive nanostructured polymers, *Sensors and Actuators A: Physical* 151 (2009) 46-52.
- [165] Shen, H., Huang, Y., Wang, R., Zhu, D., Li, W., Shen, G., Wang, B., Zhang, Y., Chen, Y., Lu, Y., Chen, H., Li, T., Sun, K., Li, B., Liu, W., Liu, J., Tao, S., *Global*

- atmospheric emissions of polycyclic aromatic hydrocarbons from 1960 to 2008 and future predictions, *Environmental science & technology* 47 (2013) 6415-6424.
- [166] Shen, X., Cui, Y., Pang, Y., Qian, H., Graphene oxide nanoribbon and polyhedral oligomeric silsesquioxane assembled composite frameworks for pre-concentrating and electrochemical sensing of 1-hydroxypyrene, *Electrochimica Acta* 59 (2012) 91-99.
- [167] Shrivastava, A., Gupta, V., Methods for the determination of limit of detection and limit of quantitation of the analytical methods, *Chronicles of Young Scientists* 2 (2011) 21-25.
- [168] Shui-Ping Wu, Bing-Yu Yang, Xin-Hong Wang, Chung-Shin Yuan, Hong, H.-S., Polycyclic Aromatic Hydrocarbons in the Atmosphere of Two Subtropical Cities in Southeast China: Seasonal Variation and Gas/Particle Partitioning, *Aerosol and Air Quality Research* 14 (2014) 1232-1246.
- [169] Sigman, M.i., Schuler, P.F., Ghosh, M., Dabestani, R.T., Mechanism of Pyrene Photochemical Oxidation in Aqueous and Surfactant Solutions, 32 (1998) 3980-3985.
- [170] Silva, T.F.d., Azevedo, D.d.A., Neto, F.R.d.A., Distribution of polycyclic aromatic hydrocarbons in surface sediments and waters from Guanabara Bay, Rio de Janeiro, Brazil, *Journal of the Brazilian Chemical Society* 18 (2007) 628-637.
- [171] Springer, *Handbook of Nanotechnology*, 2nd ed., Springer Berlin Heidelberg, 2007.
- [172] Srogi, K., Monitoring of environmental exposure to polycyclic aromatic hydrocarbons: a review, *Environmental Chemistry Letters* 5 (2007) 169-195.
- [173] Sutar, D., Aswal, D.K., Gupta, S.K., Yakhmi, J.V., Electrochemical actuator from conductive electroactive polymer polypyrrole deposited on gold, *Indian Journal of Pure & Applied Physics* 45 (2007) 354-357.
- [174] Taleat, Z., Khoshroo, A., Mazloun-Ardakani, M., Screen-printed electrodes for biosensing: a review (2008-2013), *Microchimica Acta* 181 (2014) 865-891.
- [175] Technologies, A., Improved Analysis of Polycyclic Aromatic Hydrocarbons with the Varian 920-LC and Pursuit™ PAH Column, Varian Incorporated, 2014.

- [176] Terasawa, N., Takeuchi, I., Electrochemical property and actuation mechanism of an actuator using three different electrode and same electrolyte in air: Carbon nanotube/ionic liquid/polymer gel electrode, carbon nanotube/ionic liquid gel electrode and Au paste as an electrode, *Sensors and Actuators B: Chemical* 145 (2010) 775-780.
- [177] Thummala, P., Huang, L., Zhang, Z., Andersen, M.A.E., Analysis of Dielectric Electro Active Polymer actuator and its high voltage driving circuits, *Power Modulator and High Voltage Conference (IPMHVC), 2012 IEEE International*, 2012, pp. 458-461.
- [178] Torop, J., Aabloo, A., Jager, E.W.H., Novel actuators based on polypyrrole/carbide-derived carbon hybrid materials, *Carbon* 80 (2014) 387-395.
- [179] Tovide, O., Jahed, N., Sunday, C.E., Pokpas, K., Ajayi, R.F., Makelane, H.R., Molapo, K.M., John, S.V., Baker, P.G., Iwuoha, E.I., Electro-oxidation of anthracene on polyanilino-graphene composite electrode, *Sensors and Actuators B: Chemical* 205 (2014) 184-192.
- [180] Tovide, O.O., Graphenated polyaniline nanocomposite for the determination of polyaromatic hydrocarbons (PAHs) in water, *Chemistry, University of the Western Cape, Cape Town*, 2013, pp. 327.
- [181] Trufelli, H., Palma, P., Famigliani, G., Cappiello, A., An overview of matrix effects in liquid chromatography-mass spectrometry, *Mass Spectrometry Reviews* 30 (2011) 491-509.
- [182] Tsai, H.-K.A., Ma, K.-S., Wang, C., Xu, H., Wang, C., Zoval, J., Kulinsky, L., Madou, M., Development of integrated protection for a miniaturized drug delivery system, *Smart Materials and Structures* 16 (2007) S295.
- [183] Udhayakumari, D., Velmathi, S., Azo Linked Polycyclic Aromatic Hydrocarbons-Based Dual Chemosensor for Cu²⁺ and Hg²⁺ Ions, *Industrial & Engineering Chemistry Research* 54 (2015) 3541-3547.

- [184] Vasilescu, A., Nunes, G., Hayat, A., Latif, U., Marty, J.-L., Electrochemical Affinity Biosensors Based on Disposable Screen-Printed Electrodes for Detection of Food Allergens, *Sensors (Basel, Switzerland)* 16 (2016) 1863.
- [185] Wan, B., Sayler, G.S., Schultz, T.W., Structure-activity relationships for flow cytometric data of smaller polycyclic aromatic hydrocarbons, SAR and QSAR in *Environmental Research* 17 (2006) 597-605.
- [186] Wang, H., Tjahyono, S.S., MacDonald, B., Kilmartin, P.A., Travas-Sejdic, J., Kiefer, R., Robotic Fish Based on a Polymer Actuator, *Australasian Conference on Robotics and Automation, Brisbane*, 2007.
- [187] Wang, J., Huang, L., Xue, M., Liu, L., Wang, Y., Gao, L., Zhu, J., Zou, Z., Developing a novel fluorescence chemosensor by self-assembly of Bis-Schiff base within the channel of mesoporous SBA-15 for sensitive detecting of Hg²⁺ ions, *Applied Surface Science* 254 (2008) 5329-5335.
- [188] Wang, S., Chanock, S., Tang, D., Li, Z., Jedrychowski, W., Perera, F.P., Assessment of Interactions between PAH Exposure and Genetic Polymorphisms on PAH-DNA Adducts in African American, Dominican, and Caucasian Mothers and Newborns, *Cancer epidemiology, biomarkers & prevention : a publication of the American Association for Cancer Research, cosponsored by the American Society of Preventive Oncology* 17 (2008) 405-413.
- [189] Wang, Y., Bian, K., Hu, C., Zhang, Z., Chen, N., Zhang, H., Qu, L., Flexible and wearable graphene/polypyrrole fibers towards multifunctional actuator applications, *Electrochemistry Communications* 35 (2013) 49-52.
- [190] Ward, M., Botha, S., Iwuoha, E., Baker, P., Actuation Behaviour of a Derivatized Pyrrole Accordion Type Polymer, *International Journal of Electrochemical Science* 9 (2014) 4776-4792.
- [191] Węgrzyn, E., Grześkiewicz, S., Popławska, W., Głód, B.K., Modified Analytical Method for Polycyclic Aromatic Hydrocarbons, using SEC for sample preparation and RP-HPLC with Fluorescence detection. Application to different food samples, *Acta Chromatographica* (2006) 233-249.

- [192] Wheeler, A.J., Dobbin, N.A., Heroux, M.E., Fisher, M., Sun, L., Khoury, C.F., Hauser, R., Walker, M., Ramsay, T., Bienvenu, J.F., LeBlanc, A., Daigle, E., Gaudreau, E., Belanger, P., Feeley, M., Ayotte, P., Arbuckle, T.E., Urinary and breast milk biomarkers to assess exposure to naphthalene in pregnant women: an investigation of personal and indoor air sources, *Environ Health* 13 (2014) 30.
- [193] Williamson, K.S., Petty, J.D., Huckins, J.N., Lebo, J.A., Kaiser, E.M., HPLC-PFD determination of priority pollutant PAHs in water, sediment, and semipermeable membrane devices, *Chemosphere* 49 (2002) 703-715.
- [194] Wu, Y., Alici, G., Spinks, G.M., Wallace, G.G., Fast trilayer polypyrrole bending actuators for high speed applications, *Synthetic Metals* 156 (2006) 1017-1022.
- [195] Xia, H., Byrd, D., Dekate, S., Lee, B., High-Density Fiber Optical Sensor and Instrumentation for Gas Turbine Operation Condition Monitoring, *Journal of Sensors* (2013) 10.
- [196] Xu, H., Wang, C., Wang, C., Zoval, J., Madou, M., Polymer actuator valves toward controlled drug delivery application, *Biosensors and Bioelectronics* 21 (2006) 2094-2099.
- [197] Xu, L., Chen, W., Mulchandani, A., Yan, Y., Reversible Conversion of Conducting Polymer Films from Superhydrophobic to Superhydrophilic, *Angewandte Chemie International Edition* 44 (2005) 6009-6012.
- [198] Xu, T., Duan, H., Wang, X., Meng, X., Bu, J., Fluorescence sensors for Zn²⁺ based on conjugated indole Schiff base, *Spectrochimica Acta Part A: Molecular and Biomolecular Spectroscopy* 138 (2015) 603-608.
- [199] Xue, W., Warshawsky, D., Metabolic activation of polycyclic and heterocyclic aromatic hydrocarbons and DNA damage: A review, *Toxicology and Applied Pharmacology* 206 (2005) 73-93.
- [200] Yan, J., Wang, L., Fu, P.P., Yu, H., Photomutagenicity of 16 polycyclic aromatic hydrocarbons from the US EPA priority pollutant list, *Mutation research* 557 (2004) 99-108.
- [201] Yang, D.-H., Lee, C.-S., Jeon, B.-H., Choi, S.M., Kim, Y.-D., Shin, J.S., Kim, H., An electrochemical nanofilm sensor for determination of 1-hydroxypyrene using

- molecularly imprinted receptors, *Journal of Industrial and Engineering Chemistry* (2017).
- [202] Yardım, Y., Keskin, E., Levent, A., Özsöz, M., Şentürk, Z., Voltammetric studies on the potent carcinogen, 7,12-dimethylbenz[a]anthracene: Adsorptive stripping voltammetric determination in bulk aqueous forms and human urine samples and detection of DNA interaction on pencil graphite electrode, *Talanta* 80 (2010) 1347-1355.
- [203] Yazdanbakhsh, M., Takjoo, R., Frank, W., Kaju, A.A., The preparation, spectroscopic characterization and X-ray crystal structures of the pyrrole-2-carboxaldehyde Schiff base of S-allyldithiocarbamate (HL) and its nickel(II) complex ([Ni(L)₂]), *Journal of Coordination Chemistry* 62 (2009) 3651-3660.
- [204] YouMing, Z., BingBing, S., Peng, Z., JianQiang, H., Pei, C., Qi, L., Jun, L., TaiBao, W., A highly selective dual-channel Hg²⁺ chemosensor based on an easy to prepare double naphthalene Schiff base, *Science China Chemistry* 56 (2013) 612-618.
- [205] Yu, H.-h., Xu, B., Swager, T.M., A Proton-Doped Calix[4]arene-Based Conducting Polymer, *Journal of the American Chemical Society* 125 (2003) 1142-1143.
- [206] Yu, H., Environmental Carcinogenic Polycyclic Aromatic Hydrocarbons: Photochemistry and Phototoxicity, *Journal of environmental science and health. Part C, Environmental carcinogenesis & ecotoxicology reviews* 20 (2002) 10.1081/GNC-120016203.
- [207] Yu, Y., Li, Q., Wang, H., Wang, B., Wang, X., Ren, A., Tao, S., Risk of human exposure to polycyclic aromatic hydrocarbons: A case study in Beijing, China, *Environmental Pollution* 205 (2015) 70-77.
- [208] Zainudeen, U.L., Careem, M.A., Skaarup, S., PEDOT and PPy conducting polymer bilayer and trilayer actuators, *Sensors and Actuators B: Chemical* 134 (2008) 467-470.
- [209] Zelic, M., Reverse Scan as a Source of Information in Square Wave Voltammetry, *Croatica Chemica Acta* 79 (2006) 49-55.
- [210] Zelinkova, Z., Wenzl, T., The Occurrence of 16 EPA PAHs in Food - A Review, *Polycyclic Aromatic Compounds* 35 (2015) 248-284.

- [211] Zhang, L.-X., Liu, Y., Cia, L.-H., Hu, Y.-J., Yin, J., Hu, P.-Z., Inhibitory study of some novel Schiff base derivatives on *Staphylococcus aureus* by microcalorimetry, *Thermochimica Acta* 440 (2006) 51-56.
- [212] Zhang, M., Ahmad, M., Lee, S.S., Xu, L.H., Ok, Y.S., Sorption of polycyclic aromatic hydrocarbons (PAHs) to lignin: effects of hydrophobicity and temperature, *Bull Environ Contam Toxicol* 93 (2014) 84-88.
- [213] Zhang, Y., Su, Q., Xu, J., Zhang, Y., Chen, S., Detecting of Benzo[a]pyrene Using a Label-free Amperometric Immunosensor, *International Journal of Electrochemical Science* 9 (2014) 3736-3745.
- [214] Zhang, Y., Tao, S., Global atmospheric emission inventory of polycyclic aromatic hydrocarbons (PAHs) for 2004, *Atmospheric Environment* 43 (2009) 812-819.
- [215] Zheng, X., Tian, D., Duan, S., Wei, M., Liu, S., Zhou, C., Li, Q., Wu, G., Polypyrrole Composite Film for Highly Sensitive and Selective Electrochemical Determination Sensors, *Electrochimica Acta* 130 (2014) 187-193.
- [216] Zhou, M., Heinze, J., Electropolymerization of Pyrrole and Electrochemical Study of Polypyrrole. 2. Influence of Acidity on the Formation of Polypyrrole and the Multipathway Mechanism, *The Journal of Physical Chemistry B* 103 (1999) 8443-8450.
- [217] Zhou, P., Liu, H., Chen, S., Lucia, L., Zhan, H., Fu, S., 2,3-Diaminophenazine, *Molbank* 2011 (2011) M730.
- [218] Zitka, O., Babul, P., Sochor, J., Kummerova, M., Krystofova, O., Adam, V., Havel, L., Beklova, M., Hubalek, J., Kizek, R., Determination of Eight Polycyclic Aromatic Hydrocarbons and in Pea Plants (*Pisum sativum* L.) Extracts by High Performance Liquid Chromatography with Electrochemical Detection, *International Journal of Electrochemical Science* 7 (2012) 908-927.

9. Publication 1

Polypyrrole Derivatives in the Design of electrochemically Driven Actuators

Meryck Ward^a, Priscilla Baker^{a,*}, Emmanuel Iwuoha^a, Pierre-Henri Aubert^b and Cedric Plesse^b

^aSensorLab, Department of Chemistry, University of the Western Cape, Private Bag X17, Bellville 7535, South Africa;

^bLaboratoire de Physico-chimie des Polymères et des Interfaces (LPPI, EA 2528), Université de Cergy-Pontoise, 5 Mail Gay Lussac, 95031 Cergy-Pontoise Cedex, France

Abstract: Recent developments in the field of biomimetic systems demand mechanical systems that are capable of delivering high power output per volume or mass. Volume changes within the conducting polymer layers are caused by the oxidation or reduction of the polymer. This volume change is the main source for actuators bending or deforming. Different actuator designs have been explored over the years to maximize bending, displacement or deformation. The bilayer design (two layers) incorporates a highly conductive metal layer along with the conducting polymer layer in its design. Trilayer designs (three layers) utilize an electrolyte storage layer to avoid delamination within the design. The storage layer allows for the trilayer design to operate freely in both liquid and air environments. To a limited extent zig zag conformations of polymers linked by small organic molecules or metal coordinating ligands have also been explored in the search for actuator materials with significant deformation and high current density. This review evaluates the contribution of polypyrrole and its derivatives in these actuator designs that impact on maximum displacement capability, current density and the lifetime of these actuator systems.

Keywords: Actuators, electroactive polymers (EAPs), novel polymer composites, polymer conformations, polypyrrole (PPy), volume changes.

9.1 Introduction

Extensive studies have been performed in the field of electroactive polymer (EAPs) actuators due to their muscle-like behaviour and unusual properties.[139] The polymers used in actuators can be classed as polymers that respond to electrical stimulus.[131] Bending or deformation occurs by a change in shape or potential in response to electrical stimulus.[4, 27, 177] EAPs produce actuator materials with strain, stress, work density, electrochemical coupling, relative speed cycles, flexibility, lightweight, tolerance against fracture, simple fabrication processes and the ability to convert electrical energy into mechanical energy (work) causing a force which produces large strains.[134, 164] The most attractive feature of these EAPs is their ability to mimic biological muscles. EAPs are resilient, tough and display large actuation.[20] These polymers can be classed into two categories based on their actuation mechanism, i.e. ionic EAPs (wet) and electronic EAPs (dry). Most ionic EAPs function in an electrochemical system which requires a liquid electrolyte for ion transportations while the electronic EAPs actuate due to the forces from the shift or motion in an electrical charge. Electronic EAPs are favored due to the ability to operate in air (dry environment), whereas the ionic EAPs requires a liquid medium (high safety encapsulation required for liquid media). An electric field or coulomb forces drive electronic EAPs, whereas the actuation mechanism for ionic EAPs is based upon the diffusion or mobility of ions. Electronic EAPs generally require strong electrical fields (>100 V/m) and the ionic EAPs require low driving voltages, nearly equal to 1-5V. EAPs have been used in the development of soft, lightweight actuators, sensors and energy harvesting devices that are widely applicable to robotics, haptics (sense of touch devices) and biomimetic systems.[64, 112] However, they suffer from disadvantages such as high energy requirements and low actuation force. EAP actuators based on conducting polymers particularly PPy have gained much attention due to its biocompatibility, biodegradability, ease of synthesis, low actuation power, ability to operate in liquid and air environments and stability with large volume changes. Synthesis of PPy carried out at low temperature tend to yield higher conductivities and smoother surface morphology.[99] Current density affects the rate of oxidation and therefore the polymerization of pyrrole. Synthesis at a current density of 0.1 mA.cm^{-2} displayed high surface roughness and was more rigid compared to current densities at 0.05

$\text{mA}\cdot\text{cm}^{-2}$. Current densities at $0.025 \text{ mA}\cdot\text{cm}^{-2}$ resulted in weak cohesion of the PPy and some of the regions of polyvinylidene fluoride (PVDF) remained uncoated.[100] Actuators based on PPy or other conducting polymers are electrochemically driven and may be constructed in various geometries (Makai et al., 2012).[137] The structural properties of PPy depend on the oxidation potential applied during the polymerization process (Zhou et al., 1999). Long chains (30-60 units) have been obtained using potentials close to 1.0 V with shorter chains (8-16 units) at lower potentials.

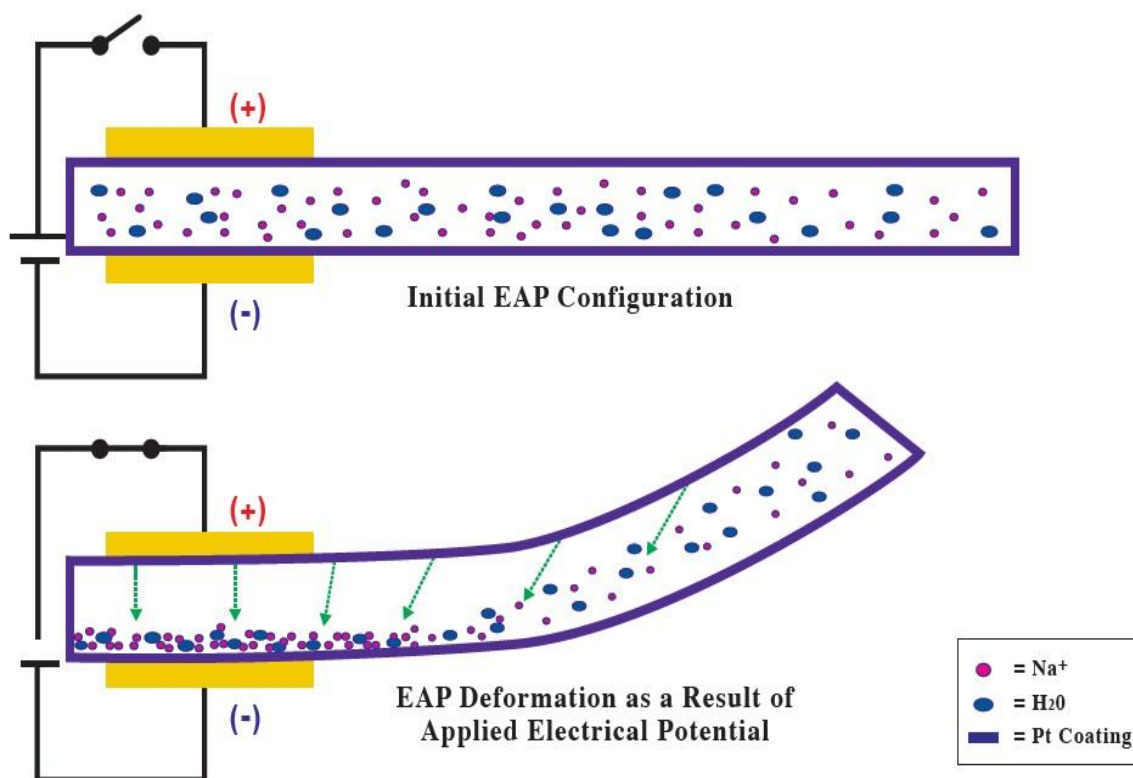
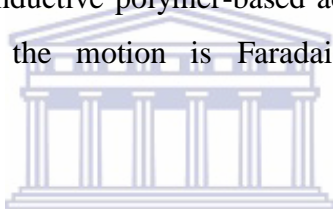


Figure 71. Possible deformation mechanism of an EAP.

Cross-linked or conjugated chains (8-16 units) were obtained from potentials between 1.0 - 1.5 V. The short chain units of PPy are based on cation movement at low potentials, with the long and cross-linked/conjugated chain units based mainly on anion movement.[104, 216] Large volume displacement is an important parameter for EAPs actuators, whose operation principle is based on the volume of expansion or contraction generated by the movement of ions during an electrochemical reaction. Bending of the EAP is induced when

positive counter ions move towards the cathode, while the negative ions that are fixed at the polymer, experience an attractive force from the anode. Simultaneously water molecules in the EAPs matrix diffuse towards the region with the highest positive ion concentration (cathode) to equalize the charge distribution. This causes the region near the anode to swell and the region near the cathode to shrink, leading to stresses which cause the EAP to bend towards anode (**Figure 74**).[44] EAPs are favoured in actuators where large deformations are required. Most EAP actuators have been synthesized to function in liquid mediums, however multi-layered EAP actuators can function in both wet and dry environments. Multi-layered actuators can be electrochemically oxidized or reduced in a continuous and reversible way which leads to bending.[63] Ordinary ‘wet’ EAP actuators operate only in electrolyte solutions whereas ‘dry’ EAP actuators work in air using ionic liquids as built in electrolytes. However, in principle, these conductive polymer-based actuators have drawbacks in their lifetime and responsivity, as the motion is Faradaically driven via oxidation or reduction.[176]



9.2 Bilayer actuators

The development of a bilayer device was proposed in 1992 by T.F. Otero who based his design on two films of material in contact with one another, having different coefficients of expansion.[144] Bilayers (**Figure 75**) provided a way in which actuation of conjugated polymers such as PPy, PANI and polythiophene (PTH) can be studied. The actuator consists of one stimuli responsive coating polymer layer which provided the swelling and contracting onto a flexible and inactive polymeric substrate which provides mechanical strength.[65]

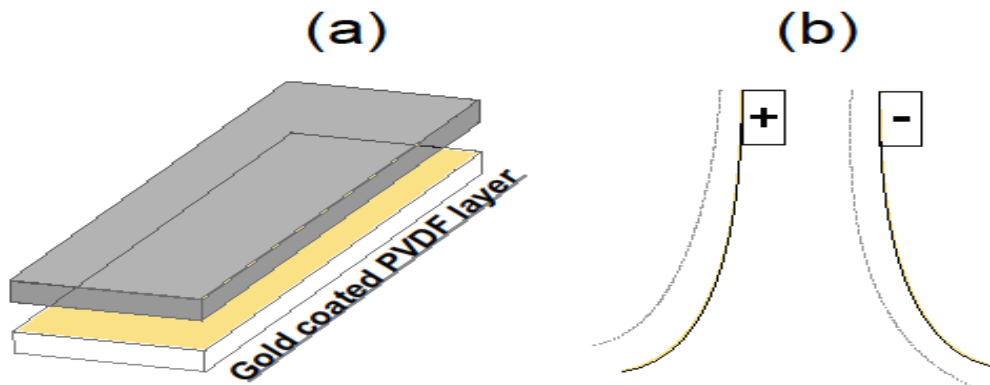


Figure 72. (a) Bilayer actuator design, (b) Operating mechanism

Implementation of conducting polymer materials in bilayer actuators allow for the possibility to operate these actuators in both wet environments (in the presence of electrolyte solutions) and dry environments (operation in air which include applications such as; used in humidity sensors).

Table 29. Modified polypyrrole bilayers.

Material		Bending Angle / Displacement	Application
PPy-DBS/Au	2006	> 60° Bending occurs – 0.3 V vs Ag/AgCl reaching the max. within 2 sec. Original position achieved at 0 V vs Ag/AgCl	Release valves for Drug Delivery Systems
PPy-DBS/Au	2007	90° Bending occurs at +2 V , reversal process occurs at -2 V	Response testing to ac/dc voltages
PPy-DBS/Au	2011	90° Neutral state at 0 V vs Ag/AgCl Bending occurs at +1 V vs Ag/AgCl at a max. frequency of 4 Hz	Mechanical microactuators for micromixing
PPy/Cellophane	2005	2.8 mm	Improving displacement performance of the actuator
PPy/Graphene	2012	120° Movement to the PPy side (- 0.8 V vs Ag/AgCl) and movement to the graphene side (+ 0.8 V vs Ag/AgCl)	Designed for the use in advanced actuation systems such as micro/nano-electromechanical systems
PPy/Graphene Fiber	2013	Symmetrical bending displacement at ± 0.8 V vs Ag/AgCl	Used in the construction of sophisticated devices such as fiber microtweezers

Note 1. PPy - Polypyrrole, Au - Gold, DBS - Dodecylbenzene Sulphonate.

Bilayer actuators (**Table 29**) resulting from the electrodeposition of PPy onto a metal electrode (Au - gold) have been used as a release valve of a drug reservoir such as biodegradable microspheres, microneedles and implantable microchips. Bending of the actuator occurred at +1.2 V vs Ag/AgCl resulting in the release of a fluorescent dye, the process was reversed by applying -1.0 V vs Ag/AgCl.[182] PPy/Au bilayer actuators was used in the development of tools such as a microrobotic arm for the manipulation of single cells. The bending/rotation of the arm was controlled by applying voltages between 0.2 V and -1.0 V vs Ag/AgCl, the arm achieved a minor sideways bending/rotation of $\sim 20^\circ$. [88] Bilayer actuators have the potential to be used in medical applications as drug delivery systems. Applied electrical stimulus to the device causes a deformation of the actuator, thus releasing any drug the reservoir might hold (**Figure 76**).

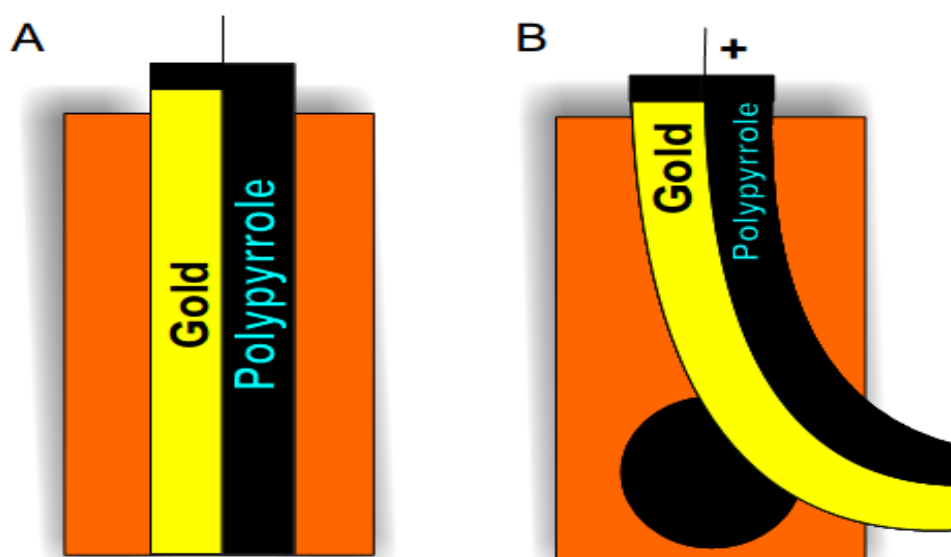


Figure 73. (a) The bilayer actuator at rest covering a reservoir, (b) Electrical stimulus applied to the bilayer actuator causing displacement and revealing the opening to the reservoir.

Aromatic dopant anions such as dodecyl benzene sulphonate (DBS^-), have been found to enhance the conductivity and mechanical strength of bilayer PPy films. Drug delivery devices employing a PPy-DBS/Au bilayer experienced bending greater than 60° between a

cycled potential of 0 V to -1 V vs Ag/AgCl. The maximum bending was reached at -0.3 V vs Ag/AgCl within 2 s, and returned to resting state at 0 V.[196] PPy doped with DBS displayed large displacements and fast responses. Bending of the EAPs (PPy-DBS) was dependent upon oxidation and reduction potential. The actuator response times was measured as 2 to 3 s for bending at ± 2 V reaching up to 90° bending.[173] Mechanical microactuators such as PPy-DBS/Au bilayer may be used for micromixing, fluid pumping or fluidic propelling of microrobots. The actuator containing the doped polymer was at a neutral state (flat conformation) at 0 V, but under positive potential of +1 V vs Ag/AgCl a bending of at least 90° was achieved at a maximum frequency of 4 Hz.[38] Bilayer actuators constructed of PPy/cellophane (electroactive paper) showed large displacement capabilities. This actuator device was constructed to improve displacement performance in electrolyte solutions for actuators of different thickness. The bilayer actuator displayed a maximum displacement of 2.8 mm at +6 V vs Ag/AgCl at a frequency of 0.5 Hz.[51] Bilayer actuators based on PPy/graphene have been designed for advanced actuation systems which are important for application in micro/nano-electromechanical systems. This modification (incorporation of the graphene layer) of the bilayer actuator exhibits improvement in movable curvature (displacement) and mechanical strength of the PPy film. The actuator experiences an electrochemical deformation of 120° with the actuator moving towards the PPy side at - 0.8 V vs Ag/AgCl and towards the graphene side at + 0.8 V vs Ag/AgCl.[119] Novel electrochemical fiber actuators based on graphene fiber/PPy have been used to fabricate multi-armed tweezers and net actuators. Symmetrical actuator bending displacement occurs at electrochemical potentials of - 0.8 V vs Ag/AgCl and + 0.8 V vs Ag/AgCl. This actuator design has demonstrated higher actuation activity and durability compared to other graphene based actuators.[189] PPy is a prime candidate for conducting polymer actuators, but has a disadvantage of decreased electronic conductivity during polymer reduction. This reduction in conductivity is the reason for not reaching high actuation speeds, the main reason for poor actuator performance. The introduction of poly(3,4-ethylene dioxythiophene), PEDOT, into a bilayer (PPy-DBS/PEDOT-DBS) actuator design improved the conductivity of the actuator due to the high conductivity of PEDOT.[208]

9.3 Trilayer actuators

Trilayer actuator addresses some of the inherent weaknesses in bilayer devices. The use of a metallic counter electrode may be avoided in order to obtain higher frequencies, whilst using the same current to produce a range of volume changes.[14] The actuator device comprises of two conducting polymer layers and one electrolyte storage (non-volume changing) layer.[63] This electrolyte storage layer, usually PVDF, allows for the actuator to operate in both wet and dry environments. A small potential difference applied between the two outer layers causes oxidation of the one layer and reduction of the other layer. Counter-ions are passed through the two conducting polymer (CP) layers via the middle electrolyte storage layer during the electrochemical switching process. Ion movement in and out of the CP layers causes swelling and de-swelling. Due to the middle electrolyte layer constraining the active layer, the whole laminated multilayer structure generates a bending motion similar to that of the cantilevered bilayer structure. The oxidized layer absorbs anions and expands while the reduced layer gives up anions and contracts (**Figure 77**) resulting in differential expansion leading to the bending of the actuator.[58, 59]

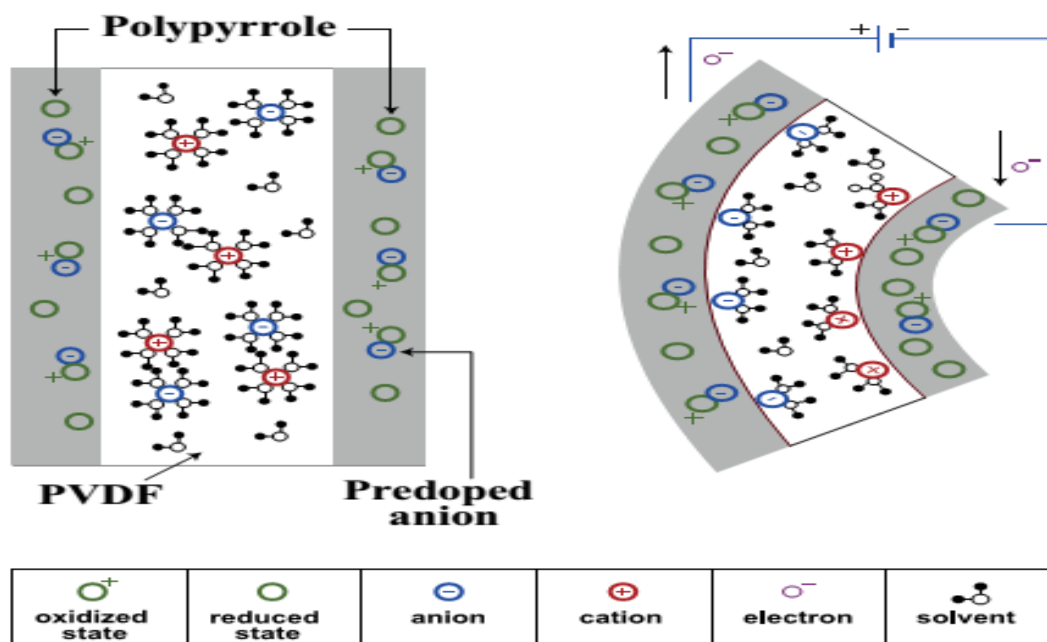


Figure 74. Illustration of the behaviour of the trilayer actuator under electrical stimulus.

Different fabrication methods have been employed in order to improve performance of the trilayer actuator material (**Table 30**).

Table 30. Modified polypyrrole trilayers.

Material	Year	Thickness	Current Density (PPy Deposition)	Bending Angle / Displacement	Application/Purpose
PPy/PVDF/PPy	2011	PVDF: ~145 μm	0.05 mA/cm ²	50 mm Maximum displacement obtained at 0.2 Hz and +3 V	Actuator studied for optimum mechanical and electrical properties
PPy/PVDF/PPy	2013	PVDF: 110 μm	0.1 mA/cm ²	18 mm Maximum displacement reached at +1.5 V at a frequency of 0.05 Hz	Development of microdevices such as comprising individually controllable actuators
PPy(DBS)/PTh/PPy (ClO ₄)	2004		2 mA.cm ⁻²	$\pm 90^\circ$ Bending at ± 1 V vs SCE	Used to determine if the polythiophene layer would provide mechanical support for the actuator
PPy/PVDF(Au)/PPy(TFSI/PF ₆)	2006	PVDF: 110 μm	0.1 mA.cm ⁻²	Displacement obtained TFSI = 60 mm, PF ₆ = 20 mm at ± 1 V at a frequency of 4 Hz	Designed for applications requiring a high speed of response
PPy/SG/RGO	2012	Actuator: 3 μm		Actuator bending occurred at -1.0 V vs SCE achieving a bending angle of + 90° and - 90° at 0.4 V vs SCE	Fabricated to improve performance and lifetime

Note 2. PTh - Polythiophene, PVDF - Polyvinylidene Fluoride, TFSI - Trifluoromethanesulfonimide, PF₆ - Hexafluorophosphate, ClO₄ - Perchlorate, SCE - Saturated Calomel Electrode, SG – Sulfonated Graphene, RGO – Reduced Graphene Oxide

Trilayers incorporating two conducting polymer layers separated by a PVDF layer, the PVDF layer can be used for both an insulator between the layers and an electrolyte reservoir. The trilayer actuators using this design was studied for optimum mechanical and electrical properties, actuator deflection, force output and stability. A maximum displacement of 50 mm was obtained +3 V at 0.2 Hz. Microdevices have been developed based on microactuators that operate in air, these microactuators use the PPy/PVDF/PPy trilayer design. A displacement of 18 mm was achieved at +1.5 V at a frequency of 0.05 Hz.[89] A trilayer conducting polymer composite film consisting of PPy-DBS/PTh/PPy-ClO₄ displayed maximum displacement of $\pm 90^\circ$ at a potential of ± 1 V vs saturated calomel electrode (SCE).[74] Trilayer actuators containing PPy doped with surfactants including

trifluoromethanesulfonimide (TFSI) and hexafluorophosphate (PF6), were prepared with TFSI producing the highest speed of response. Enhancement in the speed of bending in the trilayer actuator was achieved through mechanical resonance which also explains the effect of the dopant on the speed of actuation. Maximum displacements were reached at ± 1 V at a frequency of 4 Hz, with TFSI and PF6 generating a displacement of 60 mm and 20 mm respectively.[194] Different fabrication methods have been performed over the years to improve actuator performance, with thickness being an important parameter. At a thickness of the CP (PPy) layer exceeding 60 μm the bending movement was observed to decrease (Alici, G., et al., 2005).[7] This indicated that the PPy actuator was unable to overcome its increased resistance (flexural rigidity) while undergoing bending. Trilayer actuators have displayed great potential for a variety of applications, due to its low input voltages, biocompatibility and ability to operate in both environments. The lifetime of these actuators operating in air, was limited to the time the electrolyte solution remained in the electrolyte storage layer. The robotic fish designed by (Wang et al., 2007) encapsulated the CP layers to increase the lifetime of the actuator. The important parameters discussed when designing the robotic fish was frequency and thickness of the conducting polymer layer. Various layer thicknesses were evaluated over a frequency range between 0.03 to 10 Hz. The CP layer with a thickness of 10 μm at 1 Hz provided the best deflection of 4mm for the trilayer design.[186] Actuator conductivities determine the rate at which ions move in and out of the polymer films, therefore playing an important role in polymer material selection. PPy has relatively low conductivity but it is improved by either doping the polymer or modifying the material by incorporating materials with higher conductivity. Low conductivity actuators are responsible for slow response and deformation, whereas high conductivity actuators experience fast response and deformation. Actuator designs employing a modification of a poly(3,4-ethylenedioxythiophene), PEDOT, layer sandwiched between two PPy layers showed improved actuator performance. Improvements observed in this design were strain and force difference between redox states at faster scan rates and in actuator performance due to no delamination between the layers. The trilayer experiences a reduction in strain due to ionic diffusion and drift in an electric field. PEDOT does not affect the strain negatively but does however influence cyclic voltammetry at lower potentials. The PEDOT layer causes

PPy to be reduced at two different potentials. Actuation of the actuators occurred between a potential window of + 0.4 V to - 1.0 V against Ag/AgCl. Reduction peaks were observed at - 0.55 V (sharp peak) and - 0.95 V (broad peak). Broadening of the second peak was attributed to ions penetrating the PEDOT(DBS) layer.[208] PPy was electrodeposited onto a bilayer actuator to produce this trilayer design which exhibited a high and stable actuating performance. Graphene reduced the charge or energy that was required to reach a constant bending angle. The actuator deformed from rest at 0 V to +90° at -1.0 V vs saturated calomel electrode (SCE) towards graphene. Similarly the actuator deformed at 0.4 V vs SCE to an angle of -90°, towards PPy. The actuator displayed a disappearance of redox waves associated with PPy in the cyclic voltammogram, contributing to the gradual weakening and finally disappearance of the PPy redox waves after 5000 actuations. This was evident from SEM images where gaps were observed resulting in delamination (**Figure 78**).[118]

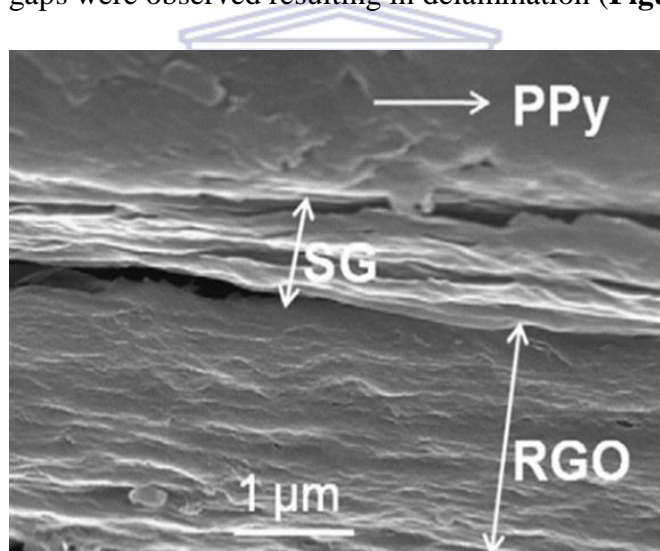


Figure 75. Trilayer experiences delamination due to excess number of actuation cycles.

Bending trilayer actuators consisting of PPy films incorporated with porous carbide-derived carbon (CDC) particles displayed properties which made them suitable for energy storage applications. This design incorporated two modified polymer layers on either side of an electrolyte storage layer. The actuation mechanism was based on the intercalation of ions due to the electric double layer charging of the electrodes. Actuators using CDC particles have been found to be more efficient and have doubled the amount of swelling per injected

charge, this improvement was very important as it overcame the low energy efficiency displayed by ionic electroactive polymers. Operations in electrolyte solutions use a design of two PPy(DBS)CDC layers on either side of a PVDF layer, this design displayed large volume changes. The bending of this fabrication in air was made possible by soaking the trilayer in Lithium bis(trifluoromethane sulfonyl) imide (LiTFSI). However, using this air operated design has shown a decrease in actuator bending from 200 μm for PPy(TFSI) to 8 μm for PPy(TFSI)CDC. The bending signal displayed more noise, due to the actuators bending response being close to the detection limit of the laser displacement sensor. The bending signal was also affected by the roughness of the PPy(TFSI)CDC actuator surface. CDC nanoparticles that have lower conductivity leads to an increase in the films overall resistance (causes actuator stiffness) thus reducing the bending ability of the actuator.[178] The image below is a further representation of trilayer actuators consisting of two PPy layers on either side of a PVDF (ion storage) layer. This actuator design has the potential to be used in a variety of potential applications, due to its fully reversible nature (Figure. 79).

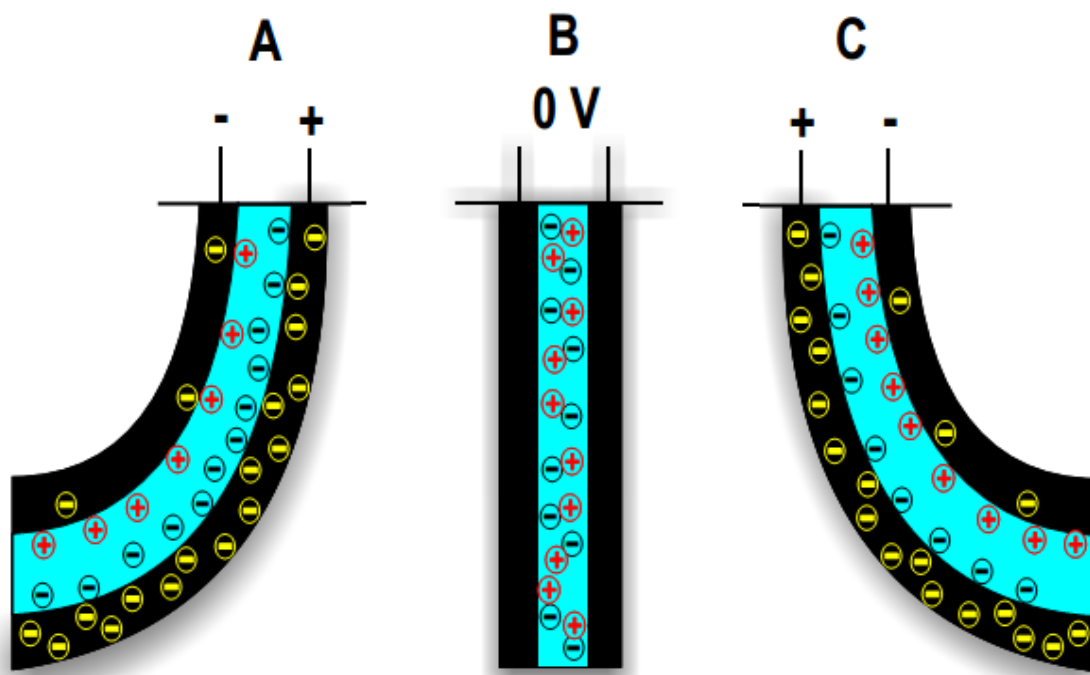


Figure 76. (a) PPy is oxidized at the positive electrode causing anion movement from the PVDF layer into the PPy layer which causes volume expansion. Reduction occurs at the

negative electrode resulting in volume reduction. (b) The trilayer actuator at rest with no electrical stimulus being applied. (c) Step A is repeated with the electrodes being switched around, allowing deformation to occur in the opposite direction.

9.4 Polymer conformations influencing actuation

Volume changes within CP films are linked to conformational changes which are generated by the presence of redox processes. Movements linked to the reduction processes are faster than oxidation processes (reactions), due to the kinetics of conformational change. Opening and closing of polymeric structures during redox switching are controlled by conformational relaxation which gives the best results for electrochemical responses of PPy-coated electrodes (Otero 1999). Electrochemical simulation and generation of free volume is transformed into a stress gradient across the polymer-polymer interface, this allows the actuator to bend.[45, 55] Polymer conformation in a zig zag structure play an important role in the actuation mechanism, not limited to ion intercalation in the bulk polymer chain upon electrochemical activation. The molecular actuation mechanism of the polymer conformation designed by (Anquetil, et al., 2002) resulted from the Π - Π stacking of the thiophene oligomers upon oxidation. A hinged molecule such as calix(4)arene interconnected by rigid rods of quarterthiophene was among the first polymers designed to have the zig-zag conformation. Attraction between the quarterthiophene rods occurred when the material was in the oxidized state which in turn contracted the overall material. Oxidation of these rods caused Π - Π stacking to produce reversible molecular displacement during actuation. These hinged rigid (zig-zag) structures which have a great amount of internal volume was found to be capable of experiencing large volume changes upon application of potentials (**Figure. 80**).[12]

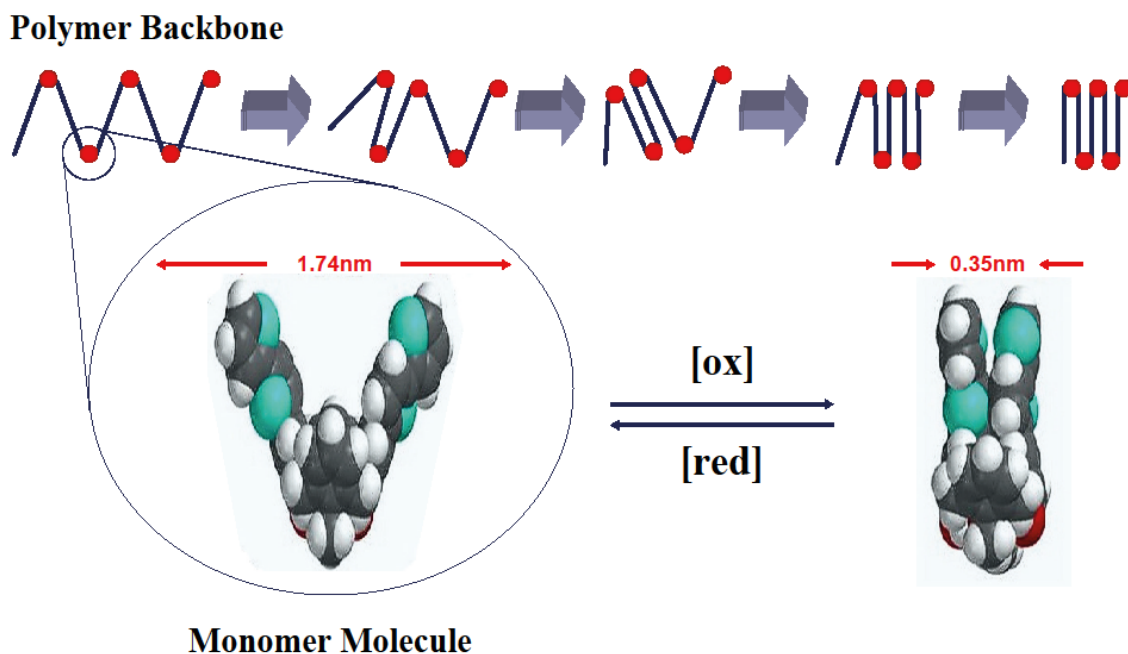


Figure 77. Zig-zag molecule containing calix(4)arene and quarterthiophene.

Other examples of zig-zag molecules used in actuation include a helical structure (with Zn centre) (**Figure. 81**), a zig-zag organometallic framework (**Figure. 82**) and molecular tweezers (**Figure. 83**).^[30, 41, 120] Films of the calixarene quarterthiophene (zig zag) material displayed conductivities of 10-1 S/m, densities between 550 and 750 kg/m³ and tensile strengths of 20 MPa in the dried form and 1.3 MPa when soaked in acetonitrile. The system also displayed a reversible strain in the order of 20%.^[205] The cyclic voltammetry of this zig zag polymer and a proton doped form of the polymer showed two redox waves with half wave potentials at 0.22 V and 0.45 V (Ag/AgCl).^[35] The contraction of the calix(4)arene based electroactive actuator was studied by microsecond atomistic molecular dynamics simulation in dichloromethane (DCM). The efficiency and rate of the contraction was found to be linked to the presence of secondary transitions in the calix(4)arene scaffold and the presence of solvent molecules.^[62]

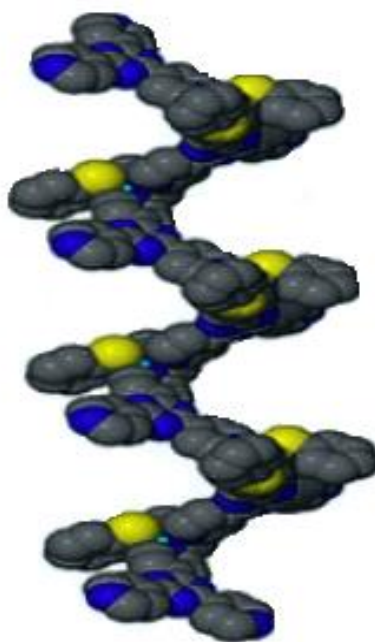


Figure 78. Helical Structure with Zn centre $\{Zn(SPh)_2(BPyVB)\}_n$.

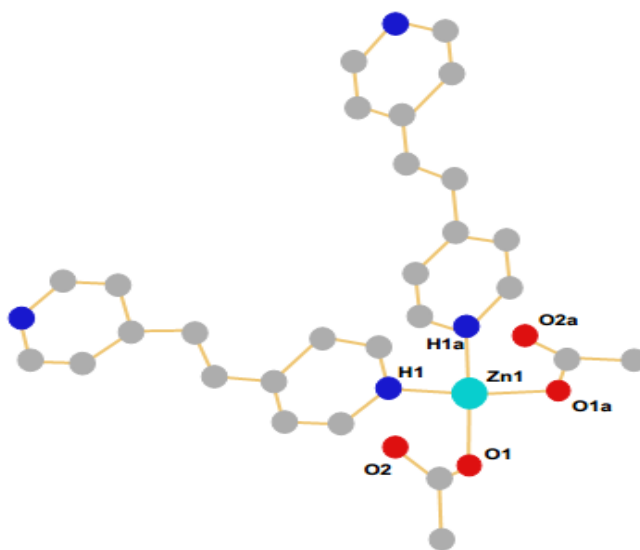
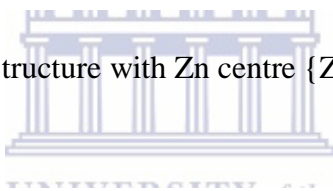


Figure 79. Organometallic framework.

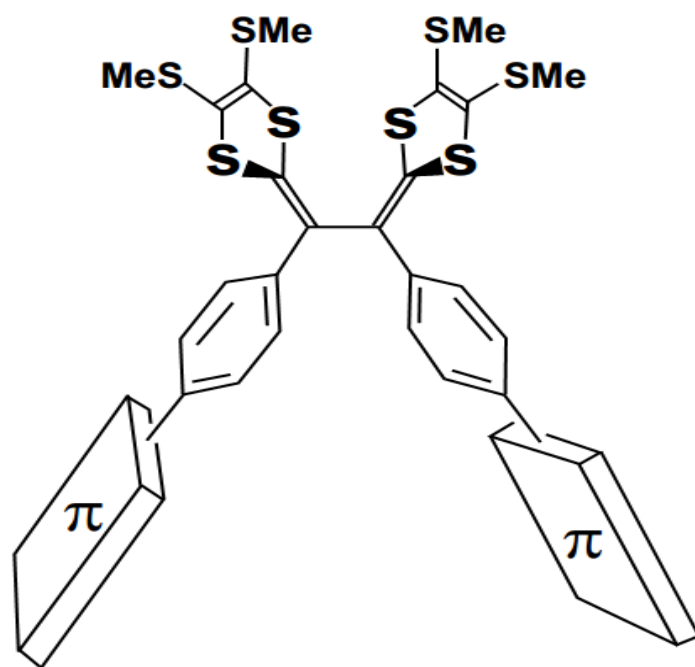


Figure 80. Molecular tweezers.

Zig zag polymers produced from digold and tetragold rings crosslinked with bis (pyridine) in which hydrogen bonding was responsible for the zig zag chains. ^{31}P NMR (nuclear magnetic resonance) and Electrospray ionization mass spectrometry (ESI-MS) was used to characterize the solid state polymer network (Burchell, et al., 2003).[35] Self-assembly of organometallic polymers through hydrogen bonding have also been explored in the production of a diplatinum(IV) complexes, through the formation of a bridging halide linking group. These types of zig zag polymers are useful for the production of molecular materials through simple self-assembly methods.[146] One dimensional zig zag polymers have also been produced from the co-ordination of Ni(II), Cu(II) and Zn(II) complexes. The bridging ligands used to produce the single strand helical structures included isophthalate, pyridyl and triazine derivatives. Extensive characterization by crystallography, spectroscopy and thermal methods, confirmed that the one dimensional chain structure was also stabilized by H-bonding.[41, 120] These zig zag materials were demonstrated to be highly efficient heterogeneous catalysts for cyanosilylation of aldehydes. These zig zag supramolecular polymers were all prepared from a materials synthesis point of view and no reports are

available about their electrochemical behaviour, actuation and conductivity characteristics. Tetrathiafulvalene (TTFV) as been used in the design of stimuli responsive molecular devices for sensing, switching and in the design of logic gates. The TTFV hinge was used to produce a tweezer like structure using various quinones as Π - backbone. The TTFV hinge was observed to have fully reversible electrochemistry.[41] Various derivatives of TTFV was applied for sensitive electrochemical detection of saccharides and fluorine.[138] A newly synthesized zig zag polymer (**Figure. 84**) containing poly(phenazine-2,3-diimino(pyrrole-2-yl)-PPDP) doped with polyvinylsulfonic acid (PVSA) and 1,4-napthaquinone sulphonic acid(NQSA) was evaluated by (Ward, et al., 2014) which by design showed promising behavior as an actuator material capturing the many advantages of PPy and conductivity favoured by a phenazine hinge. Thin films of the zig zag polymer were evaluated for actuation based on the change in capacitance (CPE) measured by electrochemical impedance spectroscopy (**Table 31**). The measured interfacial capacitance modelled at constant phase angle for redox states showed 50% higher values for the oxidized state compared to the reduced state.[190]

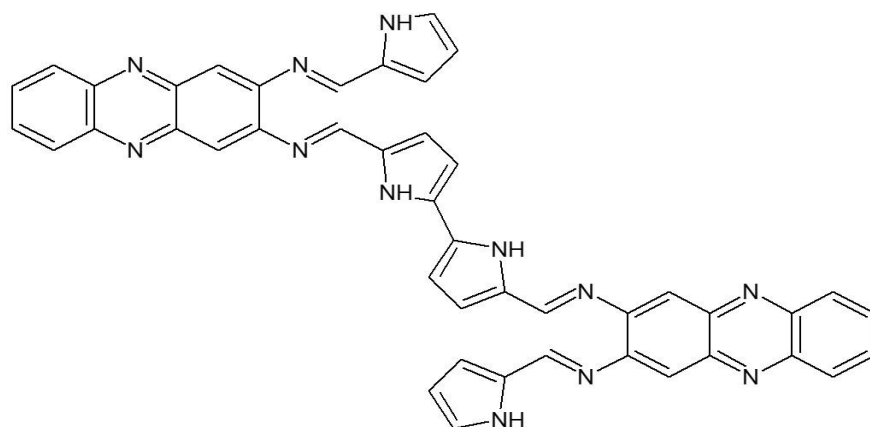


Figure 81. Zig zag structural conformation of a phenazine hinged molecule interconnected by pyrrole chains.

Table 31. Interfacial capacitance of PPDP-PVSA

	PPDP/PVSA	PPDP/PVSA	PPDP/PVSA	PPDP/PVSA
Potential / mV	-100	+100	-200	+200
Rs / Ω	105.8	106.7	106	107.4
CPE / μF	4.03	6.29	2.34	3.37
Rct / $\text{k}\Omega$	4.056	4.094	3.547	4.094

9.5 Conclusion

Polypyrrole actuators have been extensively researched due to their ability to mimic biological systems as well as their ability to operate in a wide variety of potential applications. The original actuator design in a bilayer structure was used primarily for application in a liquid medium, whereas the trilayer actuator has no such limitation. It is able to operate in both liquid and air environments. Delamination of the bilayer actuator design during bending may also be effectively addressed by the trilayer design. Both bilayer and trilayer actuators were able to realize bending angles in excess of 90°. Limited reports are available for polypyrrole actuators in the zig zag design. These materials were synthesized and characterized in terms of their physical properties and no reports are available on displacement behavior of this class of material. Further evaluation of this is confirmed through the design of new materials and evaluation of their actuation potential is necessary before finally advocating or condemning them. However they are suitable for preparation in a thin film format at conducting electrode interfaces and hold promise for a wide range of analytical applications, based on internal volume change.

CONFLICT OF INTEREST

The authors confirm that this article content has no conflict of interest.

ACKNOWLEDGEMENTS

The financial assistance of the National Research Foundation (NRF, South Africa) and the Campus France mobility fund towards this publication is hereby acknowledged.

